THE EFFECT OF STRAIN-SOFTENING COHESIVE MATERIAL ON CRACK STABILITY

Thesis by
Tawach Ungsuwarungsri

In Partial Fulfillment
of the Requirements for the Degree of
Doctor of Philosopy

California Institute of Technology
Pasadena, California

1986
(Submitted May 19, 1986)

To my parents

PREFACE

Analytical studies in elastic-plastic fracture mechanics have been mainly directed at identifying certain fracture parameters such as the J-integral, the crack tip opening displacement or angle. Although the above approach has been widely adopted and applied with some success in predicting the behavior of stable crack growth (e.g. using the J-resistance curve), it fails to provide a framework for studying in further depth the effects of the failure mechanisms in the crack tip zone on the global behavior of crack growth.

Specifically, one does not fully understand how damage-induced softening behavior of the crack tip material - which varies in characteristics with the microstructural failure mechanisms - affects the stability of the crack. In metals, cracks advance with varying degrees of ductility depending on the loading and on the environmental conditions. If the fracture is relatively brittle, the crack surfaces separate in such a way that little plastic deformation is induced in the material surrounding the crack path. On the other hand, when the crack faces are formed through void nucleation, growth and coalescence, the 'effective' fracture energy turns out to be substantially higher than the fracture energy for brittle fracture; the extent of plastic deformation in the material adjacent to the path traversed by the crack is, correspondingly, much greater than when the fracture is brittle. Thus, the material separation characteristics and toughness reflecting the failure mechanisms at the crack tip directly control the energy expenditure and the stress and strain fields around the crack front.

Seen in this light, it is clear that fracture analyses are necessarily incomplete without incorporating the proper separation laws which describe the failure modes at the crack tip; in spite of the fact that one-parameter fracture criteria serve and have served very useful purposes they seem to be of somewhat limited virtue for understanding fracture as a fundamental process.

The study reported in this thesis is focused on these aspects of fracture discussed above. The present investigation is confined to planar geometries (two-dimensional problems). Three problems have been examined. The first two are detailed analyses of the Barenblatt-Dugdale type where the cohesive forces are represented by arbitrary nonlinear force-displacement relations; these are presented in two seperate parts.

Part I analyzes the model of a beam on a nonlinear foundation appropriate to a double cantilever beam (DCB) specimen whose material is elastic with the nonlinear damage-softened material confined to a thin interlayer on the crack plane. The finding indicates that it is possible to estimate the nonlinear behavior of the damaged cohesive interlayer.

Part II examines the problem of a crack with a nonlinear cohesive zone of the Barenblatt-Dugdale character embedded in an infinite elastic medium subjected to symmetrical loading; the analysis allows the cohesive zone to be of arbitrary size and thus is appropriate for modeling crazes in polymers with the nonlinearity confined to the description of craze fibril material. These two analyses yield a number of interesting findings which show that the damage-induced softening material behavior at the crack tip plays a central role in determining the global behavior of crack propagation.

The third problem studied represents an attempt to extend the nonlinear cohesive zone model to the case where the material adjoining the cohesive 'boundary layer' along which the crack propagates is not simply elastic. In this case, the material surrounding the crack is allowed to deform plastically according to the incremental theory of plasticity thus introducing an additional dissipative mechanism. For this purpose, a finite element model in which a row of nonlinear softening springs model the behavior of cohesive layer is employed. We encounter a numerical difficulty which seems to require as remedy the

imposition of additional constraints on the manner by which the springs are allowed to deform. The finding and discussion regarding this attempt are documented in the Appendix.

ACKNOWLEDGEMENTS

It is a great pleasure to express my appreciation and gratitude to Professor W.G. Knauss for providing me with the opportunity to work on this interesting project. His physical insights, guidance and support throughout the course of this investigation were indispensable.

I would like to thank Prof. J.F. Hall for his helpful suggestions in connection with the finite element modeling in Part I of this work as well as in the Appendix. Thanks are also due to my colleagues, P. Washabaugh and S. Krishnaswamy, for their many helpful comments and discussions. I am grateful to Hibbitt, Karlsson and Sorensen, Inc. for making available the ABAQUS finite element program under a special academic license.

I am much indebted to Ms. Marta Nyiri for her help in typing Parts I & II of this thesis. I would also like to thank Mrs. Betty Wood for her help in preparing the figures and Ms. Jacquelyn Beard for typing the early draft of Part I.

The study in Part I was carried out under the sponsorship of NASA and the Air Force Office of Scientific Research. In particular the beam equation work was performed as a study on test methods for tough composite matrix materials under NAG-1-474 while the finite element work was peformed under AFOSR-84-0254 in order to become acquainted with the ABAQUS code.

The investigation in Part II was performed as part of an initiation study into nonlinear crack tip mechanics; it was supported by the Air Force Office of Scientific Research under Grant No. AFOSR-84-0254 with the initial technical contact being Capt. David Glasgow. Also support from E.I. Dupont de Nemours & Company and NASA under grant NAG-1-474 is gratefully acknowledged. In the past,

Drs. K. Palaniswamy and K. Ravi-Chandar have contributed towards the formulation of the nonlinear craze problem. Thanks are due to Professor E.J. Kramer of Cornell University for the helpful discussions regarding recent experimental findings, for providing the micrographs in Figure 1 of Part II and for the permission to duplicate some results from his papers.

I thank my wife, Pakky, for her understanding, patience and constant encouragement. Finally, I dedicate this thesis to my parents who instilled in me a belief in the value of education and encouraged me to return to Caltech to pursue my graduate studies.

TABLE OF CONTENTS

PART I

THE ROLE OF DAMAGE-SOFTENED MATERIAL BEHAVIOR IN TOUGHNESS AND FRACTURE OF COMPOSITES AND ADHESIVES

NOTATION

Lower case:

b	= beam width
d	= foundation (cohesive layer) thickness
h	= beam height (thickness)
k	= elastic foundation spring stiffness
l	= crack length
$q = q(w)$	= cohesive (foundation) restoring force per unit beam length
$w = w(x)$	= vertical displacement of the beam
x	= horizontal coordinate (measured along the undeformed beam length)

Upper case:

A, B	= constants
$C \equiv \delta/p$	= (secant) compliance
E	= elastic modulus of the beam
E_b	= beam bending energy
E_c	= elastic modulus of the cohesive foundation
F_c	= critical nodal force at which unloading starts
G	= energy release rate
$I = bh^3/12$	= moment of inertia of the beam section
K_I	= Mode-I stress intensity factor
L	= beam length
$M = M(x)$	= bending moment
M_c	= bending moment at the crack tip
N	= power law exponent (in the equation $C=al^N$)

P = applied end load

$S = S(x)$ = shear

S_c = shear at the crack tip

W = work done by the end load P

W_c = work done against the interface forces (in the ideal case)
= energy dissipated in the cohesive interlayer

Greek:

α = size of the yield zone

$\beta = (k/4EI)^{\frac{1}{4}}$

γ = fracture energy = area under q-w curve (exact value)

$\tilde{\gamma}$ = fracture energy as calculated from equation (2.16)

δ = end displacement of the beam

π = potential energy

Subscript:

$( )_c = ( )_{crack}$ (for propagating crack)

$( )_t = ( )_{tip}$ (for stationary crack)

$( )_u = ( )_{unloading}$

$( )_y = ( )_{yield}$

Superscript:

$( )', ( )'', ( )''', ( )^{(4)}$ = first, second, third and fourth derivatives of $( )$ with respect to x, respectively

$( )^*$ = dimensionless form of $( )$.

$$x^* \equiv x/d \qquad q^* \equiv qd^3/EI$$

$$w^* \equiv w/d \qquad P^* \equiv Pd^2/EI$$

$$l^* \equiv l/d \qquad M^* \equiv Md/EI$$

$$h^* \equiv h/d \qquad \gamma^* \equiv \gamma d^3/EI$$

$$b^* \equiv b/d \qquad \tilde{\gamma}^* \equiv \tilde{\gamma} d^3/EI$$

$$\delta^* \equiv \delta/d \qquad C_1 \equiv 12 \left\{\frac{E_c}{E}\right\} \left\{\frac{d}{h}\right\}^3$$

ABSTRACT

Failure mechanisms of materials under very high strains experienced at and ahead of the crack tip (such as the formation, growth and interaction of microvoids in ductile materials, microcracks in brittle solids or crazes in polymers and adhesives) are represented by one-dimensional, nonlinear stress-strain relations possessing different post-yield softening (unloading) behaviors. These reflect different ways by which the material loses capacity to carry load up to fracture. A DCB type specimen is considered in this study. The nonlinear material is confined to a thin strip between the two elastic beams loaded by a wedge. The problem is first treated as a beam on a nonlinear foundation for which the pertinent equation is solved numerically as a two-point boundary value problem for both the stationary and the quasi-statically propagating crack. A finite element model is then used to model the problem in more detail to assess the adequacy of the beam model for reduction of the experimental data.

It is found that the energy release rate[1] $G = 2(\gamma b) = \{(3P^2\delta)^2/ EI\}^{1/3}$ derived by assuming the built-in conditions at the crack tip could be used to calculate the fracture (surface) energy more accurately and conveniently than the conventional scheme even in cases where the built-in assumption is invalid. Results for the deformations of the beam prior to or during crack growth suggest ways to approximately characterize the complete material stress-strain behavior, including loading and strain-softening characteristics.

1. See table on Notation for definitions of symbols.

1. INTRODUCTION

The double cantilever beam (DCB) specimen has been extensively used in crack propagation studies due to its simple geometry which is attractive from both the experimental and theoretical standpoints. Berry [1] investigated the implications of the Griffith fracture criterion for the DCB specimen and showed that for the built-in beam, fracture initiated when the moment at the crack tip reached the critical value $M_c = Pl = \sqrt{2EI\gamma b}$ and that $3P^2\delta = (2\gamma b)^{3/2}\sqrt{EI}$. Bilek and Burns [2] in their dynamic analysis derived the same equations through the application of Hamilton's principle for nonconservative systems. Similar results were also obtained by Steverding and Lehnigk [3] using a different approach. Kanninen [4] employed a beam on an elastic foundation model to relax the built-in constraint and later [5] extended his analysis to the dynamic case introducing a Timoshenko beam on a generalized elastic foundation model to account for shear deformation and rotary inertia.

In the present work, we generalize the foundation to a nonlinear one characterized by an initial linear elastic stress-strain relation and an unloading tail reflecting loss of load carrying ability. Subsequently, fracture occurs at some critical strain where the foundation stiffness drops to zero. Thus the model allows the crack to propagate without any additional prescription of a failure criterion, so that the nonlinear DCB analysis becomes a potential tool for determining the nonlinear material characteristics of the bond-interlayer. As complete stress-strain characterizations of real materials are not yet available, we resort first to some idealized (hypothetical) material models in an attempt to extract from the solution of the problem certain measurable macroscopic quantities that might allow us to characterize the complete material behavior in the continuum sense: In this we assume that a sufficiently large number of microvoids, microcracks or craze fibrils are present in each tiny volume element under load at the "crack front" such that the damage-induced loss of load carrying

capacity can be meaningfully averaged and represented as a continuum response. Studies involving porous and damaged materials are numerous, for instance McClintock [6], Gurson [7] who developed approximate yield criteria and flow rules for dilatant ductile materials; Needleman [8], Berg [9] who proposed a continuum model for plastic deformation of microporous metal aggregates; Rice and Needleman [10] studied metals with constitutive dependence on hydrostatic stress (which promotes void nucleation and growth) in sheet metal forming processes; Krajcinovic [11] presented a constitutive model for material containing flat planar microcracks such as concrete; see also Dougill [12], Rudnicki [13] and Bazant [14]. In our studies we are primarily interested in the non-linear response of homogeneous or multiphase polymers such as those used in advanced composites and adhesives.

To simulate crack propagation in our finite element study, we employ a scheme different from the ones proposed thus far. The usual node release methods proposed by Andersson [15], Kfouri & Miller [16], Rydholm et al [17] and Malluck & King [18, 19] permit only a single node to be released at a time by reducing the reaction force at the crack tip node over several steps in some prescribed manners when a fracture criterion, such as a critical crack tip opening displacement (CTOD) or crack tip opening angle (CTOA), is reached. These methods require continual external monitoring and interruptions of the computations which become very time-consuming and inconvenient for simulation of crack growth over distances of ten or more elements. Hoff et al. [20] introduced a technique employing spring and gap elements to circumvent this problem, the method requires a subroutine to control the openings of the gap elements and thus does not put crack propagation under total control of the external loadings. In this study, we use nonlinear springs that have no restraining forces beyond a certain critical strain to imitate the failure characteristics of the cohesive material in the interlayer. Thus when a nonlinear spring joining a node along the crack path to the foundation 'fails', a node is released and the crack advances. In this way, crack propagations over distances

of tens of elements (or more) are easily simulated requiring no external monitoring whatsoever. Clearly, this 'nonlinear spring' technique can be advantageously adopted as a node release mechanism in more general situations provided the nonlinear characteristics of the "springs" are properly chosen. As an example, to release one node at a time when a critical nodal force F_c is reached (Kanninen et al. [21] showed F_c to be relatively constant during stable crack growth), the springs should be made infinitely stiff for nodal forces below F_c and may be given any unloading characteristics desired.[2] We have attempted to model quasi-static crack growth in elastic-plastic materials characterized by the J_2 incremental theory of plasticity but without much success. The difficulties encountered are documented in the Appendix. In dynamic (not necessarily steady-state) problems, this method is still applicable so long as the separation of the crack faces is monotonic (so as not to generate spurious vibrational behaviors). In this event, the loading history directly and fully dictates the crack growth history, i.e., initiation, growth and arrest. Lastly, for springs with finite initial stiffness such as the ones used in this study, the proposed method allows several nodes to be simultaneously released and thus simulates crack growth in a continuous and realistic manner.

The present problem is considered as a precursor to the more general one wherein a yield criterion based on a strain softening material is used. In that more general case one needs to be concerned with the highly triaxial stress state at the crack tip as well as with the consequences of locally unstable material behavior on global stability. In cases where the process zone is 'narrow' compared to the size of the specimen considered, a 'boundary layer' type model in which the damage-softened material behavior is confined to a thin layer adjacent

2. The unloading tail (force-displacement relation with the force decreasing from F_c to zero) might be patterned after any of the usual node release schemes. Note also that for cases where we do not have a cohesive layer, the springs must be infinitely stiff in compression since the nodes along the crack path cannot have negative vertical displacements by virtue of symmetry.

to the crack plane may prove to be a realistic and yet computationally inexpensive scheme for studying crack growth. Certain rubber toughened materials seem to obey this model very closely. Of course, much work remains before the appropriate continuum models for enigneering materials of interest are experimentally identified and numerically verified under a wide range of loading conditions.

In Section 2, we discuss the problem of the beam on a nonlinear foundation, its numerical solution schemes and the results for both stationary and propagating[3] cracks. The finite element model is presented in Section 3 and is followed by comparisons with the beam equation model in Section 4. Applications of the findings are demonstrated in Section 5, with conclusions summarized in Section 6.[4]

3. In the present investigation, no inertia (dynamic) effects are considered, therefore 'propagation' refers to 'quasi-static' propagation throughout.

4. A few other relevant works are given at the end of the list of references.

2. THE BEAM ON A NONLINEAR FOUNDATION MODEL

The model and relevant problem definitions are depicted in Figure 1. The equation for a Bernoulli-Euler beam (with constant EI) resting on a nonlinear foundation is

$$EI \frac{d^4w}{dx^4} + q(w) = 0 \tag{2.1}$$

where E is the Young's modulus of the beam, $I = \frac{1}{12}bh^3$ (for rectangular cross section), w is the vertical displacement of the beam neutral axis, and q(w) is the nonlinear restoring force per unit length of the foundation. We consider q(w) such that, typically, the small strain response corresponds to an "elasticity" modulus that is approximately an order of magnitude smaller than that of the beam.

Equation (2.1) is to be solved subject to boundary conditions at the loading end and at a distance far away from the loading end where the conditions are those of a semi-infinite beam on a linearly elastic foundation. This may always be assumed if the 'uncracked portion' of the beam is longer than two to three times the exponential decay length ($1/\beta$; see equation (2.2)).

2.1. Solution Schemes

The equation to be solved is nonlinear and involves boundary conditions at two points. A standard technique is the shooting method [22], which seeks the proper boundary conditions at one end point that also satisfy the boundary conditions at the other end point by Newton's iteration based on the Jacobian matrix formed by the miss-hits at the other end point and the current boundary conditions chosen at the first end point. The usual difficulty encountered is in obtaining convergence without requiring an excessive number of iterations; the rate of convergence depends strongly on the proximity of the initial guess of

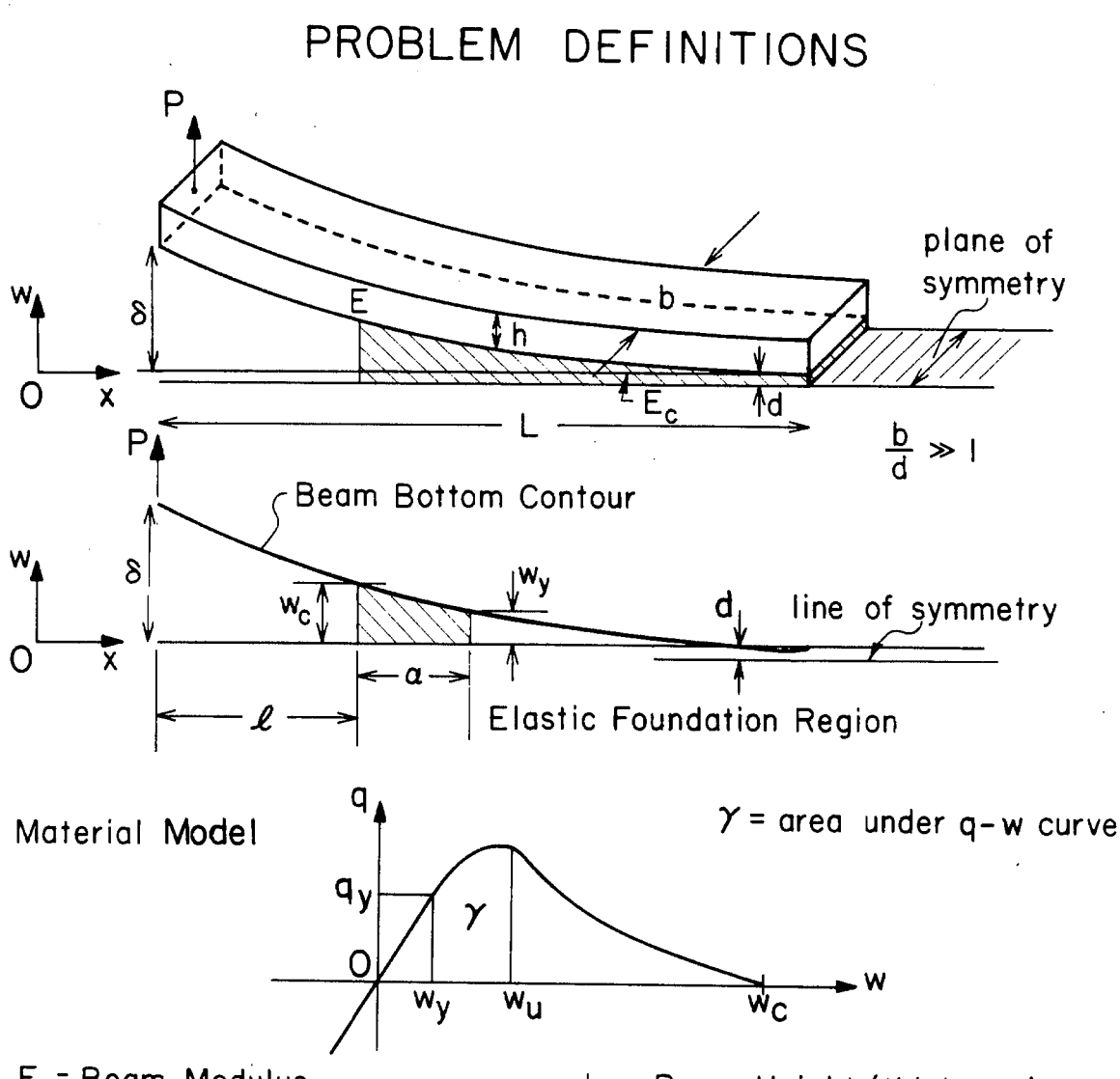

E = Beam Modulus
E_c = Cohesive Elastic Modulus
p = End Load
δ = End Displacement
w = Vertical Displacement
ℓ = Crack Length
L = Beam Length
α = Yield Zone Size

h = Beam Height (thickness)
b = Beam Width
d = Cohesive Layer Thickness
q(w) = Cohesive Restoring Force
$w_y^* = \frac{w_y}{d}$ = Yield Strain
$w_u^* = \frac{w_u}{d}$ = Unloading Strain
$w_c^* = \frac{w_c}{d}$ = Critical (crack) Strain

Figure 1. Problem definition of the geometry and material parameters.

the boundary conditions at the first end point to the correct boundary conditions.

In the present problem, we take advantage of the existence of the solution for the beam on a linear foundation by starting the integration from the region where the foundation response is linear and an analytical solution is available. We integrate up to the crack tip beyond which the beam is free of surface tractions except for the very end. For this unloaded section a simple solution can again be exploited. For convenience we set up our coordinate system as shown in Figure 2.

The solution for a semi-infinite beam on an elastic foundation (i.e., q(w)=kw in (2.1)) with boundary conditions

$$w(\infty) = w'(\infty) = w''(\infty) = w'''(\infty) = 0$$

is of the form

$$w(x) = e^{-\beta x}(A\cos\beta x + B\sin\beta x) \tag{2.2}$$

where $\beta = \left(\frac{k}{4EI}\right)^{\frac{1}{4}}$ and A, B = constants.

To start the integration of equation (2.1) from the elastic foundation region, we observe that the choice of the starting point is arbitrary; for convenience we may, therefore, choose x to be zero such that

$$w(0) = w_o \tag{2.3a}$$

$$w'(0) = 0 \tag{2.3b}$$

which yields $A = B = w_o$ and

$$w''(0) = -2\beta^2 w_o \tag{2.3c}$$

$$w'''(0) = 4\beta^3 w_o \tag{2.3d}$$

Note that it is fastest to integrate from $w_o < 0$ into the nonlinear region (see Figure 2), and that w_o has to be such that no yielding occurs in compression at the starting point x = 0. In this work, we assume that the yield strain in compression is equal to the yield strain in tension. It should be pointed out that by starting the integration from conditions derived from (2.2), we are guaranteed an exponentially decaying solution as $x \to +\infty$; this would not necessarily be the case if one were to start the integration from the loading end as any small error in the initial guess could cause the components of solution with terms proportional to $e^{\beta x}$ to enter and make the solution unbounded as $x \to +\infty$. Thus a poor initial guess at the loading end could result in extremely slow convergence or no convergence at all.

2.1.1. Stationary (Non-propagating) Case

For this case we seek the solution for a geometry with a pre-cut crack of length l under increasing load P to the point where crack propagation is imminent.

We obtain the solution by integrating[5] until $\frac{M}{P} = \frac{-M}{S} = l$ (with less than 0.1% error), here S is the shear for the free part of the beam, P is the end load, and M is the moment. We then obtain the rest of the solution from (see Figure 2)

$$\delta = \frac{Pl^3}{3EI} + |w'_t|l + w_t \tag{2.4}$$

---

5. The subroutine MODDEQ of the Caltech Computing Center which employs the Runge-Kutta-Gill method is used to solve a system of four first-order differential equations equivalent to equation (2.1).

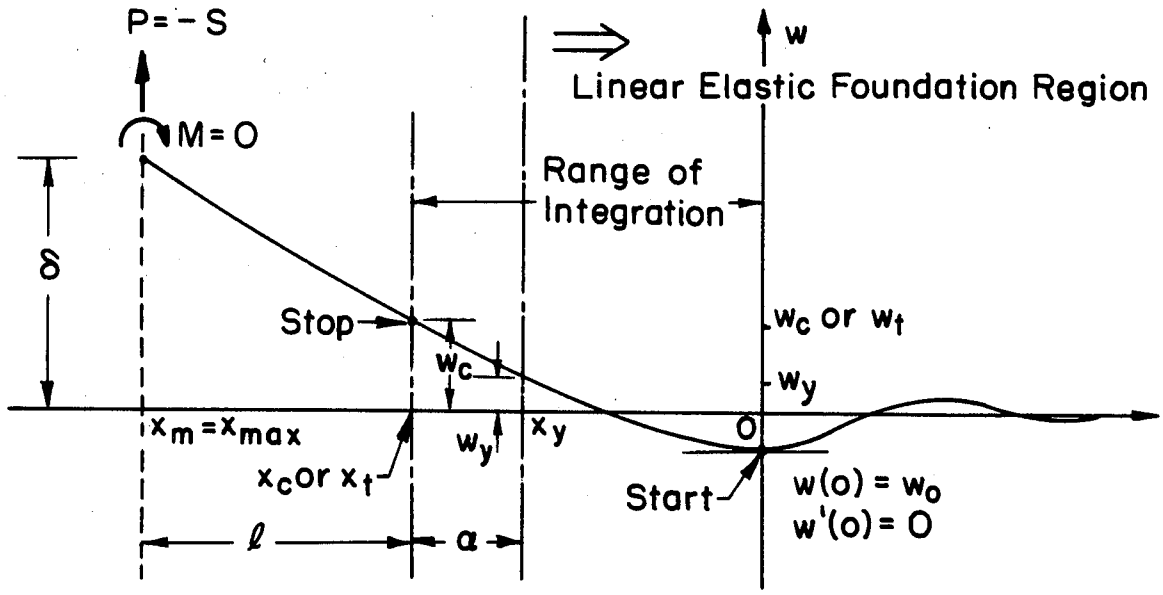

$( )_t = ( )_{tip}$ (For stationary crack)

$( )_c = ( )_{crack\ tip}$ (For propagating crack)

Stationary Case

Integrate until $\frac{M}{P} = -\frac{M}{S} = \ell$,

then

$$\Rightarrow \delta = \frac{P\ell^3}{3EI} + |w_t'|\ell + w_t$$

Propagating Case

Integrate until $w = w_c$, then

$P = -S_c$, $\quad \ell = \frac{M_c}{P}$

and

$$\delta = \frac{P\ell^3}{3EI} + |w_c'|\ell + w_c$$

Figure 2 Solution Schemes

where $w_t = w_{tip} \leq w_c$, $|w'_t|$ is the slope of the neutral axis at the crack tip. When $w_t = w_c$, we reach the point where the crack is about to grow.

2.1.2. Quasi-static Propagation Case

Here the scheme is to integrate along x until $w = w_c$ (with less than 0.001% error) and then calculate the crack length and end conditions from: (see Figure 2)

$$P = -S_c,$$

$$l = \frac{M_c}{P},$$

$$\delta = \frac{Pl^3}{3EI} + |w'_c|l + w_c \qquad (2.5)$$

where S_c and M_c are the shear and moment at the crack tip, respectively. $|w'_c|$ is the slope of the beam at the crack tip.

Other quantities such as the bending energy in the beam, E_b , the total work done, W, the work done on the interlayer, W_c , the size of the yield zone, $\alpha = |x_c - x_y|$, and the 'secant' compliance, $C \equiv \delta/p$, are readily computed. Note that for a nonlinear system, such as the one we are dealing with, it is appropriate to define the compliance C as $C \equiv \frac{d\delta}{dP}$; however in the present study, we intend to compare our results with previous findings in other studies where C has always been defined as the secant compliance which, strictly speaking, is only correct for linear systems. As there is no obvious advantage in employing the more general definition here, the usual definition is used.

2.2. Nondimensionalization

For presentation of the results it is useful to non-dimensionalize pertinent parameters. We choose the cohesive layer foundation thickness, d, as the natural length scale. For the elastic foundation region, we have

$$q(w) = b \cdot (E_c \epsilon_{22}) = E_c \left[\frac{w}{d}\right] b$$

where E_c is the elastic (small strain) modulus of the cohesive foundation. Equation (2.1) becomes

$$EI\ w^{(4)} + \left[\frac{E_c\ b}{d}\right] w = 0 \qquad (2.1a)$$

$$EI\ \frac{d^4(w/d)}{d(x/d)^4}\ \frac{1}{d^3} + E_c\ b\left[\frac{w}{d}\right] = 0$$

Define

$$w^* \equiv \frac{w}{d},\ x^* \equiv \frac{x}{d}$$

so that (2.1a) becomes

$$w^{*(4)} + C_1 w^* = 0,$$

with

$$C_1 \equiv \frac{E_c}{E} \cdot \frac{bd^3}{(bh^3/12)} = 12\left[\frac{E_c}{E}\right] \cdot \left[\frac{d}{h}\right]^3$$

Other dimensionless quantities are easily formed; they are

$$\delta^* \equiv \delta/d, \qquad l^* \equiv l/d, \qquad h^* \equiv h/d, \qquad b^* \equiv b/d$$

$$q^* \equiv \frac{qd^3}{EI}, \qquad P^* \equiv \frac{Pd^2}{EI}, \qquad M^* \equiv \frac{Md}{EI}, \qquad C^* \equiv \frac{\delta^*}{P^*}$$

and $\gamma^* \equiv \frac{\gamma d^3}{EI}$ is the non-dimensionalized fracture energy (= area under the q-w curve).

2.3. Results and Discussions

The following set of data is used throughout: E is chosen as the Young's modulus for Aluminum 2024 which is equal to 10.6×10^6 psi. E_c, the small strain modulus of the cohesive interlayer, is taken to be 1.41×10^5 psi. Also $h^* = h/d = 10.0$. These yield, $C_1 = 1.6 \times 10^{-4}$.

2.3.1. Stationary Crack Results

Here we present results for two subcases. In the first case, the materials studied possess the same fracture energy. In the second case, materials with more varied q-w characteristics but different fracture energies are used.

(a) Different material models with same γ^*

The material models[6] shown in Figure 3 are intended to examine the effects of various nonlinear material characteristics on the measurable macroscopic quantities. The results are presented in Figures 4-8. In Figure 4, the dashed lines exhibit the effects of the high compliance due to initial low foundation resistance which subsequently increases and becomes fairly constant as the yield zone, α^*, grows. (Thus the compliance decreases and then levels off.) These dashed portions are

6. The solution technique is capable of handling general nonlinear q(w), even though we only consider here piecewise-linear material models.

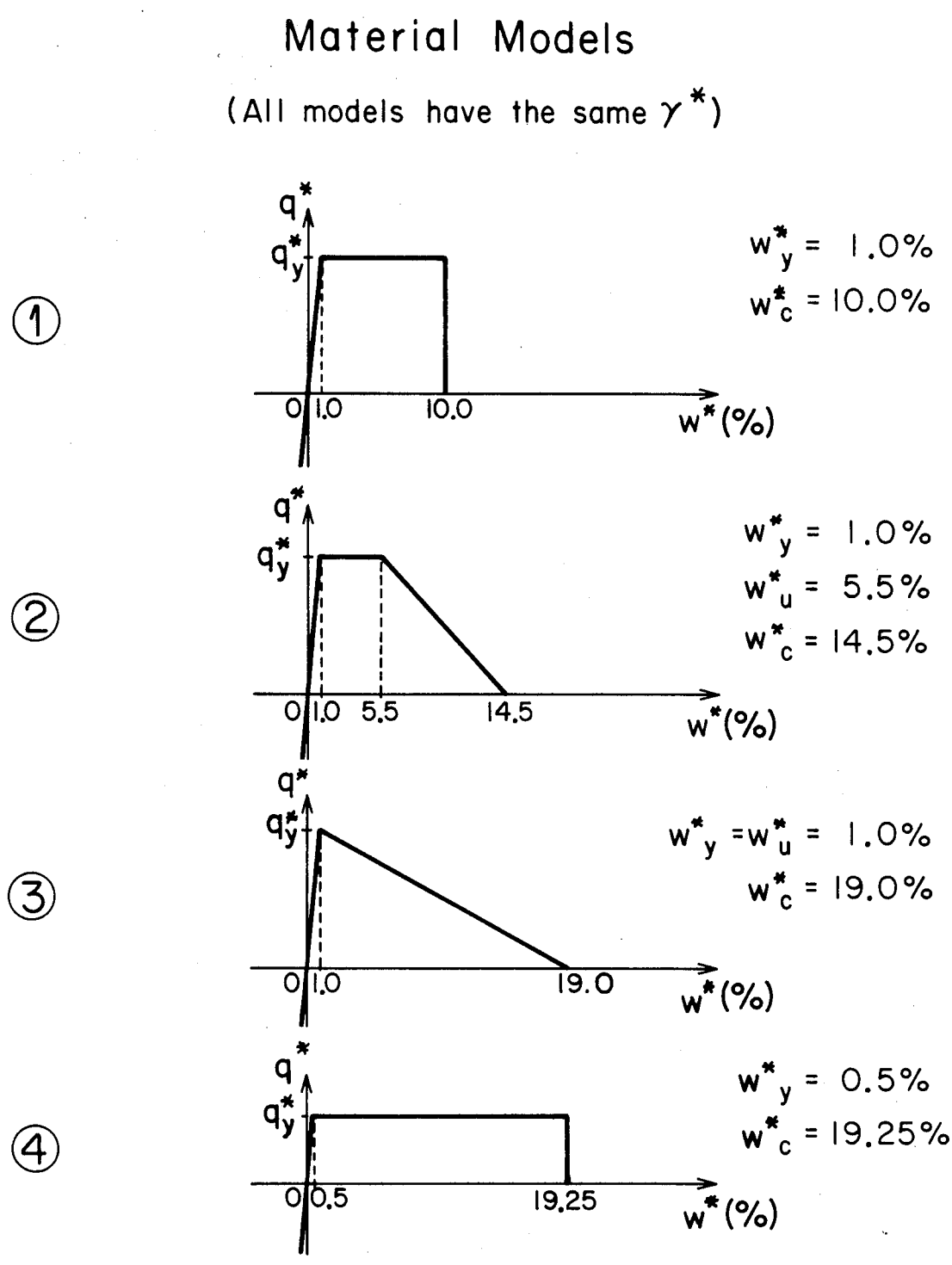

Figure 3. Material models (1, 2, 3 and 4).

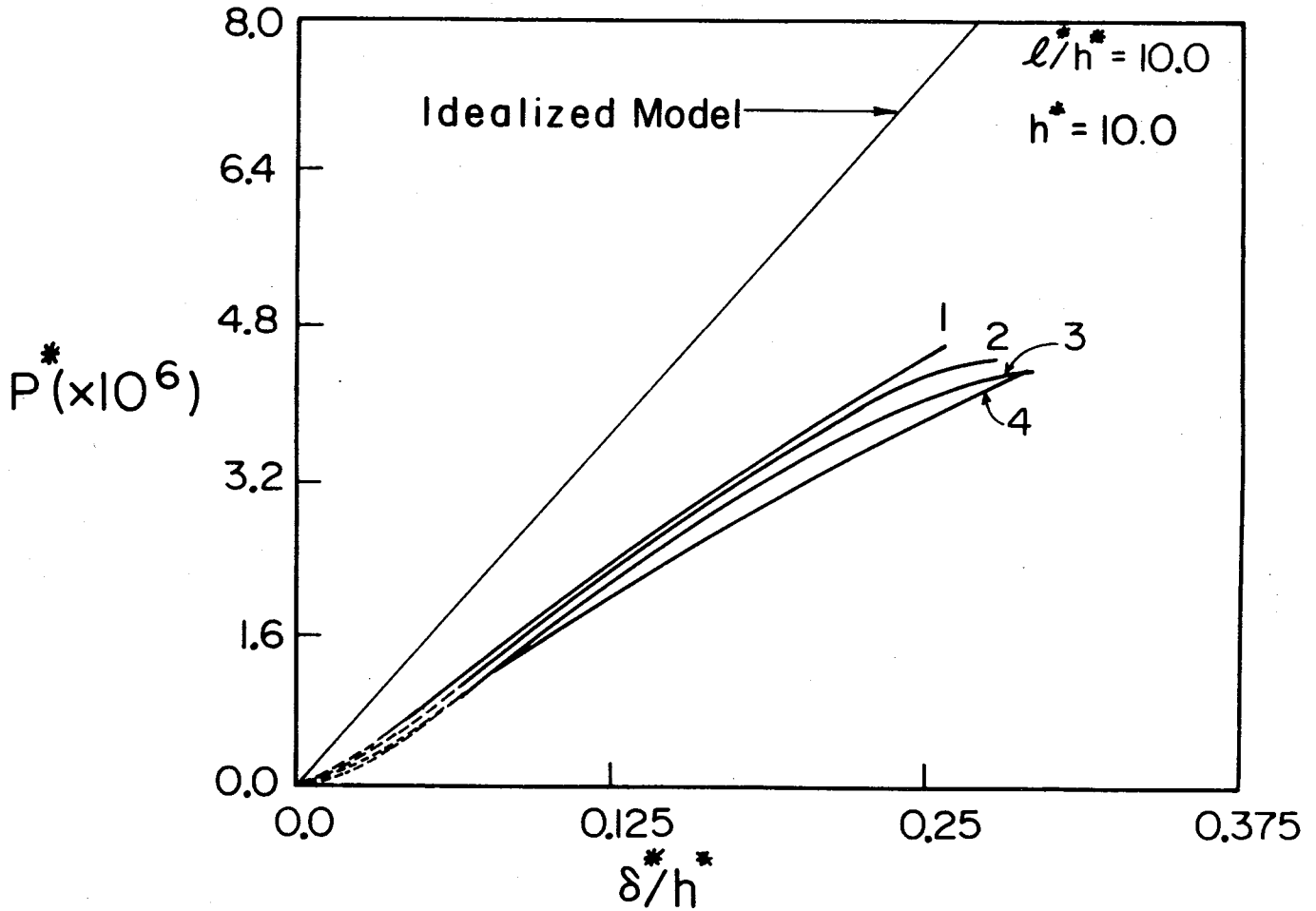

Figure 4. End load versus end displacement for the stationary crack (material models 1, 2, 3, and 4 as indicated). For explanation of the dashed portions of the P-δ curves see text.

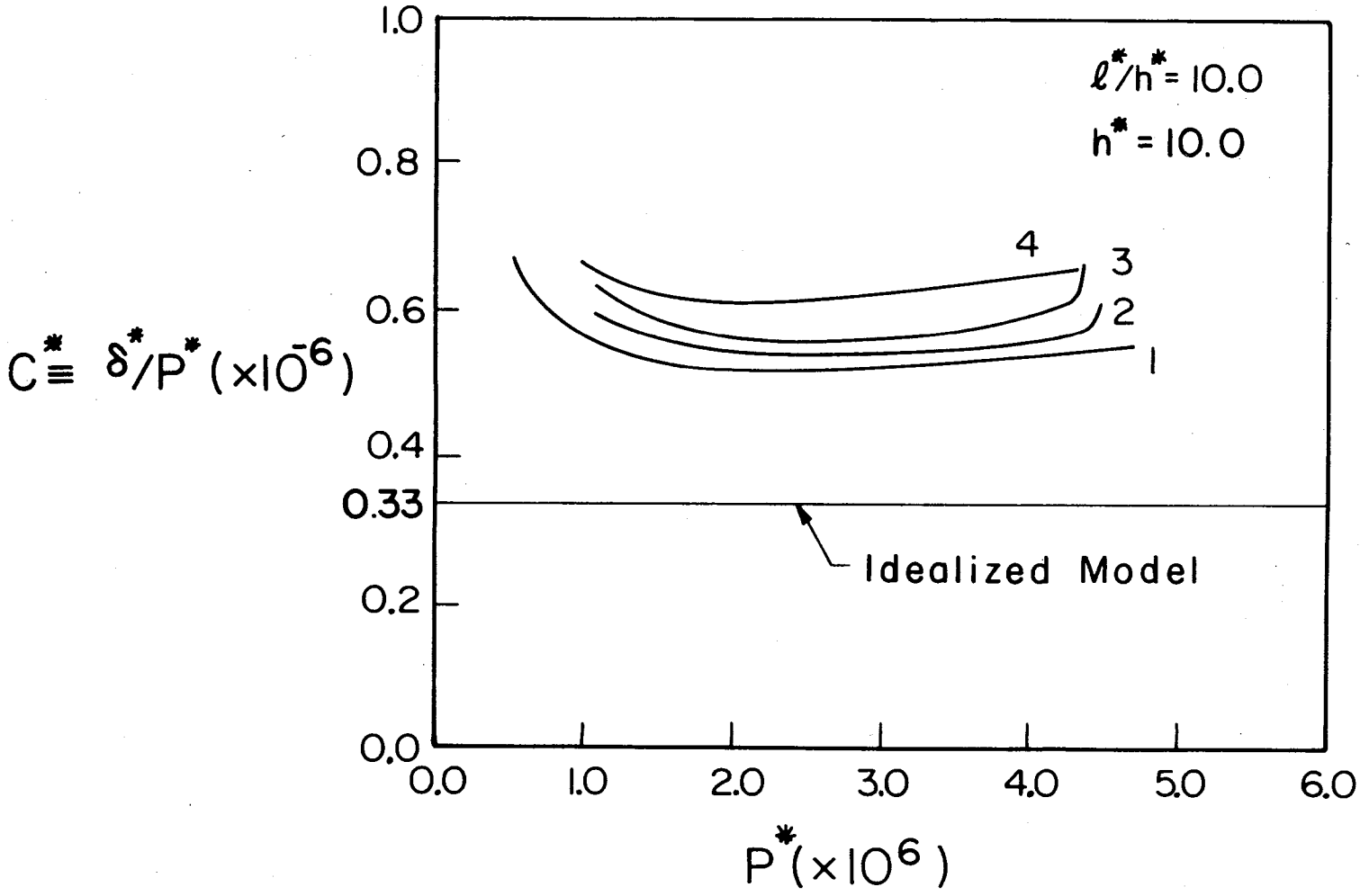

Figure 5. Compliance as a function of the end load for the stationary crack (material models 1, 2, 3 and 4 as indicated).

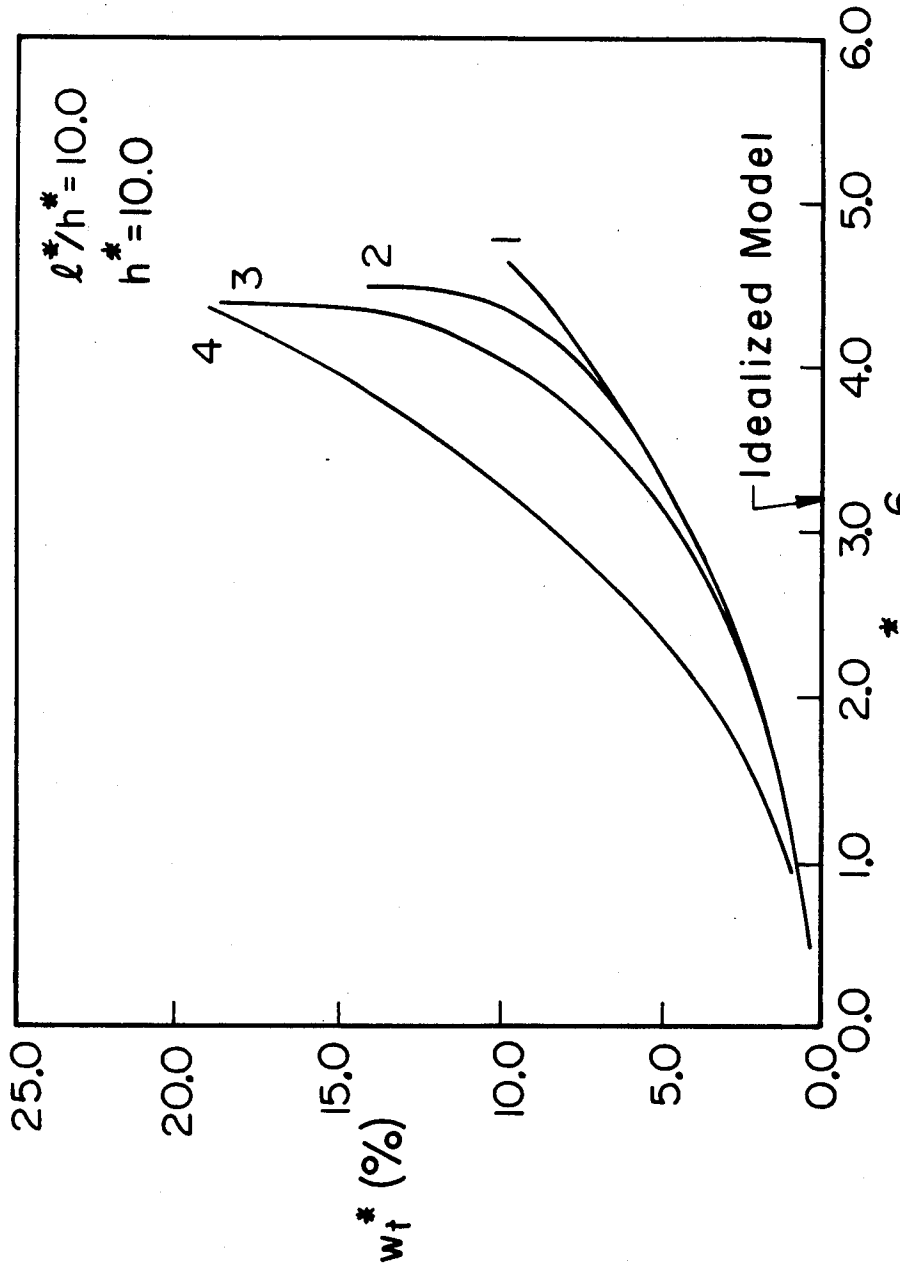

Figure 6. Crack tip displacement as a function of the end load for the stationary crack (material models 1, 2, 3 and 4 as indicated).

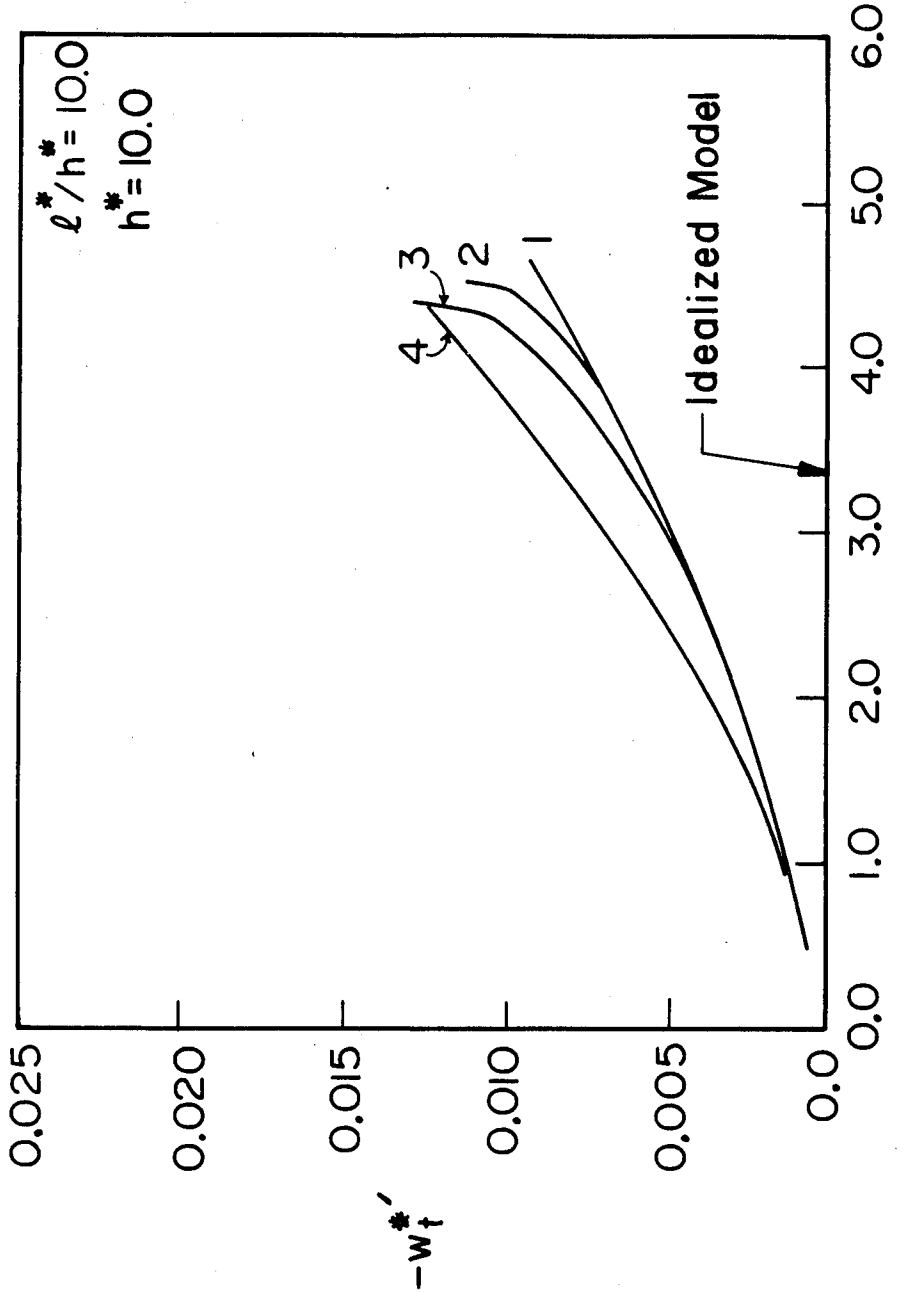

Figure 7. Slope at the crack tip as a function of the end load for the stationary crack (material models 1, 2, 3 and 4 as indicated).

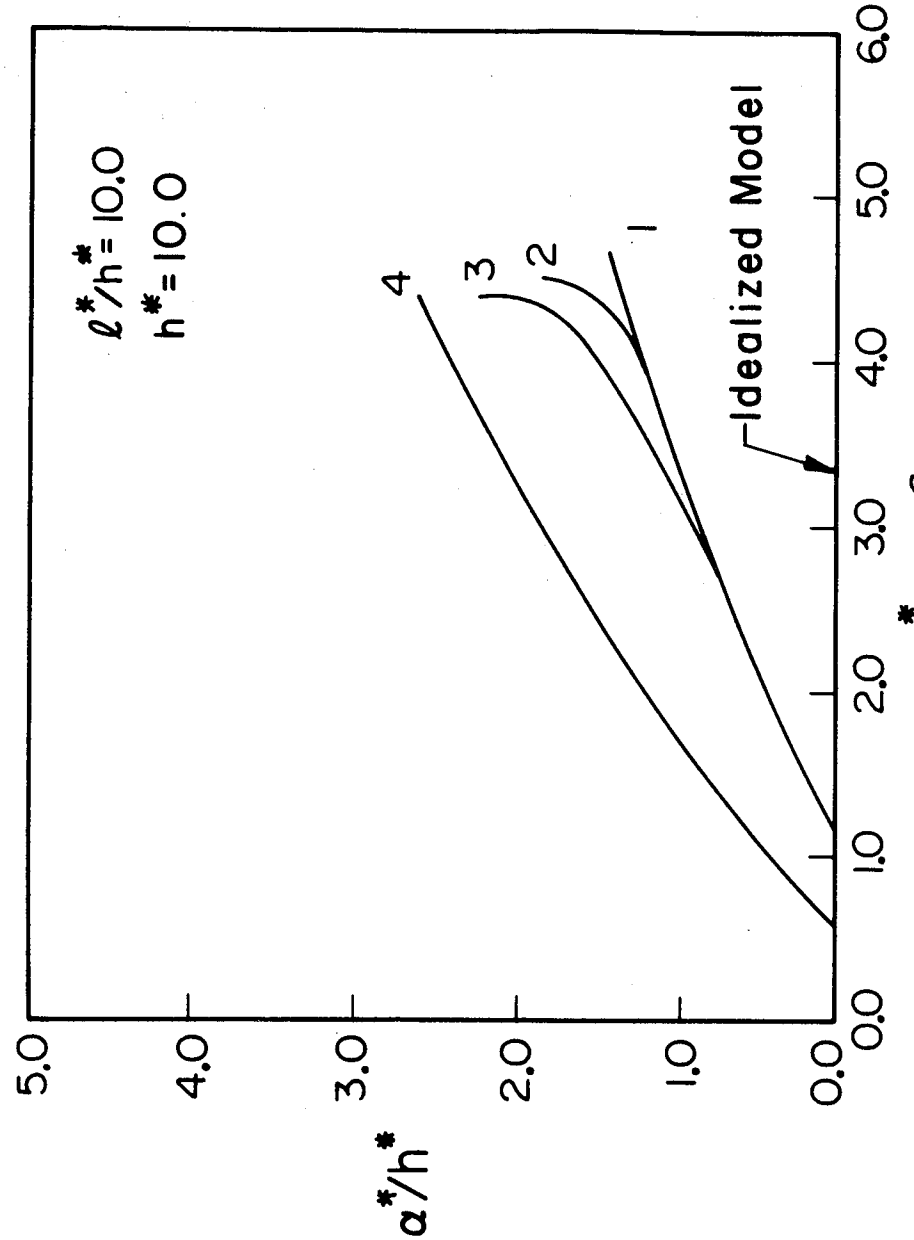

Figure 8. Yield zone size as a function of the end load for the stationary crack (material models 1, 2, 3, and 4 as indicated).

approximately extrapolated based on the compliance values from Figure 5. Clearly, the existence and the gradient of an unloading tail (as in materials 2 & 3) can be easily identified in any of these five plots as the onset of crack growth is approached, i.e., as $w_t^* \to w_c^*$. This fact can be used to approximately characterize q(w) from experimental data. In general, the compliance, C^*, the slope at the crack tip, $-w_t^{*\prime}$, and the size of the yield zone, α^*, are all monotonically increasing functions of w_c^*.

We shall discuss the application of this finding in connection with the characterization of q(w) in more detail in Section 5.2.

(b) Additional material models with different γ^*

Here we examine the material models A, B, and C in Figure 9, and show the qualitative results[7] in Figures 10-14. The figures exhibit the same features as discussed in Section 2.3.1a.

2.3.2. Quasi-static Propagation

Before dealing with the nonlinear case we consider first certain results for the idealized situation where neither the interlayer nor the elasticity of the beam allows rotation of the 'built-in' end. We first derive the equations mentioned in Section 1 for the built-in beam case. Here the coordinate system is such that the load P is applied at $x = 0$, $w(o) = \delta$ and $w(1) = w'(1) = 0$. We have for this "idealized" case,

$$\delta = \frac{Pl^3}{3EI} \qquad (2.6)$$

7. The curves are from actual computations but the scales for each curve A,B, and C are somewhat different and hence no scales are included in the Figures.

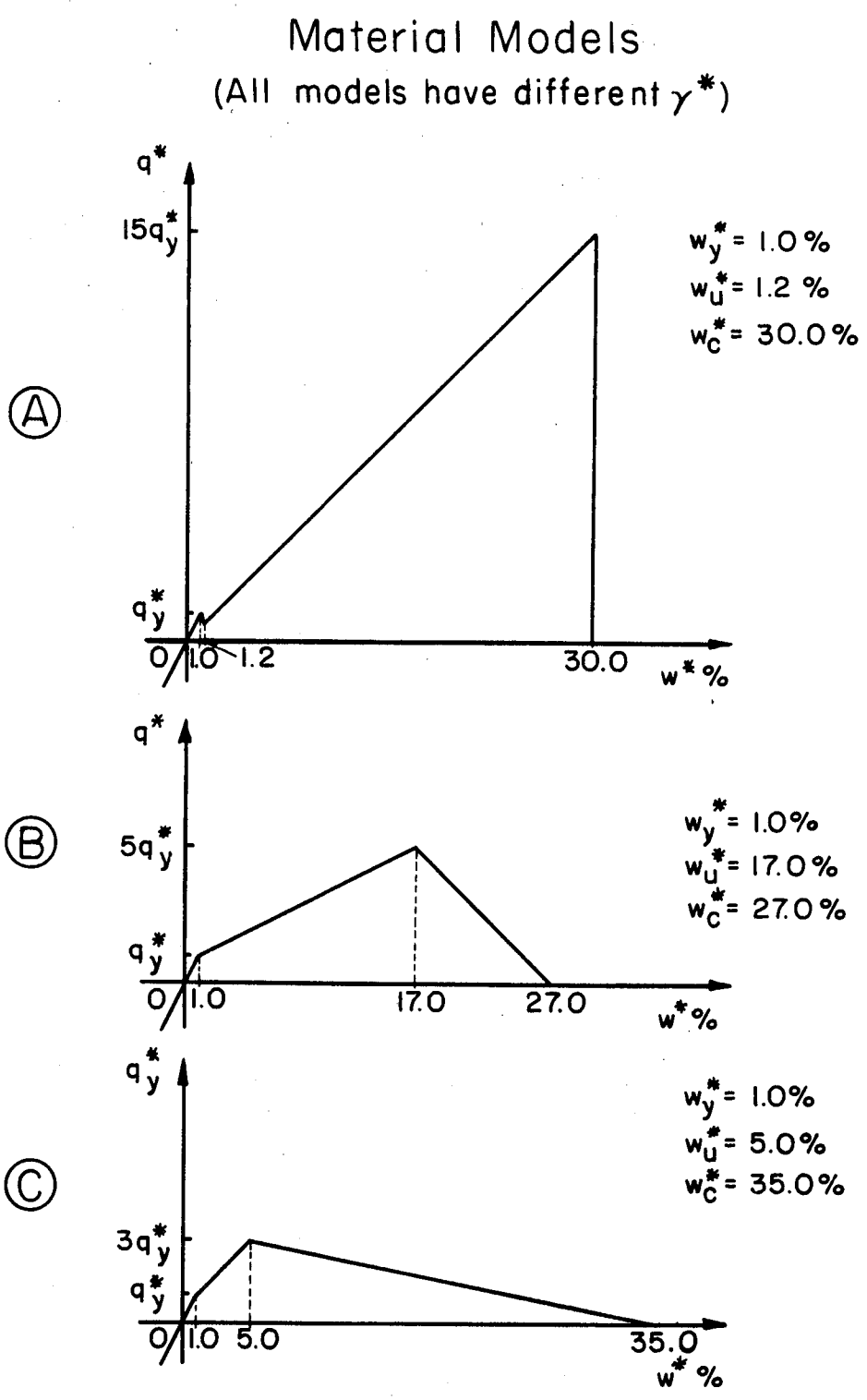

Figure 9. Material models (A, B and C).

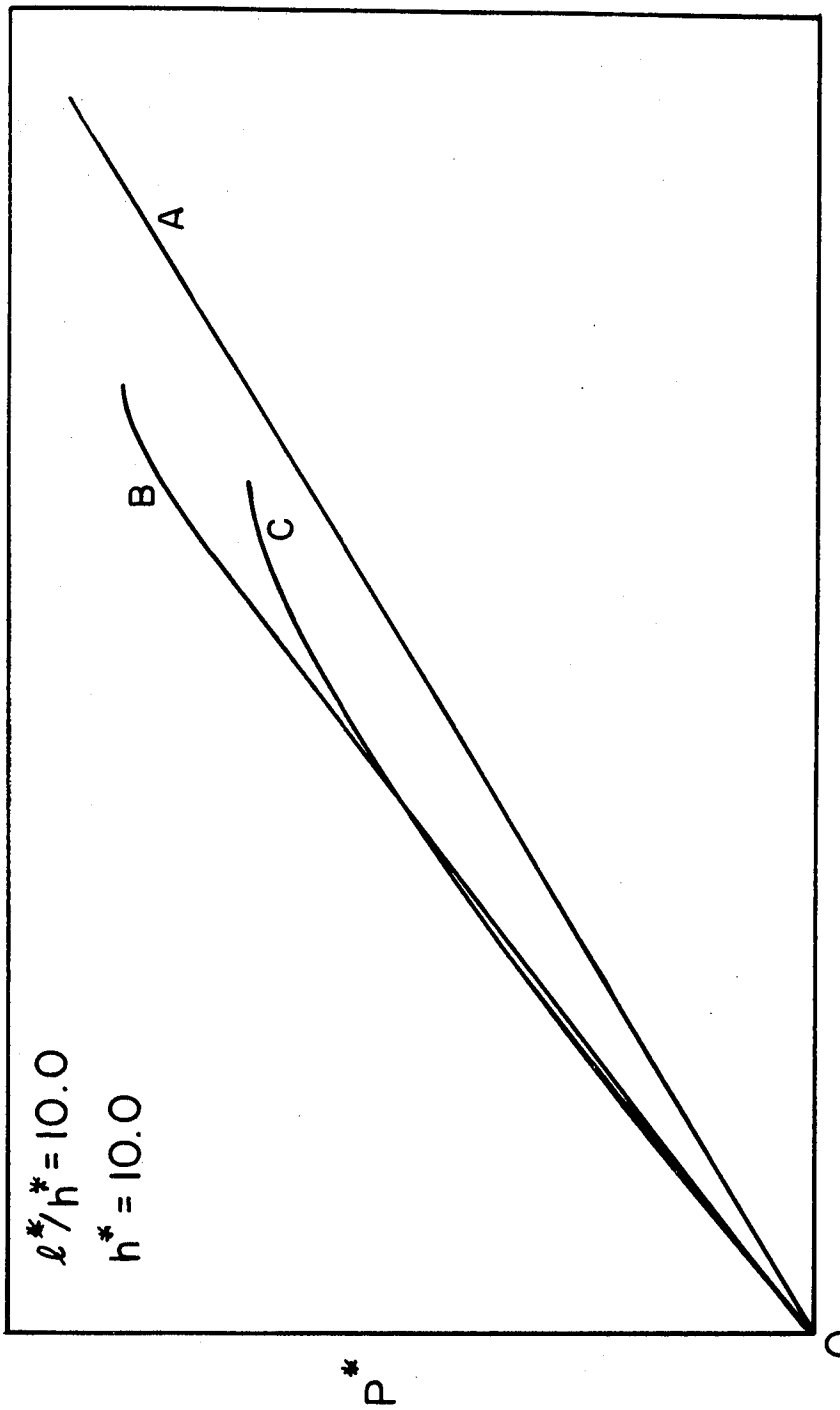

Figure 10. End load versus end displacement for the stationary crack (material models A, B and C as indicated). The scales are somewhat different for each curve, see text.

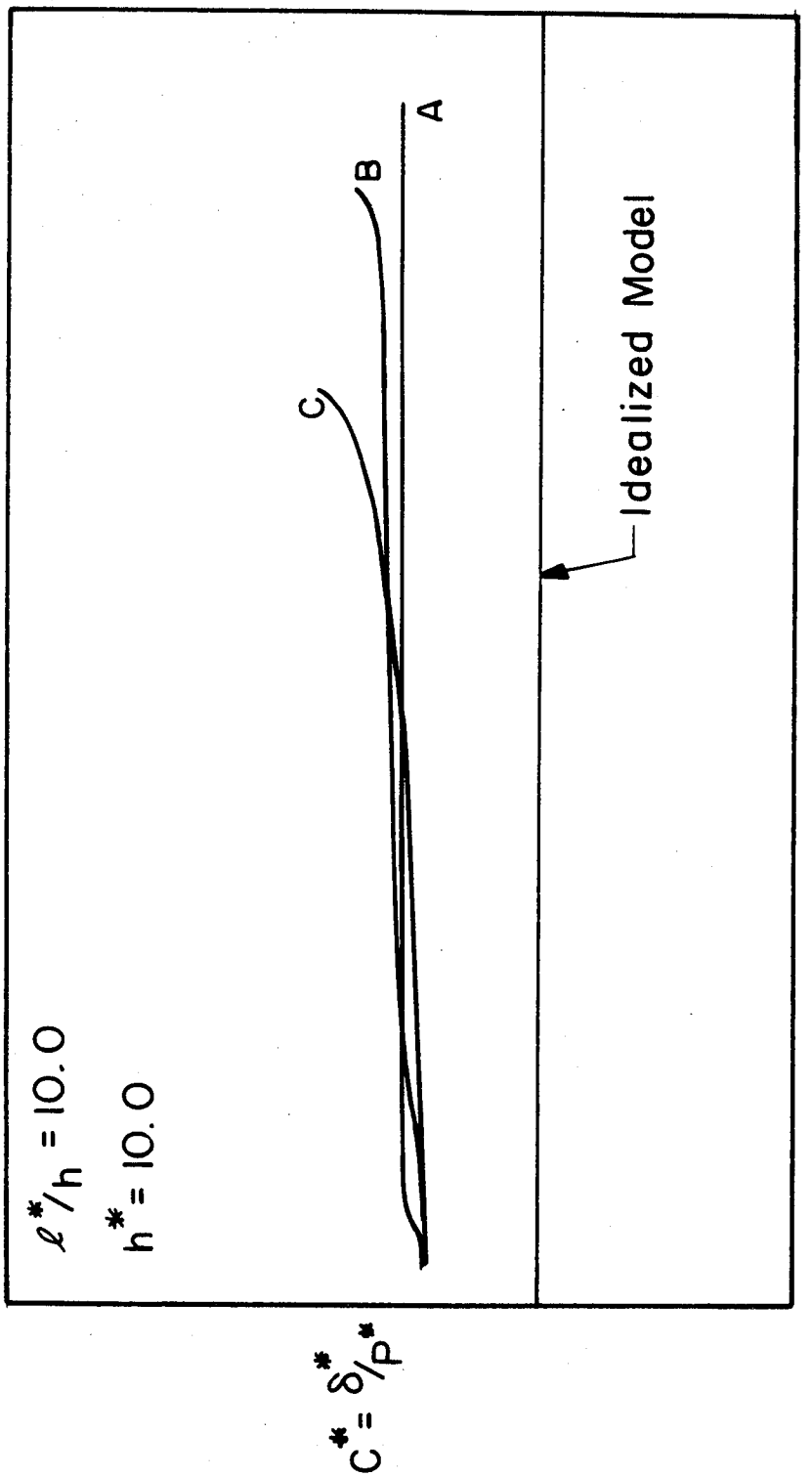

Figure 11. Compliance as a function of the end load for the stationary crack (material models A, B and C as indicated). The scales are somewhat different for each curve, see text.

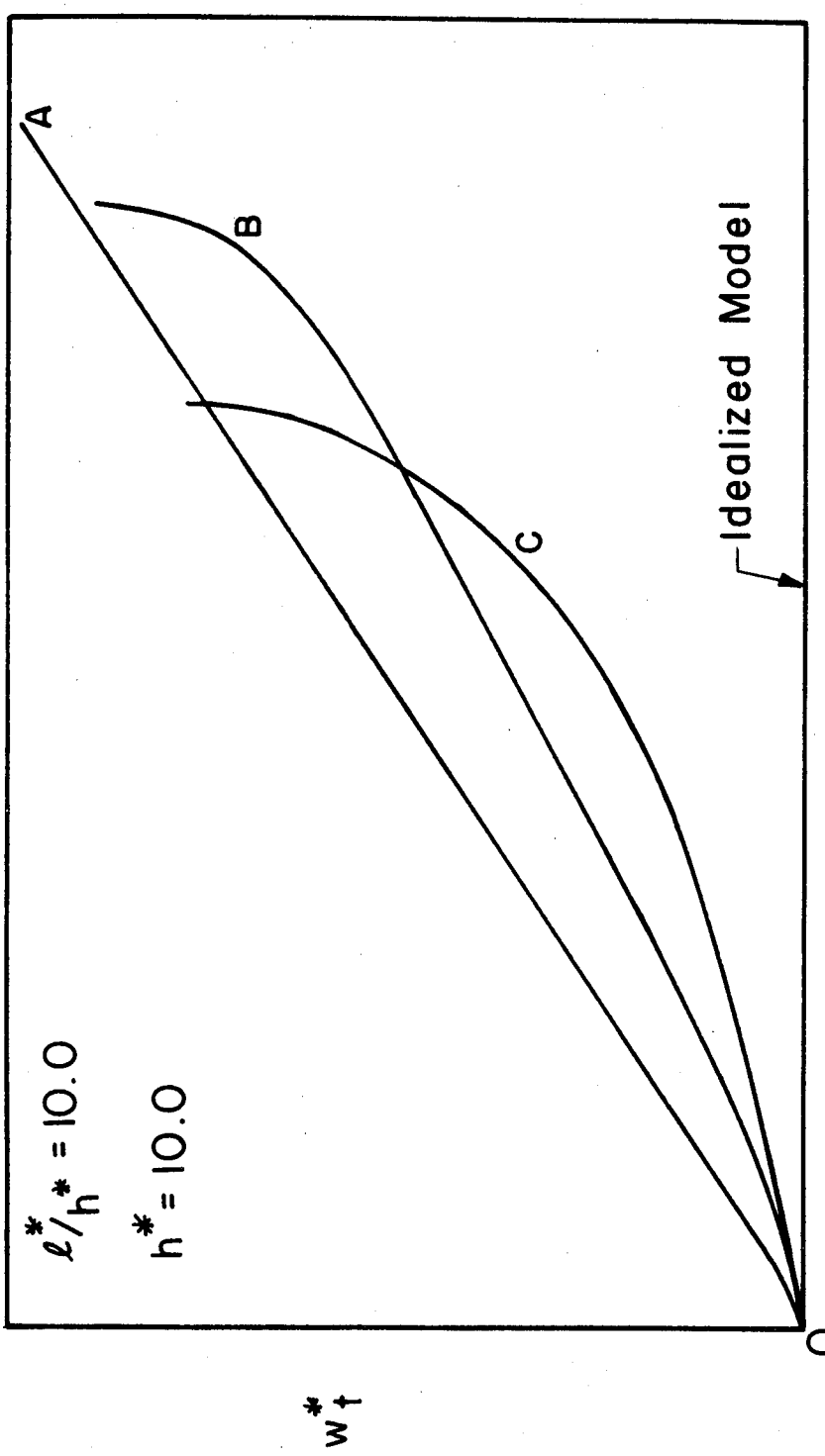

Figure 12. Crack tip displacement as a function of the end load for the stationary crack (material models A, B and C as indicated). The scales are somewhat different for each curve, see text.

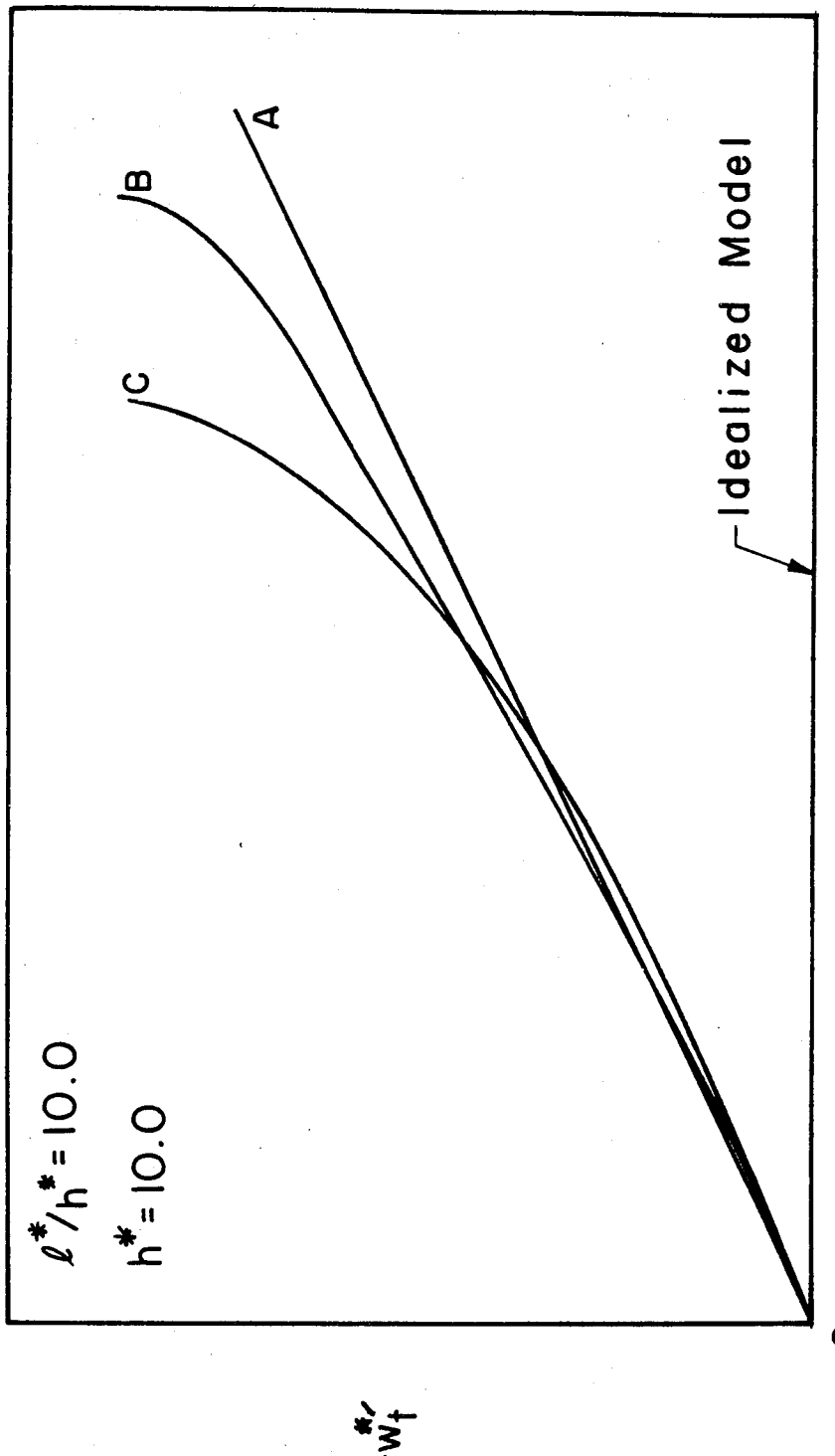

Figure 13. Slope at the crack tip as a function of the end load for the stationary crack (material models A, B and C as indicated). The scales are somewhat different for each curve, see text.

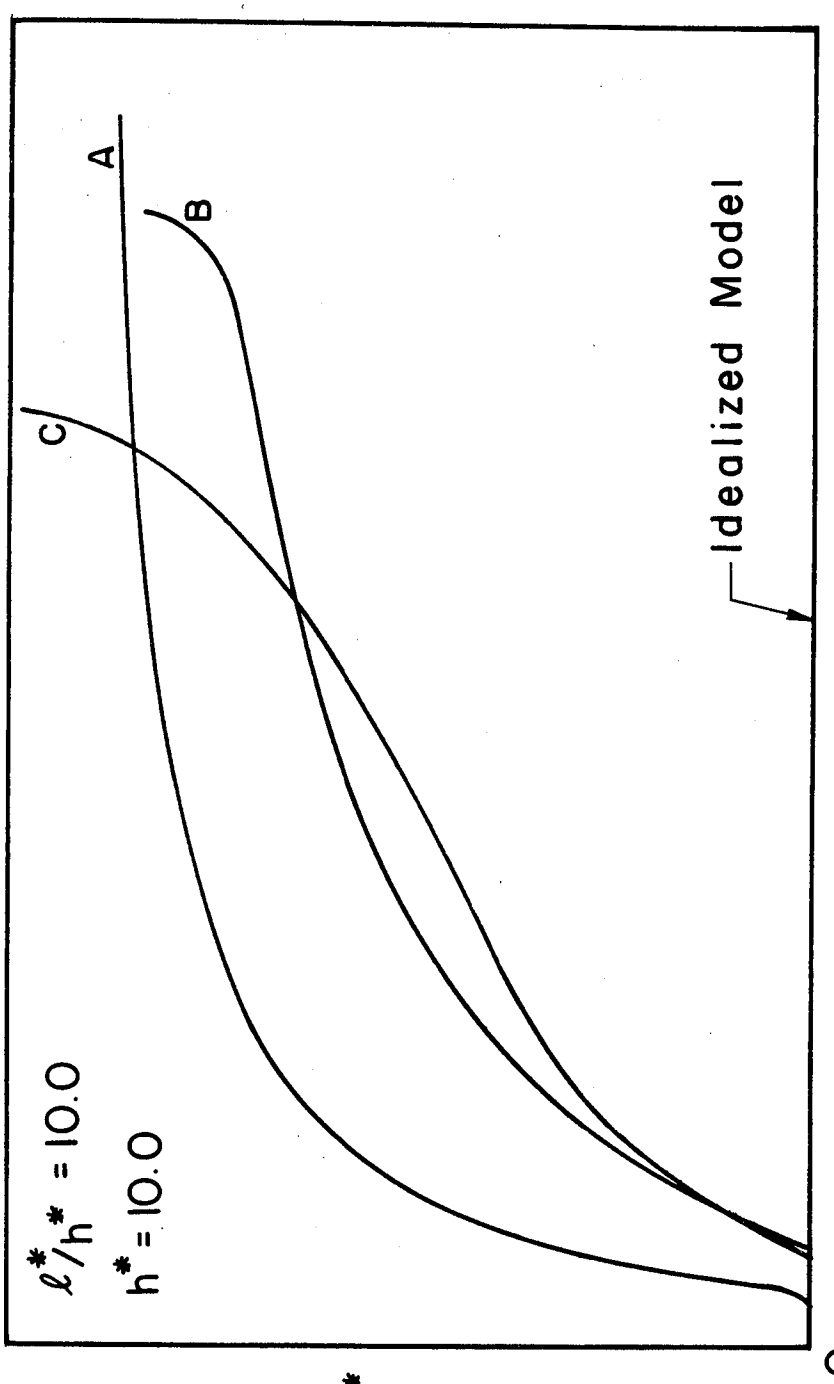

Figure 14. Yield zone size as a function of the end load for the stationary crack (material models A, B and C as indicated). The scales are somewhat different for each curve, see text.

and

$$E_b = \int_0^l \frac{M^2(x)}{2EI}dx = \frac{P^2}{2EI}\int_0^l x^2dx = \frac{P^2l^3}{6EI} \tag{2.7}$$

Griffith Condition: The energy release rate, G, is obtained from the potential energy π of the system (both beams of the DCB specimen considered and hence the factor two) as follows

$$G = -\frac{\partial\pi}{\partial l} = -\frac{\partial}{\partial l}2[E_b - P\delta] = -\frac{\partial}{\partial l}(-2\cdot\frac{P^2l^3}{6EI}) = 2\gamma b$$

Thus one has

$$G = \frac{P^2l^2}{EI} = 2\gamma b$$

Hence the moment at the crack tip required for crack growth M_c is

$$M_c = Pl = \sqrt{2EI\gamma b} \tag{2.8}$$

with the dimensionless form

$$M_c^* = \sqrt{2\gamma^* b^*} \tag{2.8a}$$

Upon writing (2.6) as

$$\delta = \frac{(Pl)^3}{3EIP^2}$$

and using (2.8) one has

$$\delta = \frac{M_c^3}{3EIP^2} = \frac{(2\gamma b)^{3/2}\sqrt{EI}}{3P^2}$$

from which follows that

$$3P^2\delta = (2\gamma b)^{3/2} \sqrt{EI} \tag{2.9}$$

Rewriting (2.9), one obtains

$$2\gamma = \frac{1}{b}\left\{\frac{(3P^2\delta)^2}{EI}\right\}^{1/3} \tag{2.10}$$

or, in dimensionless form

$$2\gamma^* = \frac{1}{b^*}(3P^{*2}\delta^*)^{2/3} \tag{2.10a}$$

In order to study how a certain quantity changes as the crack propagates quasi-statically, we denote the derivative with respect to crack length l by $\frac{d(\ )}{dl}|_{qs}$. Note that P is not constant as l increases but decreases such that quasi-static crack growth is maintained. Adopting this convention and using (2.7) and (2.8), there follows (here only half of DCB specimen is considered)

$$E_b = \frac{M_c^2 l}{6EI} = (\frac{\gamma b}{3})l$$

whence

$$\frac{dE_b}{dl}\Big|_{qs} = \frac{\gamma b}{3} \tag{2.11}$$

For this ideal case let us call W_c the work done against interface forces[8] which is related to the fracture energy γ by

---

8. When we deal with the cohesive interlayer, W_c denotes the energy dissipated in the interlayer.

$$W_c = (\gamma b)l$$

therefore

$$\frac{dW_c}{dl}\Big|_{qs} = \gamma b \tag{2.12}$$

Let W be the total work done by P, i.e., $W = \int_0^\delta P d\delta$, or $dW = Pd\delta$. Then in view of (2.6)

$$\delta = \frac{M_c l^2}{3EI}$$

hence

$$\frac{d\delta}{dl}\Big|_{qs} = \frac{2M_c l}{3EI}$$

consequently,

$$\frac{dW}{dl}\Big|_{qs} = P\frac{d\delta}{dl}\Big|_{qs} = \frac{2M_c Pl}{3EI} = \frac{2M_c^2}{3EI}.$$

In view of (2.8),

$$\frac{dW}{dl}\Big|_{qs} = \frac{4}{3}\gamma b \tag{2.13}$$

Combining now (2.11), (2.12), and (2.13) yields

$$\frac{dE_b}{dl}\Big|_{qs} = \frac{1}{4}\frac{dW}{dl}\Big|_{qs}$$

$$\frac{dW_c}{dl}\Big|_{qs} = \frac{3}{4}\frac{dW}{dl}\Big|_{qs} \tag{2.14}$$

Thus we find that for the idealized (built-in) case, 25% of the total work done is stored in the beam as bending energy while 75% is dissipated as fracture energy at the interface. Note in passing that in this idealized case the stress intensity factor is

$$K_I = (2\sqrt{3}h^{-3/2})Pl = (2\sqrt{3}h^{-3/2})M_c \tag{2.15}$$

But by (2.8), $M_c = f(\gamma, EI)$, therefore K_I is a constant as is G (the energy release rate).

Having considered this ideal case we move now to consider the situation where the nonlinear foundation allows both the displacement and the slope at the crack tip to be different from zero. The numerical results[9] in Figure 15 show that the P-δ relation depends only on γ and EI as suggested by equation (2.9) derived for the idealized case. Figure 16 indicates that M_c^* depends weakly on w_c^* and on the existence of a strain softening tail. The slope at the crack tip, $-w_c^{*\prime}$, is plotted in Figure 17 as a function of l^*/h^*. It is seen that $-w_c^{*\prime}$ depends strongly on w_c^*. The yield zone size α^* is shown to decrease and become constant as l^*/h^* increases in Figure 18. Also, α^* increases monotonically with w_c^*. In Figure 19, $P^*\delta^{*1/2}$ is shown to approach a constant value as l^*/h^* increases. In view of equation (2.9) and the behavior of $P^*\delta^{*1/2}$ exhibited in Figure 19, it seems possible that the fracture energy γ may be approximated by equations of the same form as (2.10) and (2.10a). With this in mind, let

$$2\tilde{\gamma} \equiv \frac{1}{5}\left\{\frac{(3P^2\delta)^2}{EI}\right\}^{1/3} \tag{2.16}$$

---

9. Here material #2 was not investigated, as we did not expect the use of its characteristic to contribute any more insight into the problem.

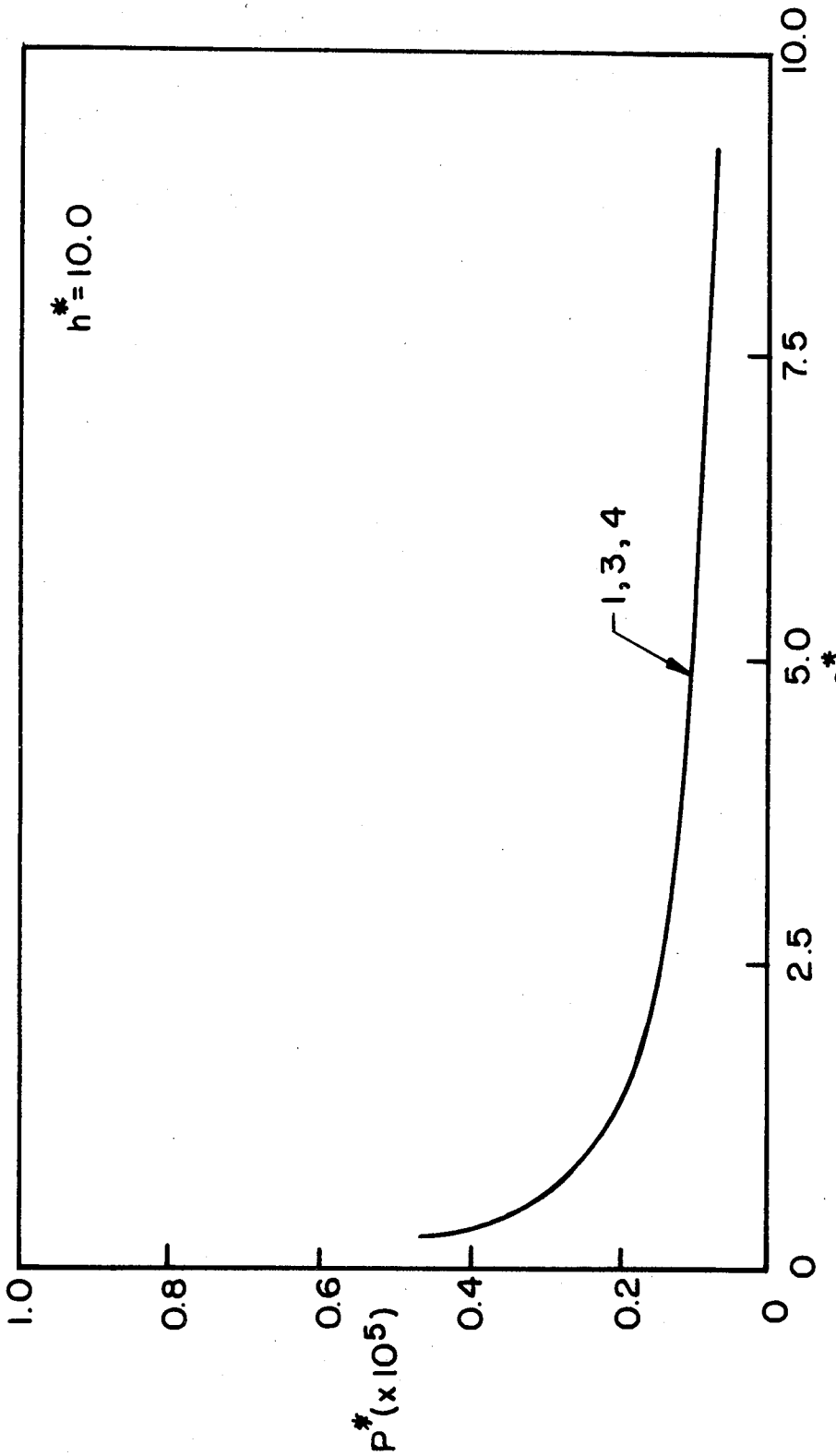

Figure 15. End load versus end displacement for the propagating crack (material models 1, 3 and 4 as indicated).

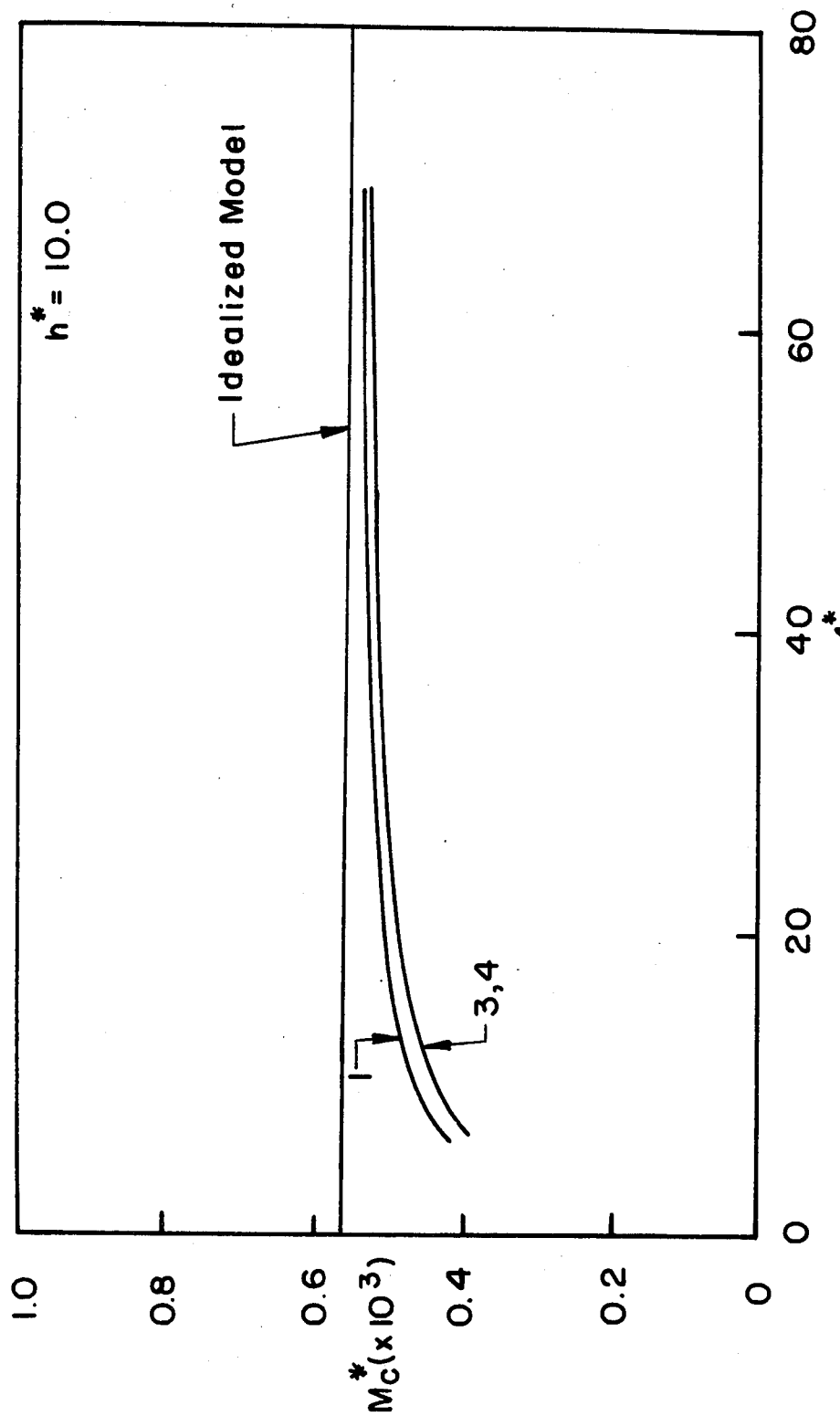

Figure 16. Moment at the crack tip as a function of crack length for the propagating crack (material models 1, 3 and 4 as indicated).

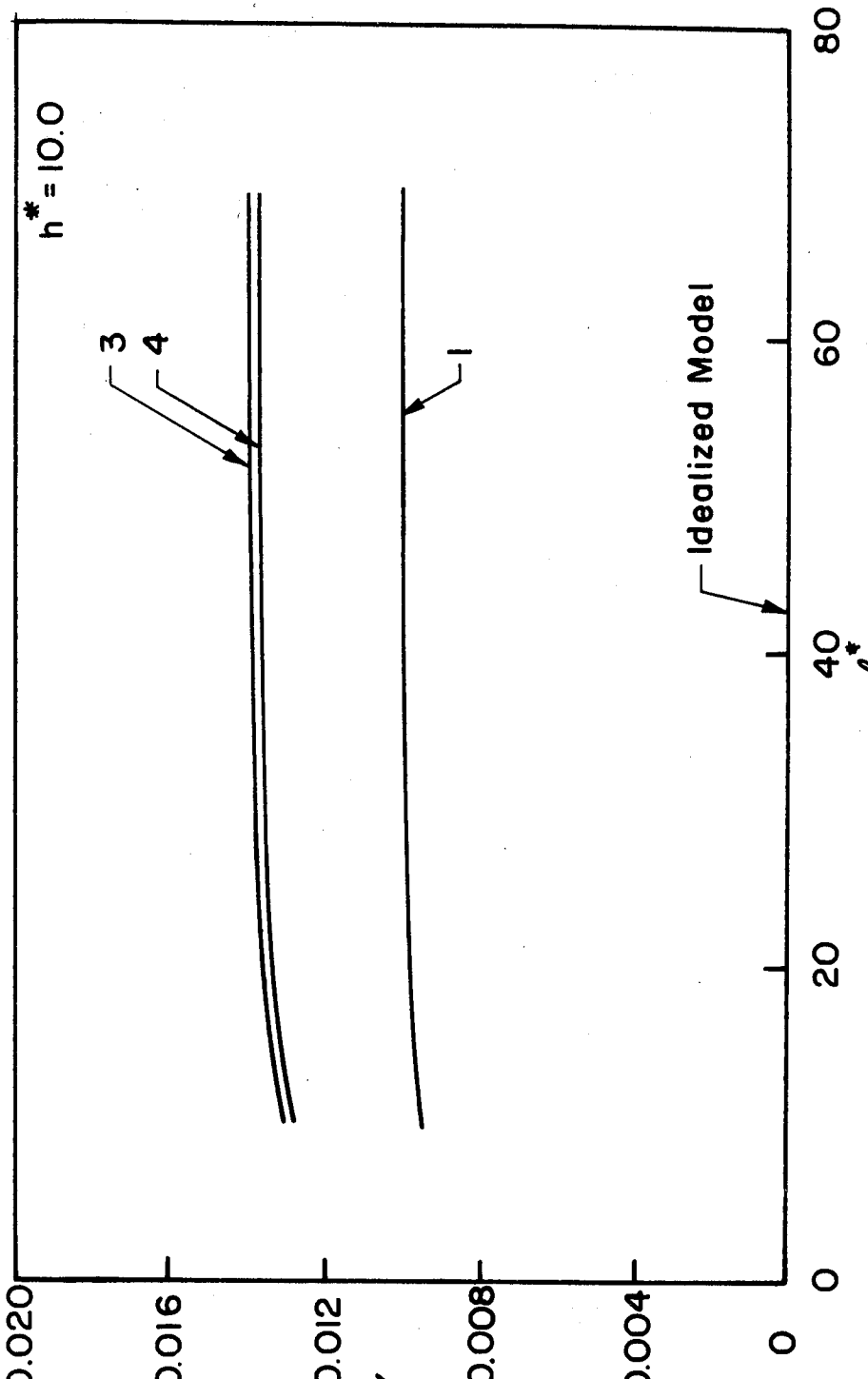

Figure 17. Slope at the crack tip as a function of crack length for the propagating crack (material models 1, 3 and 4 as indicated).

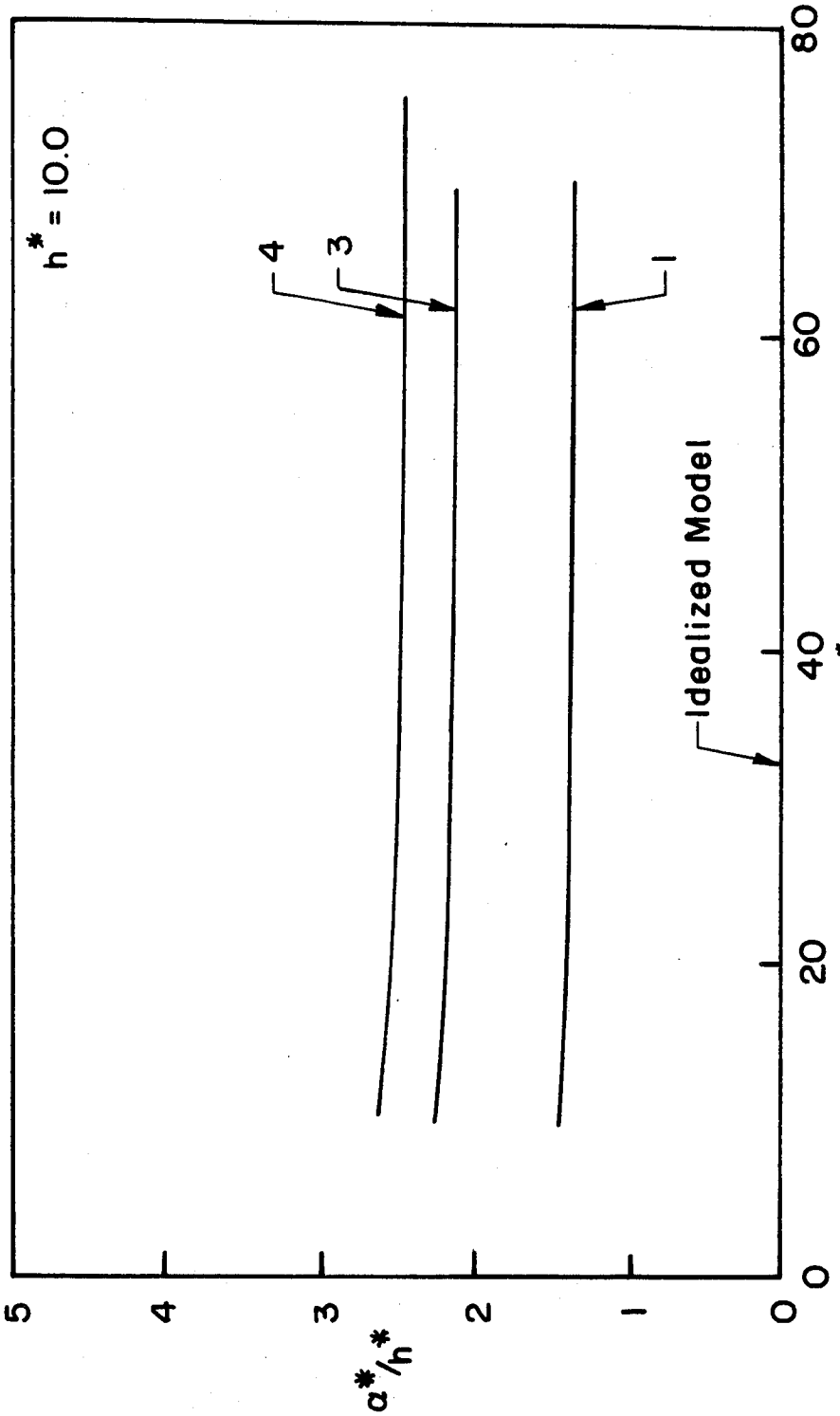

Figure 18. Yield zone size as a function of crack length for the propagating crack (material models 1, 3 and 4 as indicated).

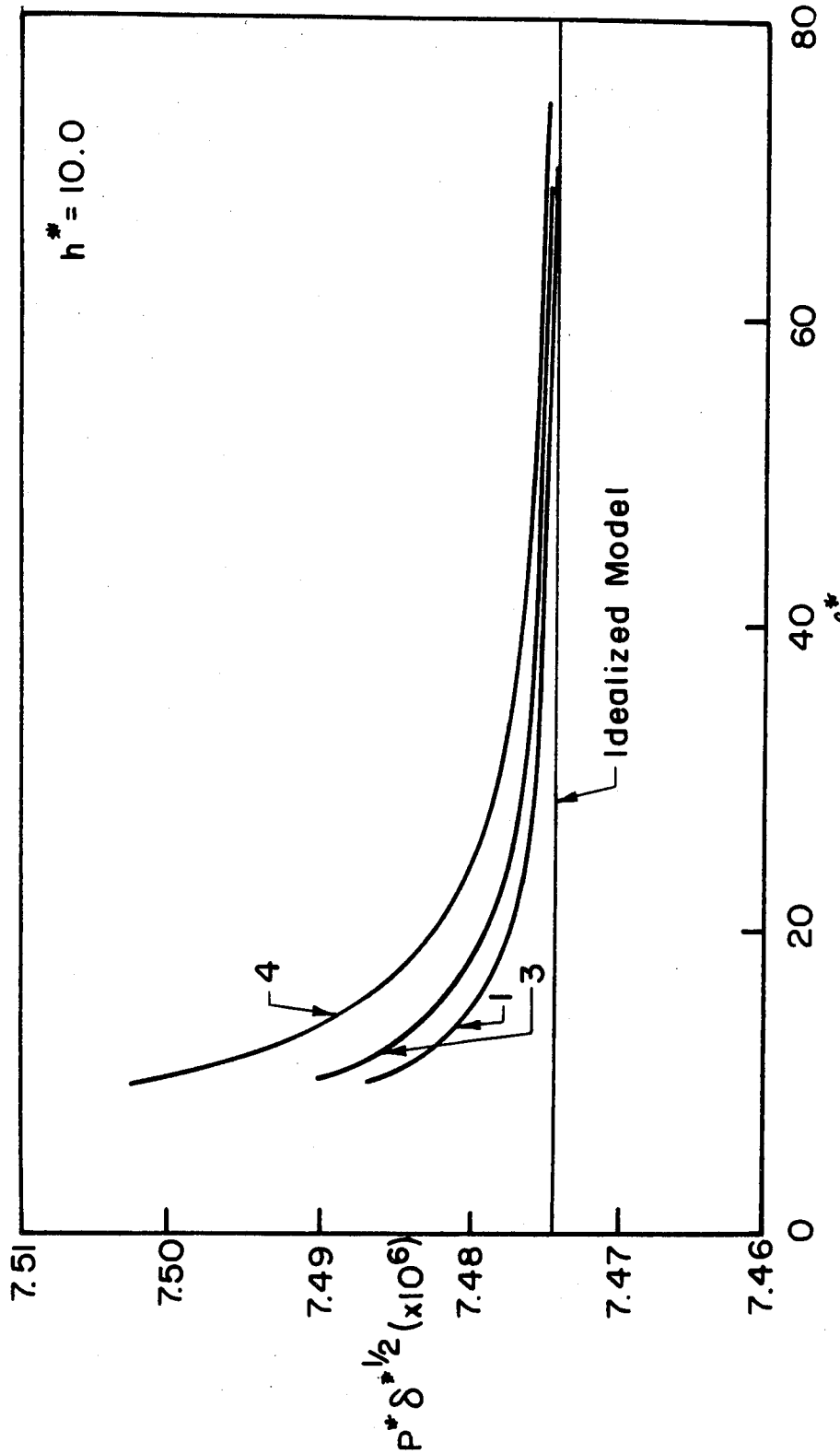

Figure 19. $P^{*}\delta^{*^{\frac{1}{2}}}$ as a function of crack length for the propagating crack (material models 1, 3 and 4 as indicated).

$$2\tilde{\gamma}^* \equiv \frac{1}{b^*}\,(3P^{*2}\delta^*)^{2/3} \tag{2.16a}$$

In Figure 20, we show the ratio of $\tilde{\gamma}^*$, the fracture surface energy as computed using equation (2.16a), to the exact value γ^* as calculated from the area under the q-w curve of the input data. Note that the vertical ordinates in Figures 19 and 20 encompass very narrow ranges of values.[10]

In these non-ideal cases, it is found that equations (2.9)-(2.14) remain valid with small errors which decrease rapidly with increasing crack length. The reason for this behavior is that the crack propagation has reached a steady state (or asymptotic condition) in the sense that neither α nor $-w_c'$ is changing much. To see this consider the following argument:

For the idealized case, equation (2.10) can be written in functional form as

$$F(P,\ \delta,\ \gamma,\ EI) = 0 \tag{2.17}$$

Note that the crack length l does not appear explicitly as it is already fixed by specifying both P and δ. In the event that the support rotates (the nonlinear foundation case), the only additional physical parameter[11] that could be involved in (2.17) is w_c', however $\frac{dw_c'}{dl}\big|_{qs} \ll 1$ for $l/h \geq 5$ (see Figure 17). In other words, the slope at the crack tip hardly changes as the crack propagates. Therefore (2.17)

10. The accuracy of these results is demonstrated in Section 2.3.3.

11. Note that we may disregard w_c as an additional parameter since it is a constant for a given q(w) under consideration. It should also be pointed out that in all cases considered $|w_c'|$ is very small (≤ 0.014) i.e. less than 0.80^o in rotation at the crack tip, but the contribution of this small slope to the end displacement δ is not at all negligible, for instance, by equation (2.5) for $l/h = 10$, $h/d = 10$; $|w_c'|l = 0.3\delta$.

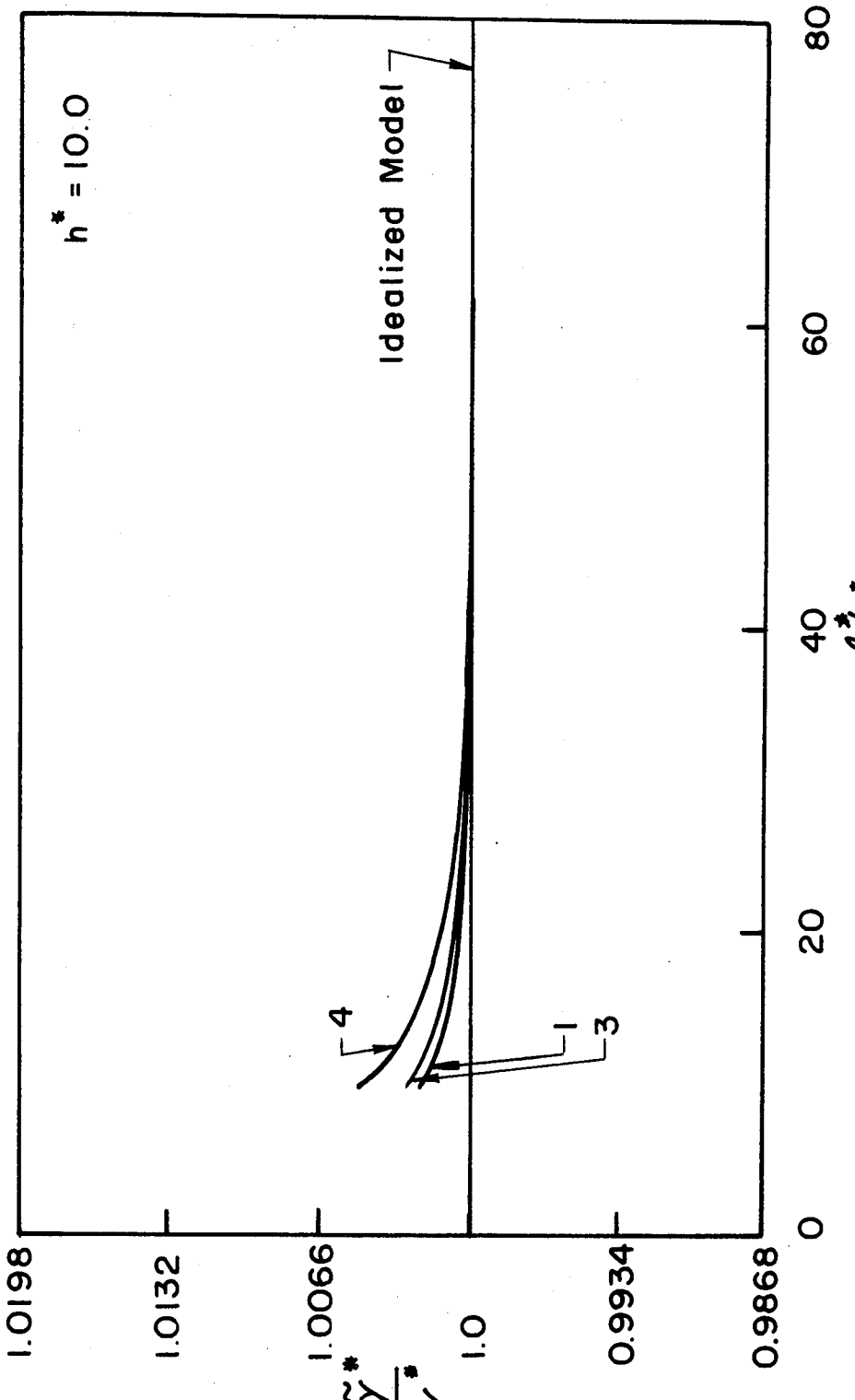

Figure 20. $\tilde{\gamma}^*/\gamma^*$ as a function of crack length for the propagating crack (Material models 1, 3 and 4 as indicated)

still holds (approximately) for $l/h \geq 5$.

One could also think of the built-in case as a special case where $q(w) = \gamma\delta(w)$ = a delta function of magnitude γ and $w_c' = \alpha = 0$. Thus for general $q(w)$, we only need to reach steady state (asymptotic conditions for long crack) where w_c' and α are approximately constant for equation (2.17) to hold.

2.3.3. The Long Crack Limit (Asymptotic Conditions)

The rate with which one approaches the asymptotic conditions is exemplified in Table I below. Material 1 with characteristics shown in Figure 3 is used. Let the subscript i denote the number of cases in the table. We take case 5 ($l/h = 60.0$, see Table I) as approximating the asymptotic conditions when l/h tends to infinity; this is reasonable since $\frac{(M_c)_5}{(M_c)_\infty} = 0.97$ and $\frac{\tilde{\gamma}_5}{\gamma} = 1.00007$ where $(M_c)_\infty = (M_c)_{\text{idealized}} = \sqrt{2EI\gamma b}$ and $\tilde{\gamma}$ is computed using equation (2.16). Also, for convenience, let $R_i \equiv (P\delta^{1/2})_i$.

Table I

i	l/h	$\frac{\alpha_i}{\alpha_5}$	$\frac{(w_c')_i}{(w_c')_5}$	$\frac{(M_c)_i}{(M_c)_5}$	$\frac{R_i}{R_5}$	$\frac{\tilde{\gamma}_i}{\tilde{\gamma}_5}$
1	2.0	1.21	0.80	0.53	1.02	1.03
2	5.0	1.11	0.90	0.75	1.006	1.008
3	10.0	1.05	0.95	0.87	1.002	1.003
4	20.0	1.02	0.98	0.94	1.0004	1.0005
5	60.0	1.0	1.0	1.0	1.0	1.0

Clearly, α and w_c' approach their asymptotic values at about the same rate which is about two to three times faster than that for M_c whereas $\tilde{\gamma}$ as computed by using equation (16) reaches its correct value with less than 1% error far sooner than α, w_c', and M_c. Therefore γ can

be determined with high accuracy and great convenience from equation (2.16) even for the case where $l/h = 2$.

3. FINITE ELEMENT MODEL

The finite element program ABAQUS (version 4) running on a VAX-11/780 was used to model the beam and the nonlinear foundation. We use 4-noded bilinear plane elements to model the beam, and nonlinear springs restraining vertical motion of the beam to model the foundation. The 4-noded element is chosen for convenience in discretizing the foundation and in interpolating to locate the crack tip. The force-displacement relations of the nonlinear springs are patterned precisely after the material models shown in Figure 3.

The discretization of the foundation is accomplished by attaching two identical nonlinear springs with total restraining forces equal to that of a continuous foundation to the bottom two nodes of each element of the beam at the interface. (For 8-noded biquadratic elements, this simple scheme would not work.)

The three meshes used for the beam are shown in Figure 21. Mesh #1 has 402 elements, 67 springs, 476 nodes, and a total of 952 degrees of freedom with the smallest element size of $0.1h \times 0.05h$. Mesh #2 has 540 elements, 90 springs, 637 nodes, and 1274 degrees of freedom with the same smallest element size as Mesh #1. Mesh #3 has 480 elements, 120 springs, 605 nodes and 1210 degrees of freedom with smallest element size of $0.25h \times 0.1h$. (For Mesh #2, an iteration takes approximately 75 CPU seconds and each increment requires 2 or 3 iterations.)

Mesh #1 is designed to capture the displacement details around the crack tip for $l^*/h^* = 10.0$ while mesh #2 is intended to study a shorter specimen and shorter crack lengths, i.e., $l^*/h^* \leq 3.5$. Mesh #3 is a more uniform mesh than the previous two and gives better results for a larger range of l^*/h^* (from 0.0 to 10.5). It is of interest to note here that for identical end displacements ($\delta^*/h^* = 0.29$), mesh #3 renders $l^*/h^* = 9.65$ while Mesh #1 gives $l^*/h^* = 10.05$, an error of 4%. More on this in Section 4.

Beam on Nonlinear Cohesive Foundation

Finite Element Meshes

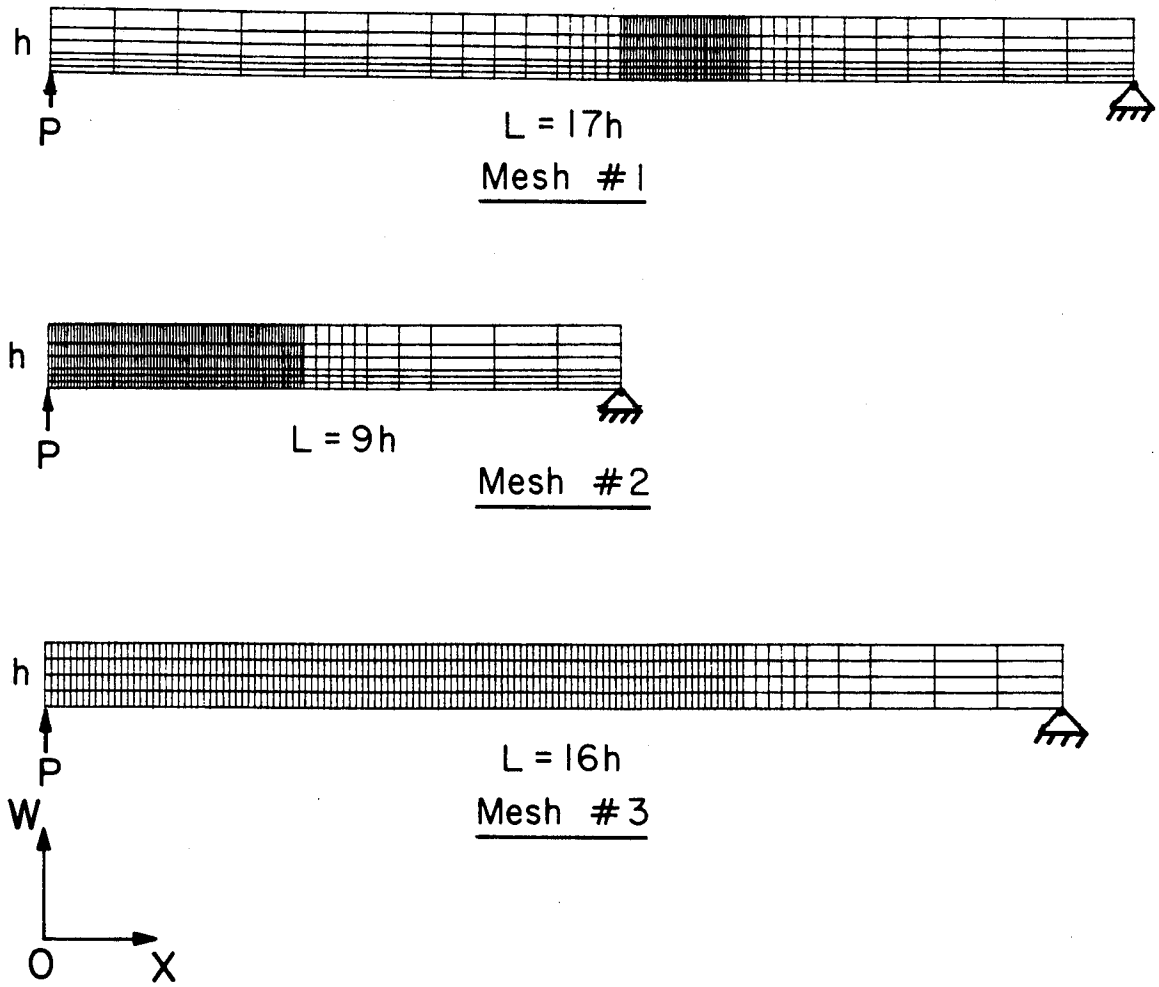

Figure 21. Finite element meshes.

The loading is done by prescribing the end displacement (δ) at the first node on the bottom line of the beam; the reaction force is then equal to P. The crack length is obtained by linear interpolation between a node where $w > w_c$ and an adjacent node where $w < w_c$. (This convenience would be lost if 8-noded biquadratic elements were used.) Convergence is considered attained when all forces at all nodes except those with prescribed displacements fall below 0.2% of the typical actual force values (in this case P). Since the beam is linearly elastic and the nonlinear springs simply supply the proper boundary conditions, the typical residuals for the convergent solutions are $= 10^{-14}$ P which were much smaller than the set tolerance.

Besides the results presented in Section 4, the contours for the stresses in the beam were also plotted. We omit them in this report as they do not contribute to any new insights.

4. COMPARISONS OF RESULTS OBTAINED FROM THE BEAM EQUATION AND FROM THE FINITE ELEMENT STUDY

In this section, the effects of including shear deformations accounted for in the finite element model but neglected in the beam equation model are examined. The finite element results show that, excepting the beam end where the point force is applied, the stress components σ_{12} and σ_{22} in the beam are always less than 10% of the maximum value of σ_{11}. The maximum equivalent (von Mises) stress in the beam only reaches a value $\approx 0.53\ \sigma_y$ where σ_y is the yield stress for Aluminum 2024 = $50. \times 10^3$ psi. For beams that are made of materials of low yield stress one must ensure that no yielding occurs for the present analysis to be applicable.

All comparisons shown here are for material model 3 only (see Figure 3). In Figure 22, the displacement contours of the top center and bottom of the beam are compared with the solution to the beam equation (the neutral axis or center line displacement) at the same crack length to determine if experimental measurments can be taken at the top of the DCB specimen instead of at the bottom (interlayer) where it would be more difficult to measure without incurring unacceptable errors. Figures 23 and 24 give the actual and the percent differences of the two results. It should be noted that the <u>percent</u> differences increase rapidly for $x^*/h^* > 11.0$ where w^* is very small and the mesh becomes coarse.

The $P^*-\delta^*$ relationships obtained from both methods are compared in Figure 25. The finite element results for Mesh #2 and #3 give also the $P^*-\delta^*$ points before crack propagation commences (the peak in the upper left hand corner). The best matching is obtained by using a uniform mesh (#3). Figure 26 shows comparison for P^* versus l^*, and Figure 27 δ^* versus l^*.

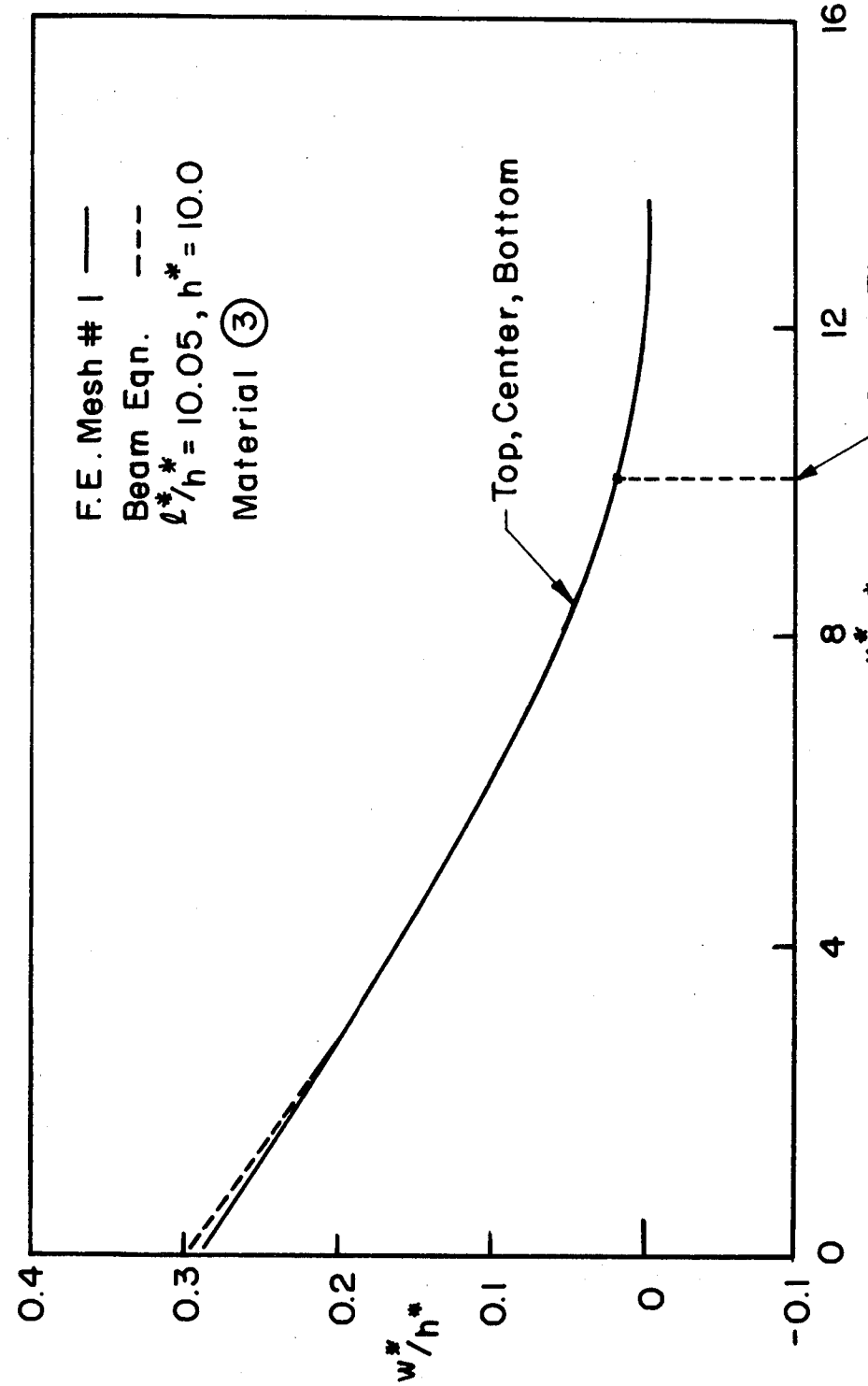

Figure 22. Comparison between Finite Element solution and Beam Equation: Vertical displacement as a function of x (for the same crack length).

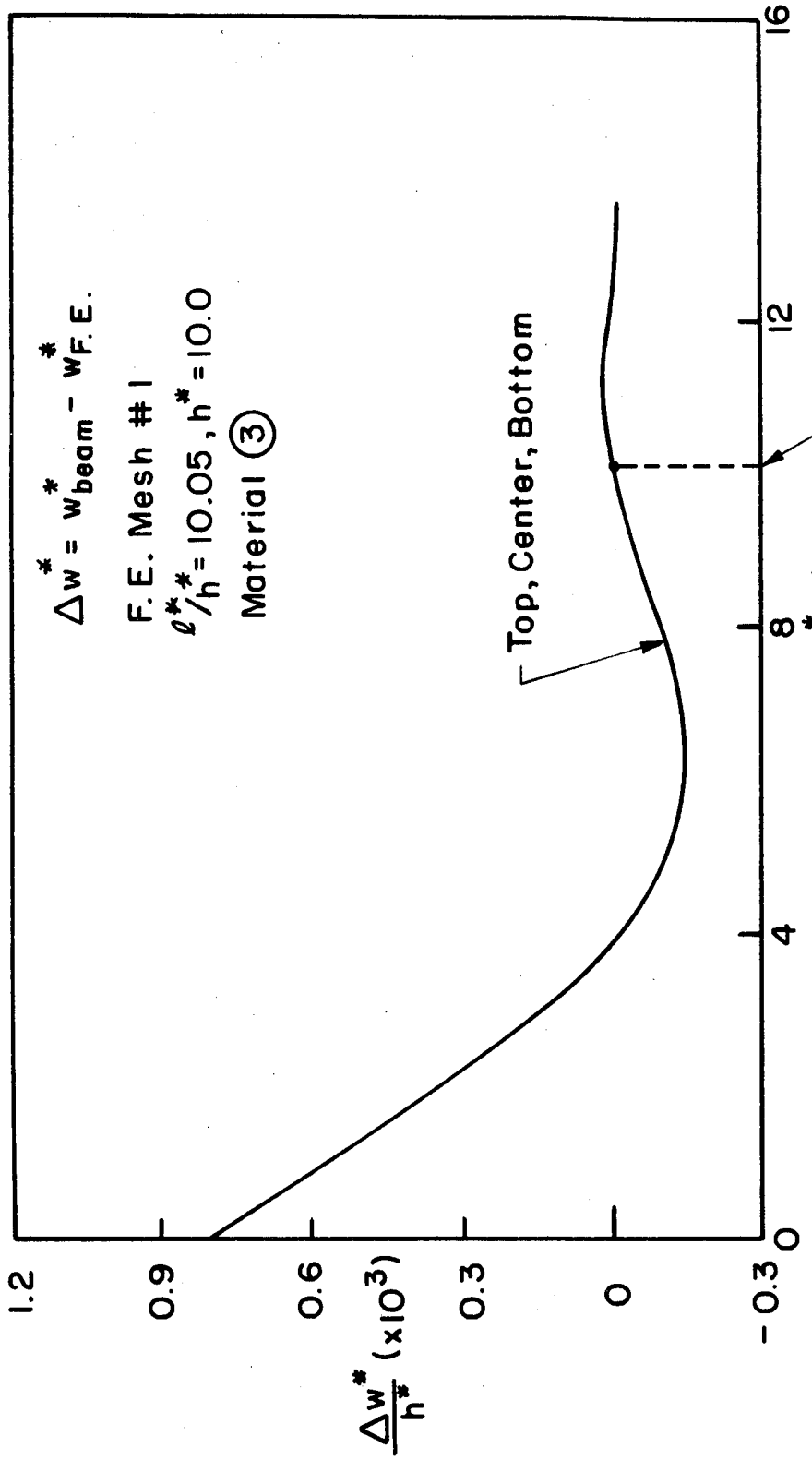

Figure 23. Comparison between Finite Element and Beam Equation: Difference in vertical displacement as a function of x (for the same crack length).

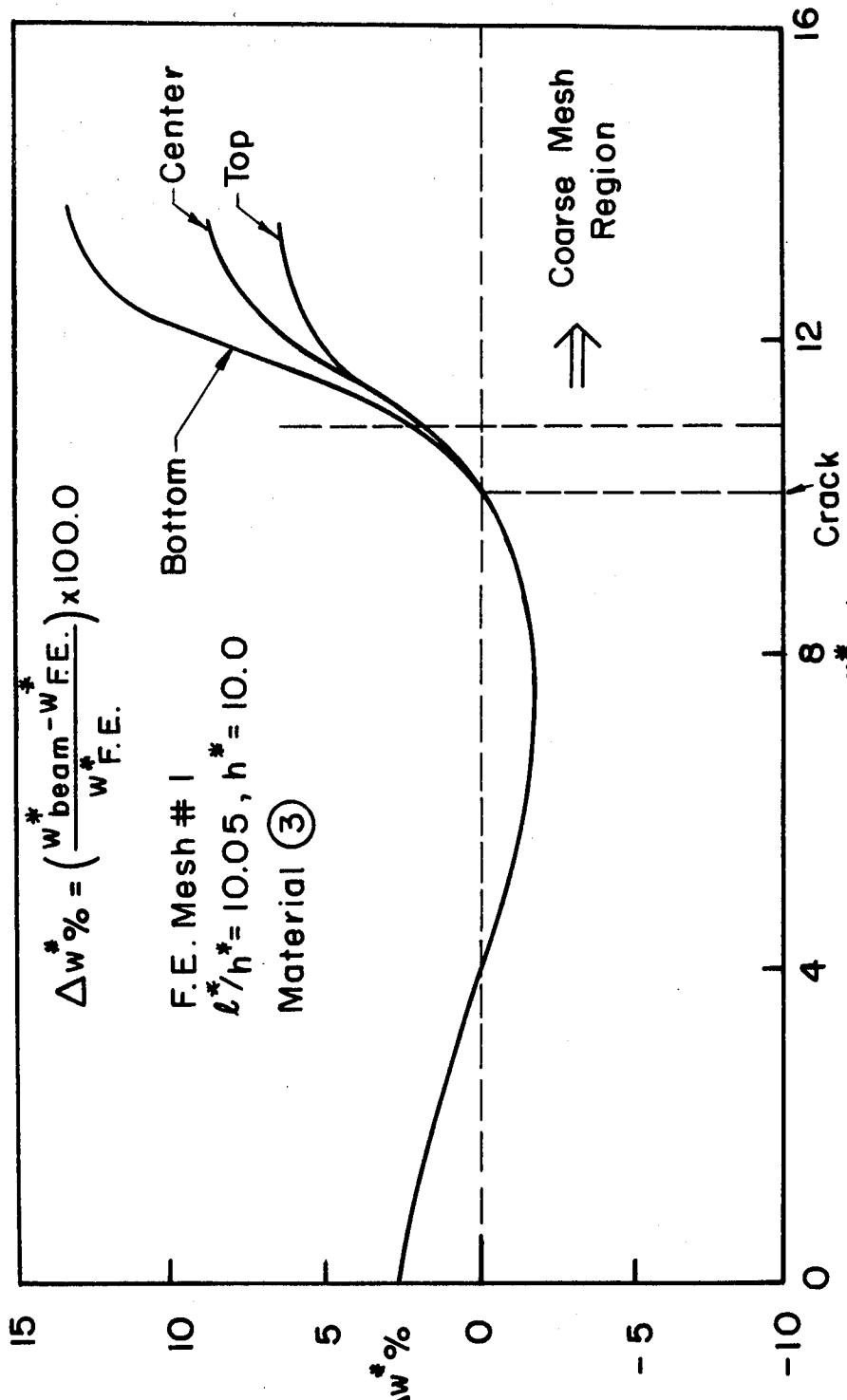

Figure 24. Comparison between Finite Element and Beam Equation: Percent difference in vertical displacement as a function of x (for the same crack length).

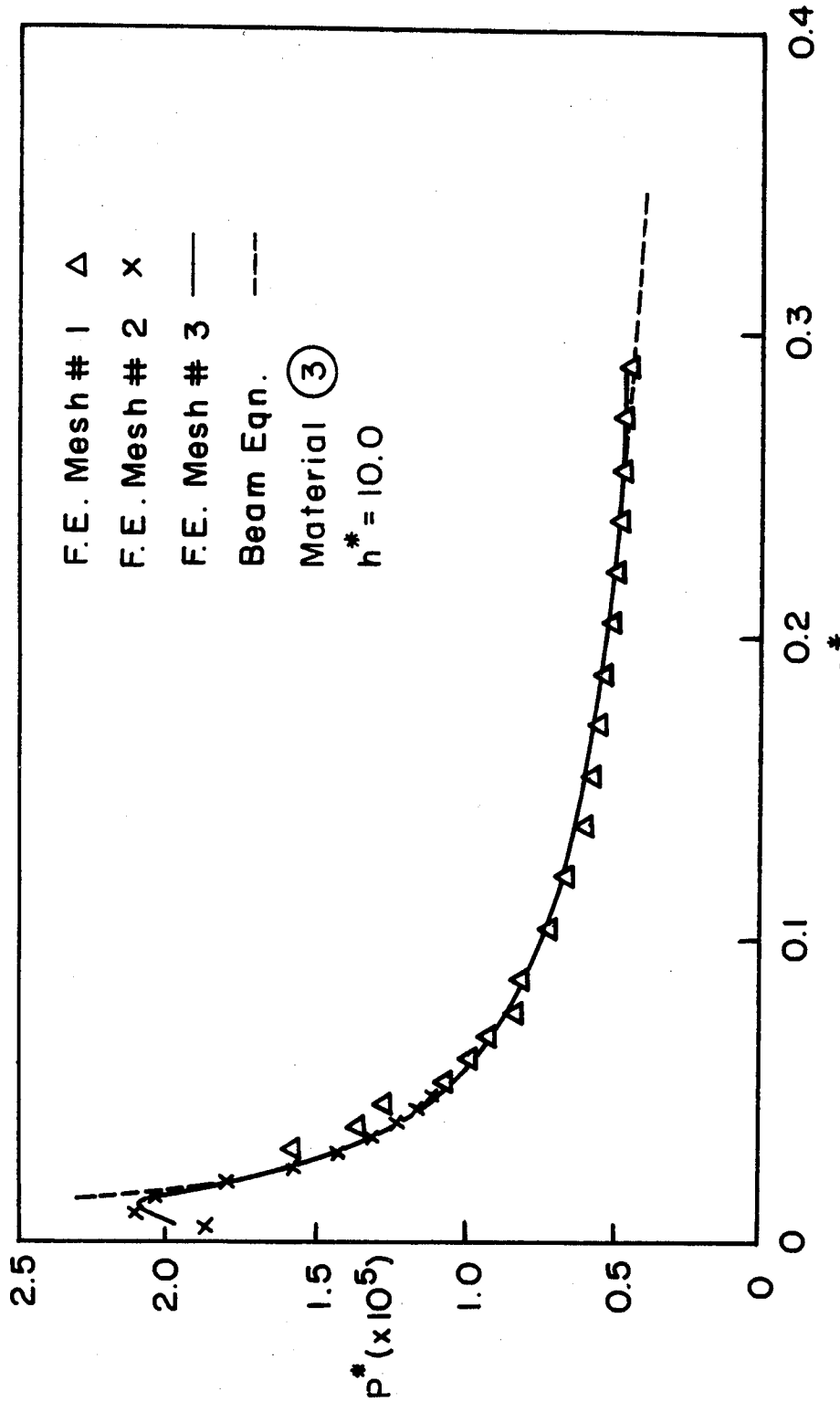

Figure 25. Comparison between Finite Element and Beam Equation: End load versus end displacement for 3 different Finite Element meshes. (The higher discrepancy at $\delta^*/h^* > 2.7$ is due to the coarse mesh region.)

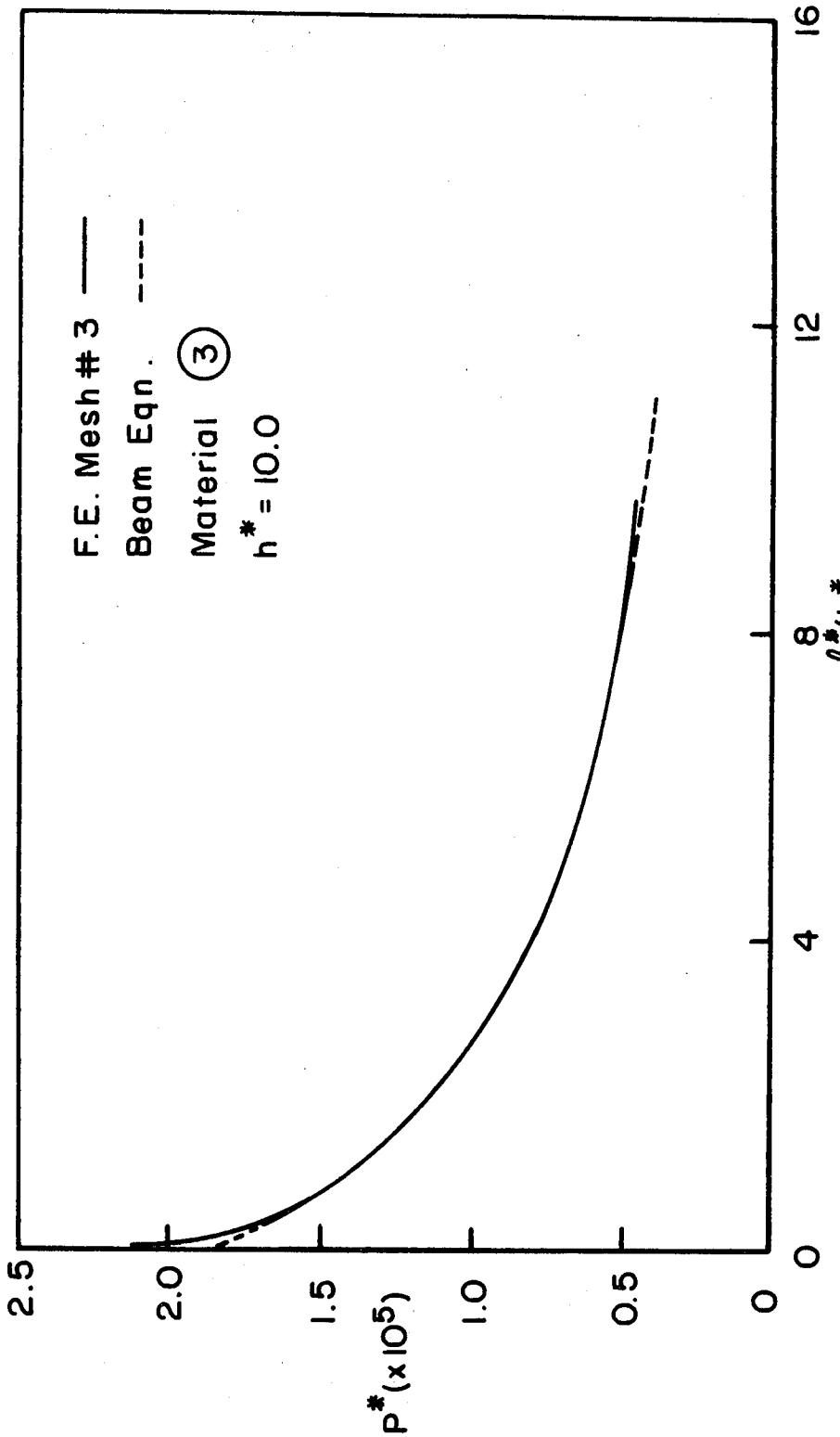

Figure 26. Comparison between Finite Element and Beam Equation: End load versus crack length for Finite Element Mesh #3. (The higher discrepancy at $l^*/h^* > 8.0$ is due to the coarse mesh region.)

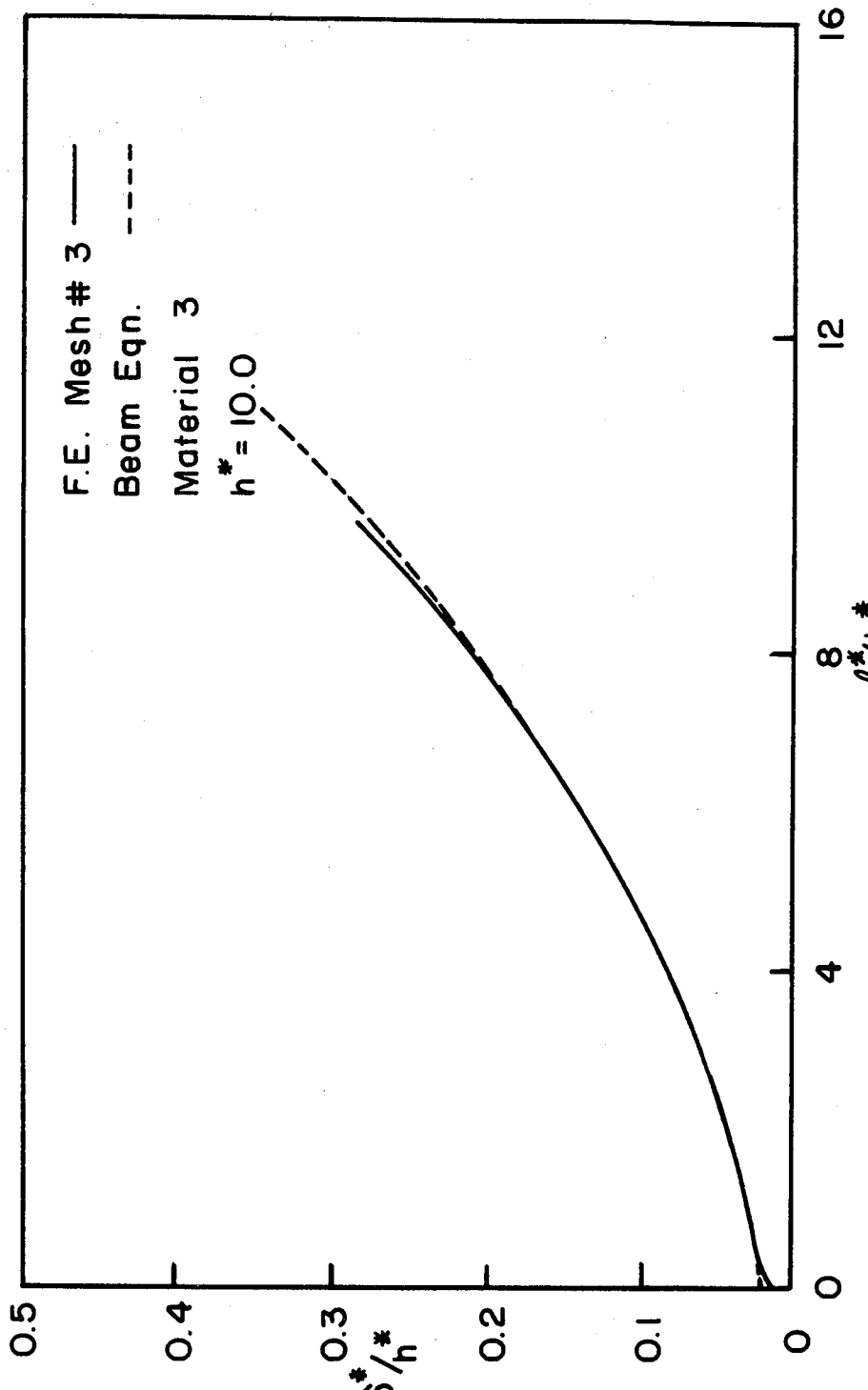

Figure 27. Comparison between Finite Element and Beam Equation: End displacement versus crack length for Finite Element Mesh #3. (The higher discrepancy at $\ell^*/h^* > 8.0$ is due to the coarse mesh region.)

The stress distributions in the cohesive foundation are compared in Figure 28 and again show good agreement. The stress distributions with the crack tip as the origin for different crack lengths are compared in Figure 29, and it is clear that with increasing crack length the size of the yield zone decreases.

Next, we compare the finite element and beam equation results to examine discrepancies in the calculated crack lengths and end loads for the same end displacements. It is found that the beam equation predicts crack lengths slightly larger than the finite element values by less than 2% for $2.5 < l^*/h^* < 8.5$. This is expected because shearing in a real beam (as modeled by finite element) allows more vertical deformation (sagging) than in the Bernoulli-Euler beam model where shearing is neglected. (See Figures 30 and 31).

In Figures 32 and 33, the errors in the predicted end loads required to obtain the same end displacement are plotted versus the actual end displacement and crack length (finite element results) respectively. Here the shear stress allowed in the finite element model makes the structure stiffer and thus higher end load P is required to displace the end to a given displacement δ than for a beam under pure bending without shear deformation.

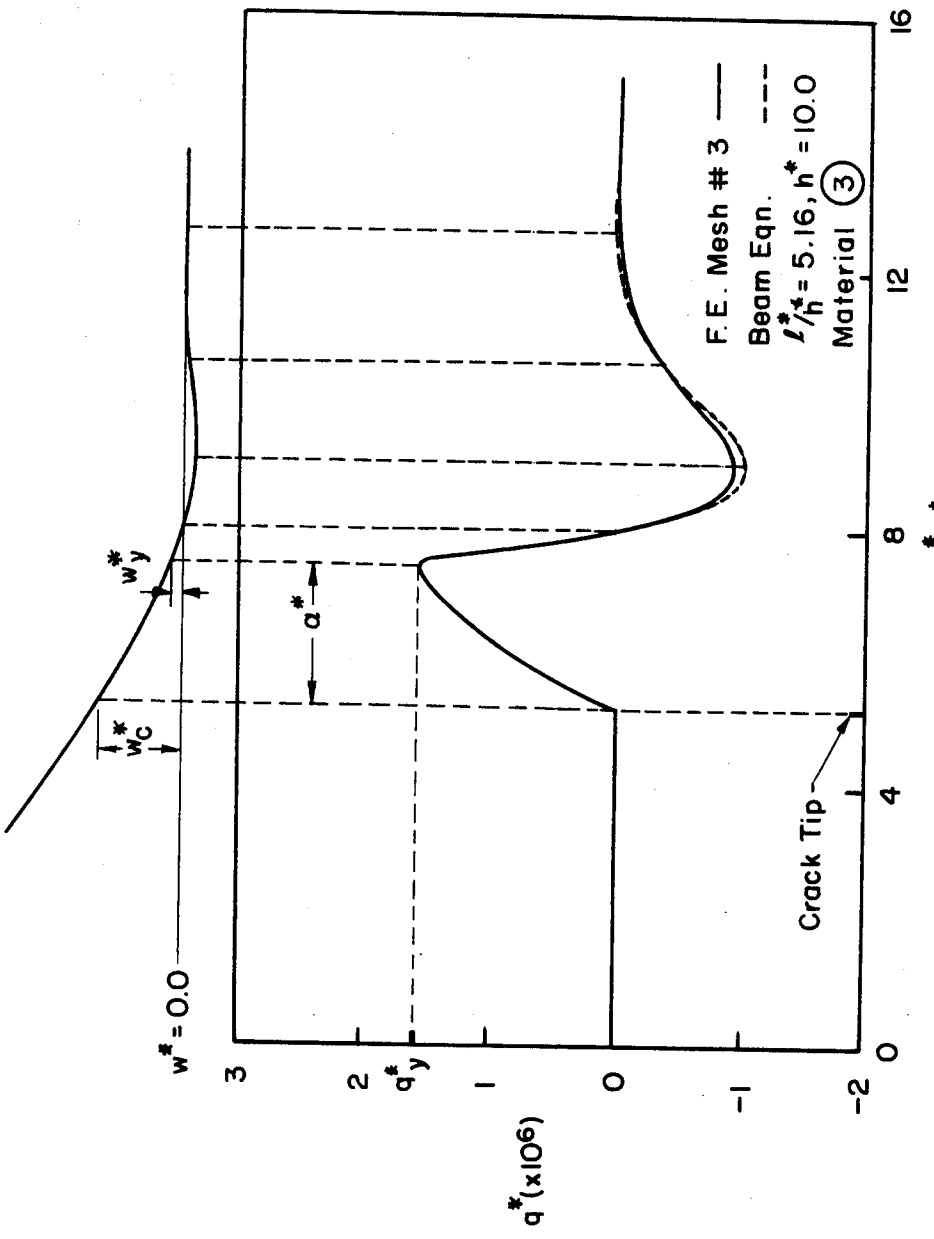

Figure 28. Comparison between Finite Element and Beam Equation: Cohesive stress distribution for the same crack length.

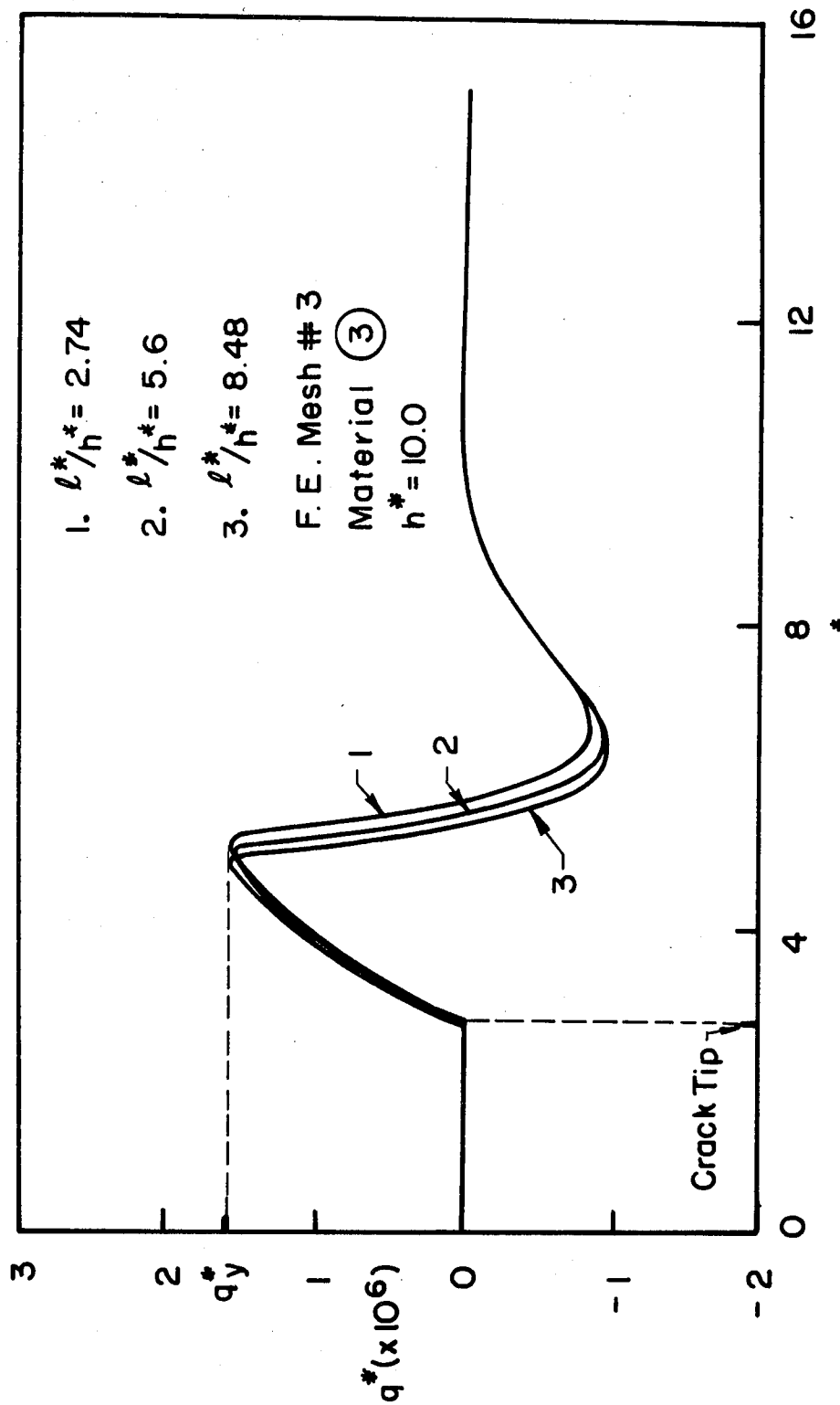

Figure 29. Cohesive stress distributions for different crack lengths.

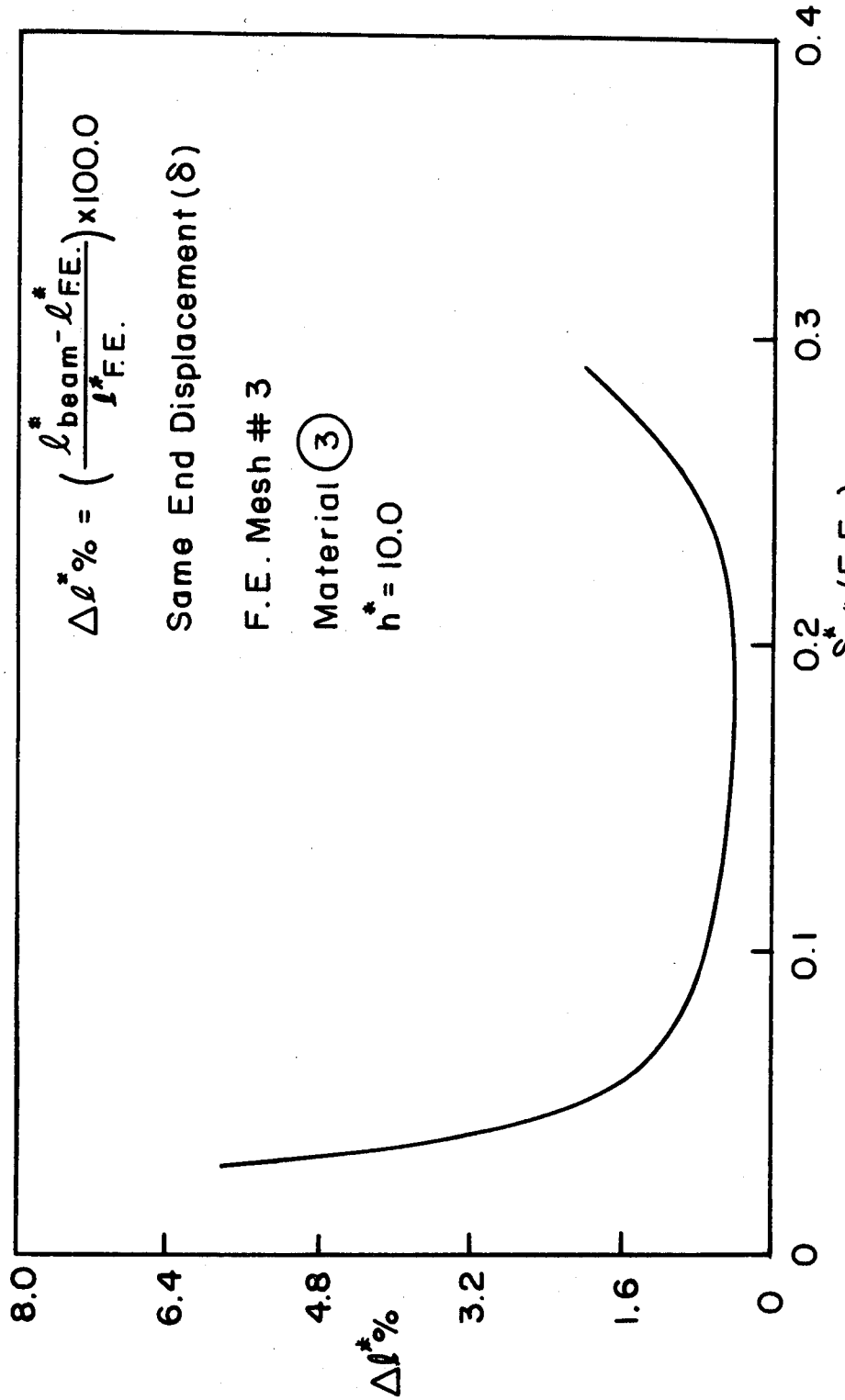

Figure 30. Error in the predicted crack length as a function of the end displacement using the beam equation (for the same end displacement δ).

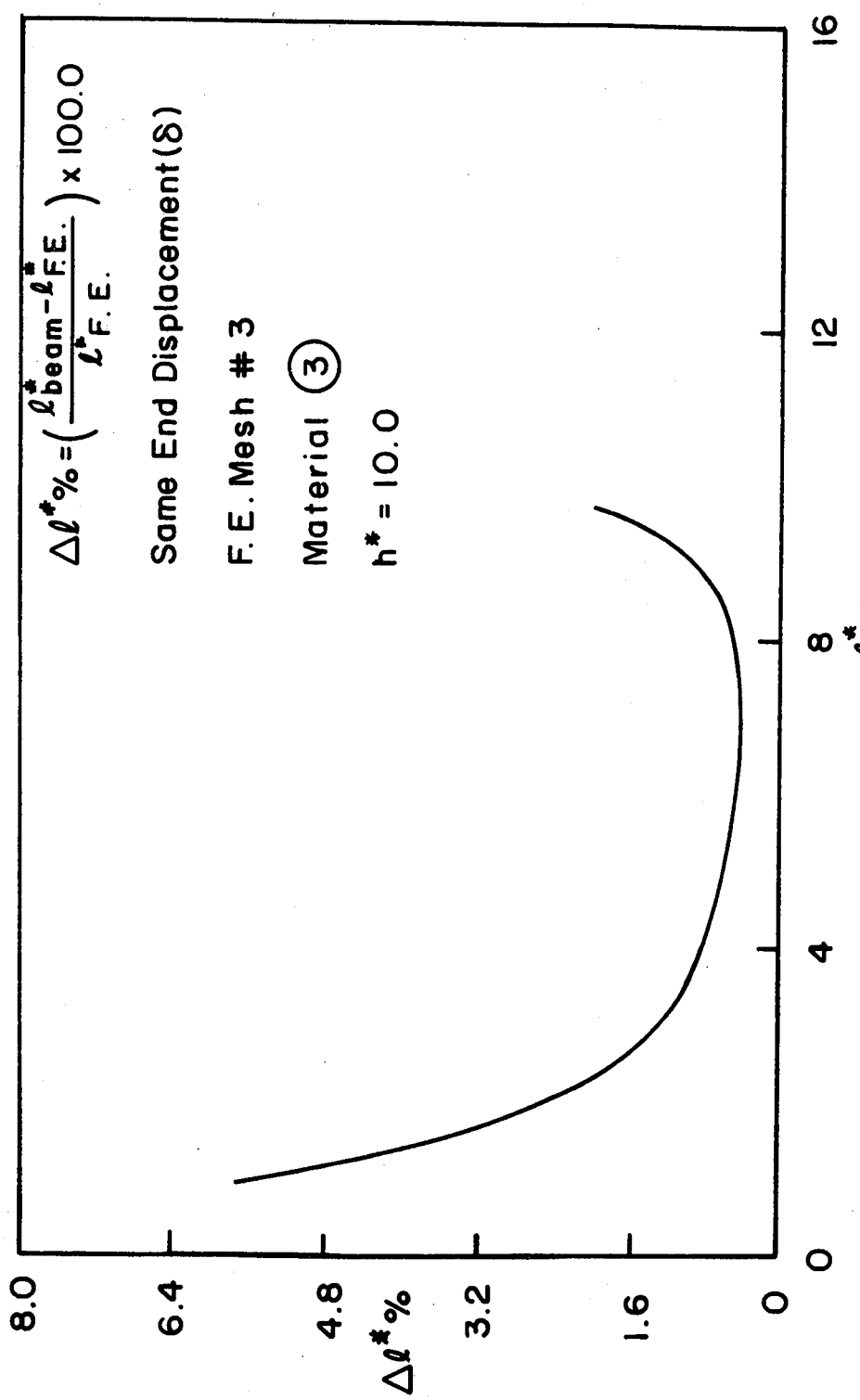

Figure 31. Error in the predicted crack length as a function of the crack length using the beam equation (for the same end displacement δ).

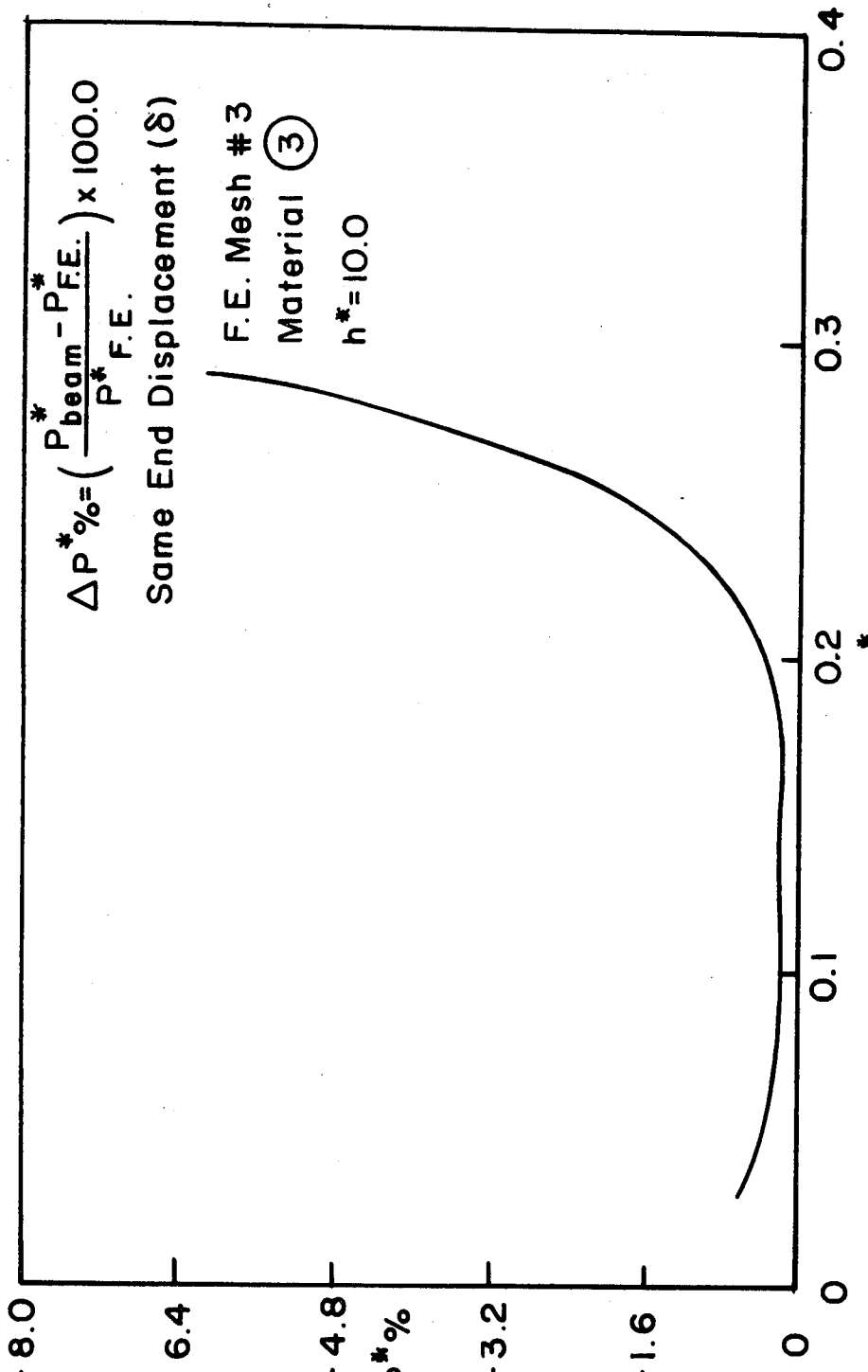

Figure 32. Error in the predicted end load as a function of the end displacement using the beam equation (for the same end displacement δ).

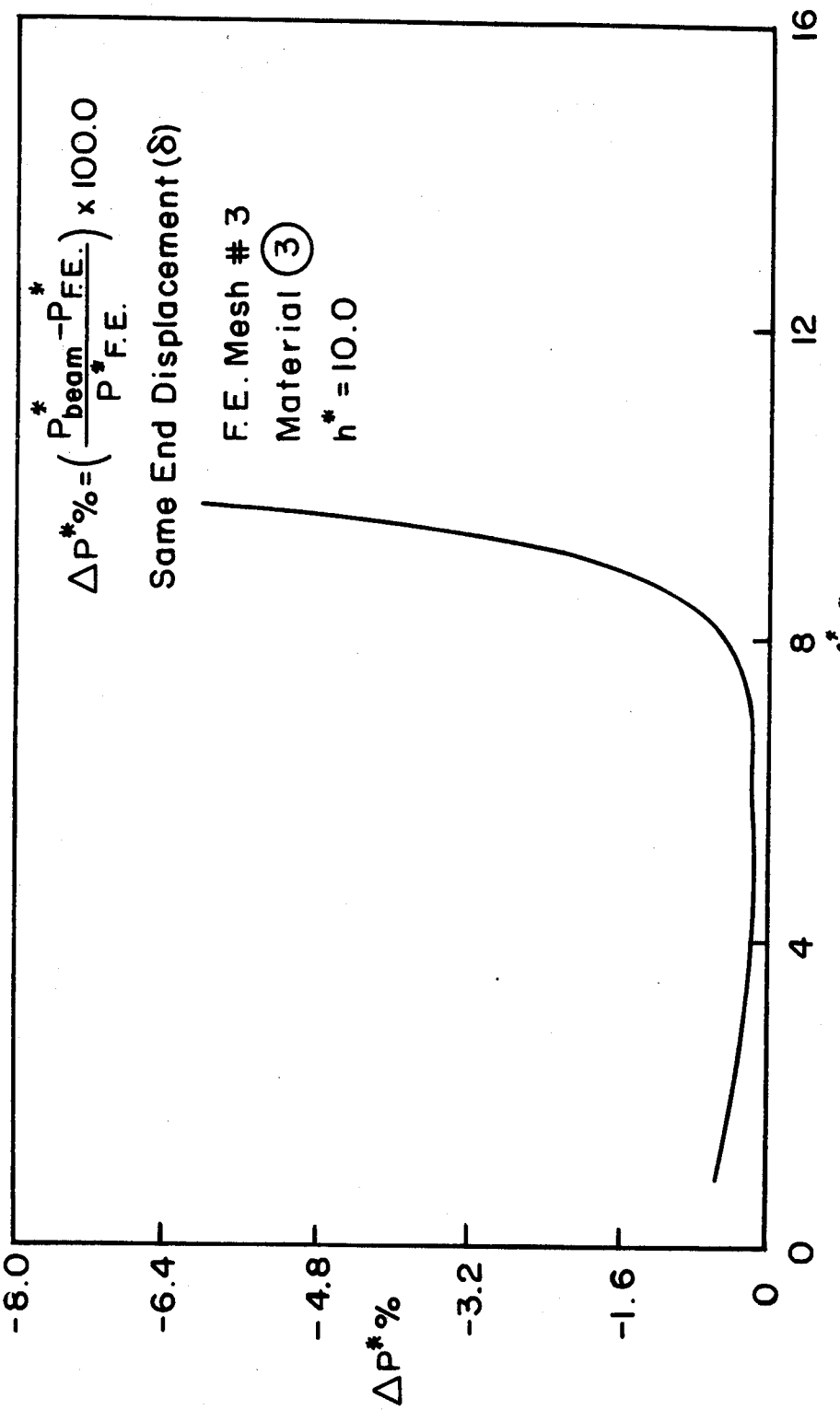

Figure 33. Error in the predicted end load as a function of crack length using the beam equation (for the same end displacement δ).

5. APPLICATIONS

We now discuss two practical applications of the findings, one is a simpler method for determining the fracture surface energy, the other which is the primary goal of this study, is the characterization of $q(w)$.

5.1. Surface Energy Determination

As the results for the propagating crack in Section 2.3.2 suggest (see Figure 20), equation (2.16) can be used to calculate γ more conveniently and accurately than the conventional scheme proposed by Berry [23], outlined as Method (A) below, even when the built-in conditions are not valid.

Method (A): Assume

$$C \equiv \frac{\delta}{P} = a l^N$$

where a is a function of EI. Plot log C versus log l and determine the slope N. Then the energy release rate G is

$$G = 2\gamma b = \frac{NP\delta}{l}$$

Here, we shall adopt the notations

$$G^{(A)} = 2\gamma^{(A)} b = \frac{NP\delta}{l} \qquad (A)$$

Apparently, one needs to measure several sets of P, δ and l to be able to determine N accurately from the plot of log C versus log l.

Method (B): The method we propose is simply the application of equation (2.16),[12] i.e. we henceforth let,

$$G^{(B)} \equiv 2\gamma^{(B)}b \equiv \left\{\frac{(3P^2\delta)^2}{EI}\right\}^{1/3} \qquad (B)$$

where $\gamma^{(B)}$ is simply $\tilde{\gamma}$ defined by (2.16).

For comparison, both schemes are applied to experimental data on composite delamination taken from H.Chai's Ph.D. thesis [26]. The details are given below:

12. This method was proposed and used earlier in [24,25] for cases where the 'built-in' conditions are assumed to be valid.

Material: Composite T300/5208, $E = 1.9 \times 10^7$ psi

Set A #1: $N = 2.68$, $h = t/2 = 0.119$ in, $b = 0.205$ in.

$I = 2.88 \times 10^{-5}$ in^4, $(EI)_{A\#1} = 547.0$ lb-in^2

l/h	P(lb)	l(in)	δ(in)	$2\gamma^{(A)}$	$2\gamma^{(B)}$	$\frac{2\gamma^{(A)}}{2\gamma^{(B)}}$
22.3	3.05	2.65	0.105	1.58	1.22	1.30
24.9	3.12	2.96	0.135	1.86	1.49	1.25
33.8	2.31	4.02	0.220	1.65	1.38	1.20
44.9	1.75	5.34	0.375	1.61	1.36	1.18
47.6	1.82	5.67	0.425	1.78	1.56	1.14
52.5	1.50	6.25	0.480	1.51	1.31	1.15
56.9	1.42	6.77	0.540	1.48	1.31	1.13
62.8	1.37	7.47	0.690	1.65	1.47	1.12
			$2\gamma_{ave.}$ (lb/in)	1.65	1.39	
			Standard Deviation	0.12	0.10	

$$\frac{2\gamma^{(A)}_{ave}}{2\gamma^{(B)}_{ave}} = 1.19$$

Set A #2: N = 2.85, h = t/2 = 0.118 in, b = 0.217 in.

$I = 2.97 \times 10^{-5}$ in^4, $(EI)_{A\#2} = 564.5$ lb-in^2

l/h	P(lb)	l(in)	δ(in)	$2\gamma^{(A)}$	$2\gamma^{(B)}$	$\frac{2\gamma^{(A)}}{2\gamma^{(B)}}$
23.1	3.70	2.72	0.115	2.05	1.57	1.31
30.7	2.65	3.62	0.170	1.63	1.31	1.24
39.6	1.85	4.67	0.250	1.30	1.05	1.24
45.9	1.62	5.42	0.350	1.37	1.10	1.25
53.8	1.43	6.35	0.475	1.40	1.14	1.23
59.7	1.38	7.05	0.625	1.61	1.30	1.24
66.5	1.29	7.85	0.770	1.66	1.37	1.21
			$2\gamma_{ave}$(lb/in)	1.57	1.26	
			Standard Deviation	0.24	0.17	

$$\frac{2\gamma^{(A)}_{ave}}{2\gamma^{(B)}_{ave}} = 1.25$$

Sets A #1 and A #2

	(A)	(B)
$2\gamma_{ave}$(lb/in)	1.61	1.33
Standard Deviation	0.19	0.15

$$\frac{2\gamma^{(A)}_{ave}}{2\gamma^{(B)}_{ave}} = 1.21$$

To check the validity of Berry's assumption, we plot $\log_{10} C^*$ vs $\log_{10} (l^*/h^*)$ in Figure 34, it is seen that the straight line approximation as proposed by Berry is valid only for a finite range of $\log_{10} (l^*/h^*)$. This can be seen more clearly by plotting N versus l^*/h^*. Figure 35 shows that N increases with l^*/h^* and approaches N = 3 which corresponds to the idealized case (see equation (2.6)) as $l^*/h^* \to \infty$.

We also calculate G based on method (A). Using a continuously varying N (as shown in Figure 35), the results are very accurate but still less accurate than the straight forward application of equation (B). As an example, for $l^*/h^* = 60, \frac{G^{(A)}}{G} = 1.001$ and $\frac{G^{(B)}}{G} = 1.0001$, where $G = 2\gamma b$.

When we simply pick an intermediate value of N and use equation (A), it is obvious that greater errors would result.[13] Keeping this in mind, we compute $\frac{G^{(B)}}{G^{(A)}} = \frac{2\gamma^{(B)}}{2\gamma^{(A)}}$ in the last column of the Appendix. The surprisingly monotonic decreasing trend with increasing l^* of the above ratio in both data sets A#1 and A#2 suggest that somehow high values for N's (N = 2.68 and N = 2.85) corresponding to long crack length were obtained from the log C versus log l plots.

A word of caution is in order, as the experiments from which the data are taken were done on nonsymmetric DCB speciments, i.e., the heights of the two beams were not necessarily equal, due to lack of more detailed data, we assume δ to be the average of the sum of the δ's of each beam. Figure 36 taken from reference 26 illustrates the points made. A fractured specimen is shown in Figure 37.

---

13. The fact that we find N in Berry's method to be a function of l indicates that the power law assumption is erroneous (as should be the case since a theoretical basis is lacking in the first place) and that our proposed method is inherently more accurate.

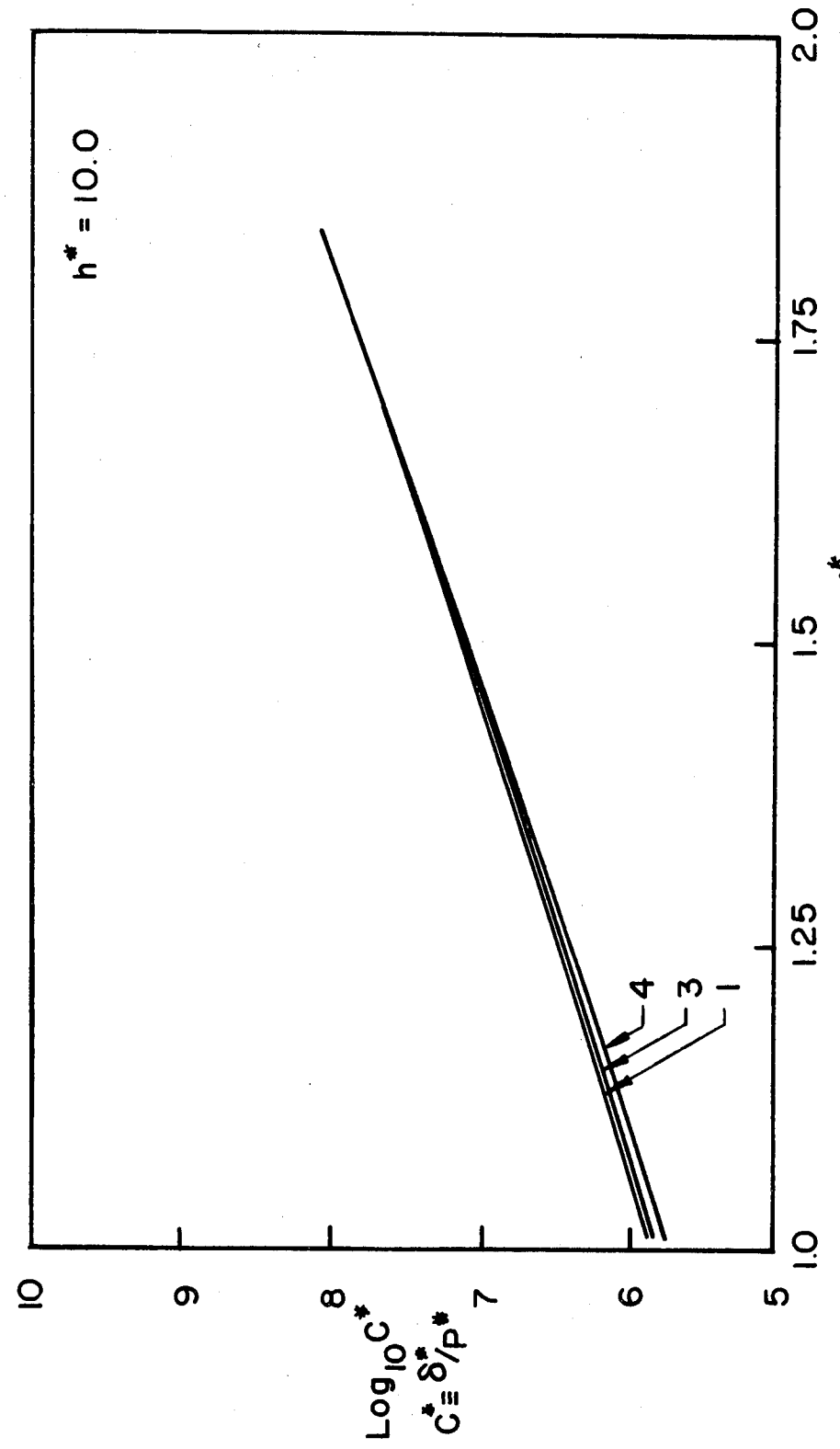

Figure 34. Compliance as a function of crack length for the propagating crack (material models 1, 3 and 4 as indicated).

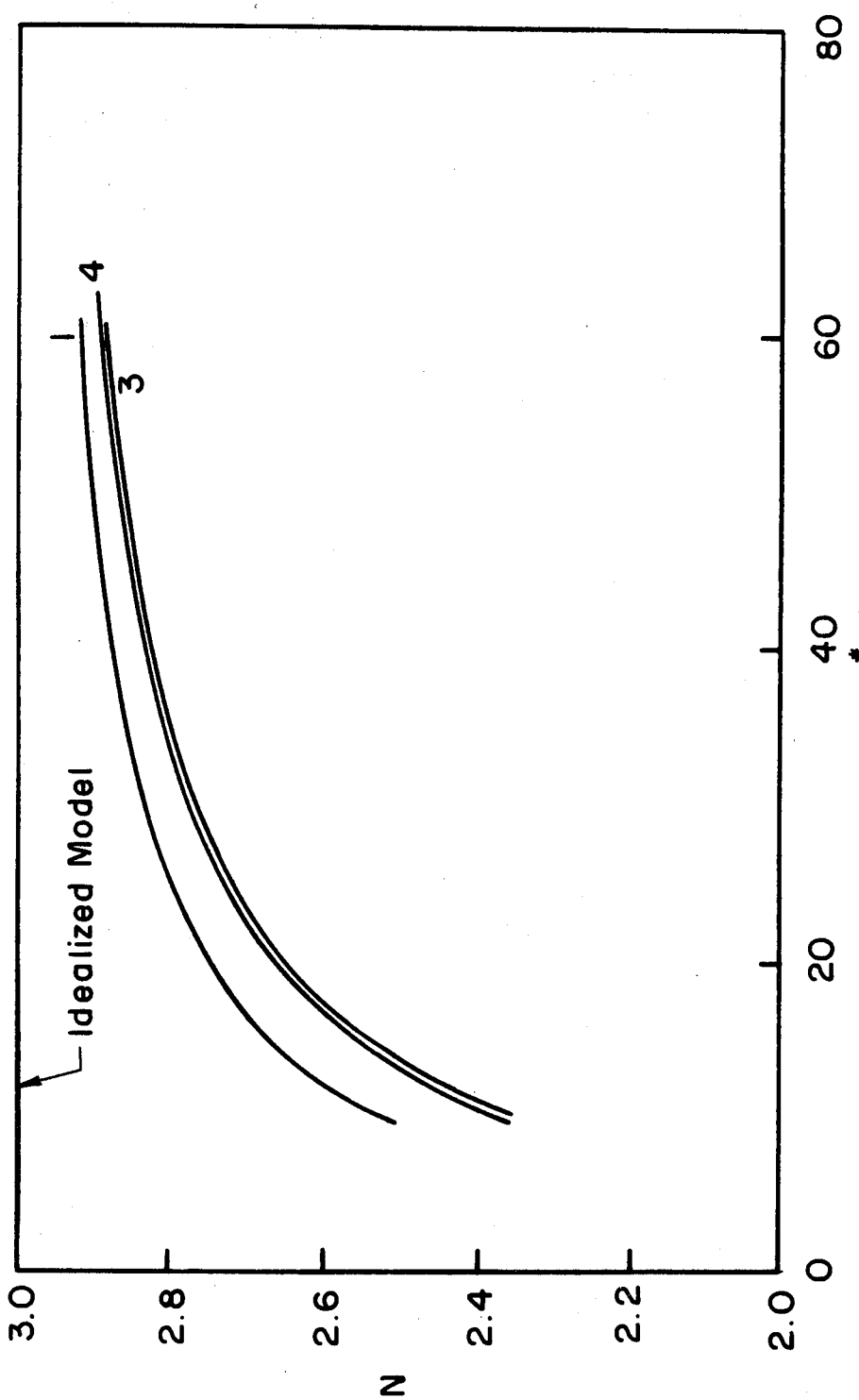

Figure 35. The exponent N in the assumed power law $C = a\ell^N$ as a function of crack length for the propagating crack (material models 1, 3 and 4 as indicated).

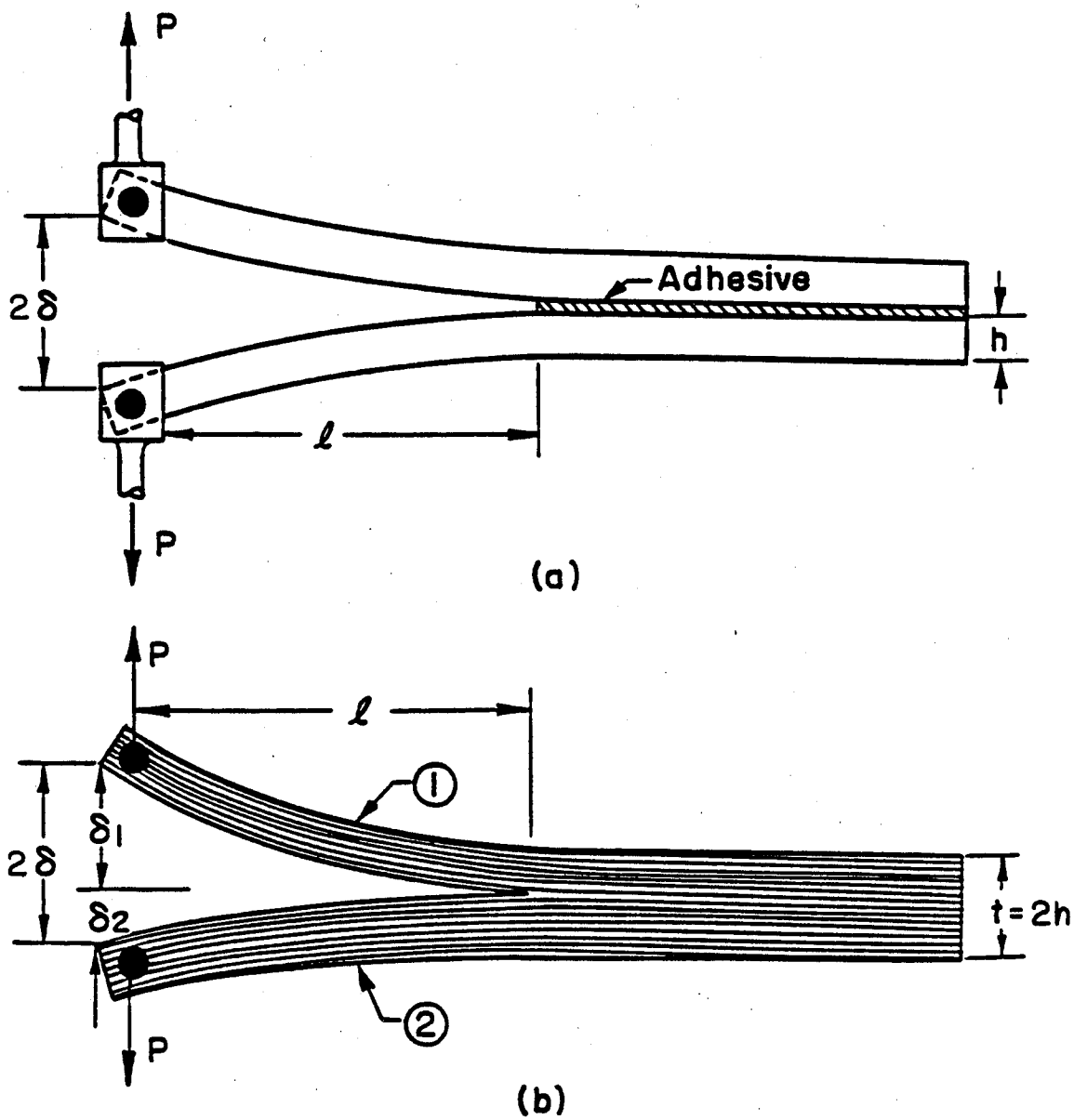

Figure 36 CLEAVAGE SPECIMEN;(a)-PROTOTYPE, (b)-MODIFIED (From ref. [26])

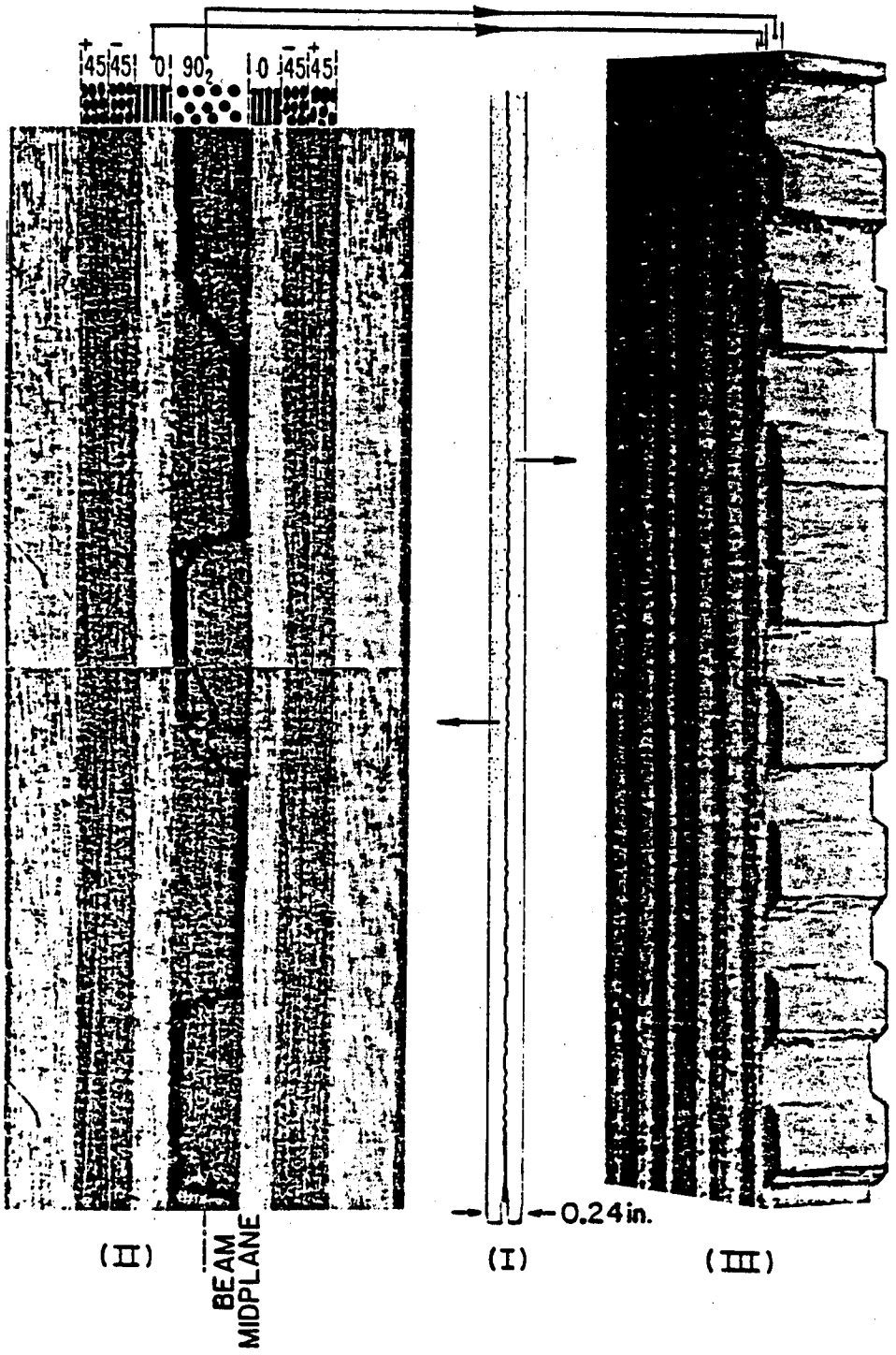

Figure 37 FRACTURE SURFACE OF A 48-PLY T300/5208 LAMINATE; TEST #A1 (From ref. [26])

5.2. Characterization of q(w)

We next discuss how the nonlinear characteristics of q(w) may be determined to first-order based on information gathered from basic material testings and DCB specimen tests. The properties of q(w) we are interested in are E_c, w_y, w_c, γ as well as the existence and gradient of an unloading tail. We outline below the methodology by which the characterization may proceed:

a. E_c and w_y can be directly taken from uniaxial tests.

b. w_c may be obtained from ultimate strain tension tests or optical measurements of the displacement contour from the DCB specimen tests.[14]

c. γ is easily computed using equation (2.16) or equation (B) as discussed at length in Section 5.1.

d. The existence and the gradient of an unloading tail can be identified and estimated by plotting C, $w_t, -w_t'$ and α as a function of P using DCB specimen test results for the stationary crack case (see Section 2.3.1a, Figures 5-8).

All these properties are sufficient to give a bound on the shape of q(w). Refinements of this approximate characterization can then be obtained by solving[15] the beam equation for various assumed q(w)'s (within the above bound) to better match the experimental results.

---

14. Note that from results depicted in Figures 22-24, displacement measurements can be conveniently taken at the top surface of the beam with less than 3% error over most portion of the beam.

15. We mention in passing that the solutions of the beam equation are relatively inexpensive compared to the finite element solutions.

6. CONCLUSIONS AND SUGGESTIONS FOR FURTHER WORK

We have shown how the problem of a beam on a nonlinear foundation can be solved economically and that the simple model renders results which compare well with more elaborate finite element models. We gain insights into how the behavior of the system is affected by the nonlinear material behavior of the cohesive foundation.

The finding suggests a simple way to determine the fracture energy. It also shows the shortcoming of the conventional method. The approximate characterization of the complete shape of q(w) appears to be possible.

As discussed in the introduction, the crack propagation scheme using nonlinear springs can be employed in more general situations with great promise for example it can be used to investigate how brittle or ductile material behavior (modeled by the spring characteristics) affects the dependence of the stress intensity factor on the crack velocity. (See the Appendix for further discussion on and results of one such attempt.) It is also interesting to study crack growth for materials that soften (after an appropriate amount of hardening) and fail under high strain using yield criteria and flow rules that account for the failure mechanisms involved (in the continuum sense). Many other problems along this line readily come to mind, all centered around determining the proper continuum constitutive models for damaged materials and applying the models to engineering problems of interest.

7. REFERENCES

1. Berry, J.P., "Some Kinetics Considerations of the Griffith Criterion for Fracture, Parts I & II," J. Mech. Phys. Solids, Vol. 8, 1960, pp. 194-216.

2. Bilek, Z.J. and Burns, S.J., "Crack Propagation in Wedged DCB Specimen," J. Mech. Phys. Solids, Vol. 22, 1974, pp. 85-95.

3. Steverding, B. and Lehnigk, S.H., "The Propagation Law of Cleavage Fracture," Int. J. Fracture, Vol. 6, 1970, pp. 223-232.

4. Kanninen, M.F., "An Augmented DCB Model for Studying Crack Propagation and Arrest," Int. J. Fracture, Vol. 9, 1973, pp. 83-92.

5. Kanninen, M.F., "A Dynamic Analysis of Unstable Crack Propagation and Arrest in the DCB Test Specimen," Int. J. Fracture, Vol. 10, 1974, pp. 415-430.

6. McClintock, F.A., "A Criterion for Ductile Fracture by the Growth of Holes," J. Appl. Mech., Vol. 35, 1968, pp. 363-371.

7. Gurson, A.L., "Continuum Theory of Ductile Rupture by Void Nucleation and Growth: Part 1 - Yield Criterial and Flow Rules for Porous Ductile Media," J. Eng. Mat. Tech., Vol. 99, 1977, pp. 2-15.

8. Needleman, A., "Void Growth in an Elastic-Plastic Medium," J. Appl. Mech., Vol. 39, 1972, pp. 964-970.

9. Berg, C.A., "Plastic Dilation and Void Interaction," Proc. of Batelle Memorial Inst. Symposium on Inelastic Processes in Solids, 1969, pp. 171-209.

10. Rice, J.R. and Needleman, A., "Limits to Ductility Set by Plastic Flow Localization," Mechanics of Sheet Metal Forming, D.P. Koistinen and N.M. Wang (Eds.), Plenum, New York, 1978, pp. 237-267

11. Krajcinovic, D., "Constitutive Equations for Damaging Materials," J. Appl. Mech., Vol. 50, 1983, pp. 355-360.

12. Dougill, J.W., "On Stable Progressively Fracturing Solids," J. Appl. Math. Phys., (ZAMP), Vol. 27, 1976, pp. 423-436.

13. Rudnicki, J.W., "A Class of Elastic-Plastic Constitutive Laws for Brittle Rock," J. Rheology, Vol. 28, 1984, pp. 759-778.

14. Bazant, Z.P., "Work Inequalities for Plastic Fracturing Materials," Int. J. Solid Structures, Vol. 16, 1980, pp. 873-901.

15. Andersson, H., "A Finite Element Representation of Stable Crack Growth," J. Mech. Phys. Solids, Vol. 21, 1973, pp. 337-356.

16. Kfouri, A.P. and Miller, K.J., "Crack Separation Energy Rates in Elastic-Plastic Fracture Mechanics," Proc. Inst. Mech. Eng. (London), Vol. 190, 1976, pp. 571-584.

17. Rydholm, G., Fredricksson, B. and Nilsson, F., "Numerical Investigations of Rapid Crack Propagation," Numerical methods in Fracture Mechanics, A.R. Luxmoore and D.R.J. Owen (Eds.), Univ. College of Swansea, Swansea, Wales, Jan. 1978, pp. 660-672.

18. Malluck, J.F. and King, W.W., "Fast Fracture Simulated by a Finite Element Analysis Which Accounts for Crack-Tip Energy Dissipation," Numerical methods in Fracture Mechanics, A.R. Luxmoore and D.R.J. Owen (Eds.), Univ. College of Swansea, Swansea, Wales, Jan. 1978, pp. 648-659.

19. Malluck, J.F. and King, W.W., "Fast Fracture Simulated by Conventional Finite Elements: A Comparison of Two-Energy Release Algorithms," Crack Arrest Methodology and Applications, ASTM STP 711, G.T. Hahn and M.F. Kanninen (Eds.), 1980, pp. 38-53.

20. Hoff, R., Rubin, C.A., and Hahn, G.T., "A New Finite Element Technique for Modelling Stable Crack Growth," J. Eng. Fracture Mech., special issue: Dynamic Fracture Mechanics, Vol. 23, 1, 1986, pp. 105-118.

21. Kanninen, M.F. et al., "Elastic-Plastic Fracture Mechanics for Two-Dimensional Stable Crack Growth and Instability Problems," Elastic-Plastic Fracture, ASTM STP 668, J.D. Landes, J.A. Begley, and G.A. Clarke (Eds.), 1979, pp. 121-150.

22. Keller, H.B., "Numerical Solution of Two Point Boundary Value Problems," Series: Regional Conf. in Appl. Math., Vol. 24, SIAM, 1976.

23. Berry, J.P., "Determination of Surface Fracture Energies by the Cleavage Technique," J. Appl. Phys., Vol. 34, 1963, pp. 62-68.

24. Asbeck, W.K., "Forces in Coatings Removal by Knife Cutting Methods," Adhesion and Cohesion, Amsterdam, P. Weiss (Ed.), 1962, pp. 101-120.

25. Malyshev, B.M. and Salganik, R.L., "The Strength of Adhesive Joints Using the Theory of Cracks," Int. J. Fracture, Vol. 1, 1965, pp. 114-128.

26. Chai, H., "The Growth of Impact Damage in Compressively Loaded Laminates," Ph.D. Thesis, Calif. Inst. of Tech., 1982, pp. 102-126.

Other Relevant Works:

1. Tsai, N.C. and Westmann, R.A., "Beam on Tensionless Foundation," J. Eng. Mech. Div., Proc. ASCE., 1967, pp. 1-12.

2. Chang, D.J., Muki, R. and Westmann, R.A., "Double Cantilever Beam Models in Adhesive Mechanics," Int. J. Solids Structures, Vol. 12, 1976, pp. 13-26.

3. Franklin, J.N. and Scott, R.F., "Beam Equation with Variable Foundation Coefficient," J. Eng. Mech. Div., ASCE, 1979, pp. 811-827.

PART II

A NONLINEAR ANALYSIS OF AN EQUILIBRIUM CRAZE IN AN INFINITE MEDIUM SUBJECTED TO SYMMETRICAL LOADING

NOTATION

Dimensional Variables:

A = crack length

C = craze length

E = Young's modulus of the elastic medium

H = $H(C,X,T)$ = kernel defined by (2.11)

I_M = the integral defined by (2.6)

K_I = Mode-I stress intensity factor

M = $M(C,X,T)$ = kernel defined by (2.5)

P = cohesive stress or fibril restoring force

T = dummy variable

V = net vertical displacement of the craze/crack boundary $\equiv W - W_o$

V_c = critical crack tip opening displacement (CTOD)

W = actual craze contour

W_o = primordial craze contour

X = horizontal coordinate measured along the craze major axis

Y = vertical coordinate

Σ_∞ = far-field applied stress in the Y-direction

θ = temperature

Reference Parameters (used for non-dimensionalization):

$C_{ref} = C_o$ = reference craze length

$\Sigma_{ref} = E/2$ for plane stress

$= E/2(1 - \nu^2)$ for plane strain

$U_{ref} = C_o^2 \Sigma_{ref}$ = reference energy

Dimensionless Variables:

a = A/C_o

a_o = initial crack length of the precut crack in Section 7

c = C/C_o

c_{cr} = critical craze length defined by equation (7.1)

d = half length dimension of the infinite (large) plate

e = natural logarithm base

G = energy release rate

$h(c,x,\tau)$ = the kernel in equation (2.10a)

$l(c,\tau)$ = the kernel in equation (2.19)

$m(c,x,\tau)$ = the kernel in equation (2.18)

p = P/Σ_{ref}

p_m = Dugdale cohesive stress

R = the exponent in equation (2.13)

τ = T/C_o

U_p = elastic strain energy in a plate with no crack or craze

U_c = energy required to form a craze of length 2c with an internal crack of length 2a

v = V/C_o

v_c = V_c/C_o

w = W/C_o

w_o = W_o/C_o

x = X/C_o

y = Y/C_o

α = c-a = craze zone size

β = $\frac{\pi v_c}{2p_m}$

γ = $\int_0^{v_c} p(v)dv$

= area under the p-v curve

= fibril fracture energy

σ_∞ = $\Sigma_\infty/\Sigma_{ref}$

Π = potential energy

Superscript:

$\dot{(\ )}$ = time derivative of ( )

$(\ )^{o}$ = the initial guess of ( )

$(\ )^{k}$ = the k^{th} approximation of ( )

ABSTRACT

This study investigates the effects of nonlinear fibril behavior on the mechanics of craze and crack growth. We developed a numerical method for determining the equilibrium shape of a craze in an infinite elastic plane whose fibrils exhibit very general nonlinear force-displacement (P-V) behavior, including strain softening characteristics.[1]

The problem formulation is based on the superposition of the relevant elasticity Green's function. The solution is effected by using Picard's successive approximation iterative scheme. Both field equilibrium and the Barenblatt condition for vanishing stress and strain singularities (K_I=0) are satisfied simultaneously, rendering the craze tip profile cusp-like as observed experimentally. The formulation allows the stress distribution profile and the corresponding P-V relation to be computed from experimentally measured craze/crack contours with certain advantages over the methods proposed to date.

Further numerical investigations indicate that only certain classes of the fibril P-V relations are consistent with realistic craze profiles, i.e., profiles with nonnegative displacements at all points. In addition, it is found that for a given P-V relation, nontrivial solutions[2] exist only for certain ranges of craze lengths depending on the P-V characteristics under consideration.

Quasi-static growth of a craze with a central crack is analyzed for different nonlinear P-V relations for the craze fibrils. A 'critical crack tip opening displacement' (CTOD) or more precisely, 'critical

1. See 'Notation' table for definitions of symbols.

2. The 'trivial solution' refers to the solution corresponding to a fully closed craze, i.e., zero displacements throughout or, simply: No craze exists.

fibril extension' is employed as the criterion for fracture. The P-V relation is further assumed to be invariant with respect to the craze and crack lengths. For comparison purposes, the results are compared and contrasted with the Dugdale model. The craze zone size and the energy dissipation rate are shown to approach asymptotic values in the limit of long cracks.

The problem of craze growth from a precut crack under increasing far-field loading is then studied. Instability is shown to occur in the case where the P-V relation is monotonically softening: The crack could start to grow unstably before the crack tip opening displacement reaches its critical value.

1. INTRODUCTION

When glassy polymers are subjected to strains larger than about 0.2%, they begin to exhibit local 'plastic' deformation. Two distinct processes of plastic deformations have been observed, one being mainly a shearing phenomenon such as diffuse shear yielding and localized shear band formation, and the other being caused by cavitation and void growth commonly called 'crazing'. The latter process is characterized by a loss of intermolecular cohesion, molecular flow and reorientation as well as a significant decrease in local density [1]. In this work, we shall concern ourselves only with the phenomenon of crazing.

The subject of crazing has been extensively studied by both material (polymer) scientists and applied mechanicians. Literature addressing various aspects of crazing can be found in references 1 through 8. We shall discuss here briefly the pertinent physical concepts and the motivations leading to the present investigation.

It has been recognized for some time that fracture in thermoplastic polymers is usually preceded by the formation of crazes. Crazes are formed in the bulk polymer along planes normal to the direction of maximum principal tensile stress. Crazes tend to nucleate at microdefects or inclusions and grow by the formation of fibrils from the bulk polymer [4,5]. They thicken through a combination of two distinct mechanisms: 'surface drawing' and 'creep'. In surface drawing, new polymer is drawn from the bulk into the craze in the form of fibrils. In the creep mechnism, existing fibrils are simply stretched, mostly locally around the weak portions. Note that although 'creep' implicitly signifies a time dependent process, we will exclude time consideration from this work.[3] For our purpose it is sufficient to recognize that the interplay of these two mechanisms gives rise to an

3. For an analysis accounting for these two basic mechanisms, see a recent paper by Kramer and Hart [9].

effective force-displacement (P-V) behavior which we consider to be initially prescribed. Here 'force' represents the cohesive stress exerted by the fibril on the craze/bulk polymer boundary. 'Displacement' refers to the net displacement of the craze boundary (see Section 2.1 for details).

Electron microscopy shows that the typical craze thickness is on the order of 1 μm and the length to thickness (aspect) ratio is approximately 10^2 to 10^3. Crazes generally consist of a network of fibrils between 10 to 40 nm in diameter, interspersed by voids of similar dimensions. The transition boundary between a craze and the bulk polymer where surface drawing takes place is very thin, i.e., less than 2 nm. Craze fibrils have been shown to exhibit considerable strength [7,8]. Therefore, crazing could, under certain conditions, substantially enhance the toughness of bulk polymers. However the presence of crazes does not necessarily enhance the strength of the overall structure. In many instances, uncontrolled craze growth tends to induce fracture, causing structures to fail 'prematurely'. For more in-depth discussions on microstructures and properties of crazes, see references 5 and 8. Figure 1 shows a typical craze and its tip region.[4]

We next review briefly the analytical approaches that have been attempted in modelling the crazing phenomenon to date. Barenblatt considered the problem of equilibrium cracks in brittle fracture [10]; even though the analysis was carried out in the context of cracks, the basic propositions and concepts apply to crazes equally well. His proposition eliminates the infinite stresses and strains at the crack tip by incorporating cohesive stresses distributed over a cohesive zone of finite length such that the crack is in 'equilibrium' and the stress intensity factor vanishes. Assuming constant cohesive (yield) stress in this cohesive zone, Dugdale derived a simple relationship between

4. The micrographs were taken by L. Berger and made available to us by Professor E.J. Kramer.

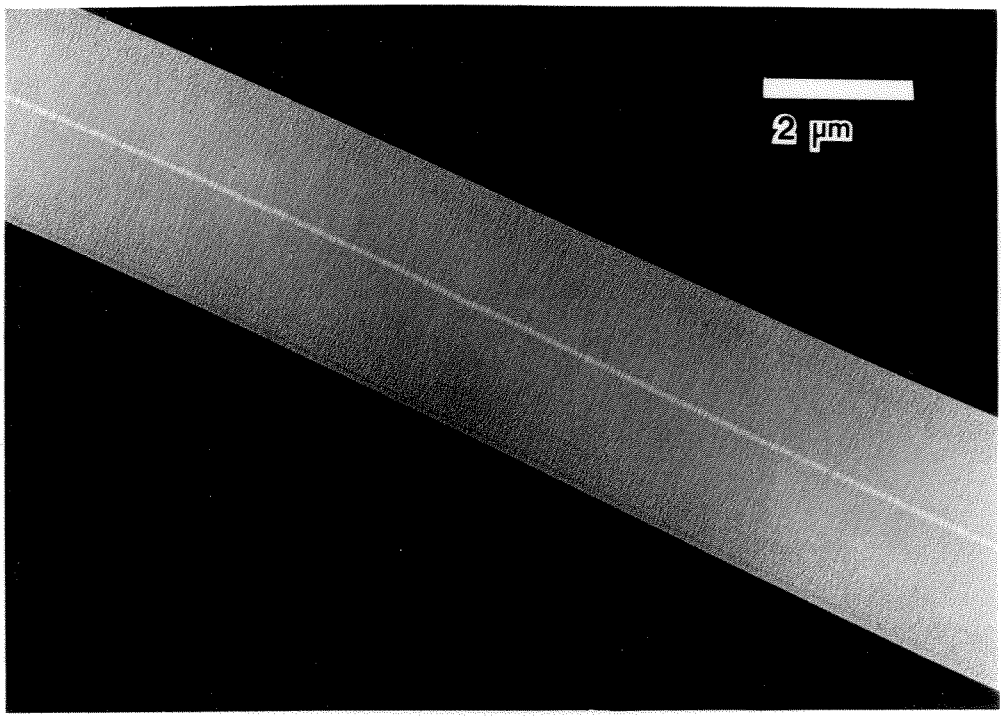

(a)

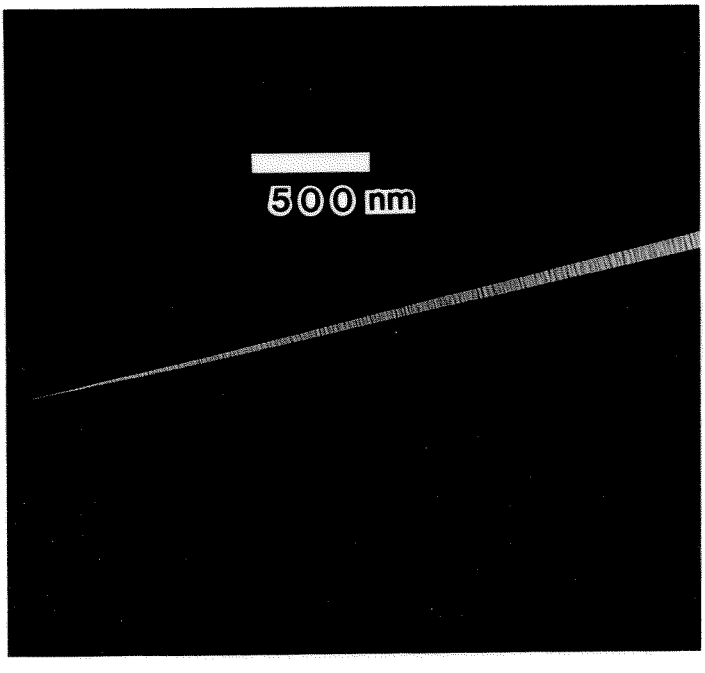

(b)

Figure 1 Electron micrographs of a craze (a) and its tip region (b). (Courtesy of L. Berger and E.J. Kramer.)

its size and the applied stress [11]; this study was then considered by Rice in greater detail using the rigid-plastic strip model [12]. Goodier and Field calculated the rate of plastic work dissipation for the same model with an added assumption that a crack propagates with a self-similar geometry [13]. In this, the authors assumed that the far-field stress remained constant during quasi-static crack propagation; however, this assumption will be shown to be incompatible with the critical crack tip opening displacement criterion employed in the present work (see Section 6).

Goodier and Kanninen introduced a crack propagation model using nonlinear atomic separation laws and indicated how the cohesive stress distribution changed as the crack extended [14]. Atkinson proposed an iterative scheme for solving axially symmetric problems relating to cracks opening under a displacement-dependent internal stress without, however, satisfying the Barenblatt condition [15]. Andersson and Bergkvist solved a crack problem using a strip model [16]. The strip material behavior was piecewise-linear with a 'linear softening' characteristic; the strip extended to infinity and the displacements decreased gradually to zero, so that the stresses were bounded everywhere, similar to reference 14. E. Smith derived a class of acceptable force-displacement relationships by starting with displacement profiles chosen so as to yield simple solutions to the integral equation relating the displacement and stress within the cohesive zone [17]. In this instance, the smooth closure (Barenblatt) condition was satisfied a priori. The resulting class of the P-V relations is in general agreement with our present findings. Some of the P-V relations (normalized) are excerpted in Figure 2.[5]

In addition to these stress analyses, there are a number of contributions concerned with the mechanics of craze growth. In 1965, Knight [18] employed the Fourier transform method [19] to calculate the

5. Taken from reference 17.

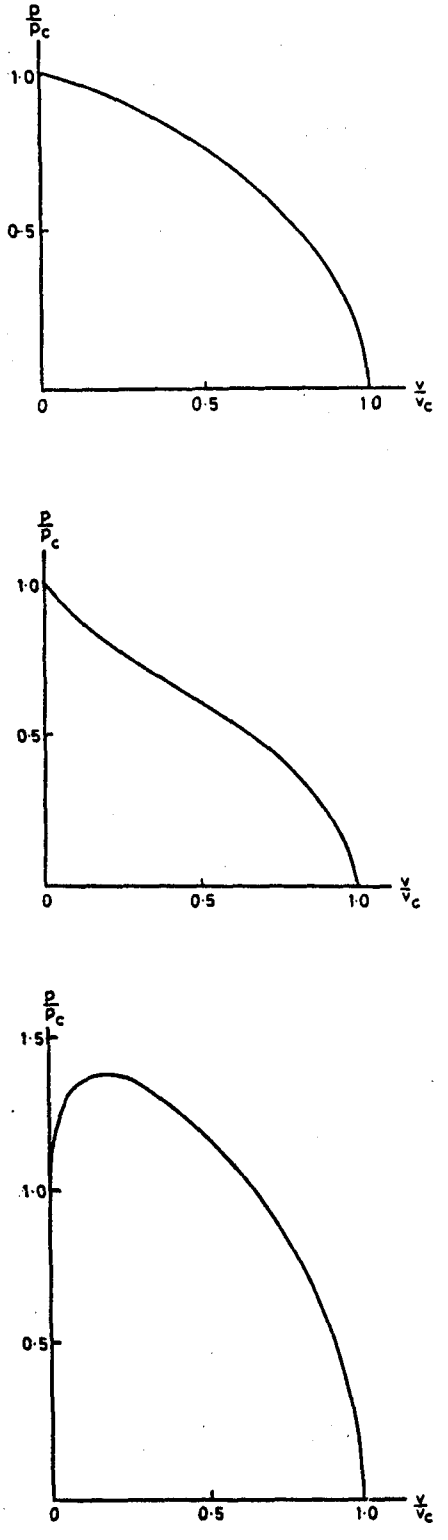

Figure 2. Some 'acceptable' p-v relations from reference 17: p_c and v_c denote the maximum values of cohesive stress and CTOD respectively.

stress distribution along a craze, but due to the erroneous craze profile used, the resulting stress distribution was incorrect. Knauss presented a boundary-layer model (formulated for a semi-infinite crack) which is extendable to account for rate-dependent cohesive stress-displacement behavior [20]. The critical strain (displacement) criterion was employed and it was found that for materials with softening force-displacement characteristics, the crack tip cohesive stress decreased rapidly to zero while the size of the cohesive zone rose sharply as the critical strain was approached at the crack tip. Figure 3a illustrates the cohesive stress and strain employed and Figures 3b,c, the results discussed.[6]

Verheulpen-Heymans and Bauwens presented a modified Dugdale model with a constant cohesive stress acting over a short distance behind the craze tip and a lower constant cohesive stress acting over the rest of the craze length [21]. Lauterwasser and Kramer performed experiments in which accurate measurements of the density of the craze materials together with the craze profile permitted the determination of the stress distribution profile [5] through use of the Fourier transform technique [19]. They also demonstrated conclusively that surface drawing was the dominant process in craze thickening. As we shall see later, this finding is of general significance in determining the appropriate P-V relations for craze fibrils. Subsequently, Wang and Kramer employed a distributed dislocation model to calculate the far field applied stress as well as the surface stress profile along the craze from the experimental displacement profile in the craze zone [22]. The method gave results in good agreement with the Fourier transform method. The only disadvantage of this method lies in the inherent errors associated with the computation of the derivative of the experimentally determined displacement profile required in applying the scheme. The stress profiles obtained in this way for polystyrene and polycarbonate exhibited stress concentrations at the crack tip as

6. Taken from reference 20.

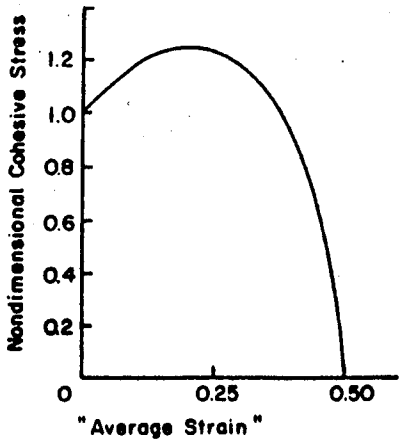

Fig. 3a Relation Between Cohesive Stress and "Strain" in the Cohesive Zone

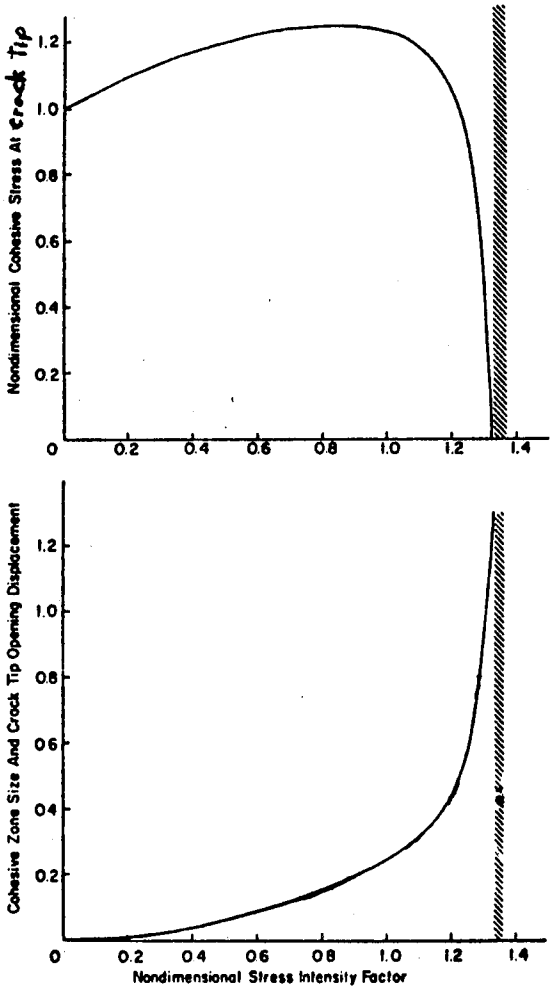

Fig. 3bc Force at Crack Tip (Above), Displacement ("Strain") at Crack Tip and Cohesive Zone Size (Below) as a Function of Stress Intensity Factor

Figure 3. (a) Cohesive stress and strain relation; (b,c) Crack tip cohesive stress and displacement as functions of the stress intensity factor (from reference 20).

well as at the craze tip and approximately constant stress in between. Donald and Kramer later studied five polymers and obtained similar qualitative results [23] which we reproduce in Figure 4.

Attempts to determine stress distribution profiles for given displacement profiles by using other methods such as finite element and boundary element analyses were made by Bevan [24] and Sun and Hsiao [25], where the latter authors also allowed yielding in the bulk polymer in their finite element study. Although the results of both studies agreed generally (within 5%) with those obtained by Kramer et al [5] through the Fourier transform method, the accuracy and efficiency seems lacking.

So far we have reviewed studies in which the stress distribution along the craze boundary is calculated from the experimental displacement profile using various analytical techniques. The main purpose of the present study is, however, to address the more difficult problem where one seeks solutions for both the stress and displacement profiles together with the far-field applied stress, given a craze length and a nonlinear fibril P-V relation, such that the Barenblatt's condition is also satisfied. This problem has thus far not been solved correctly. Recently, Walton and Weitsman presented a solution scheme for the special case in which the fibril P-V relation is linear [26] and later Weitsman [27] extended the analysis to include the case where the P-V relation is nonlinear. The analyses in references 26 and 27 are, however, deficient in several aspects. For instance, in reference 26 the solution did not satisfy the Barenblatt condition but had to be 'corrected' later by imposing additional cohesive stresses in a small 'tip zone' to make the stress intensity vanish. This arbitrary correction is artificial and results in stress distribution profiles inconsistent with those deduced experimentally as illustrated in Figure 5. In reference 27, Weitsman attempted to extend his analysis to the nonlinear case and made use of the stress-strain relations obtained by Kambour as the P-V relations for craze fibrils [7]. In view of the

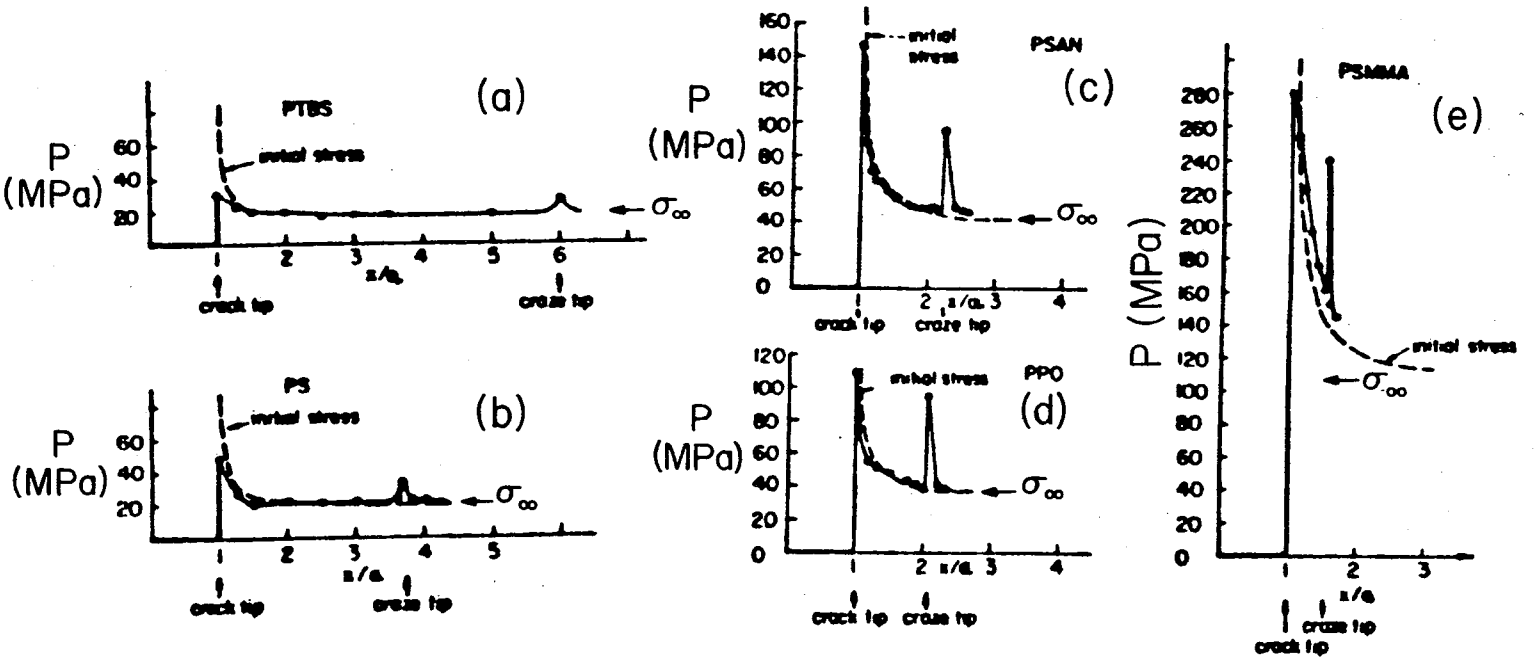

Surface stress profiles P(x) in (a) PTBS, (b) PS, (c) PSAN, (d) PPO, and (e) PSMMA. 'a' denotes crack length, the applied stress σ_∞, and the form of the initial crack stress profile are marked.

Figure 4. Experimental stress distribution profiles for crazes with internal cracks (from reference 23).

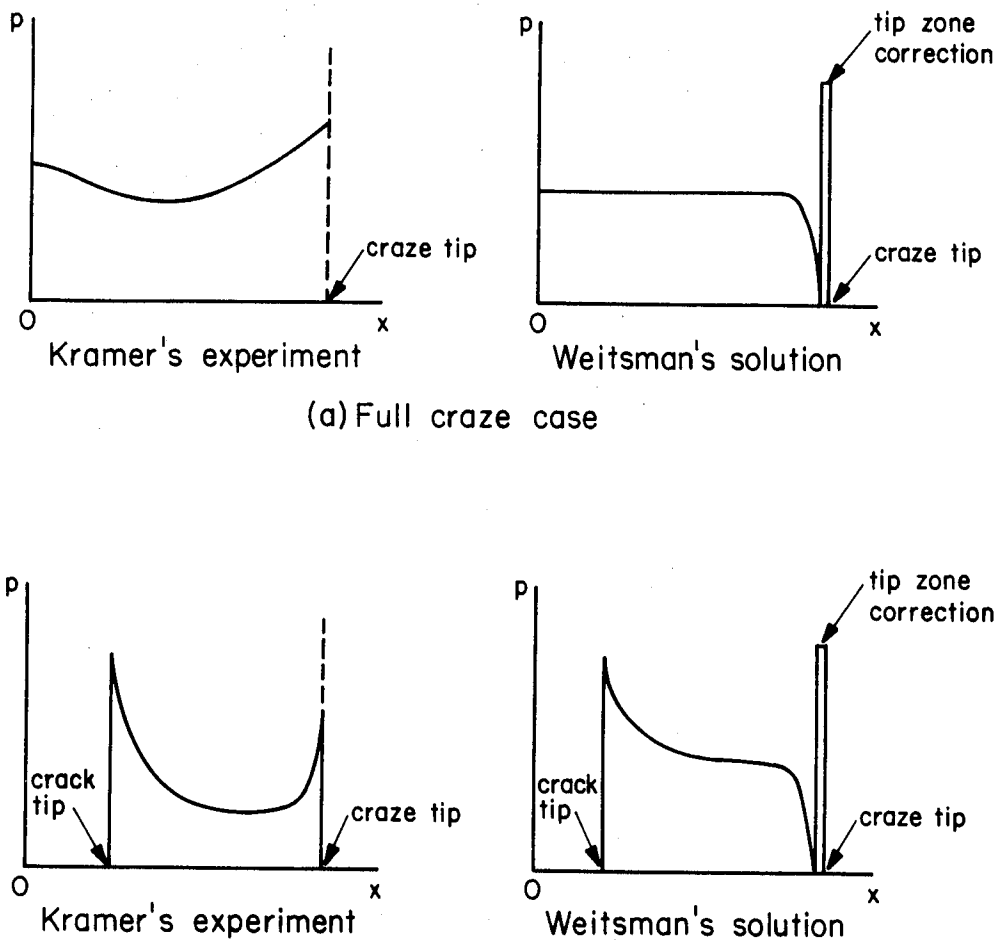

Figure 5. Comparisons between actual stress distribution profiles and those derived from analyses in reference 26.

fact that Kambour performed his experiments using 'dried' polycarbonate and observed no surface drawing whatsoever [28], it is clear that one could use the resulting stress-strain relations as fibril behaviors only when the crazes thicken solely by creep (fibril stretching). In contrast and as mentioned earlier, Kramer found that crazes thicken and grow mainly by fibrillation and surface drawing [5]. It is clear that the incorrect choices for the fibril P-V relations invalidated the results of the analyses in references 26 and 27. In addition, the 'energy release rate' as calculated in [27] by summing the contributions of the artificial stress intensity factor (which should be zero) and the plastic work release rate, are devoid of any physical meaning. This is because no consistent fracture criterion was applied, therefore the variation of the crack length without varying the craze length as was done in [27] was totally arbitrary and incorrect.

In view of these past contributions, it becomes clear that an analytical and computationally efficient method for determining the displacement and stress profiles of a craze with prescribed nonlinear fibril P-V behavior under satisfaction of both equilibrium and the smooth-closure conditions is still lacking. The primary objective of this work is to present such an analysis and to use it in the study of various aspects of the mechanics of craze and crack growth in thermoplastic materials.

In the following sections, we discuss the model for representing a craze. The idealizations made to model the problem are explained in Section 2.1. The mathematical formulation including non-dimensionalization and discretization for final implementation then follow in Sections 2.2, 2.3 and 2.4. In Section 3, two alternate methods for computing stress distribution profiles from craze displacement contours are presented for the case of a full craze and for a craze with a central crack. Because of their simplicity, these methods are both computationally more efficient and inherently more accurate (for the same degree of discretization) than those used in the past by

other investigators.

In Section 4.1, the general applicability and performance of the solution algorithm are examined and assessed. Some characteristics of the fibril P-V relations that are inconsistent with realistic craze profiles are identified in Section 4.2. The existence and uniqueness of solutions are addressed; certain interesting conclusions are drawn through use of heuristic arguments.

We next employ the solution scheme developed in Section 2 to investigate how the nonlinear fibril P-V characteristics affect the mechanics of craze and crack growth. The critical crack tip opening displacement (CTOD) is employed in a natural way as a fracture criterion. The applicability of this CTOD criterion to crazes containing cracks is based on experimental evidence and is discussed in the Section 5. We further assume that under quasi-static conditions the fibril P-V relation does not change its character as the craze and crack propagate. This assumption is made for lack of experimental data and because of an inadequate understanding of the fibril behavior at the present time.

Quasi-static propagation of a craze with a central crack is studied in detail in Section 6. In Section 7, we examine the problem of a craze initiating from an existing (precut) crack with special interest on the effect of 'softening' fibril behavior on crack stability. In both analyses, the results for several nonlinear P-V relations are compared and contrasted with the Barenblatt-Dugdale model. Finally, conclusions and suggestions for further work are given in Section 8.

2. PROBLEM FORMULATIONS AND SOLUTIONS

In this section, we reduce the physical problem to a mathematically manageable one through suitable approximations. The resulting equations are non-dimensionalized and solved through a numerical algorithm based on Picard's iteration.

2.1. Geometric and Mathematical Idealization

We consider first the geometry of the problem as depicted in Figure 6a. A craze of length C with an (internal) central crack of length A is embedded in an infinite plate subjected to a remote and uniform tensile stress Σ_∞ applied normal to the major axis of the craze. X,Y are the coordinates and W(X) denotes the Y-displacement of the craze contour. We let P(X) represent the cohesive force (stress) distribution exerted by the fibrils.

As shown by Lauterwasser and Kramer, a craze is formed from a primordial craze, characterized by a contour $W_o(X)$: this contour contains the bulk polymer material which is subsequently transformed into craze fibrils through the surface drawing process [5]. Thus the dashed contour $W_o(X)$ in Figure 6b is displaced in the drawing process to the solid contour W(X) due to the application of Σ_∞. Since we know from experiments that $W_o(X)$ is much smaller than C and that the slope, $W'_o(X)$, is also very small everywhere, we can recast the geometry of the problem as shown in Figure 6c where V(X) is the net displacement of the craze profile caused by the applied stress as measured from $W_o(X)$ so that $V(X) = W(X) - W_o(X)$. Cast in this light, the force-displacement (P-V) relation may be represented schematically as shown in Figure 6d. Keeping in mind that $V < 0$ corresponds to the primordial craze under small strain prior to fibrillation, the dashed portion of the P-V curve is assumed linear with a slope equal to Young's modulus, E, for the bulk polymer. At V=0, the threshold (or fibrillation) stress P_o is reached and henceforth the P-V relation is nonlinear.

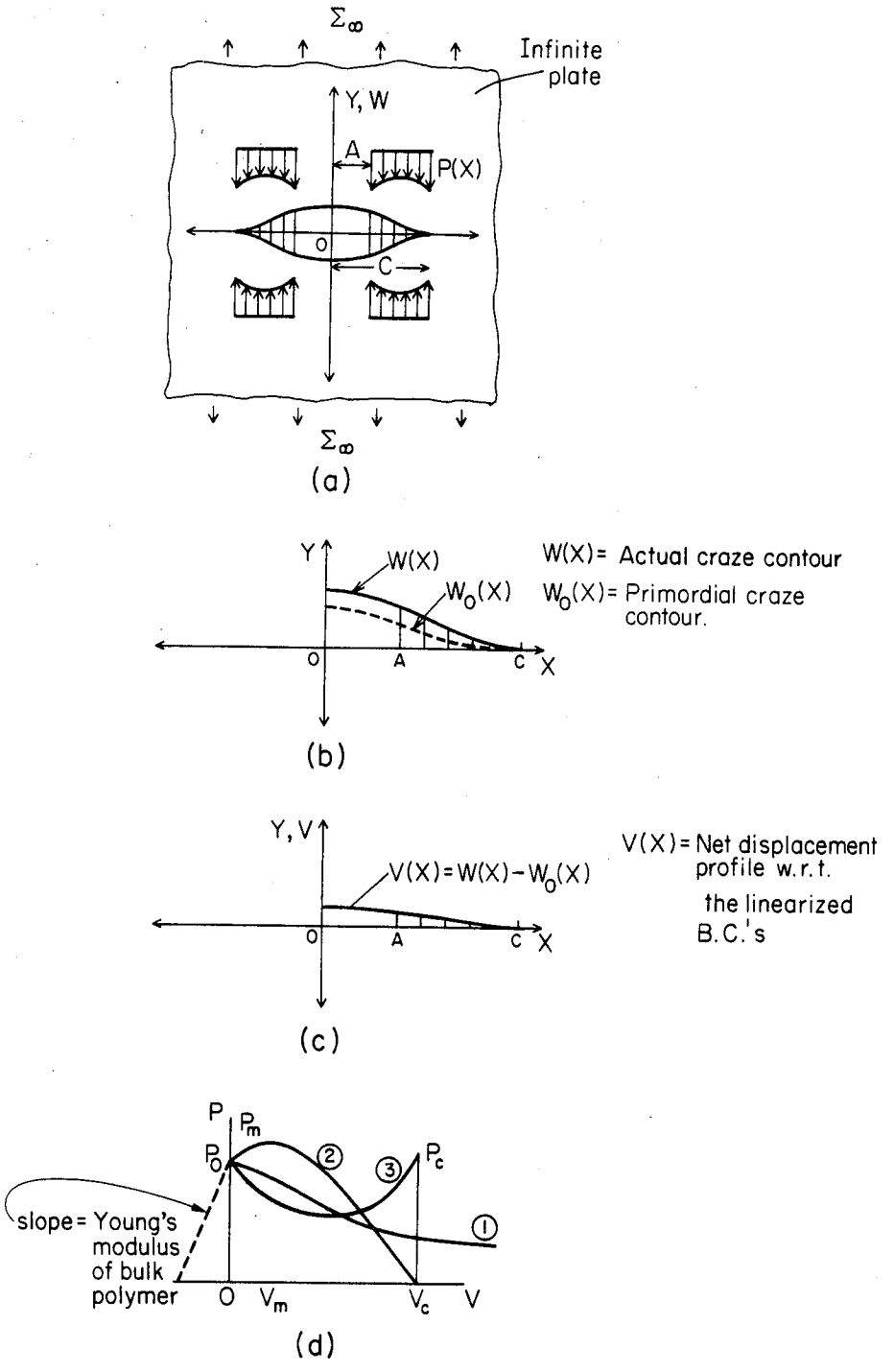

Figure 6. (a) Problem geometry definition
(b) Actual craze contour with primordial craze contour
(c) Linearized geometry: net displacement profile
(d) Model for craze fibril p-v relation

Three P-V relations are illustrated, curve #1 is representative of a craze that does not contain a crack. We shall later refer to such a craze as a 'full-craze'. Curve #2 allows for continued hardening before softening to failure (fibril degradation and rupture) at V_c. Curve #3 is typical of a craze with a central crack; this rehardening behavior may be understood in the context of the midrib behavior [5].[7]

2.2. The Mathematical Formulation

Consider a mathematically sharp crack of length 2C embedded in an infinite elastic medium loaded symmetrically as shown in Figure 7a, by using the Westergaard stress function method [29], the following Green's solutions are obtained

$$V(X) = \left(\frac{1+\eta}{4\mu}\right) \frac{P}{\pi} \log \left| \frac{\sqrt{C^2-X^2}+\sqrt{C^2-T^2}}{\sqrt{C^2-X^2}-\sqrt{C^2-T^2}} \right| \tag{2.1}$$

$$K_I = \frac{2P}{\sqrt{\pi C}} \frac{C}{\sqrt{C^2-T^2}} \tag{2.2}$$

where $\eta = \left(\frac{3-\nu}{1+\nu}\right)$ for plane stress and $(3-4\nu)$ for plane strain; ν= Poisson's ratio; μ= shear modulus = $E/2(1+\nu)$. K_I is the mode-I stress intensity factor, and V(X) is the displacement due to the load P . Note that V(X) is singular at X=T.

Turning now to the problem at hand depicted in Figure 7b, the solutions to the problem can readily be written down by superposition[8]

---

7. The midrib is formed initially at the craze tip due to fibril drawing at high stress. As the craze grows, the midrib is unloaded as it becomes part of the mature (developed) craze. The introduction of a crack in the craze causes the stress at the crack tip to rise, so that the midrib is reloaded and therefore must sustain higher stress.

8. Huang independently employed an identical formulation in studying the size of the crack tip cohesive zone based on an interatomic

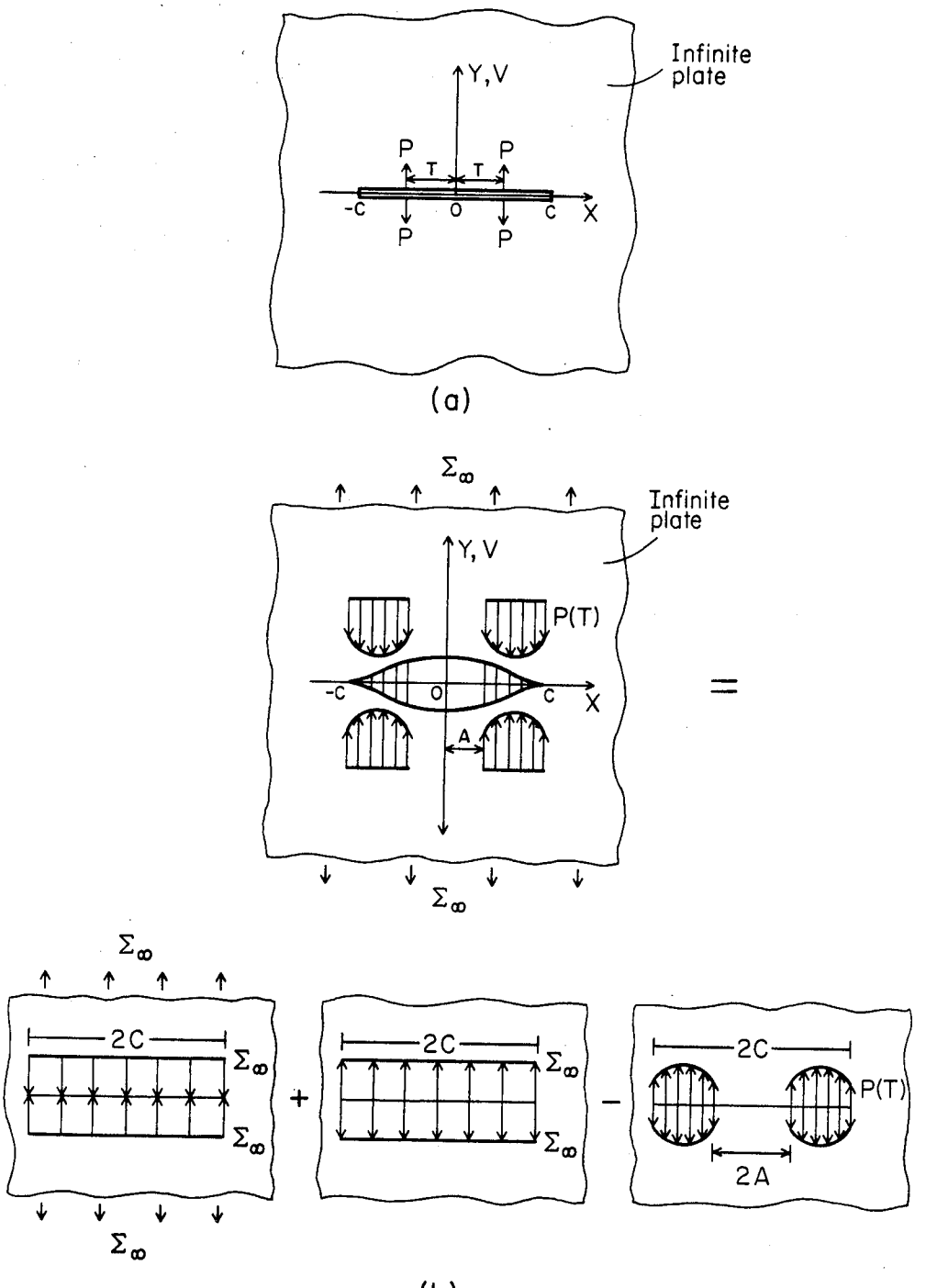

Figure 7. (a) The Green's problem
(b) Decomposition of the craze problem

$$V(X) = \left(\frac{1+\eta}{4\mu}\right) \frac{1}{\pi} \int_0^C (\Sigma_\infty - P(T)) \log \left| \frac{\sqrt{C^2-X^2}+\sqrt{C^2-T^2}}{\sqrt{C^2-X^2}-\sqrt{C^2-T^2}} \right| dT \tag{2.3}$$

$$K_I = 2\sqrt{\frac{C}{\pi}} \left[\int_0^C \frac{\Sigma_\infty - P(T)}{\sqrt{C^2-T^2}} dT \right] \tag{2.4}$$

It is convenient to denote the kernel in equations (2.3) by

$$M(C,X,T) = \frac{1}{\pi} \log \left| \frac{\sqrt{C^2-X^2}+\sqrt{C^2-T^2}}{\sqrt{C^2-X^2}-\sqrt{C^2-T^2}} \right| \tag{2.5}$$

This kernel is integrable in closed-form which proves to be a very useful property in numerical implementation (see Section 2.4). Denoting by I_M, the integral of M, one has

$$I_M \equiv \int M(C,X,T)dT = \frac{1}{\pi} \left[T\log \left| \frac{\sqrt{C^2-X^2}+\sqrt{C^2-T^2}}{\sqrt{C^2-X^2}-\sqrt{C^2-T^2}} \right| - 2\sqrt{C^2-X^2}\cos^{-1}\left(\frac{T}{C}\right) \right.$$

$$\left. + X\log \left| \frac{X\sqrt{C^2-T^2}-T\sqrt{C^2-X^2}}{X\sqrt{C^2-T^2}+T\sqrt{C^2-X^2}} \right| \right] \tag{2.6}$$

Equations (2.3) and (2.4) can be simplified to

$$V(X) = \left(\frac{1+\eta}{4\mu}\right) \left[\Sigma_\infty \sqrt{C^2-X^2} - \int_0^C M(X,C,T)P(T)dT \right] \tag{2.7}$$

$$K_I = \Sigma_\infty \sqrt{\pi C} - 2\sqrt{\frac{C}{\pi}} \int_0^C \frac{P(T)}{\sqrt{C^2-T^2}} dT \tag{2.8}$$

Clearly, for P(T) = 0, we recover the familiar crack solutions

---

potential [30].

$$V(X) = \left(\frac{1+\eta}{4\mu}\right) \Sigma_\infty \sqrt{C^2-X^2}$$

$$K_I = \Sigma_\infty \sqrt{\pi C}$$

For the stress at the craze tip to be finite, or equivalently, for the craze tip to close smoothly, i.e., $V'(C) = 0$, it is necessary and sufficient that K_I vanish. Then (2.8) gives

$$\Sigma_\infty = \frac{2}{\pi} \int_0^C \frac{P(T)}{\sqrt{C^2-T^2}}\, dT \tag{2.9}$$

Substituting Σ_∞ from (2.9) into (2.7), one obtains

$$V(X) = \left(\frac{1+\eta}{4\mu}\right) \int_0^C \left[\frac{2}{\pi} \sqrt{\frac{C^2-X^2}{C^2-T^2}} - M(C,X,T) \right] P(T)\, dT$$

or

$$V(X) = \left(\frac{1+\eta}{4\mu}\right) \int_0^C H(C,X,T)\, P(T)\, dT \tag{2.10}$$

where

$$H(C,X,T) = \frac{2}{\pi} \sqrt{\frac{C^2-X^2}{C^2-T^2}} - M(C,X,T) \tag{2.11}$$

The formulation is completed by specifying the fibril force-displacement behavior

$$P(X) = P[V(X)] \tag{2.12}^9$$

Equations (2.10) and (2.12) must be solved simultaneously. This is

9. The more general case, $P(X) = P[V(X),X]$ can be handled within the

accomplished by using Picard's method of successive approximation outlined below[10]

We start with an initial guess of the form,

$$V^{o}(X) = \Sigma_{\infty}^{o}(C - X)^{R} \tag{2.13}$$

where Σ_{∞}^{o} and R are to be appropriately chosen. Of course, other forms of $V^{o}(X)$ are also acceptable.

The k^{th} approximation is given by

$$V^{k}(X) = \left(\frac{1+\eta}{4\mu}\right) \int_{o}^{C} H(C,X,T)P(V^{k-1}(T))dT \; ; \quad k = 1,2,... \tag{2.14}$$

We consider that a solution has been attained when $V^{k}(X)$ differs from $V^{k-1}(X)$ at all (discretized) points by 0.1% or less. The convergence of the scheme is found to be relatively insensitive to the choice of the initial guess of Σ_{∞}^{o} and R as will be demonstrated in Section 3.1.

It is worthwhile to note that in the case where a crack is present as determined by the critical crack tip opening displacement (CTOD) criterion (see Section 4 for further discussion), the crack length is not fixed a priori but is obtained as part of the solution.[11] We next non-dimensionalize the relevant parameters prior to discretization for

---

framework of our formulation using the same solution scheme. A P-V relation with explicit dependence on X is a more realistic candidate; however due to lack of any such data, we confine our attention to the form (2.12).

10. As it turns out, this simple scheme is more efficient than the Newton iterative scheme which was also implemented and yielded the same results.

11. In all past contributions, the crack and craze lengths were fixed a priori as no consistent fracture criterion was employed.

numerical implementation.

2.3. Non-dimensionalization

For presentation of the results, it is helpful to non-dimensionalize pertinent parameters. We let a craze length C_o be the reference length scale. The stresses are scaled by $(\frac{4\mu}{1+\eta})$; in this fashion, the Poisson's ratio is absorbed for both cases of plane stress or plane strain. In short,

$$C_{ref} = C_o$$

$$\Sigma_{ref} = \mu(1+\nu) = \frac{E}{2} \qquad \text{for planestress}$$

$$\frac{\mu}{(1-\nu)} = \frac{E}{2(1-\nu^2)} \qquad \text{for plane strain}$$

We shall use lower case letters for dimensionless quantities and define

$$c \equiv \frac{C}{C_o}, \quad a \equiv \frac{A}{C_o}, \quad x \equiv \frac{X}{C_o}, \quad y \equiv \frac{Y}{C_o}$$

$$w \equiv \frac{W}{C_o}, \quad w_o \equiv \frac{W_o}{C_o}, \quad v \equiv \frac{V}{C_o}, \quad \tau \equiv \frac{T}{C_o}$$

and, $\sigma_\infty \equiv \frac{\Sigma_\infty}{\Sigma_{ref}}, \quad p \equiv \frac{P}{\Sigma_{ref}}$

Thus, in dimensionless forms, equations (2.9), (2.10), and (2.12) become

$$\sigma_\infty = \frac{2}{\pi} \int_o^c \frac{p(\tau)}{\sqrt{c^2-\tau^2}}\, d\tau \tag{2.9a}$$

$$v(x) = \int_o^c h(c,x,\tau)p(\tau)d\tau \tag{2.10a}$$

$$p(x) = p[v(x)] \tag{2.12a}$$

Other equations can be easily non-dimensionalized by simply replacing each upper case letter by a lower case one and removing $(\frac{1+\eta}{4\mu})$. Having done this, we are ready to discretize the equations for numerical

implementation.

2.4. Discretization and the Resulting Algorithm

Because the kernels M(C,X,T) and H(C,X,T) defined by (2.5) and (2.11) can be evaluated in closed forms, the integration of these 'singular' integrals can be performed very accurately without requiring excessive subdivisions of the domain.[12] We discretize the domain of integration into n equal intervals of length Δx as shown in Figure 8, where

$$\Delta x = \Delta \tau = c/n$$

and x_i, τ_i, v_i, p_i are evaluated at the center point of each interval. With this in mind, an integral I(x) can be approximated as[13]

$$I(x_i) \equiv \int_0^c f(c,x_i,\tau)\cdot p(\tau)d\tau \equiv \bar{f}_j(c,x_i)p_j = \bar{f}_{ij}p_j \qquad (2.15)$$

where

$$\bar{f}_{ij} \equiv \bar{f}_j(c,x_i) \equiv \int_{\tau_j-\Delta\tau/2}^{\tau_j+\Delta\tau/2} f(c,x_i,\tau)\, d\tau \qquad (2.16)$$

Integrals of the form (2.16) in this study are easily evaluated in closed forms; specifically, from (2.7) and (2.6), one obtains

$$v_i = v(x_i) = \sigma_\infty \left| \sqrt{c^2-x_i^2} - \int_0^c m(c,x_i,\tau)p(\tau)d\tau \right.$$

or

12. For contributions about the singular points, the Cauchy Principal values of the integrals are used.

13. Repeated indices indicate summation from 1 to n.

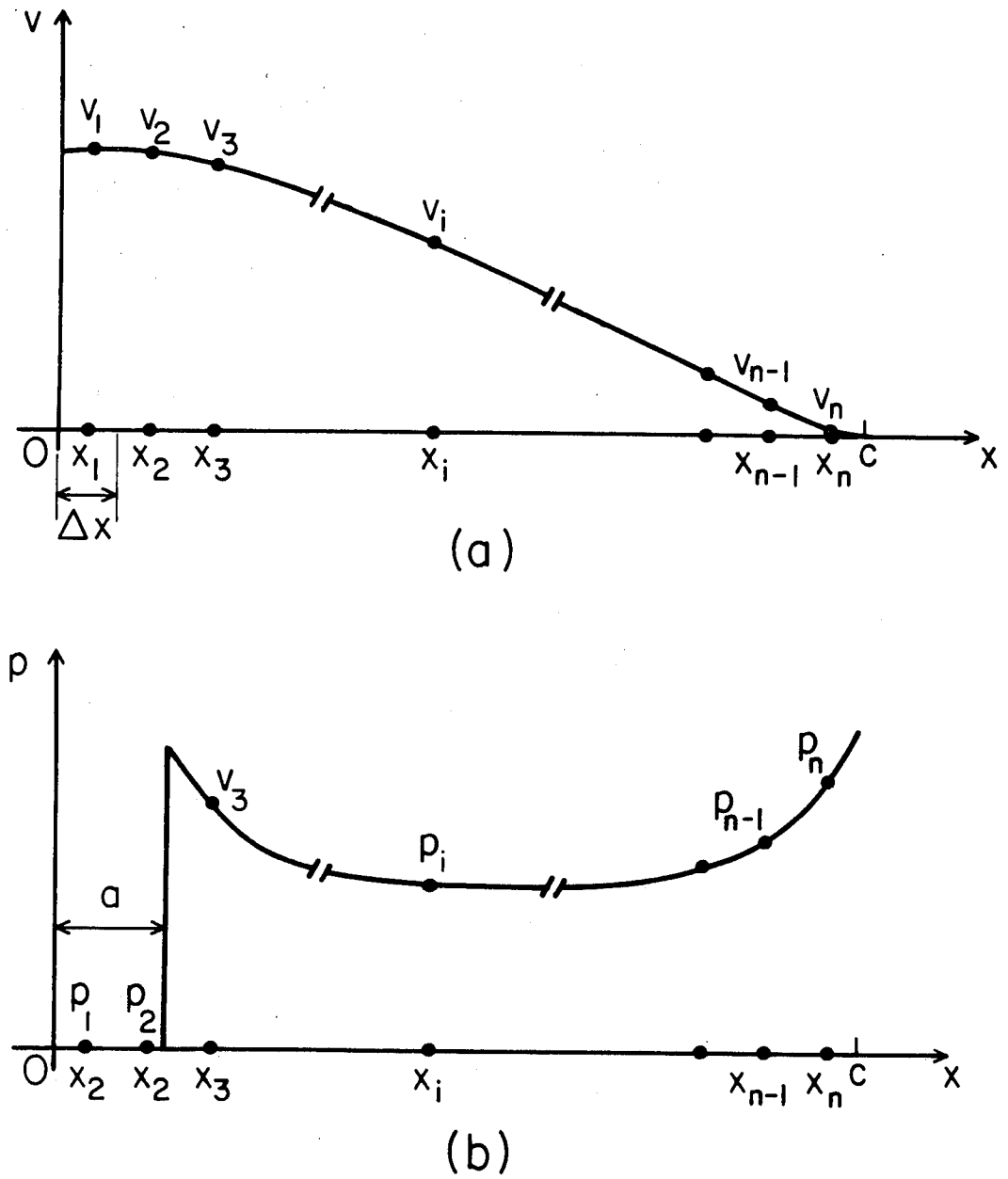

Figure 8. (a,b) Discretization scheme for numerical implementation.

$$v_i = \sigma_\infty \sqrt{c^2-x_i^2} - \bar{m}_{ij} p_j \tag{2.17}$$

where

$$\bar{m}_{ij} \equiv \int_{\tau_j-\Delta\tau/2}^{\tau_j+\Delta\tau/2} m(c,x_i,\tau)\,d\tau \equiv \frac{1}{\pi} \int_{\tau_j-\Delta\tau/2}^{\tau_j+\Delta\tau/2} \log \left| \frac{\sqrt{c^2-x_i^2}+\sqrt{c^2-\tau^2}}{\sqrt{c^2-x_i^2}-\sqrt{c^2-\tau^2}} \right| d\tau$$

or

$$\bar{m}_{ij} \equiv \frac{1}{\pi} \left[\tau \log \left| \frac{\sqrt{c^2-x_i^2}+\sqrt{c^2-\tau^2}}{\sqrt{c^2-x_i^2}-\sqrt{c^2-\tau^2}} \right| - 2\sqrt{c^2-x_i^2}\cos^{-1}\left(\frac{\tau}{c}\right) \right.$$

$$\left. + x_i \log \left| \frac{x_i\sqrt{c^2-\tau^2}-\tau\sqrt{c^2-x_i^2}}{x_i\sqrt{c^2-\tau^2}+\tau\sqrt{c^2-x_i^2}} \right| \right]_{\tau=\tau_j-\Delta\tau/2}^{\tau=\tau_j+\Delta\tau/2} \tag{2.18}$$

Similarly, (2.9) may be written as

$$\sigma_\infty = \int_0^c l(c,\tau)p(\tau)\,d\tau = \bar{I}_j p_j \tag{2.19}$$

where $l(c,\tau) = \frac{2}{\pi} \frac{1}{\sqrt{c^2-\tau^2}}$ and

$$I_j \equiv \int_{\tau_j-\Delta\tau/2}^{\tau_j+\Delta\tau/2} l(c,\tau)\,d\tau = \frac{2}{\pi}\left[\sin^{-1}\left(\frac{\tau}{c}\right)\right]_{\tau=\tau_j-\Delta\tau/2}^{\tau=\tau_j+\Delta\tau/2} \tag{2.20}$$

In view of (2.17)-(2.20), (2.10), and (2.11), we obtain in compact form,

$$v_i \equiv v(x_i) = \int_0^c h(c,x_i,\tau)p(\tau)d\tau = \bar{h}_{ij}p_j \tag{2.21}$$

where

$$\bar{h}_{ij} \equiv \int_{\tau_j-\Delta\tau/2}^{\tau_j+\Delta\tau/2} h(c,x_i,\tau)p(\tau)d\tau$$

$$\equiv \int_{\tau_j-\Delta\tau/2}^{\tau_j+\Delta\tau/2} \left[\sqrt{c^2-x_i^2}\, l(c,\tau) - m(c,x_i,\tau) \right] d\tau$$

$$\bar{h}_{ij} \equiv \sqrt{c^2-x_i^2}\, \bar{l}_j - \bar{m}_{ij} \tag{2.22}$$[14]

$$\bar{h}_{ij} \equiv \frac{1}{\pi}\left[\tau \log \left| \frac{\sqrt{c^2-x_i^2}-\sqrt{c^2-\tau^2}}{\sqrt{c^2-x_i^2}+\sqrt{c^2-\tau^2}} \right| \right.$$

$$\left. + x_i \log \left| \frac{x_i\sqrt{c^2-\tau^2}+\tau\sqrt{c^2-x_i^2}}{x_i\sqrt{c^2-\tau^2}-\tau\sqrt{c^2-x_i^2}} \right| \right]_{\tau=\tau_j-\Delta\tau/2}^{\tau=\tau_j+\Delta\tau/2} \tag{2.23}$$

It turns out that, from equations (2.18), (2.20), and (2.23), $\bar{l}_j$ is independent of c while $\bar{m}_{ij}$ and $\bar{h}_{ij}$ are homogeneous in c. These properties prove to be very useful when we employ the numerical algorithm to study craze and crack growth in Sections 6 and 7. In concise form, one has

---

14. Note that the matrix $\bar{h}_{ij}$ is singular, i.e., given a displacement profile v(x), the cohesive stress profile can only be determined up to an additive constant. This, however, does not affect the validity of our algorithm.

$$\bar{l}_j = \bar{l}_j(c,n) = \bar{l}_j(1,n) \tag{2.24}$$

$$\bar{m}_{ij} = \bar{m}_{ij}(c,n) = c \cdot \bar{m}_{ij}(1,n) \tag{2.25}$$

$$\bar{h}_{ij} = \bar{h}_{ij}(c,n) = c \cdot \bar{h}_{ij}(1,n) \tag{2.26}$$

Thus, for a given degree of discretization n , $\bar{l}_j$, $\bar{m}_{ij}$ and $\bar{h}_{ij}$ only need to be computed once for c=1 and stored for later use. In the simulation of craze and crack growth in Sections 6 and 7, c increases continually, thus the properties exhibit in (2.24)-(2.26) reduce the computation time substantially. Note that $\bar{l}_j$, $\bar{m}_{ij}$ and $\bar{h}_{ij}$ are independent of the p-v relation considered.

The algorithm can now be summarized. Given a craze length c and a p-v relation, we seek solutions in the form of p(x), v(x) and σ_∞ according to the following procedure:

Prescribed p-v relation : $p(x_i) = p_i = p(v(x_i)) = p(v_i)$ (2.27a)

Initial guess : $v^o(x_i) = v_i^o = \sigma_\infty^o (c-x_i)^R$ (2.27b)

k^{th}-iteration : $v_i^k = v^k(x_i) = \bar{h}_{ij}(c,n)p(v_j^{k-1})$ (2.27c)

$$p_i^k = p(v_i^k) \tag{2.27d}$$

$$\sigma_\infty^k = \bar{l}_j p_j^k \tag{2.27e}$$

Convergence is considered achieved when the minimum change for any v_j is less than 0.1% between two successive iterations.

3. SCHEMES FOR DETERMINING STRESS PROFILES FROM DISPLACEMENT PROFILES

As mentioned in the introduction, for the case of a full craze, the stress distribution profile $p(x)$ may be obtained from the measured displacement profile $v(x)$ and σ_∞ using the Fourier transform method [19]. However, for a craze with a central crack, only the displacement profile in the craze zone is needed to determine both $p(x)$ and σ_∞ using a distributed dislocation scheme [22]. Here we present two alternative methods for determining the stress profiles based on the formulation in the previous section; one method is suitable for a full craze, the other for a craze containing a central crack. Both schemes have been fully tested and found to be numerically more efficient than the methods previously proposed [5,22,24,25].

First we discuss the method suitable for the problem of a full craze. Given $v(x_i)$ and σ_∞, equation (2.17) can be rewritten as

$$\bar{m}_{ij} p_j = (\sigma_\infty \sqrt{c^2 - x_i^2} - v_i) \tag{3.1}$$

Equation (3.1) is a system of n linear equations from which p_j can be determined either by Gaussian elimination or by inverting $\bar{m}_{ij}$. In the latter case, (3.1) and (2.25) gives

$$p_j = \bar{m}^{-1}_{ij}(c,n)\ (\sigma_\infty \sqrt{c^2 - x_i} - v_i) \tag{3.2}$$

where

$$\bar{m}^{-1}_{ij}(c,n) = \bar{m}^{-1}_{ij}(1,n)/c \tag{3.3}$$

Note that $\bar{m}^{-1}_{ij}(1,n)$ only needs to be computed once and stored for later use.

For demonstration purposes, this scheme is applied to v(x) and σ_∞ as presented in reference 5 (see Figure 9). The resulting cohesive force distribution p(x) shown in Figure 10 and that derived in [5] through the Fourier Transform method are virtually identical. The p-v relation obtained by combining Figures 9 and 10 is plotted in Figure 11.

This method is, of course, also applicable to a craze with an internal crack. However, since the measured displacement profiles in the crack region are usually not reliable on a point-by-point basis (see [22]), an alternative scheme using only the displacement profile in the craze zone as boundary data is preferable. Such a method has been presented by Kramer and Wang [22]; however, the method requires differentiation of the experimentally measured displacement profile which incurs additional error. In view of this shortcoming, we present here a scheme which requires as inputs only the displacement v_j in the craze zone and the crack tip location. The outputs are the stress profile p(x), the applied stress σ_∞ and the displacement in the crack region.

Let i_t be such that the fibril cohesive force at the i^{th} station is

$$\begin{aligned} p_i &= 0 \qquad \text{for} \qquad i < i_t \\ p_i &\neq 0 \qquad \text{for} \qquad i \geq i_t \end{aligned} \tag{3.4}$$

Given the displacement in the craze zone, v_i for $i \geq i_t$, we wish to find σ_∞ and p_i for $i \geq i_t$ and v_i for $i < i_t$. Consider equation (2.21),

$$v_i = \bar{h}_{ij} p_j \ , \qquad i,j = 1,2,\ldots,n \tag{2.21}$$

In light of (3.4), (2.21) reduces to

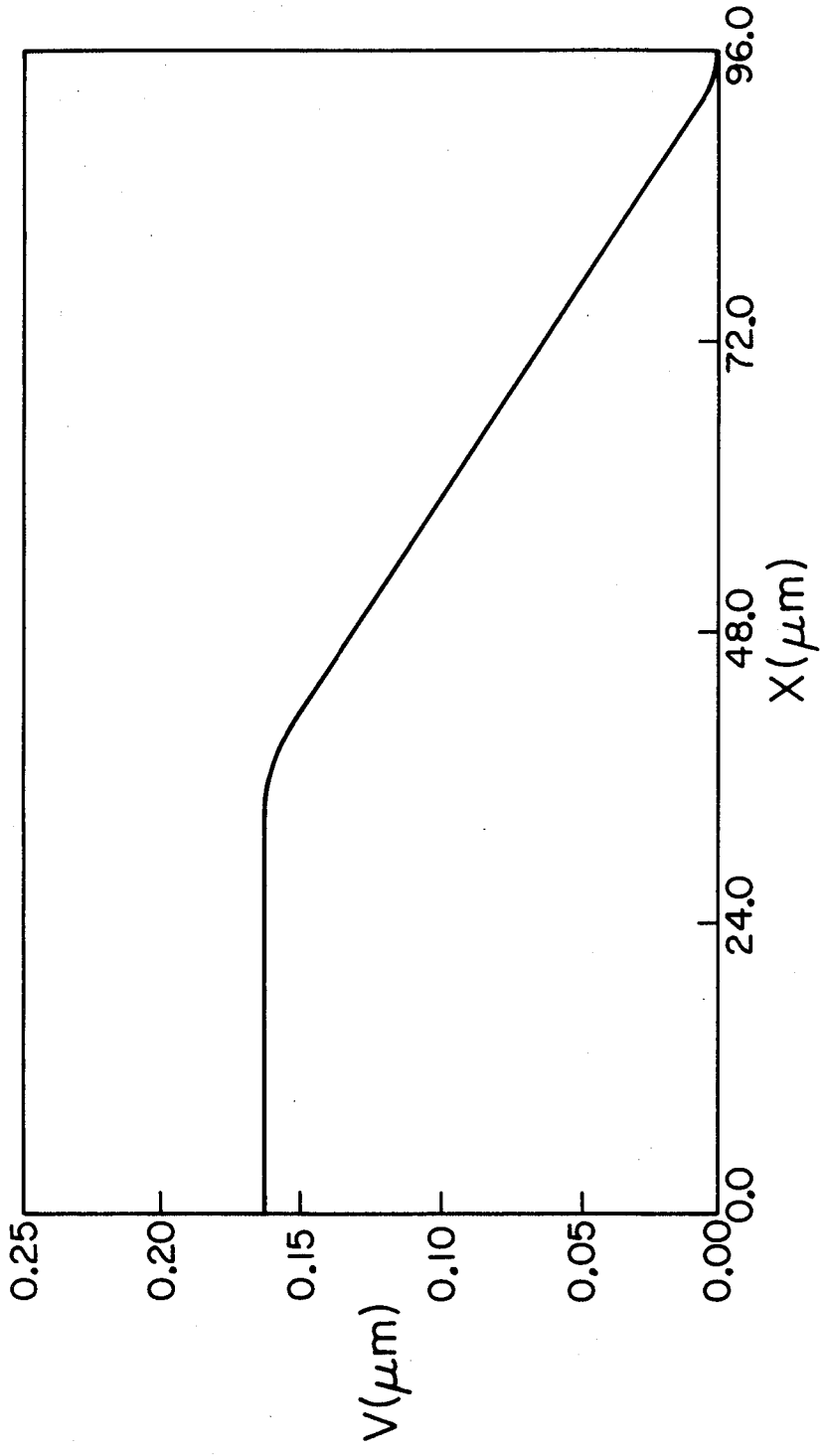

Figure 9. Experimental craze contour from reference 5.

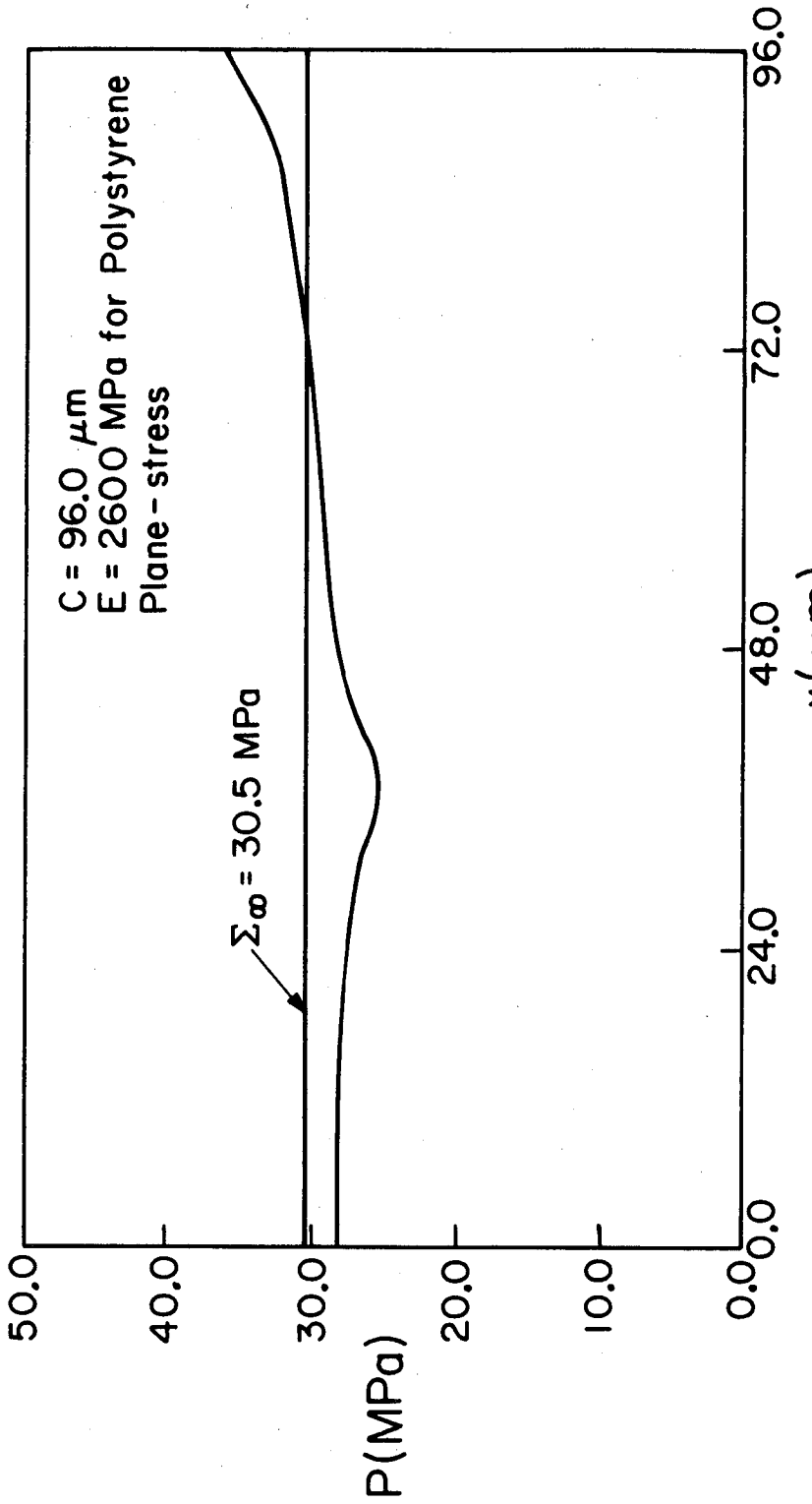

Figure 10. Stress distribution profile derived from V(X) in Figure 9 using the method in Section 3.

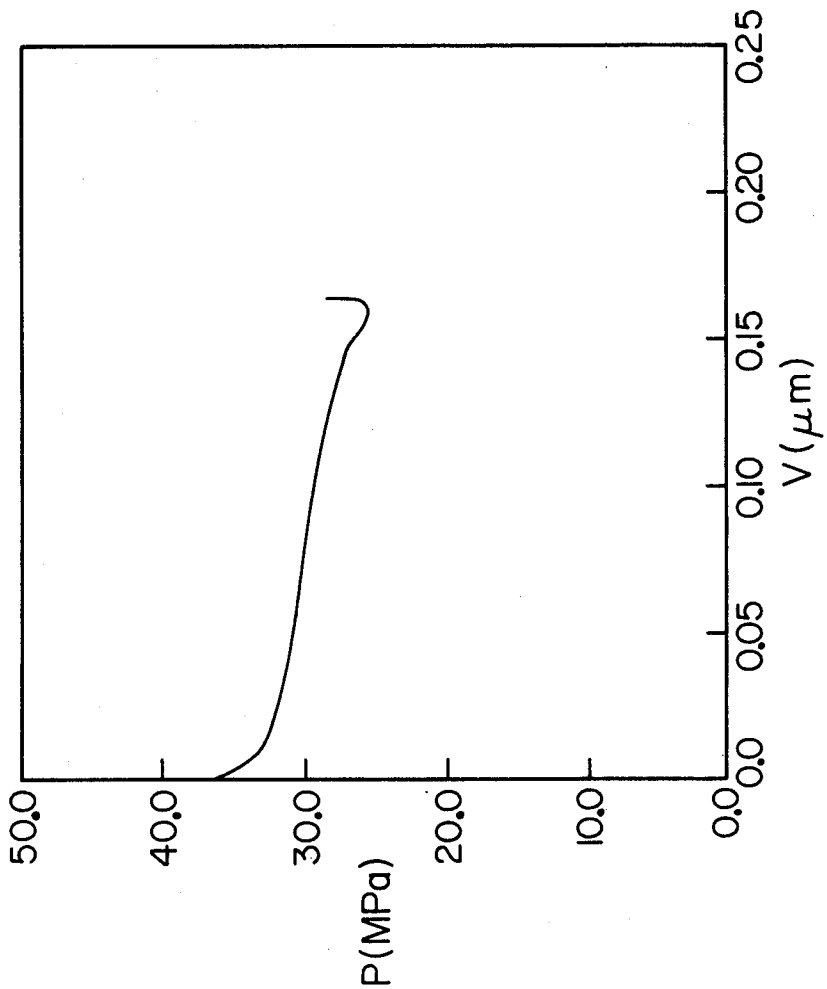

Figure 11. The p-v relation derived from Figures 9 and 10.

$$v_l = 0 \quad ; \qquad l = 1,2,\ldots,i_t-1 \tag{3.5a}$$

$$v_l = \bar{h}_{lk}p_k \; ; \qquad l,k = i_t, i_t+1,\ldots,n \tag{3.5b}$$

Equation (3.5b) can be solved for p_k, $k = i_t,\ldots,n$, by Gaussian elimination. Then by (2.19) and (2.21)

$$\sigma_\infty = \bar{l}_j p_j = \bar{l}_k p_k \; , \qquad k = i_t,\ldots,n \tag{3.6}$$

$$v_i = \bar{h}_{ik}p_k \; , \qquad i = 1,\ldots,i_t-1 \;\text{ and }\; k = i_t,\ldots,n \tag{3.7}$$

This completes the presentation of the two alternative schemes for computing p(x) from v(x).

4. THE CHARACTERISTICS OF THE ALGORITHM AND THE p-v RELATION

We examine next two aspects of the craze problem from a general viewpoint. First we report on the convergence characteristics of the algorithm and attempt to give some broad criteria on its applicability and effectiveness. Then two models of p-v relations are studied with the aim of determining how the existence of a solution depends on the nonlinearity of the p-v relation. The findings indicate that there are restrictions on the characters of the p-v relations if realistic craze profiles are to result, i.e., profiles with nonnegative (non-interpenetrating) displacements at all points.

4.1. The Convergence of the Algorithm

Having discussed the algorithm and the convergence criterion in Sections 2.2 and 2.4, we proceed to consider the characteristics of the algorithm as applied to specific problems. In Figures 12-15, we show how the solutions v(x) and p(x) for a half-cosine p-v relation[15] are approached using two different initial guesses of the form

$$v^0(x) = \sigma_\infty^0 (c - x)^R$$

where in these examples, the initial guesses are $\sigma_\infty^0 = 0.05$ and 0.01 with R = 1.5. For $\sigma_\infty^0 = 0.05$, nine iterations are required for convergence and the results are presented in Figures 12 and 13. In Figures 14 and 15, σ_∞^0 is 0.01 and twelve iterations are needed for convergence. (Each iteration takes about 1.2 CPU seconds on a VAX 11-780.) The solution for σ_∞ is 0.0176. Again, a displacement tolerance of 0.1% is used as the convergence criterion. For n=200, we find that checking for convergence at only 20 or 100 equi-spaced points give identical results to checking at all 200 points. This is because the convergence is quite uniform for most p-v relations as is illustrated in Figures 12-

15. Specifically, the p-v relation #1 in Figure 28 is used.

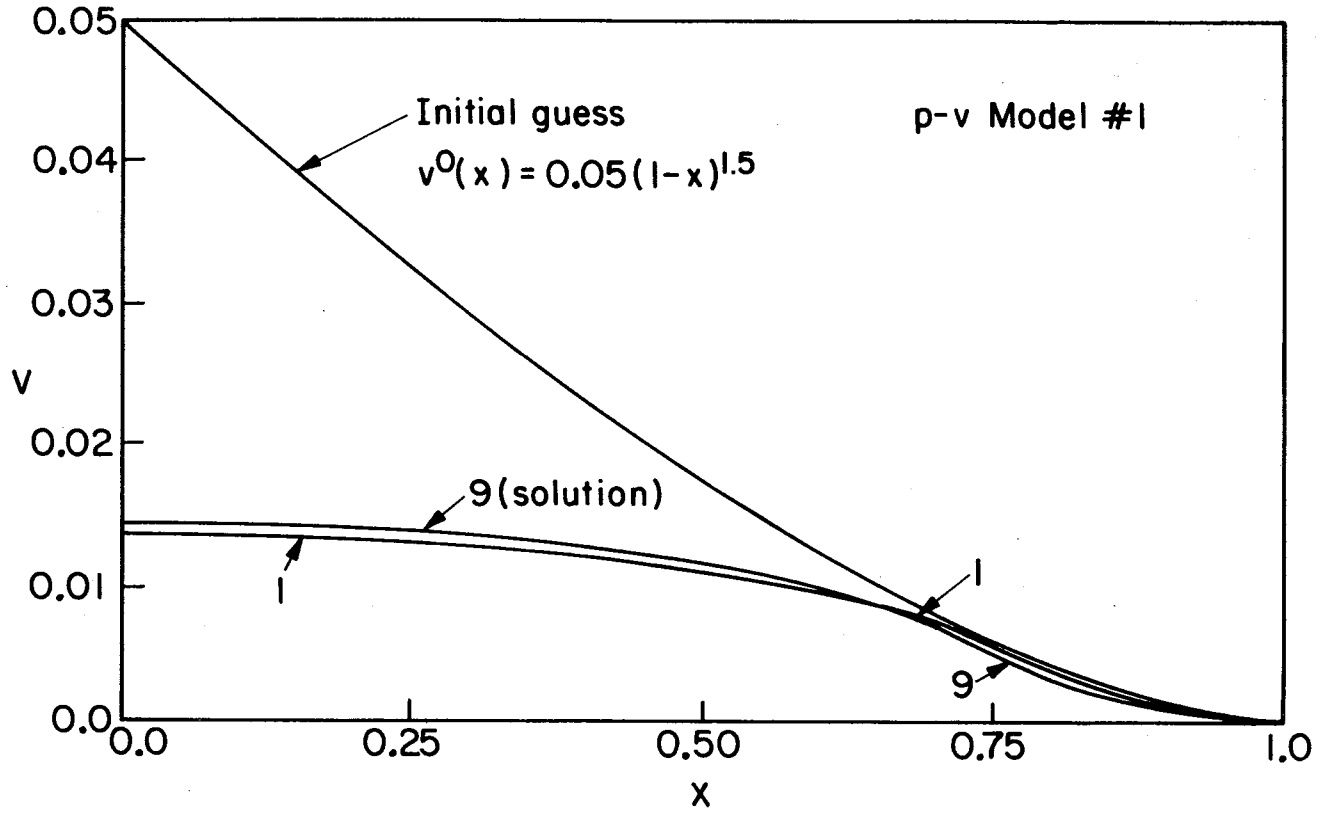

Figure 12. Convergence illustration v versus x ($\sigma_\infty^0 = 0.05$, R = 1.5). Iterations # 2-8 are confined in between iterations # 1 & 9.

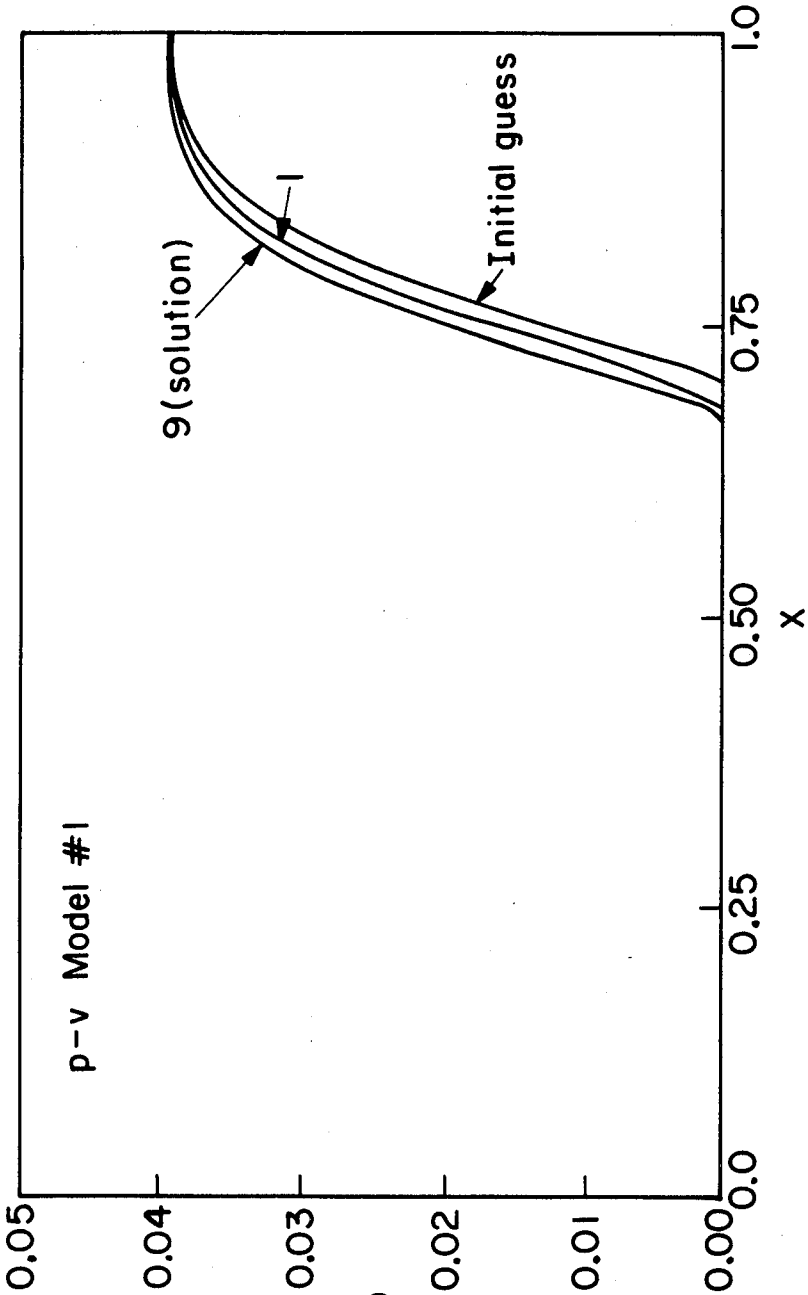

Figure 13. Convergence illustration p versus x (σ_∞^o = 0.05, R = 1.5). Iterations # 2-8 are confined in between iterations # 1 & 9.

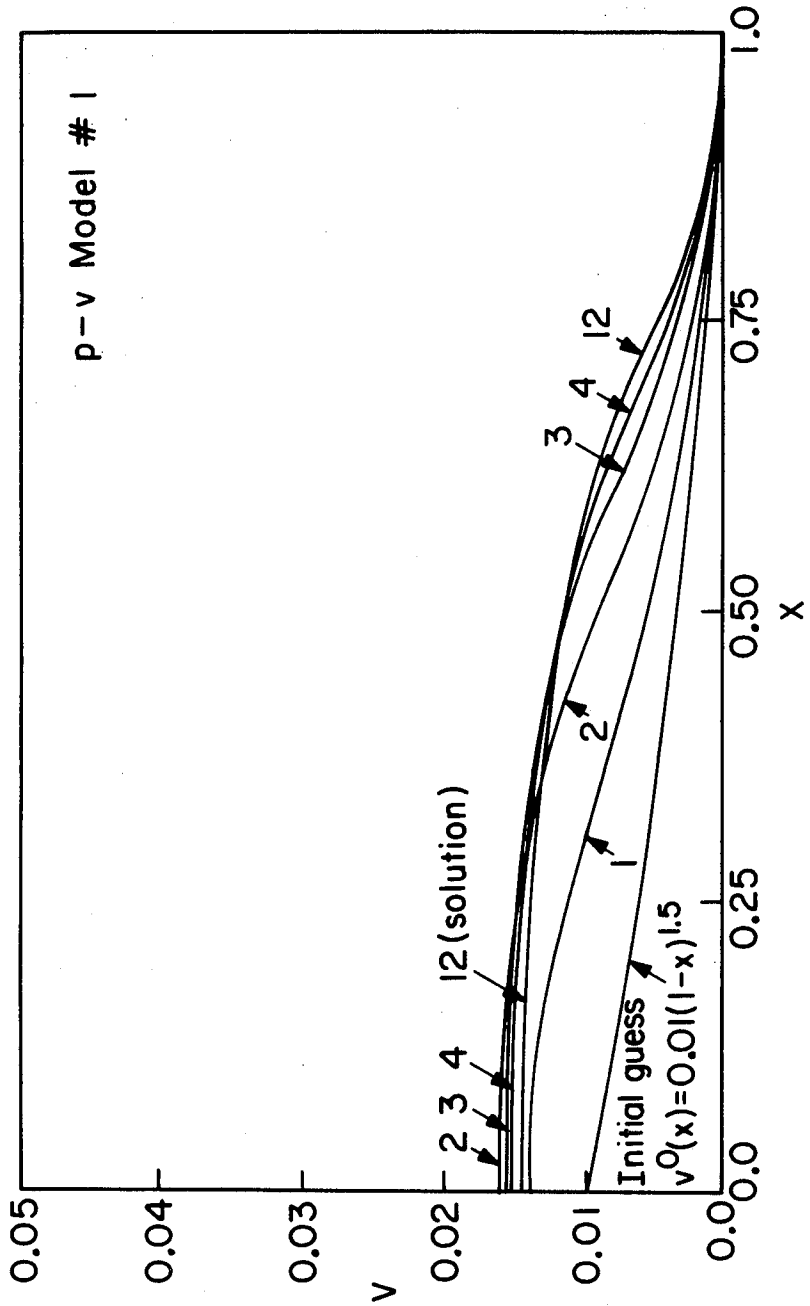

Figure 14. Convergence illustration v versus x (σ_∞^0 = 0.01, R = 1.5). Iterations # 5-11 are confined in between iterations # 4 & 12.

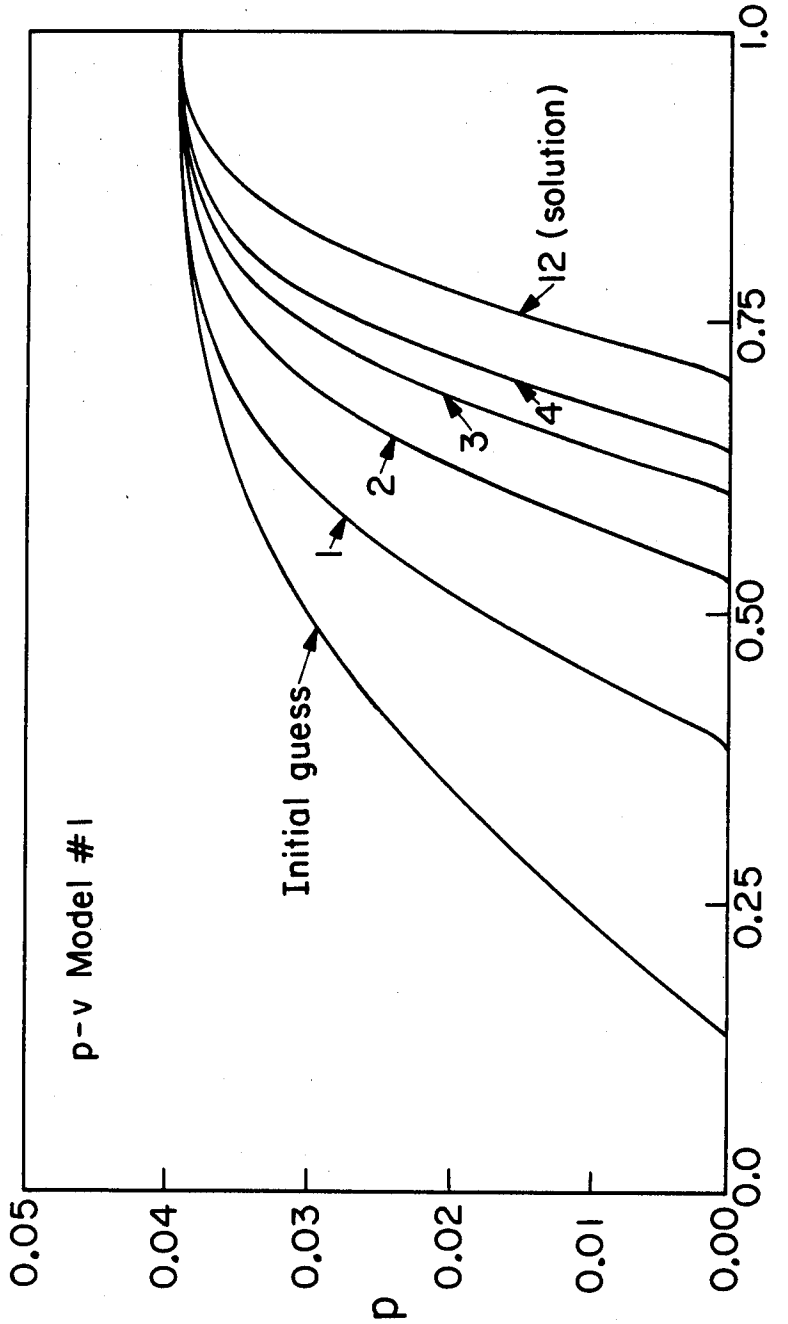

Figure 15. Convergence illustration p versus x (σ^0_∞ = 0.01, R = 1.5). Iterations # 5-11 are confined in between iterations # 4 & 12.

15. Throughout this work, we conservatively use 100 checkpoints for n=200.[16]

With regard to the general applicability of the algorithm, we find that the initial guess does not need to be very close to the correct solution for the scheme to work as illustrated in Figures 12-15. It is found that the exponent 'R' in equation (2.27b) for the initial guess $v^0(x)$ may range from 0.5 to 2.0 but R = 1.5 seems to work best in most instances. When there is no solution such as those situations to be discussed later in Section 4.2, the algorithm quickly diverges for a wide range of initial guesses. For p-v relations which soften initially and then reharden such as model #6 in Figure 28, the convergence could be very slow and 30-70 iterations may be required, depending on the initial guess.

In cases where the algorithm did not converge, the Newton iterative scheme was tried but did not yield convergence either. Per iteration, the Newton scheme takes about 250 times the CPU time needed for Picard's method (for n=200). For all cases studied Picard's iterative scheme yielded the same results as the Newton method.

4.2. The Characteristics of Admissible p-v Relations

In the following, we examine how the various characteristics of a given nonlinear p-v relation affect the existence of a solution. This issue is of considerable importance as little is known regarding the fibril p-v behavior that is consistent with observed craze displacement profiles. When improper p-v behaviors are used, the results obtained are necessarily incorrect as discussed in Section 1 concerning recent works in references 26 and 27. (E. Smith [17] and Knauss [20] presented some admissible p-v relations for the crack tip cohesive

16. We tried n=50, 100, 200, 300, 400, 500 and found n=200 to be the best compromise between the integration accuracy (within 0.0001%) and the computing time.

zone.)

In the present study, we find that there are certain restrictions on the p-v relations for the algorithm to converge. Heuristic arguments, such as the ones presented in connection with the findings (1) and (2) below, were used to demonstrate that the proposed algorithm is capable of seeking out a solution for a given p-v relation and craze length, if such a solution exists. Otherwise, our numerical studies show it to be most likely that algorithm divergence indicates the absence of a solution. The question of uniqueness is then addressed.

Consider the two families of p-v relations depicted in Figure 16.[17] The two models are designated A and B respectively. Analytically, they are given by

Model A:

$$p(v) = \begin{cases} p_o + (p_m - p_o)\left(\frac{v}{v_m}\right) & \text{for } 0 \le v \le v_m \\ p_m\left(\frac{v-v_c}{v_m-v_c}\right) & \text{for } v_m \le v \le v_c \\ 0 & \text{for } v \ge v_c \end{cases} \tag{4.1}$$

Model B:

17. Note that in both models, the fibril stress vanishes for displacements greater than a critical value v_c ; we thus deal with a critical crack tip opening displacement (CTOD) criterion which can be justified on physical grounds as is discussed at length in Section 5.1.

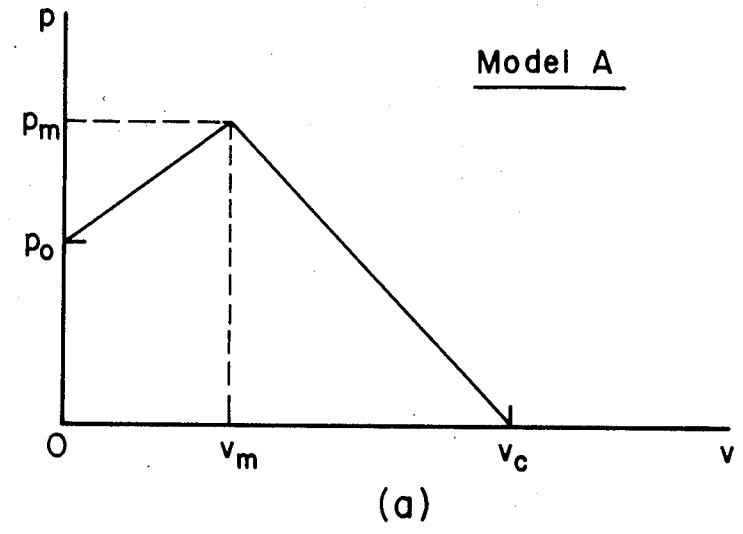

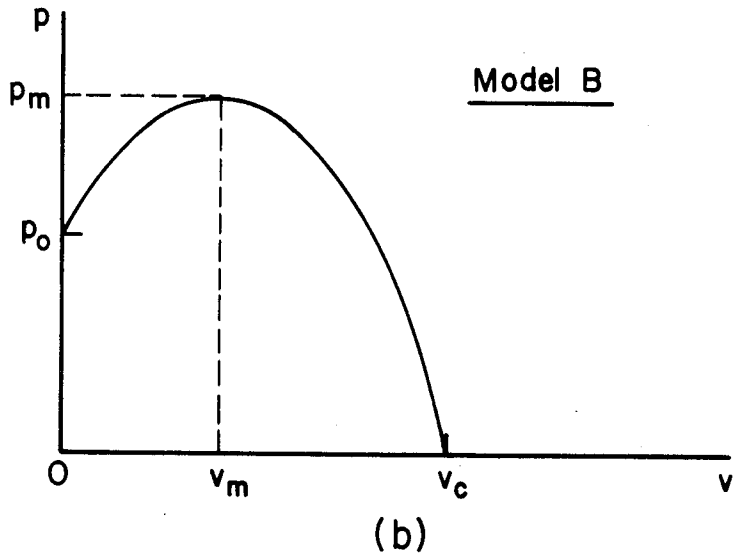

Figure 16. Two p-v relations used in studying characteristics of 'admissible' p-v relations.
(a) piecewise-linear model
(b) cosine model

$$p(v) = \begin{cases} p_m \cos\{\frac{\pi}{2}(\frac{v-v_m}{v_c-v_m})\} & \text{for } 0 \le v \le v_c \\ 0 & \text{for } v \ge v_c \end{cases} \qquad (4.2)$$

Both models are designed so as to allow the relative amount of hardening and softening in the p-v behavior to be adjusted by varying a few parameters. It is easy to see that v scales with c, thus we need only study the case c = 1. Based on the convergence criterion stated at the end of Section 2.2, the findings regarding the restrictons on the p-v relations are summarized below:

Case A.1: $p_o = p_m = 1.0$, $v_m = 0$; vary v_c
for $0 < v_c \le 0.36$: convergence to solutions with cracks
for $v_c \ge 0.37$: convergence to the trivial solution where $p(x) = 1.0$ and $v(x) = 0.0$ for all x

Case A.2: $p_o = 0.5$, $p_m = 1.0$, $v_m = 0.05$; vary v_c
for $0 < v_c \le 0.11$: convergence to solutions with cracks
for $v_c \ge 0.12$: divergence - no solution

Case A.3: $p_m = 1.0$, $v_m = 0.15$; $v_c = 0.3$; vary p_o
for $p_o \ge 0.97$: convergence to solutions with cracks
for $p_o \le 0.96$: divergence - no solution

Case B.1: $p_m = 1.0$, $v_m = 0.0$; vary v_c
for $0 < v_c \le 0.35$: convergence to solutions with cracks
for $v_c \ge 0.36$: convergence to the trivial solution as in Case A.1

Case B.2: $p_m = 1.0$, $v_c = 0.3$; vary v_m
for $0 < v_m \le 0.058$: convergence to solutions with cracks
for $v_m \ge 0.059$: divergence - no solution

All these variations are presented graphically in Figure 17. Qualitatively, the following conclusions are drawn:

(1) Monotonically softening p-v relations as in cases A.1 and B.1: We observe that when v_c exceeds certain values, only the trivial solution results, otherwise a nontrivial solution exists. In other words, the parameter $\frac{(v_c/c)}{p_o}$ determines the existence of a nontrivial solution.

To support the above conclusion, consider the following heuristic argument: When the algorithm yields the trivial solution for a prescribed p-v relation and a given craze length, there exist only two possibilities.

The first possibility is that as the parameter $\frac{(v_c/c)}{p_o}$ increases (v_c increases), we have a craze with a shorter and shorter crack or no crack at all and there no longer exists a nontrivial pair of p(x) and v(x) that simultaneously satisfies equation (2.21) and the prescribed p-v relation. This simply tells us that a different p-v relation or a p-v relation with explicit dependence on x must be considered for the short crack and the full craze solution regimes.

The other possibility is that while a nontrivial solution may exist, our algorithm fails to seek it out. Such a solution, if it indeed exists, must correspond to a very thin craze with a slowly varying stress distribution as depicted in Figure 18a, yielding a displacement field (obtained using (2.21)) as shown in Figure 18b. Combining p(x) and v(x) from Figures 18a & 18b results in a p-v relation as plotted in Figure 18c. It is seen that the fibril stress, p, has to drop sharply at large values of displacement, v (circled area). Such behavior is not present in either the linear (case A.1) or the half-cosine (case B.1) p-v relation prescribed, thus, it is most unlikely that such a solution exists. Several other stress distributions

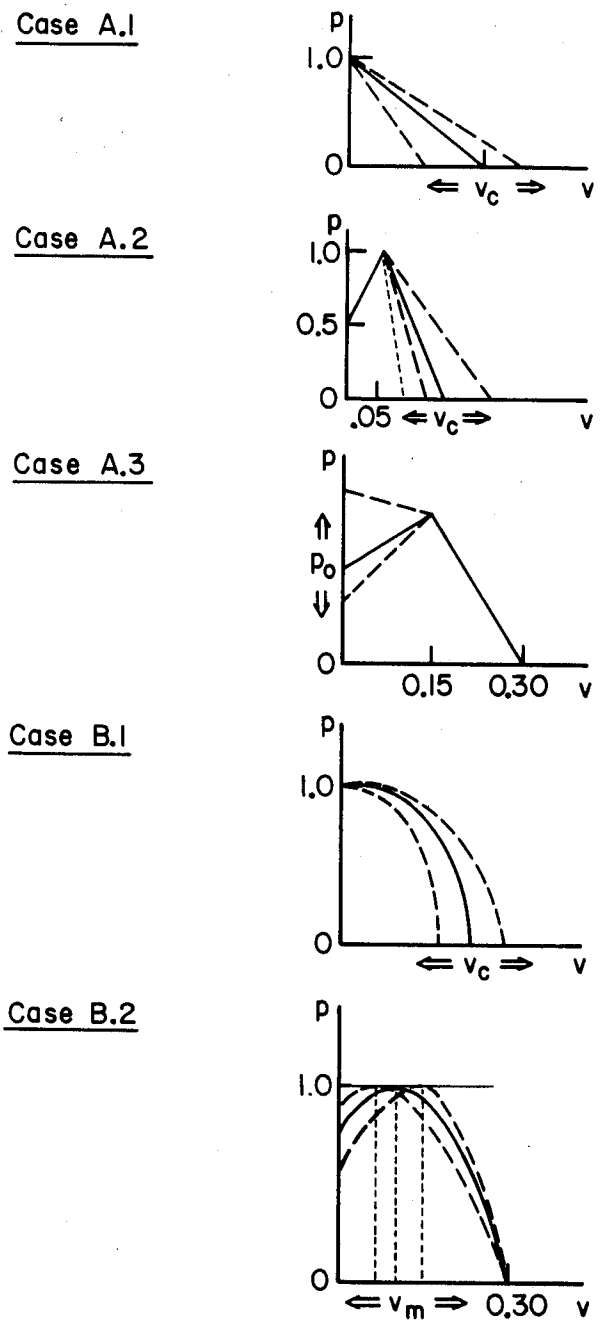

Figure 17. Illustrations of the study of bounds on the p-v relations in Section 4.2.

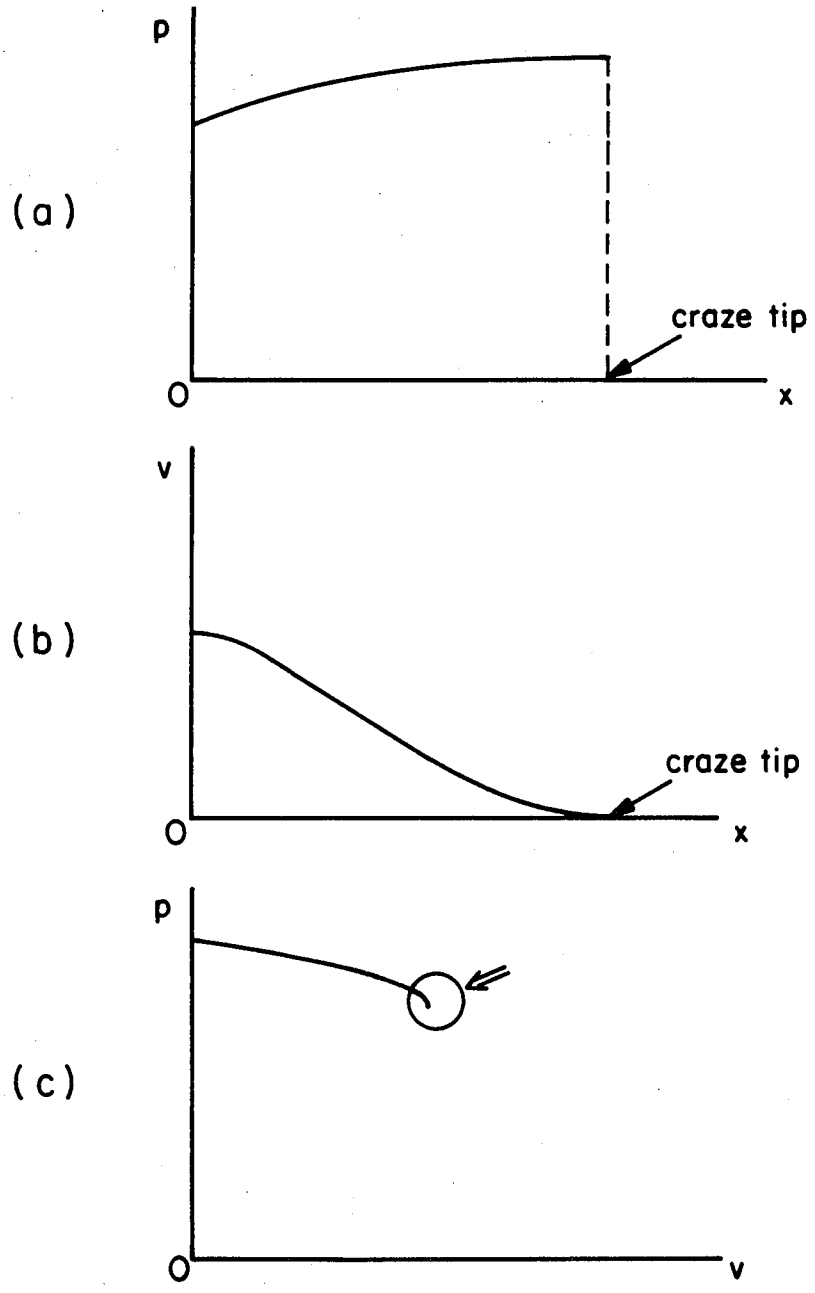

Figure 18. Demonstration of the nonexistence of nontrivial 'full craze' solutions for cases A.1 and B.1. See discussion in Section 4.2.

covering a wide range of possible solutions are tested by the same procedure and yield no prospective solution consistent with the prescribed p-v relation. This demonstrates quite clearly that one cannot 'force' a prescribed p-v relation on a given craze length and expects a non-trivial solution to always exist.

The above heuristic argument is not a proof that establishes our conclusions rigorously but represents the our best effort in trying to gain some insights into the behavior of the nonlinear problem at hand. The arguments presented here were conceived in connection with the extensive experience acquired through the course of the study which adds confidence to the conclusions we drew. We will resort to this line of argument on a few more occasions in later investigations mainly to assure ourselves of the nonexistence of a solution when the algorithm fails to seek out one.

(2) p-v relations with hardening followed by softening as in cases A.2, A.3 and B.2: It is seen that only a 'limited' amount of hardening prior to softening is permissible for a solution to exist.

To demonstrate this finding, consider another heuristic argument illustrated in Figures 19a-e. Let us first assume that a reasonable craze profile, i.e., a profile v(x) that is continuous and has zero slope and displacement at its tip, as shown in Figure 19a is the result of prescribing a p-v relation in Figure 19b. Then, without considering continuum mechanics, the corresponding p(x) deduced from v(x) in Figure 19a and the p-v relation in Figure 19b would be of the character shown in Figure 19c. However, on mechanical ground, i.e., using (2.21), this p(x) gives rise to a displacement profile $\tilde{v}(x)$ as shown in Figure 19d which exhibits interpenetration in the craze tip region unlike the assumed v(x) in Figure 19a. The p-$\tilde{v}$ relation (Figures 19e) derived from figure 19c and 19d also bears little resemblance to the assumed p-v relation in Figure 19b. Thus through this somewhat roundabout argument, we conclude that when the prescribed p-v relation hardens by

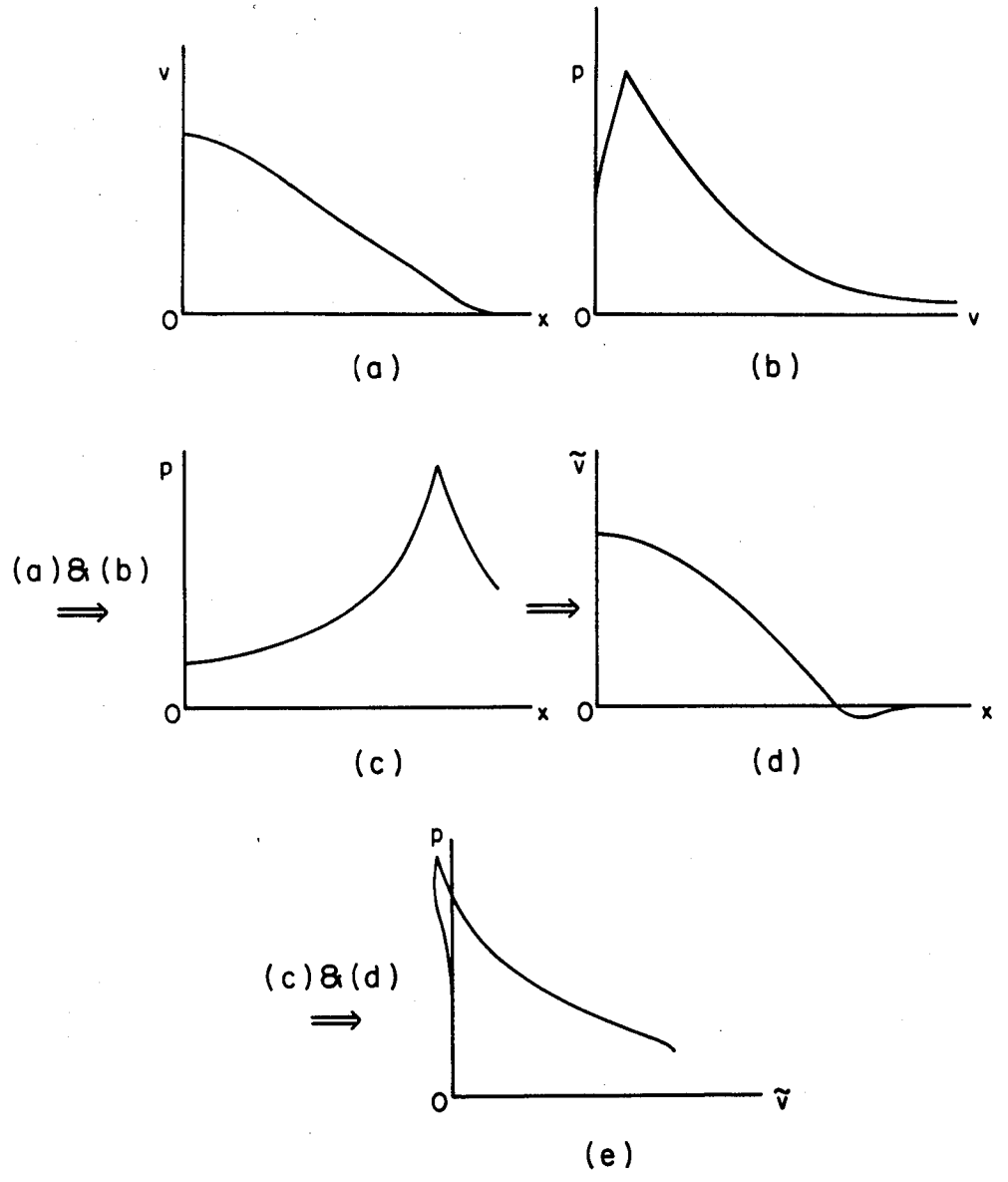

Figure 19. Demonstration of the nonexistence of solution for cases A.2, A.3 and B.2. See dicussion in Section 4.2.

an 'appreciable' amount prior to softening (as in Figure 19b) and our solution algorithm diverges (i.e. cannot find a solution) for a wide range of trial initial guesses, there is no solution for the p-v relation prescribed.

Before moving on to Section 5, three comments are in order:

(a) In all cases studied the Picard's iterative scheme yields the same results as the Newton method with much less CPU time.

(b) From the arguments presented above and experimental observations that crazes/cracks exist in continuum spectra, we can conclude that the p-v relations can only be invariant with respect to a 'limited' range of craze lengths. (See the discussion on the 'first possibility' associated with the finding (1) above regarding monotonically softening p-v relations.)

(c) The question of the uniqueness of solution will not be answered rigorously here. As is the case in most nonlinear problems, uniqueness is very difficult to establish. Nevertheless, based on the extensive experience acquired during the course of this study, we are convinced that for a given craze length and σ_∞, the solution p(x) and v(x) found using Picard's algorithm is unique. However we find that for a given craze length, there may be two different values of σ_∞ and two corresponding sets of p(x) and v(x) which form solutions: The solution with the higher σ_∞ corresponds to a full craze or a craze with a very short internal crack, while the other one with the lower σ_∞ is invariably the solution of a craze with a 'longer' central crack. These aspects are discussed in more detail in Section 6.

5. THE TWO BASIC ASSUMPTIONS

In this section we discuss the 'crack tip opening displacement' criterion (CTOD) and the 'invariance' assumption regarding the fibril p-v behavior as the craze and crack grow in the light of existing experimental results before employing them in the study in the following sections. Of these separate issues we address first

5.1 The CTOD Criterion

When a central crack is present within a craze, the crack may or may not propagate as the far-field load σ_∞ is increased. If the crack does not propagate, it is clear that the fibril at the crack tip can sustain additional growth (lengthen) though not necessarily higher stress or strain. This is the consequence of two physical mechanisms that operate simultaneously, namely, surface drawing and fibril creep.[18] If surface drawing alone operates a fibril will never break and the crack will never advance. This possibility is contrary to experimental observations since cracks do grow within crazes. As can be explained in terms of craze and fibril microstructures, a crack that propagates quasi-statically through a craze either runs right along the midrib where the fibrils are weakest or propagates in a 'patch' or 'mackerel' pattern [5,8]. In the first situation, the heightened stress at the crack tip causes the previously unloaded midrib to stretch until the local extension ratio exceeds the maximum sustainable by the bundles of polymeric molecule chains that constitute the fibril, thus leading to fracture. In the latter event, usually observed at higher crack velocities [8], the high crack tip stress causes fibrils at the craze-polymer interface to be drawn at high local strains [5]. One observes then that the crack, in this case, prefers to run along

18. Surface drawing is the process by which bulk polymer is converted (drawn) into fibrillar craze material. Fibril creep is simply the stretching of an existing fibril without drawing additional polymer material into the craze from the bulk.

either interface where the fibrils are locally weaker than at the midrib, creating the familiar mackerel pattern [5,8]. In either case, the above situations support the use of a critical crack tip opening displacement (or a critical fibril extension). This is also confirmed by experiments performed by Döll et al [31,32] who found further that the CTOD is relatively constant for a wide range of crack velocity. Specifically, these authors showed that the maximum craze widths at the crack tip (critical CTOD or v_c in our notation), measured for PMMA compact tension specimens for crack speeds ranging from 10^{-8} to 20 mm/sec, are essentially constant with a standard deviation of about 8% .[19] Their findings suggest that the fibrils spanning the tip of the crack can only sustain a limited, relative, displacement of their ends. An interpretation of the experimental result in terms of molecular behaviors is given in reference 32; such discussions are beyond the scope of the present work. For our purpose, it suffices to assume that the surface drawing mechanism is somehow constrained at the crack tip and creep invariably gives rise to fibril breakage at a roughly constant CTOD.[20] We assume in this study, therefore, that for a given polymer, a critical CTOD exists and is constant.

5.2 Comments on the Invariance of the p-v Relation

To study craze and/or crack growth, one needs to know whether the p-v relation changes as propagation proceeds and if so, how ? The

19. In private communication Professor Kramer indicated the observation that under a low crack speed of about 1 micron/sec the critical CTOD increases substantially. This casts some doubt on the validity of the number 10^{-8} mm/sec given in references 31 and 32. However, for the speed range between 10^{-3} and 20 mm/sec, the constancy of the CTOD (for PMMA) appears acceptable. See the introduction of reference 9 for further discussion on this point.

20. It is worthwhile to note that cracks are observed to form in 'full' crazes at the polymer/craze interface and not at the midrib. The locations of the first formed crack in a full craze are also not necessarily at the center part of the craze where the fibrils are longest.

question can only be answered by experiments, i.e., by measuring v(x) for crazes with or without cracks of various lenths and compute p-v relations for each craze length. Since no experimental data on this particular topic exist, we feel free to assume further that the p-v relation is 'invariant' with respect to both the craze and the crack lengths for quasi-static propagation under a 'controlled' environment.[21] As it turns out, on the basis of the previous (see comment (b) in Section 4.2) and subsequent studies (see Section 6), this assumption can only be valid over a limited range of craze and crack lengths.

21. Temperature, pressure, moisture content, chemical environment (such as the presence of alcohol or any chemical agents affecting fibril drawing and creep) are all kept unchanged.

6. NUMERICAL SIMULATIONS OF CRAZE AND CRACK PROPAGATION

We proceed now to apply the solution scheme to study how the nonlinear fibril (cohesive) p-v characteristics affect the mechanics of craze and crack growth. Given a craze length and a p-v relation for the fibrils, the problem is to find $p(x)$,$v(x)$ and σ_∞ such that both equilibrium and the smooth closure (Barenblatt's) condition are satisfied simultaneously.[22] The solution scheme has been presented in Section 2.

Quasi-static craze and crack growth is simulated by varying the craze length c continuously. Based on the discussion in Section 5, we assume the fibril force-displacement relation of the form

$$p(x) = p[v(x)] \tag{6.1}$$

The effect of several p-v relations will be examined. We start by first reviewing the Barenblatt-Dugdale model [10,11] shown in Figure 20a. The critical CTOD v_c is used as the fracture criterion throughout; the physical justifications of which have been discussed at length in Section 5.1. It is worth emphasizing that the invariance of the p-v relation with respect to the crack and craze lengths as implicitly assumed in using equation (6.1) is only a conjecture as discussed in Section 5.2. However, this assumption may be a good approximation over a 'limited' range of crack and craze lengths.

---

22. In this paper, the (net) stress intensity factor is always zero and thus does not enter the discussion as a pertinent parameter. The external loading is completely characterized by σ_∞ which is related to the 'loading' stress intensity factor by $K_I = \sigma_\infty \sqrt{\pi c}$. Note that the stress states at both the crack tip and the craze tip are determined by the nonlinearity of the fibril p-v relation rather than the 'usual' K-field.

6.1. The Barenblatt-Dugdale Model

This simplest model assumes the cohesive (fibril) stress to be constant throughout the cohesive (craze) zone as denoted by p_m in Figure 20a. The problem has been analyzed by Rice [12] and Goodier and Field [13], we summarize below the pertinent results. These are obtained directly from the equations presented in Section 2.

The Barenblatt condition requires

$$\sigma_\infty = \frac{2}{\pi} p_m \cos^{-1}\left(\frac{a}{c}\right) \tag{6.2}$$

The displacement v(x) is

$$v(x) = \frac{p_m}{\pi}\left[a\log\left| \frac{\sqrt{c^2-x^2}+\sqrt{c^2-a^2}}{\sqrt{c^2-x^2}-\sqrt{c^2-a^2}} \right| + x\log\left| \frac{x\sqrt{c^2-a^2}-a\sqrt{c^2-x^2}}{x\sqrt{c^2-a^2}+a\sqrt{c^2-x^2}} \right| \right] \tag{6.3}$$

At x=a, v equals v_c the critical CTOD, thus applying L'Hospital's rule, one obtains

$$v(a) = v_c = \frac{2p_m}{\pi} a \log\left(\frac{c}{a}\right) \tag{6.4}$$

Equation (6.4) may be rewritten as

$$c = ae^{\beta/a}, \qquad \beta \equiv \frac{\pi v_c}{2p_m} \tag{6.5}$$

Note that β= constant for a given set of values of v_c and p_m.

Let ω denote the size of the craze (yield) zone, i.e.,

$$\omega \equiv c - a = a(e^{\beta/a} - 1) \tag{6.6}$$

Another quantity of interest is the aspect ratio, α , defined by (using equation (6.3))

$$\alpha \equiv \frac{v(o)}{c} = \frac{p_m}{\pi}\left(\frac{a}{c}\right)\log \left| \frac{c+\sqrt{c^2-a^2}}{c-\sqrt{c^2-a^2}} \right| \tag{6.7}$$

By analyzing the data for six polymers in references 5 and 23, we find that the dimensionless parameters p_m and v_c have values in the ranges of

$$0.01 \leq p_m \leq 0.1$$

$$0.001 \leq v_c \leq 0.01$$

We shall use these numbers later as guidelines for bounding the various parameters in the p-v relations to be studied so that the results of our analyses will be quantitatively realistic.

Further, let γ be the 'fibril fracture energy' (or 'the surface energy') which is the work expended in pulling a fibril from v=0 to $v=v_c$. For the Dugdale model, we have thus

$$\gamma \equiv p_m v_c \tag{6.8}$$

To study how p_m and v_c affect the behaviors of the solutions, it is best to keep γ (which characterizes the energy dissipation of the system) constant. In Figures 20b-f, five sets of p_m and v_c are considered, i.e.,

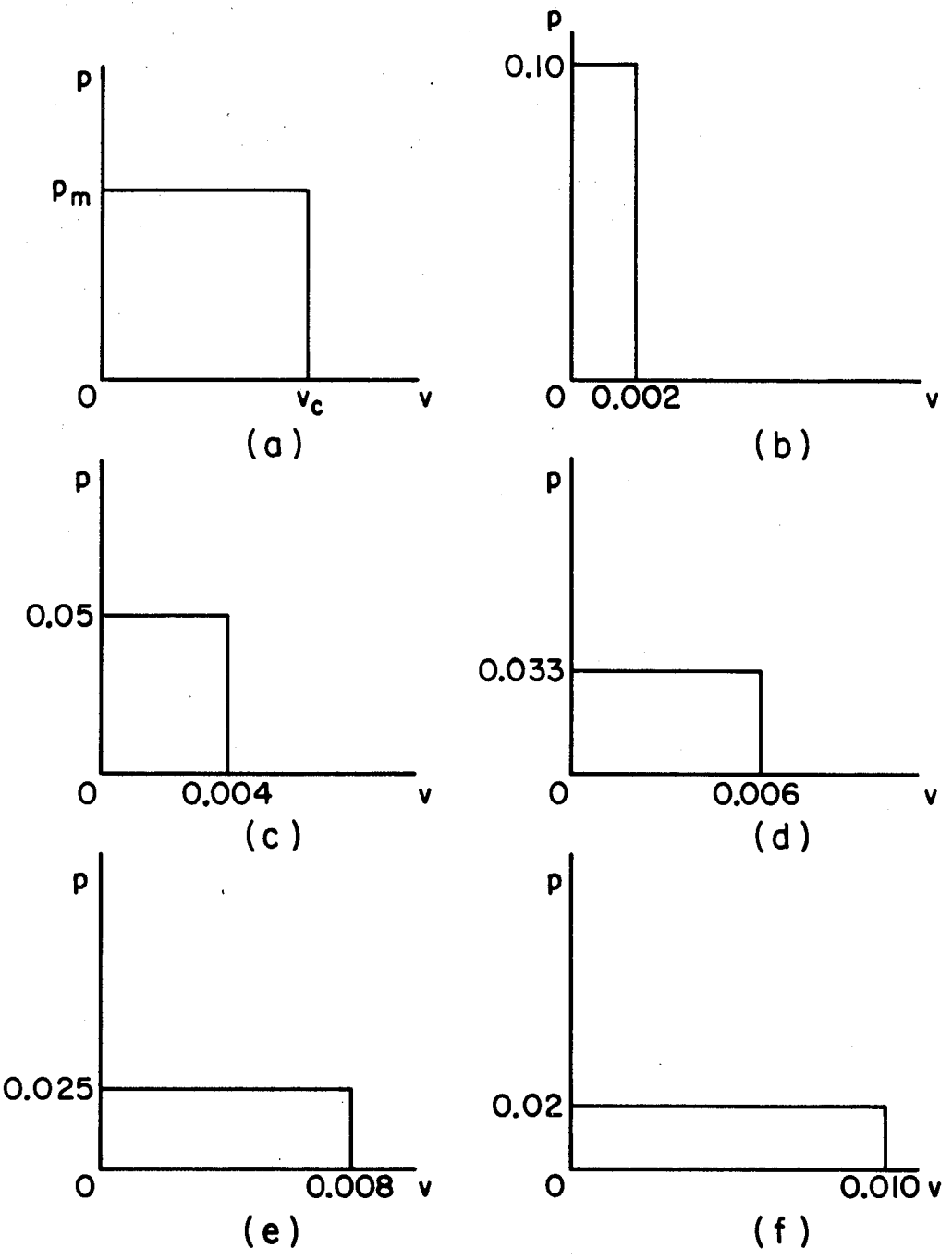

Figure 20. The Barenblatt-Dugdale models.

p_m	v_c	γ
0.1	0.002	2×10^{-4}
0.05	0.004	2×10^{-4}
0.033	0.006	2×10^{-4}
0.025	0.008	2×10^{-4}
0.02	0.010	2×10^{-4}

Using (6.5), c can be plotted as a function of 'a' as shown in Figure 21. Note that there is a minimum in the craze length c for each curve. The minimum can be obtained by setting $\frac{dc}{da} = 0$, yielding the coordinates of the minimum point as

$$(a_{min}, \quad c_{min}) = (\beta, \quad \beta e)$$

where 'e' is the natural logarithm base.

The branch on which $a < a_{min}$ is plotted as a broken line, it is 'nonphysical' in the sense that as 'a' increases, c decreases, which is not possible since craze formation is an irreversible process (a craze cannot 'shrink' unless heated externally to 'heal', which we do not consider here). Note that as $a \to 0$, $c \to \infty$, this is necessary to maintain $v(a) = v_c$ and physically we have a thin long 'full' craze in the limit of $a = 0$.

For $a > a_{min}$, we see that 'a' and c increase together. This is the branch on which we will concentrate our attention as it describes the propagation of a crack within a growing craze.

The craze zone size ω is plotted as a function of 'a' in Figure 22. Note that the craze zone ω decreases and tends asymptotically to β as 'a' increases; see equation (6.6). Observe also that ω is an increasing function of v_c. Figure 23 shows that σ_∞/p_m decreases as 'a'

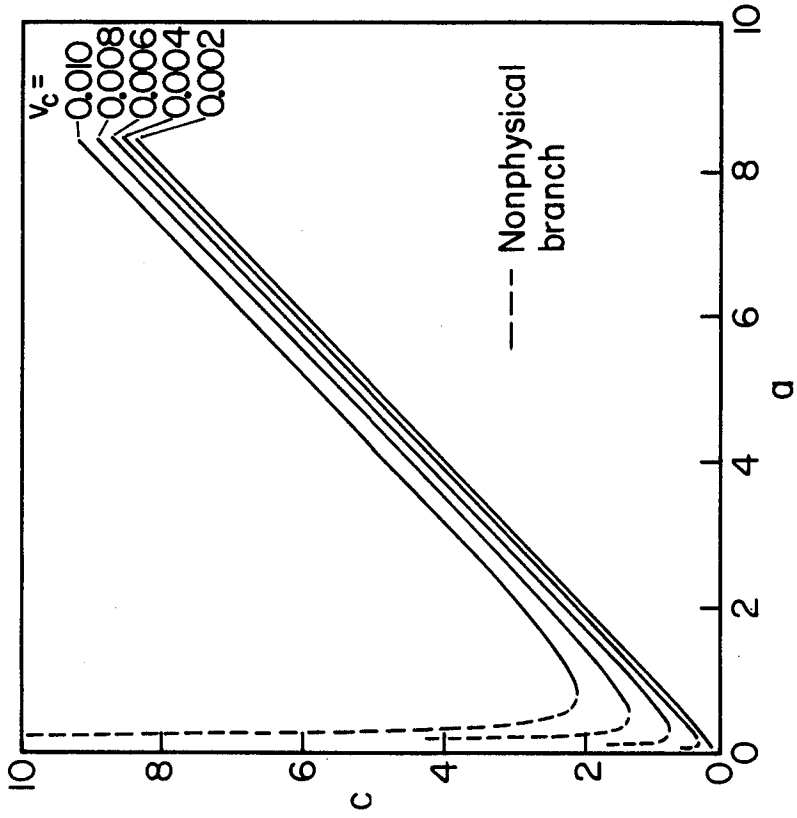

Figure 21. c as a function of 'a' for the Dugdale models.

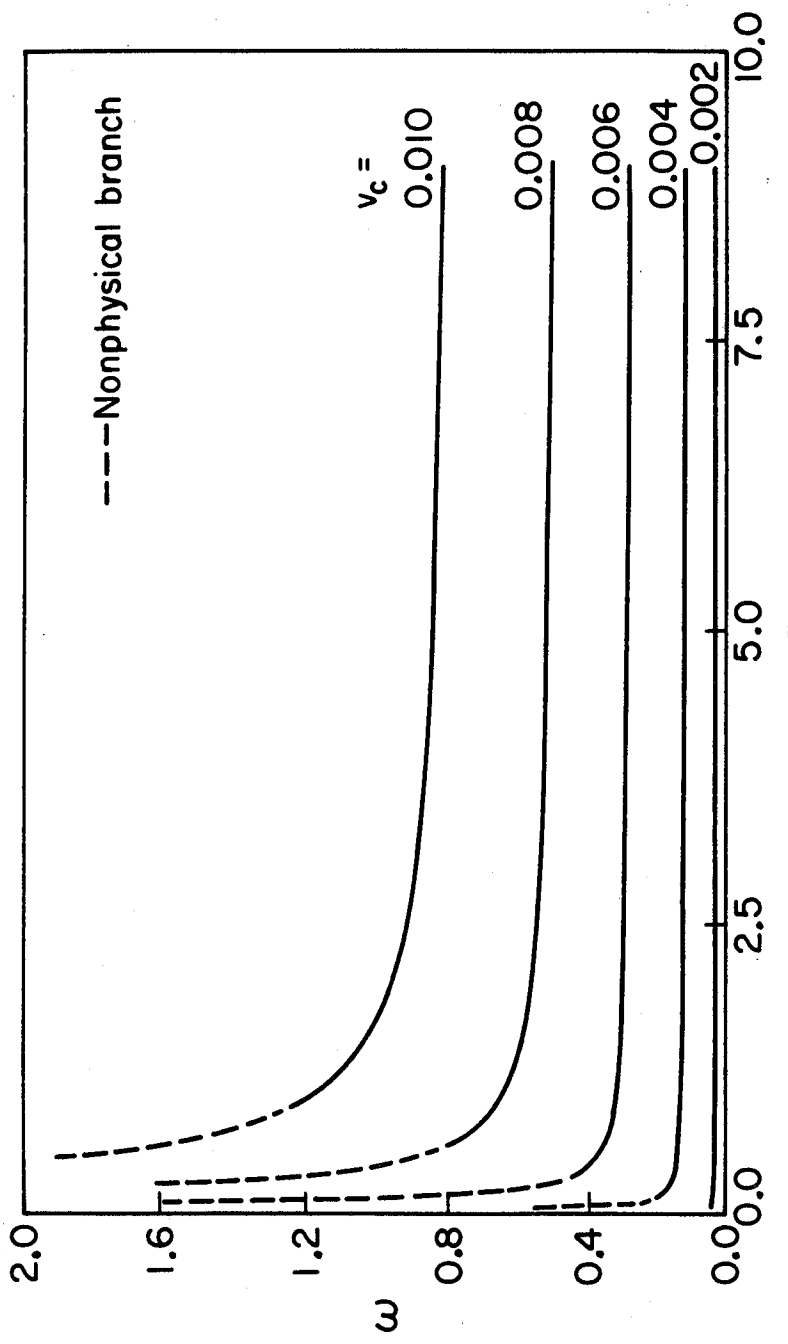

Figure 22. The craze zone ω as a function of 'a' for the Dugdale models.

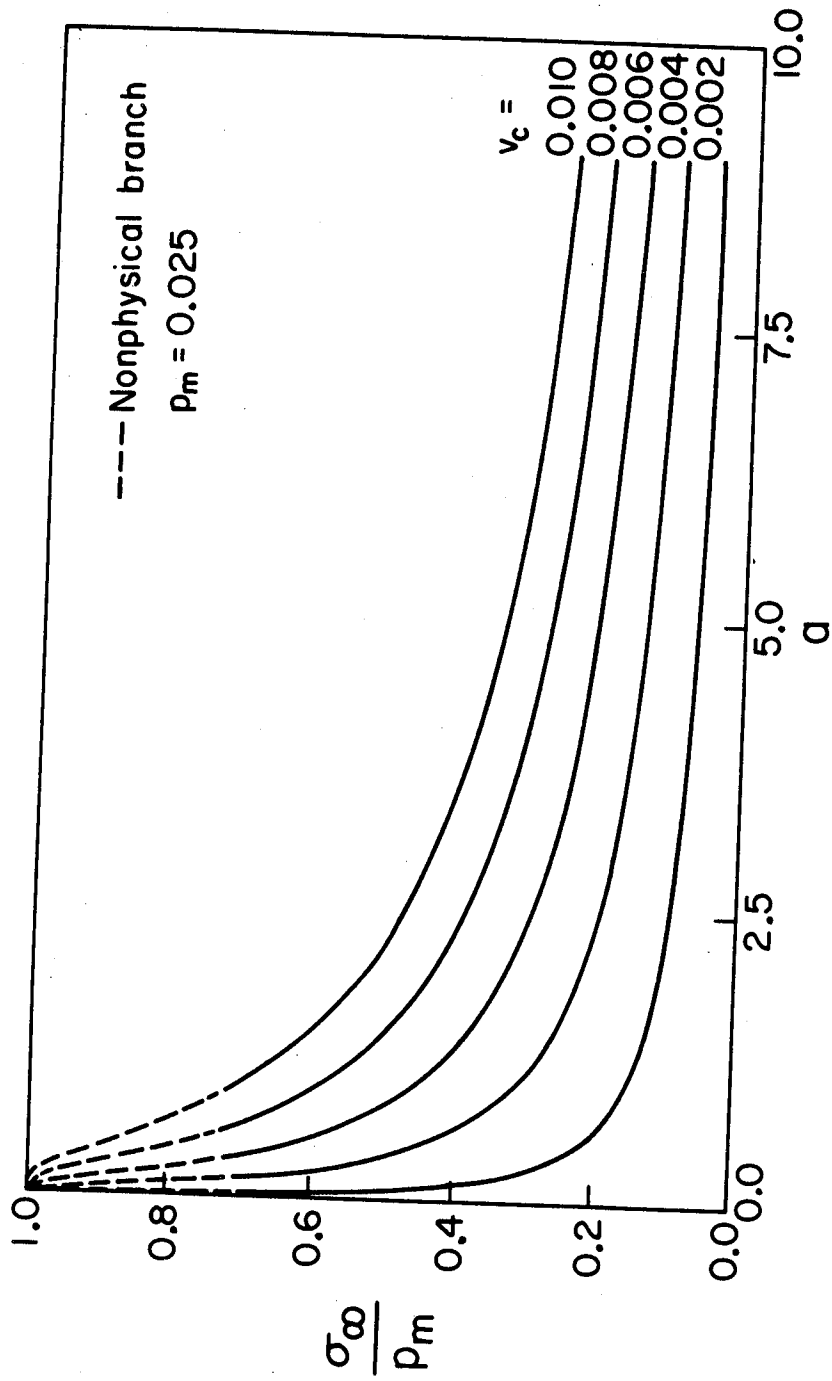

Figure 23. $\frac{\sigma_\infty}{p_m}$ as a function of 'a' for the Dugdale models.

increases, whereas, as a function of c, σ_∞/p_m increases on the 'nonphysical' branch and decreases with c on the 'physical' branch as shown in Figure 24. This illustrates the comment (c) made at the end of Section 4.2 that, for a given craze length, there may be two solutions. The one corresponding to the higher σ_∞ represents a craze with a very short crack ($< a_{min}$), the other, at a lower σ_∞, is a craze with a longer crack ($> a_{min}$). The displacement at the center of the craze, v(o), is shown in Figure 25 to increase monotonically as 'a' increases. Observe that v(o) is relatively insensitive to v_c. The aspect ratio α ($\equiv$ v(o)/c) is plotted versus 'a' in Figure 26. α tends to zero as 'a' tends to zero since in this limit c becomes unbounded (see Figure 21). The aspect ratio exhibits a maximum at a value of 'a' that slightly exceeds a_{min} and then decreases as 'a' (and c) increases. Note that α is a decreasing function of v_c.

We examine next the energy release rate of the system. Let U represent the elastic energy of the system. In general, the energy release rate G is defined as[23]

$$G = - \frac{\partial \Pi}{\partial a} \tag{6.9}$$

Consider the case where the plate is clamped at infinity so that no external work is done during the course of crack propagation. The potential energy Π of the system is then equal to U, and equation (6.9) reduces to

$$G = - \frac{\partial U}{\partial a} \tag{6.10}$$

---

23. To comply with conventional usage, here G, Π, U_p and U_c are dimensionless even though upper case letters are used. The nondimensionalization factor U_{ref} is simply $C_o^2 \Sigma_{ref}$. The dimensionless strain energy density is $\sigma_\infty^2/4$.

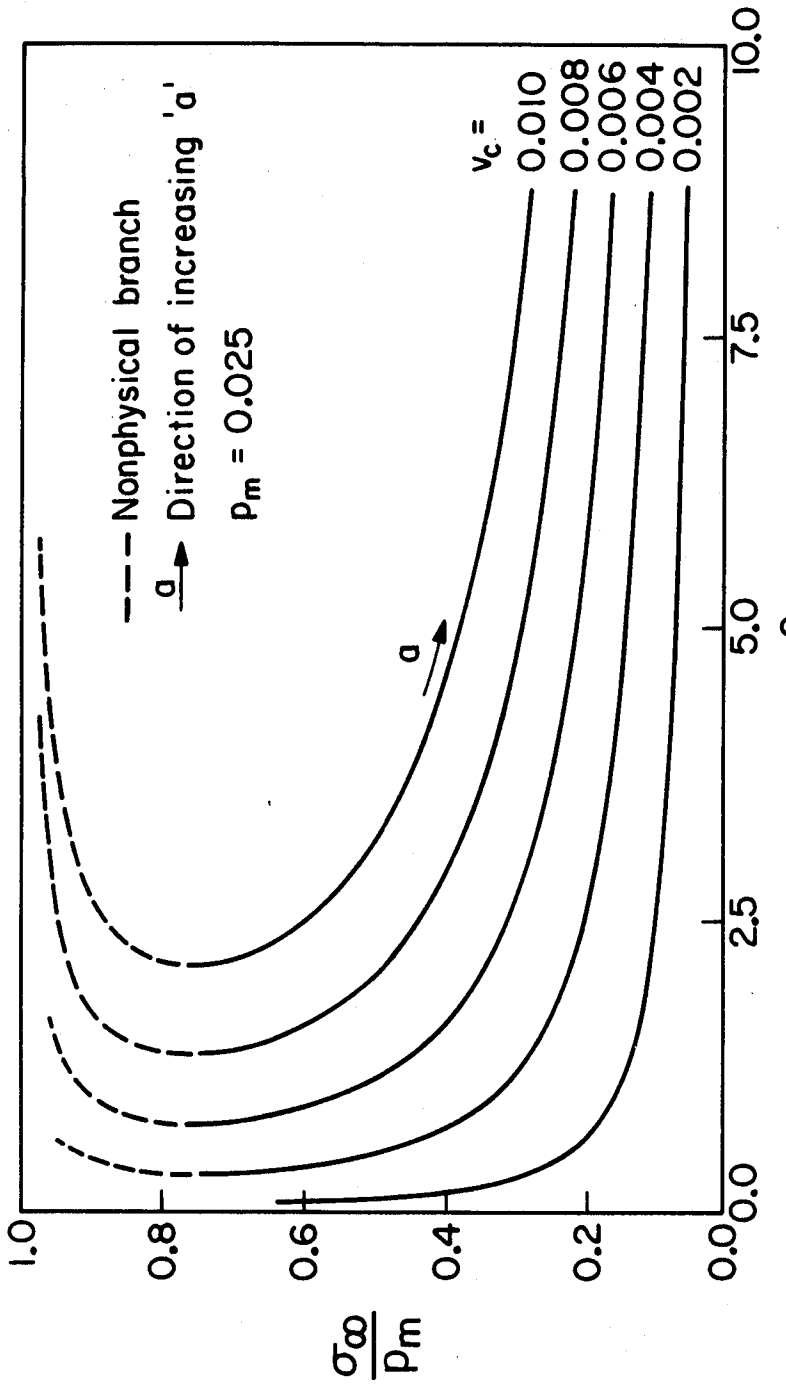

Figure 24. $\frac{\sigma_\infty}{p_m}$ as a function of c for the Dugdale models.

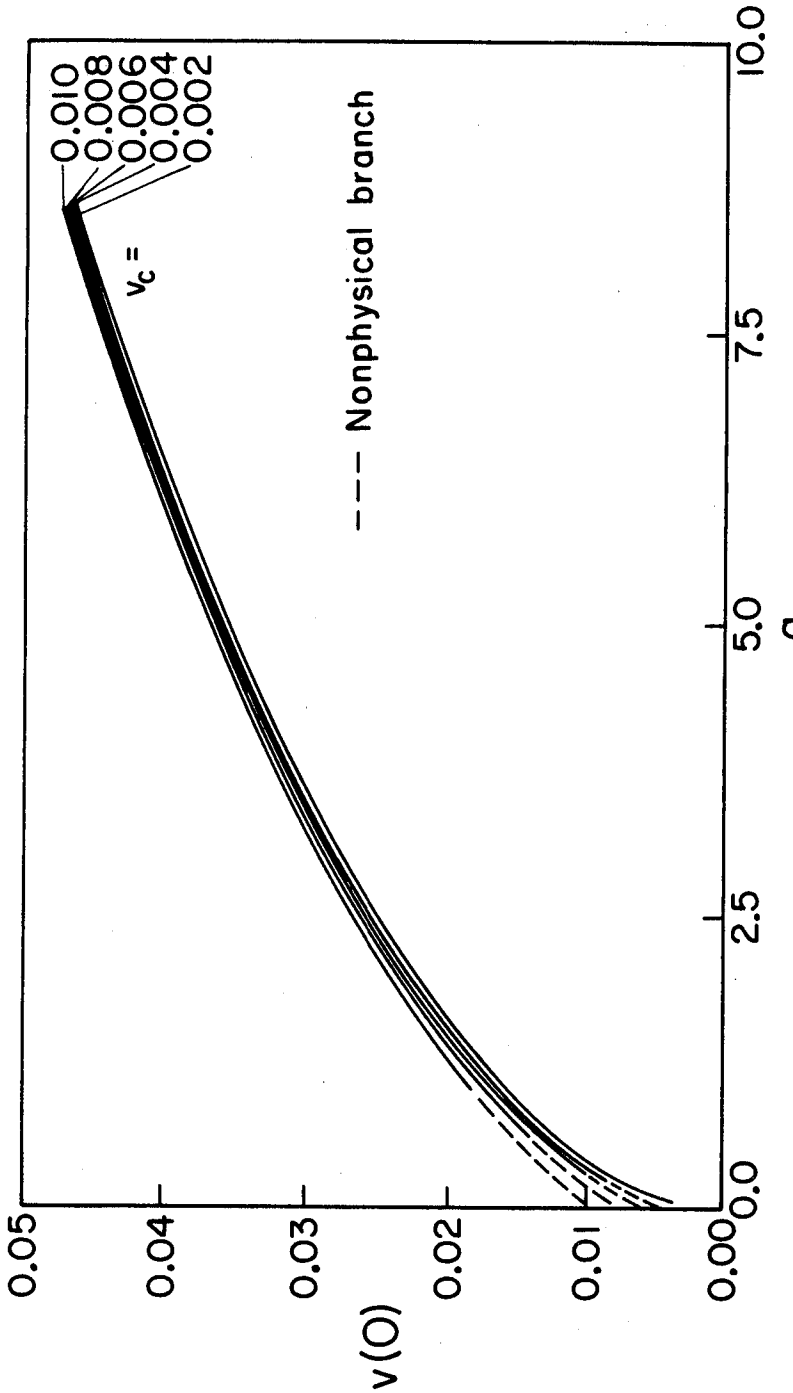

Figure 25. The displacement at the center of the craze v(o) as a function of 'a' for the Dugdale models.

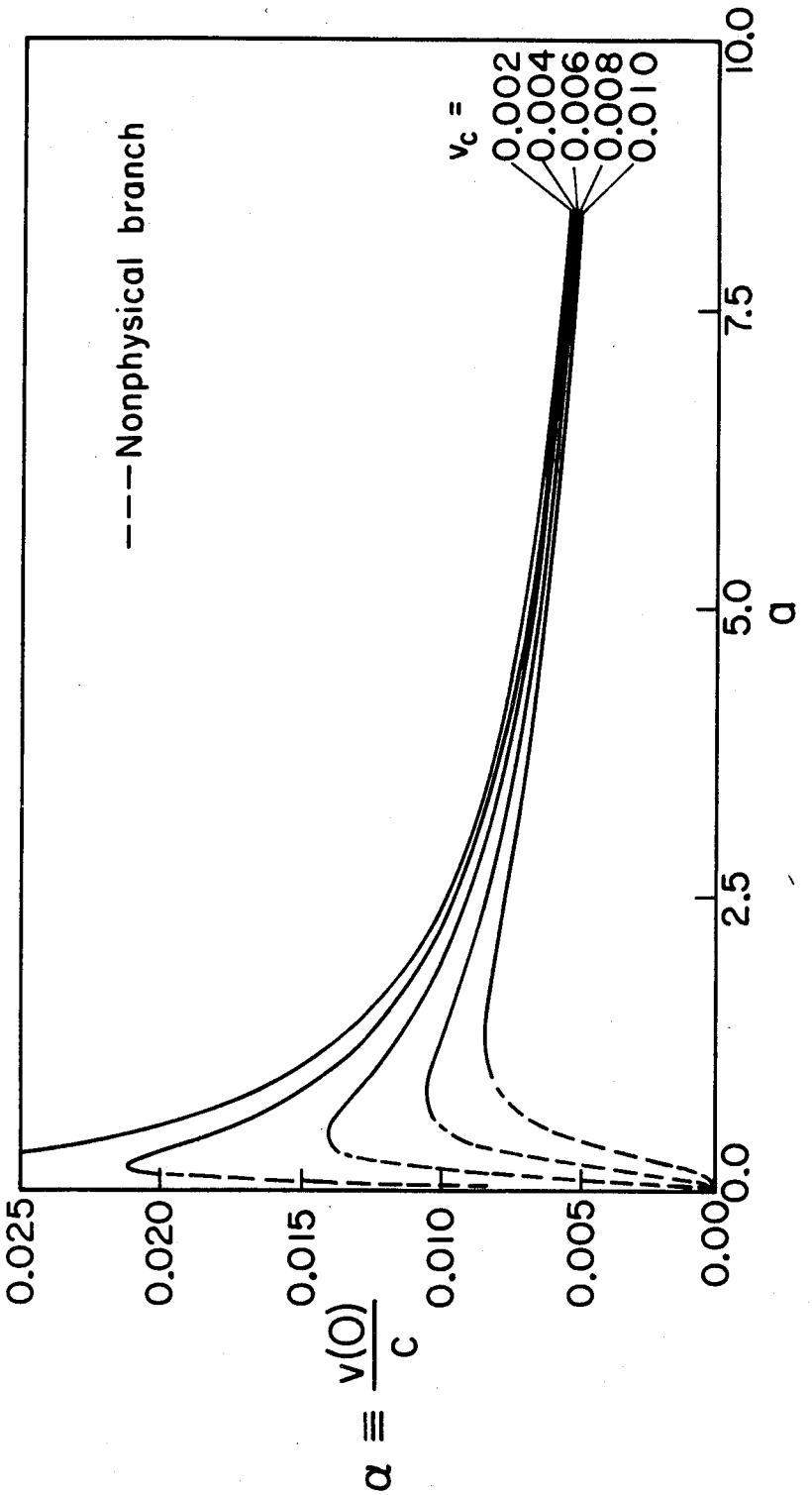

Figure 26. The aspect ratio α as a function of 'a' for the Dugdale models.

Now U is given by the elastic energy stored initially in the plate (planar body), U_p, minus the energy U_c which is required to form a crack of length 2a and two craze zones of length ω each. (This energy comes from the unloading of the plate as the craze boundaries are displaced and work is done against the fibrils.) We have then

$$U = U_p - U_c \tag{6.11}$$

$$U_p = \sigma_\infty^2 d^2 \tag{6.12}$$

where we let 2d denote the dimension of this 'infinite' square plate, i.e., d is very large compared to c. U_c is given by

$$U_c = 4[\ \gamma a + \int_a^c p_m v(x)dx\ ] \tag{6.13}$$

where the factor of four arises because all 4 quadrants have to be accounted for. Substituting v(x) from (6.3) and making use of (6.2) and (6.4), one obtains after some lengthy algebra

$$U_c = 4a[\ \gamma + \frac{p_m}{2}\ \{\ \sigma_\infty \sqrt{c^2-a^2}\ - 2v_c\ \}\ ] \tag{6.14}$$

Using (6.11) and (6.12) in (6.10) yields

$$G = -2\sigma_\infty d^2\ (\ \frac{\partial \sigma_\infty}{\partial a}\ ) + \frac{\partial U_c}{\partial a} \tag{6.15}$$

At this point an important question enters our discussion: What is the criterion for crack propagation (fracture) ?

Goodier and Field [13] assumed that the crack grows in a self-similar manner, such that

$$\frac{\partial c}{\partial a} = \frac{c}{a} \tag{6.16}$$

This condition is the consequence of assuming σ_∞ to be constant as the crack and craze grows. Under these conditions, $\frac{\partial \sigma_\infty}{\partial a}$ vanishes and G becomes, in view of (6.15), $\frac{\partial U_c}{\partial a}$, which is the 'plastic' (cohesive) work rate. However, the crack tip opening displacement $v(a) = v_c$ as given by (6.4) becomes a linear function of 'a'. Thus the CTOD in Goodier and Field's model increases as the crack grows. This behavior is inconsistent with experimental observations as discussed in Section 5.1.

In the present model, the critical CTOD, v_c, is kept constant; this condition in turn requires that σ_∞ decreases as 'a' increases (see Figure 23), in order to maintain the quasi-static condition, i.e.,

$$\frac{\partial \sigma_\infty}{\partial a} \Big|_{v_c} < 0 \tag{6.17}$$

Viewing (6.15) in this light, it is evident that G becomes unbounded if d is unbounded, no matter how small $\sigma_\infty(\frac{\partial \sigma_\infty}{\partial a})$ may be, since $\frac{\partial U_c}{\partial a}$ is always finite.

Therefore, in this geometry, a crack the tip displacement of which has reached the critical value is always unstable.[24] This statement can be directly verified from Figure 23 which indicates that unless σ_∞ is reduced as 'a' increases in the manner shown, quasi-static crack and craze growth cannot be maintained. To this result we only need to add the reminder that for a clamped infinite (very large) plate, a small enlargement of an internal crack would hardly affect the far-field σ_∞ sufficiently to keep the crack and craze growing quasi-statically.

24. If the tip displacement is less than v_c, the crack does not grow as the tip fibril is not broken. For softening p-v relations, however, instability may occur before v_c is reached (see Section 7.2).

Therefore once a crack (with or without a cohesive zone) starts growing, and the fracture criterion such as a critical CTOD is satisfied, catastrophic failure ensues. We shall see in the next section that the converse is not true.

It is of interest to see how the plastic work dissipation rate, $\frac{\partial U_c}{\partial a}$, changes as the crack grows. Making use of (6.5), the constancy of v_c requires

$$\frac{\partial c}{\partial a} = \frac{c}{a}(1 - \frac{\beta}{a}) \tag{6.18}$$

Also, differentiating (6.2) and using (6.18) yields

$$\frac{\partial \sigma_\infty}{\partial a} = - \frac{v_c}{a\sqrt{c^2-a^2}} \tag{6.19}$$

Differentiating (6.14) and using (6.18) and (6.19), there results

$$\frac{\partial U_c}{\partial a} = 4\gamma + 2p_m \left[\sigma_\infty (2\sqrt{c^2-a^2} - \frac{c^2\beta}{a\sqrt{c^2-a^2}}) - 3v_c \right] \tag{6.20}$$

This plastic work rate calculated using the CTOD criterion differs markedly from the result obtained by Goodier and Field under the assumption of self-similar growth [13]. The work rate given by (6.20) in this work is plotted in Figure 27; note that the plastic work rate increases as 'a' increases and approaches the constant value 4γ rapidly. Physically, for a short crack, one has a relatively large craze (yield) zone ω ; to advance the crack by Δa, very little energy is needed since c increases more slowly than 'a' (i.e. ω shrinks). For longer cracks, the size of the yield zone tends toward a constant value and thus the craze zone simply translates as the crack propagates. In this latter case, the dissipated energy is thus 4γ per unit crack advance.

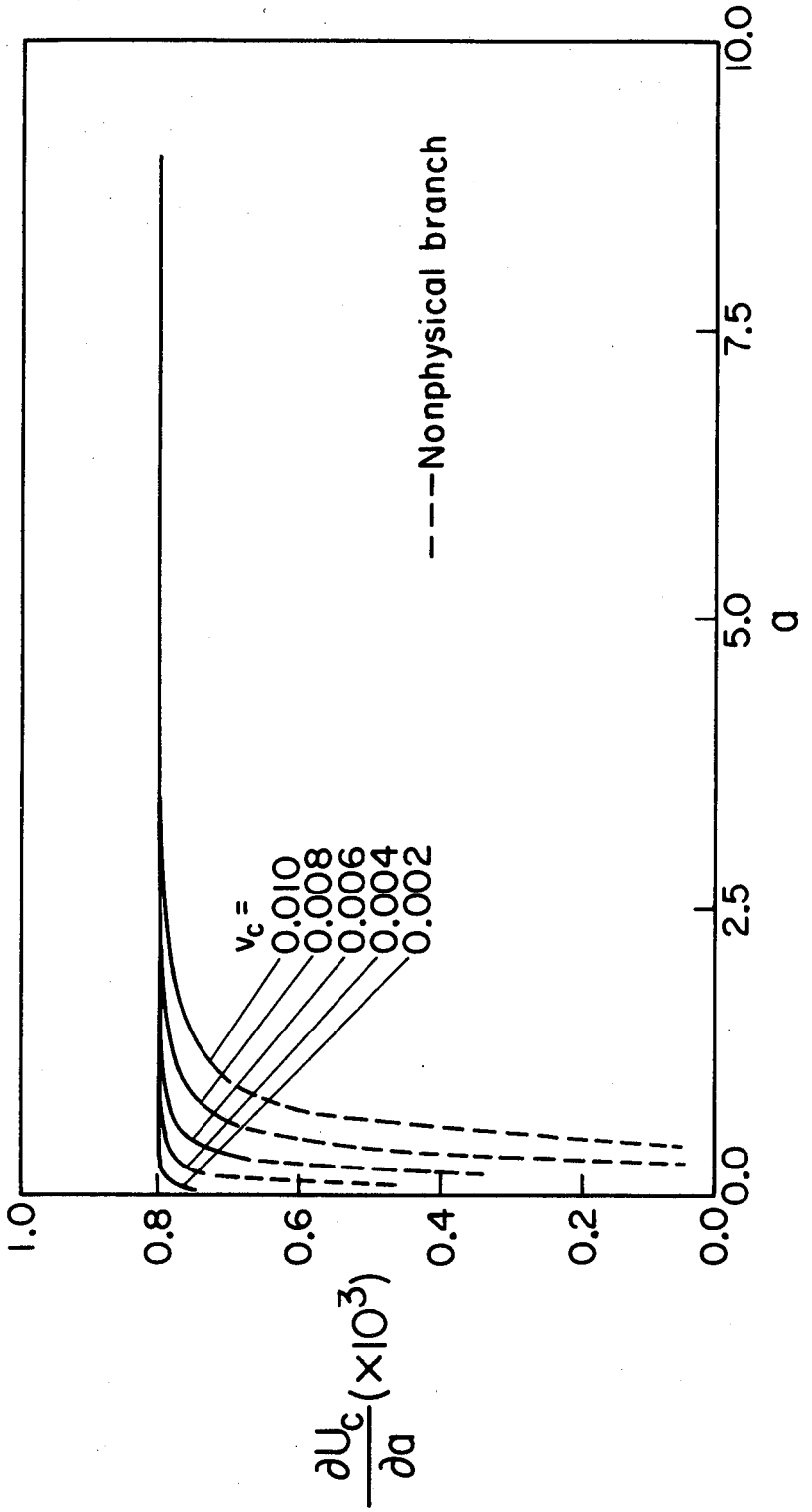

Figure 27. The rate of plastic work dissipation $\frac{\partial U_c}{\partial a}$ as a function of 'a' for the Dugdale models.

6.2. General p-v Models

Next we examine six different p-v relations labeled #1 through #6 in Figure 28 and compared the results to the Dugdale model labeled 'D'. Models #1 and #2 are of the half-cosine form given by (4.2) with $v_m = 0$. Models #3 and #4 are linear-softening defined by (4.1) with $v_m = 0$. The p-v relation #5 is hypothetical.[25] It is designed with the intention to examine the effects of a highly-softening fibril behavior coupled with subsequent mildly-softening behavior on the mechanics of crack and craze growth. The last model (#6) is of a 'bi-parabolic' form, i.e., the initial softening with subsequent rehardening behavior is modeled by two parabolic curves (joined at the transition point with zero slopes). The motivation for this design is based on the experimental findings of Kramer et al. [22,23] as reproduced in Figure 4. The model should approximate the realistic p-v behaviors of craze fibrils as it is known today reasonably well. As a check, we employ this model to simulate craze and crack growth. The resulting craze contours and stress distribution profiles are depicted in Figures 29 and 30 respectively. They do closely resemble the experimental v(x) and p(x) obtained by Kramer and his coworkers.

To compare the results for all these different p-v relations, it is necessary to have a benchmark. For this purpose we use a Dugdale model (labeled 'D' in Figure 28) with $p_m = 0.025$ and $v_c = 0.008$. All the p-v models are designed so that the area under each p-v curve, γ, is constant and equal 2×10^{-4}, the same as that of the Dugdale model employed. This is done to 'filter out' the possible effects on the results that may be caused by the differences in the values of fracture toughness among the various p-v models.

---

25. Meaning, no experimental evidence suggests the existence of such a form of p-v relation.

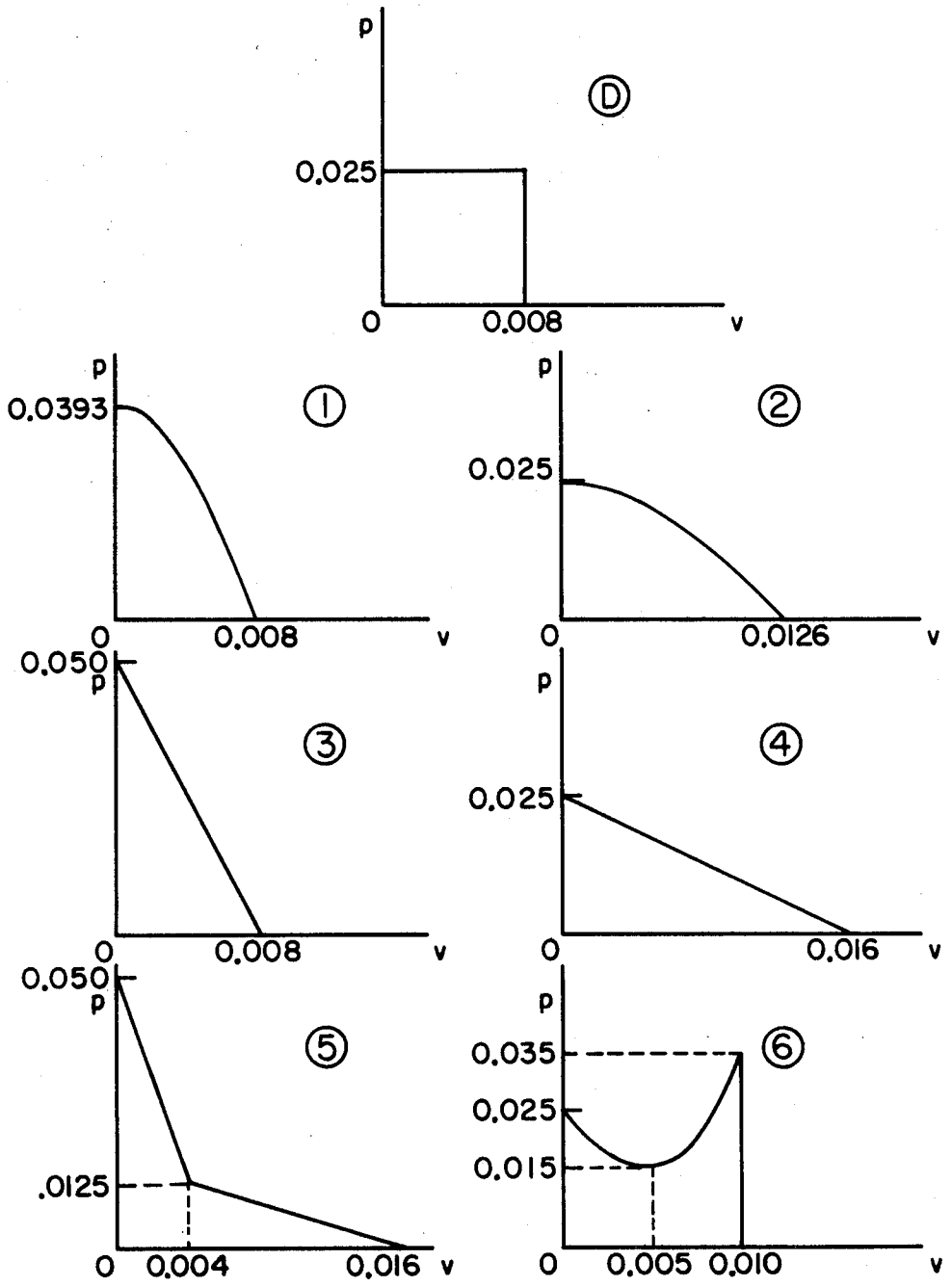

Figure 28. p-v models used in the nonlinear craze and crack propagation studies in Sections 6 and 7. All models have the same γ .

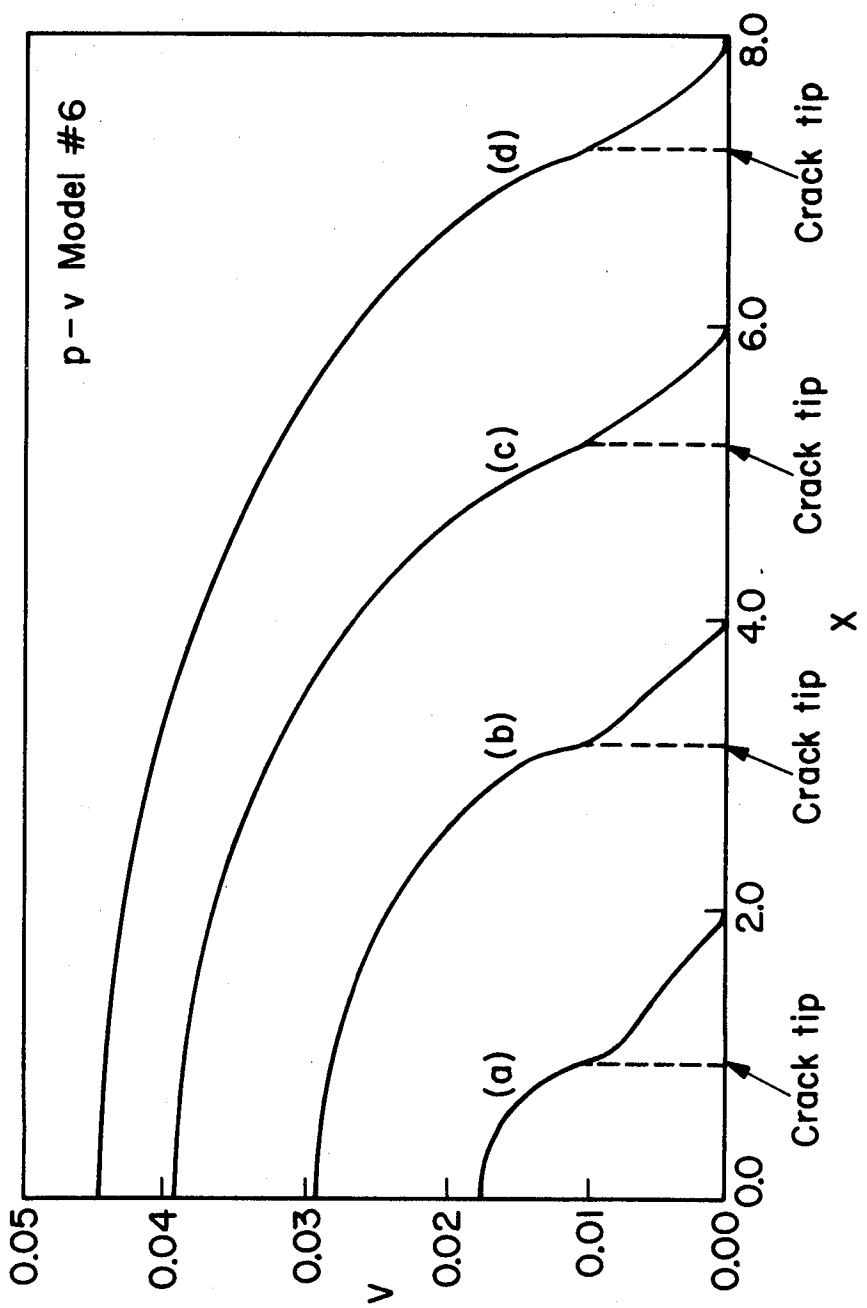

Figure 29. Craze and crack propagation simulations for p-v model #6: Displacement profiles.

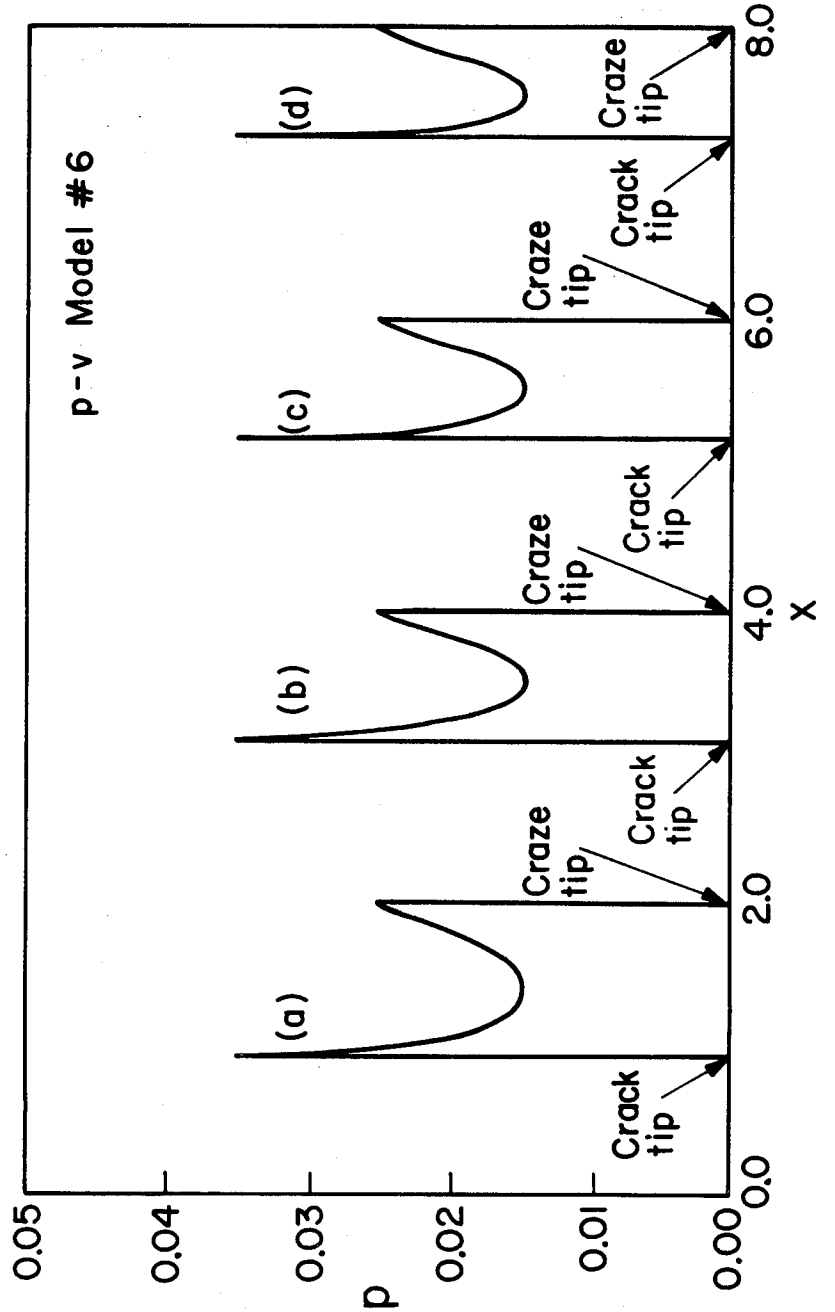

Figure 30. Craze and crack propagation simulations for p-v model #6: Stress distribution profiles.

The numerical procedures have been presented earlier in Section 2.4. Here a few remarks are in order: First, the computation time is cut substantially by employing relations (2.24)-(2.26) in the evaluations of integrals involved for the wide range of craze lengths studied. The craze length is varied from the c=0.0 to c=10.0, the increment Δc ranges from 0.01 to 0.2. Smaller increments for Δc are necessary to capture the behavior of the system for short crack lengths, particularly in calculating the rate of plastic dissipation, $\frac{\partial U_c}{\partial a}$.[26] During the course of these craze growth simulations, it was found that convergence is generally attained in fewer iterations if $v_i(c)$ is used as the initial guess of $v_i(c+\Delta c)$. (This is not the case for p-v model #6, however.)

In Figure 31 and 32, c and ω are plotted as functions of 'a', respectively. The general behaviors for all p-v models are the same as those of the Dugdale models shown in Figure 21 and 22. Note that ω is primarily dependent on v_c but also depends weakly on the character of the p-v relation. In Figure 33, σ_∞ is normalized by $p_m = 0.025$ of the Dugdale model and plotted against 'a'. We see that p-v relations with the same v_c (1&3 and 4&5) yield identical curves, i.e., σ_∞ decreases monotonically as 'a' increases with the short crack length behavior controlled by v_c and p_o (p at v = 0).

In Figure 34, the far-field stress σ_∞ normalized by $p_m = 0.025$ is plotted versus c for the various p-v models. Except for the 'nonphysical' branch of the Dugdale model shown by the dashed line, the remotely applied stress decreases monotonically as the craze/crack grows which is necessary to maintain quasi-static growth. This confirms the conclusion reached in Section 6.1 from the energy release rate analysis that once the critical CTOD is reached the crack will grow unstably if

---

26. U_c is obtained by integrating numerically

$$U_c = 4\left[\gamma a + \int_a^c ev(v(x))dx\right] \qquad \text{where} \qquad ev(v) = \int_o^v p(v')dv'$$

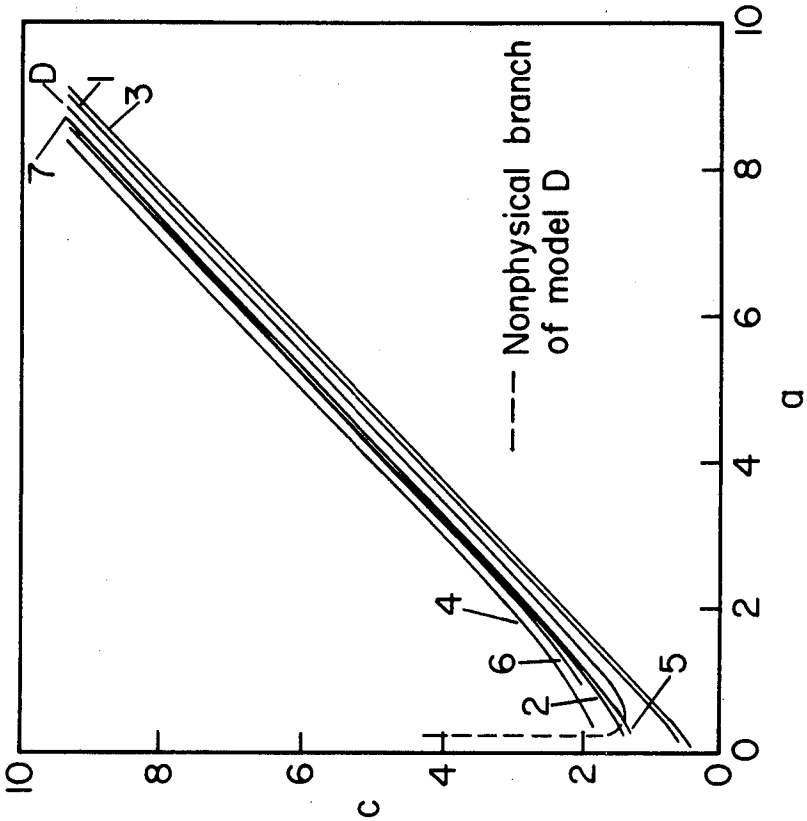

Figure 31. c as a function of 'a' for various nonlinear p-v models (p-v models as indicated).

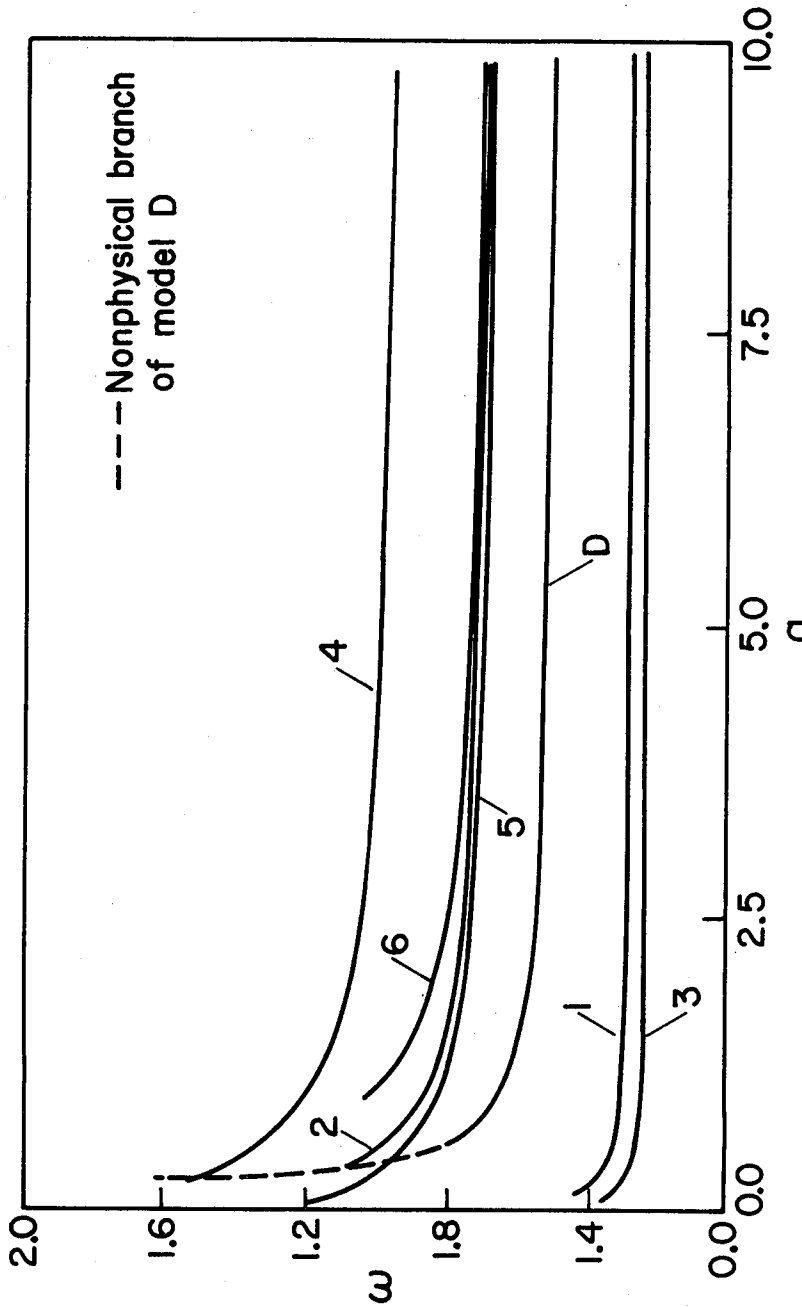

Figure 32. The craze zone ω as a function of 'a' for various nonlinear p-v models (p-v models as indicated).

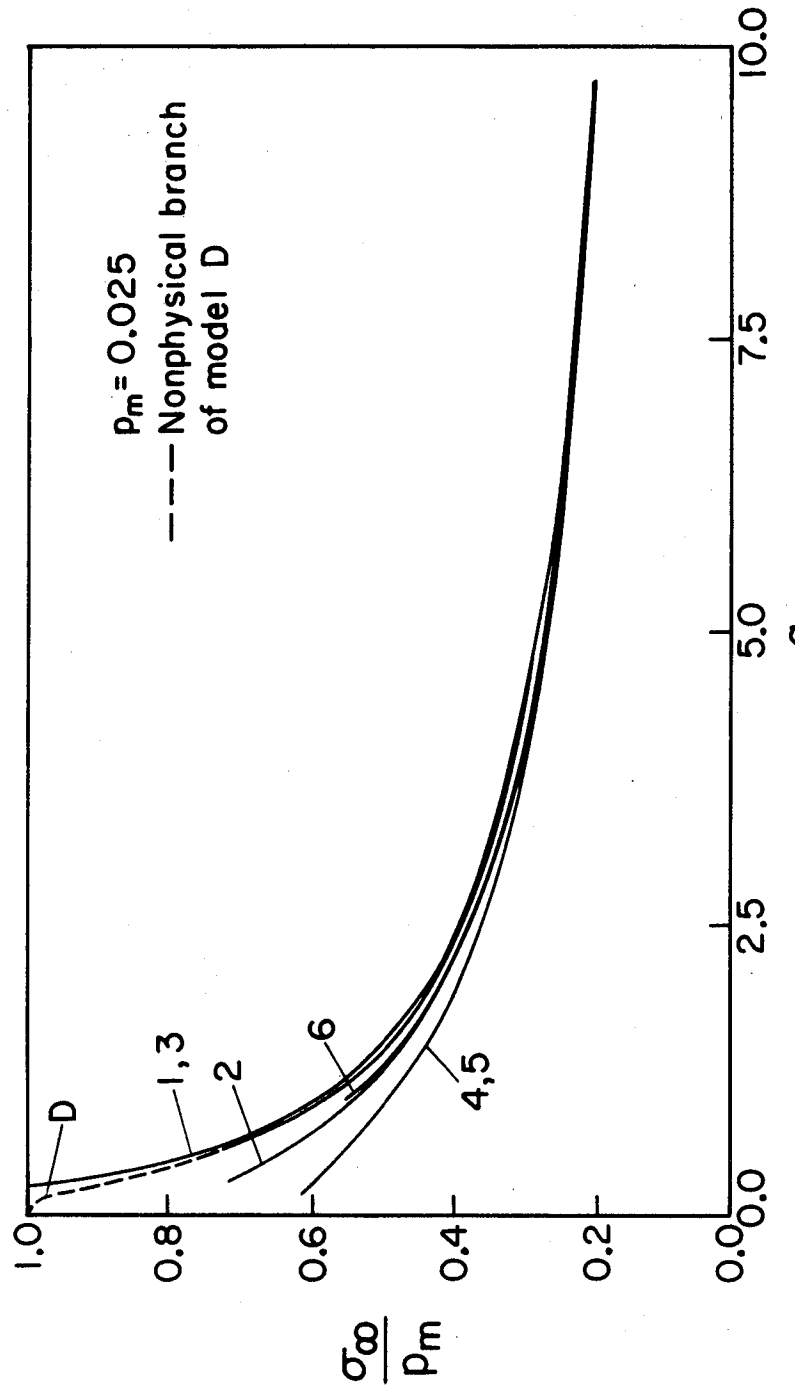

Figure 33. $\frac{\sigma_\infty}{p_m}$ as a function of 'a' for various nonlinear p-v models (p-v models as indicated).

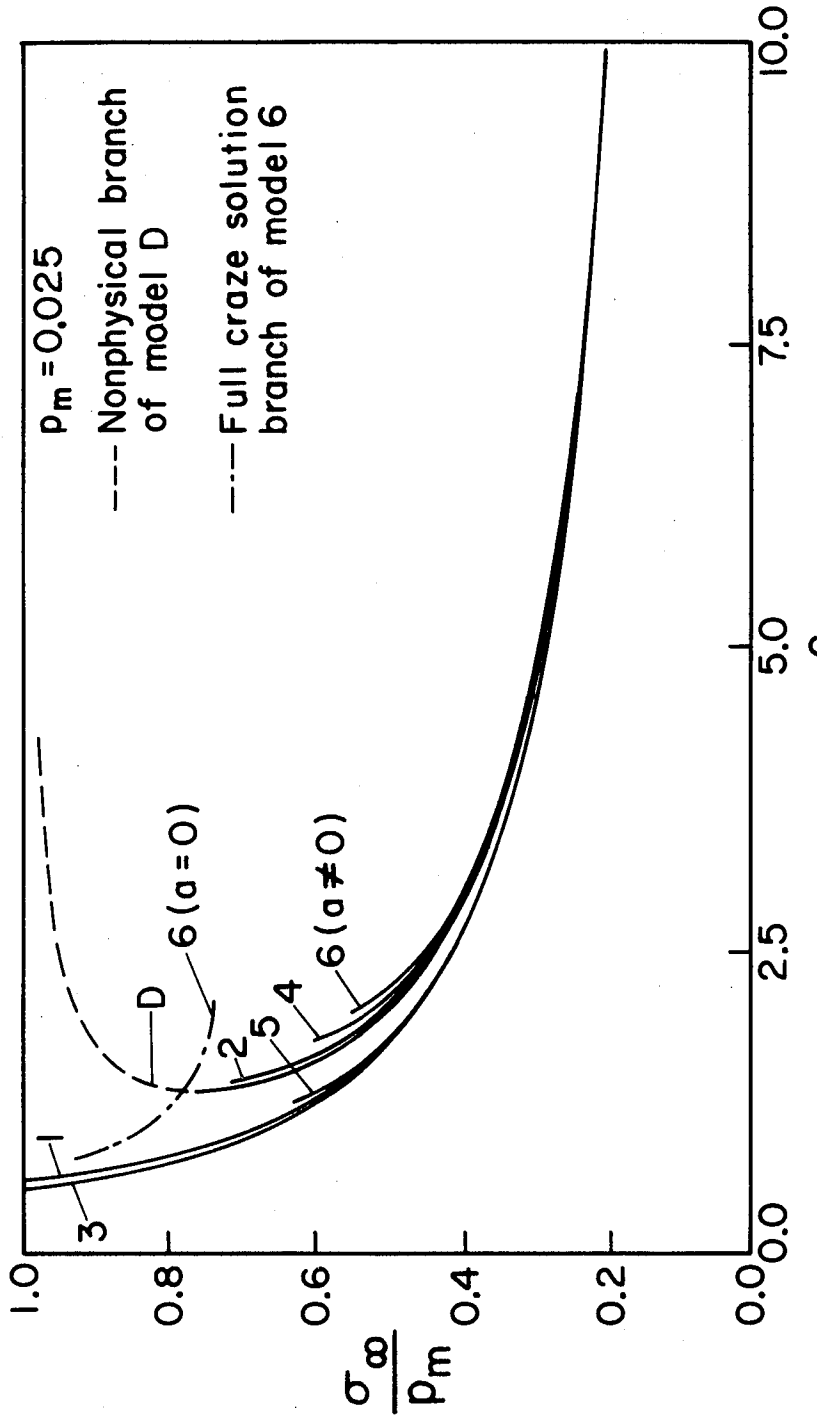

Figure 34. $\frac{\sigma_\infty}{p_m}$ as a function of c for various nonlinear p-v models (p-v models as indicated).

the remotely applied stress is maintained constant. An interesting feature is exhibited by the dash-dot curve which represents a 'full craze' (a=0) solution branch and is present only in the p-v model #6 (among all models studied here). This unusual behavior merits further elaboration:

One finds that for the craze length c < 0.8, the algorithm converges to the trivial solution in which the craze is fully closed (v(x) = 0) at all points (see Figure 46 for better details). For c greater than 0.8, there exists a 'full craze' solution regime up to c = 2.2. At c = 2.2, the solution shows that v(o) is approximately 0.006 and thus p(x) has a minimum at v(x) = 0.005 (see Figure 28). For c larger than 2.2, there is no full craze solution (the algorithm 'jumps' and converges to solutions with cracks, i.e., a ≠ 0). This behavior can again be explained using a contradiction-type argument similar to the ones used earlier in Section 4.2 (and illustrated in Figures 18 and 19). In the present case, consider the following heuristic argument:

With a little exaggeration, let us assume that for a craze length greater than 2.2, a solution exists with p(x) as shown in Figure 35a. The corresponding displacement profile v(x) and the p-v relation, derived through use of equation (2.21), would be as depicted in Figures 35b and c, respectively. Evidently, the p-v behavior in Figure 35c hardly resembles that of model #6. Thus it is unlikely that a solution consistent with p-v model #6 and c > 2.2 exists.

On the other hand, for crazes with nonzero crack lengths, it is found that for c < 1.87 and a < 0.98, there is no solution with nonzero crack length 'a'. As c is decreased below 1.87, a transition in the character of the solution occurs; the solution 'jumps' from the branch on which 'a' is nonzero to another branch on which a = 0 or the full craze solution branch. Note that for 1.87 < c < 2.2, the solutions are not unique, i.e., for a given c in this range, we either have a full craze solution at a higher σ_∞ or a crack/craze solution at a lower

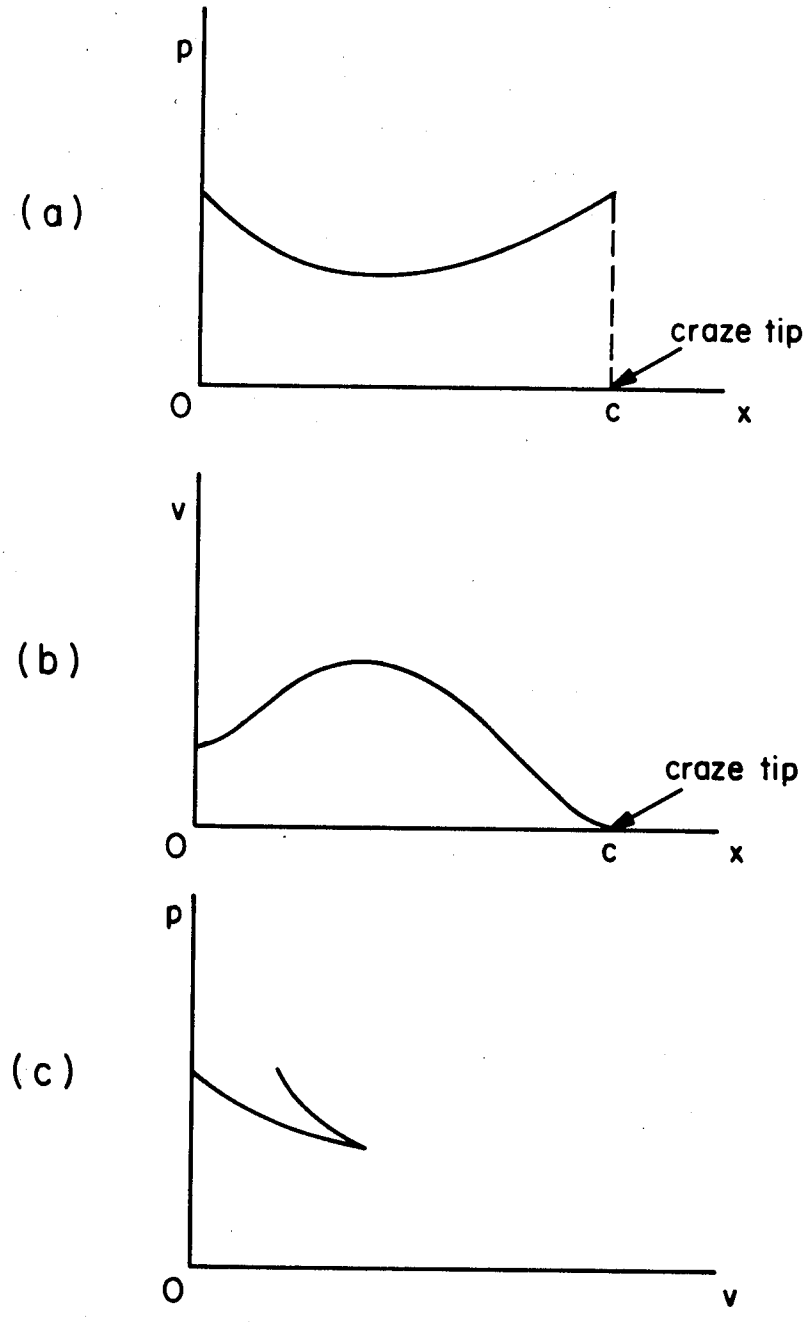

Figure 35. Demonstration of the nonexistence of nontrivial 'full craze' solutions for p-v model #6 for c > 2.2. See discussion in Section 6.2.

σ_∞.[27]

As an assurance, we now check the conclusion that for $c < 1.87$ and $a < 0.98$, there is no solution with $a \neq 0$. This is achieved through another heuristic argument. Assuming that a solution with a short crack length exists, a fibril stress distribution p(x) of the form plotted in Figure 36a seems reasonable. The resulting v(x) and p-v relation are shown in Figures 36b and c. As before the p-v relation needed for such a solution to exist is quite different from the prescribed p-v relation in model #6 .

The above result indicating the lack of solutions for the prescribed p-v relation (#6) over some ranges of craze and/or crack lengths may seem, at first sight, contradictory to our physical intuition that crazes and/or cracks of different sizes exist in a continuous size 'spectrum'. This seeming contradiction is easily resolved by recognizing that, most probably, the p-v relation is not 'invariant' with respect to all values of the crack and craze lengths as initially assumed.[28] More elaborate modelling of the fibril p-v characteristic is therefore needed; see Section 8 for further discussion.

Figure 37 indicates that v(o) increases monotonically with 'a' and is an increasing function of v_c. In Figure 38, the aspect ratio α is shown to behave essentially as for the Dugdale counterparts (cf. Figure 26). The plastic work dissipation rate, $\frac{\partial U_c}{\partial a}$, approaches the asymptotic limit 4γ fairly quickly as illustrated in Figure 39.[29]

---

27. This non-uniqueness situation is qualitatively different from that of the Dugdale model (see Figure 24 for comparison).

28. Note that this conclusion is based solely on mechanics analysis.

29. The curve representing p-v model #6 has been smoothed out for $a > 2.5$. For this particular p-v relation, to get accurate v_c in the craze zone (whose size equals 0.8 for $a > 2.5$), finer discretization is required to capture the steep rise and fall of the stress distribution in the craze zone.

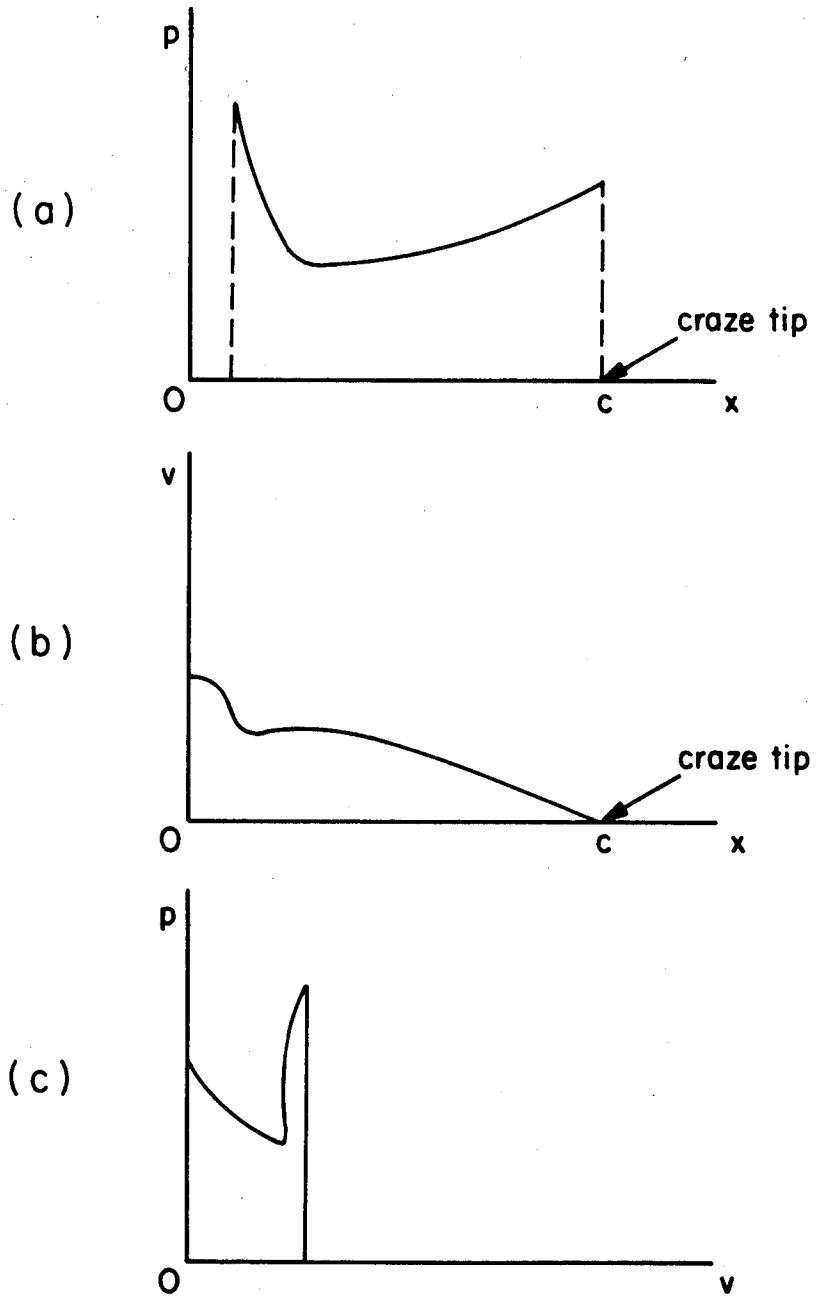

Figure 36. Demonstration of the nonexistence of 'short crack' solutions for p-v model #6 for c < 1.87. See discussion in Section 6.2.

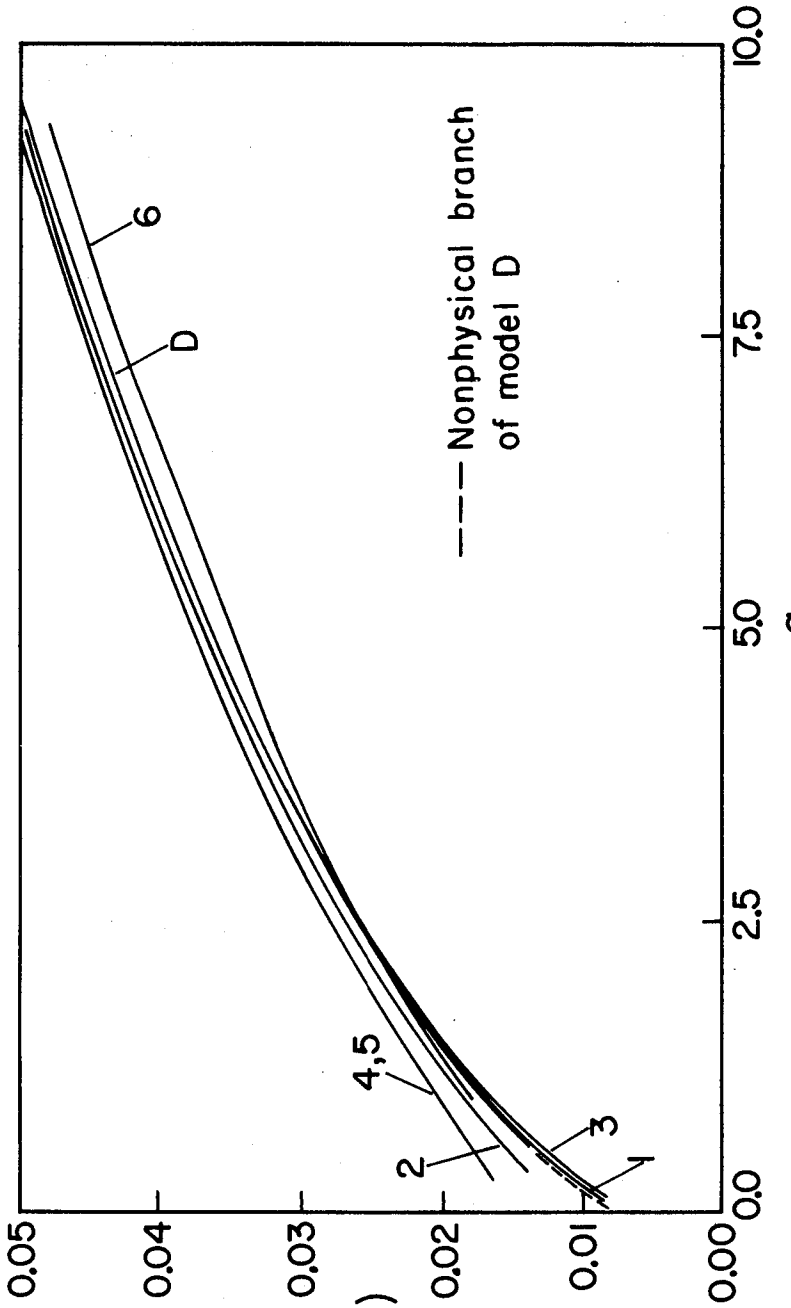

Figure 37. The displacement at the center of the craze v(o) as a function of 'a' for various nonlinear p-v models (p-v models as indicated).

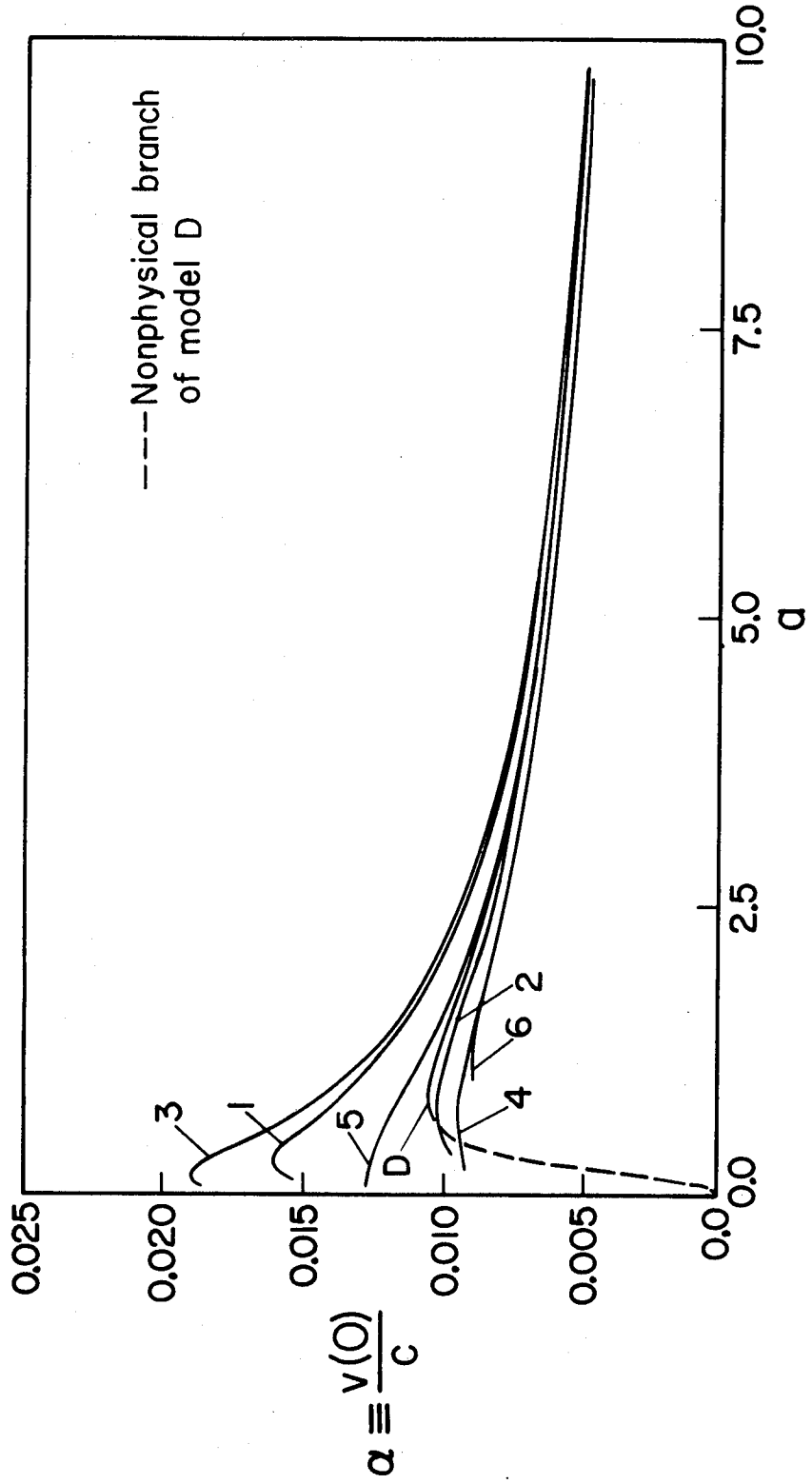

Figure 38. The aspect ratio α as a function of 'a' for various nonlinear p-v models (p-v models as indicated).

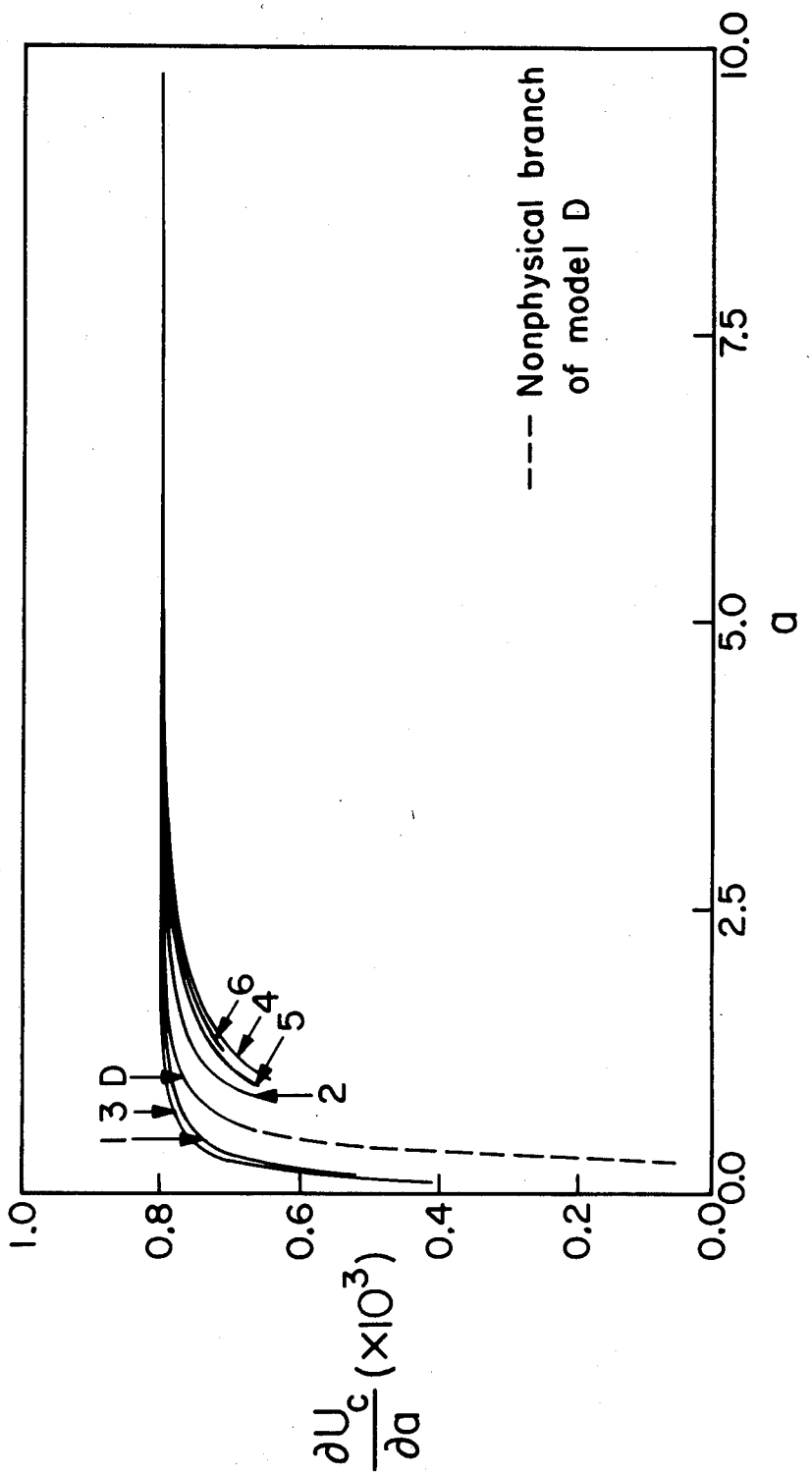

Figure 39. The rate of plastic work dissipation $\frac{\partial U_c}{\partial a}$ as a function of 'a' for various nonlinear p-v models (p-v models as indicated).

7. CRAZE GROWTH INITIATING FROM A PRECUT CRACK

In this section, we consider the problem of a craze growing from a precut slit as shown in Figure 40. Under the assumption of a CTOD criterion, one would expect the crack to start advancing when the far-field applied stress σ_∞ is high enough to make the crack tip displacement v(a) reach the value v_c. Thereafter the crack and craze would grow unstably as discussed in the previous section.

However, it is conceivable that for certain p-v relations, σ_∞ may reach its maximum value before the crack tip displacement reaches its critical value v_c, thus resulting in instability before the CTOD criterion is satisfied. We shall show that this is indeed the case for p-v relations that soften monotonically up to fracture (fibril breakage). To start, let us first study the Barenblatt-Dugdale model for later reference.

7.1. The Barenblatt-Dugdale Model

We start with a precut crack of length $2a_o$. Initially, this 'initial' crack length, a_o, is equal to the initial craze length, i.e. at the moment $c = a_o$ and $\omega = 0$. We then increase σ_∞ gradually until v(a) reaches v_c. By equation (6.5) when $v(a) = v_c$, the 'critical' craze length c_{cr} is

$$c_{cr} = a_o e^{\beta/a_o}, \qquad \beta \equiv \frac{\pi v_c}{2p_m} \tag{7.1}$$

Hence for $a_o \le c < c_{cr}$, the remotely applied stress σ_∞ can be obtained from (6.2), i.e.,

$$\sigma_\infty = \frac{2p_m}{\pi} \cos^{-1}\left(\frac{a_o}{c}\right), \qquad a_o \le c < c_{cr} \tag{7.2}$$

Based on (7.1) and (7.2), we can plot the applied stress σ_∞ as a

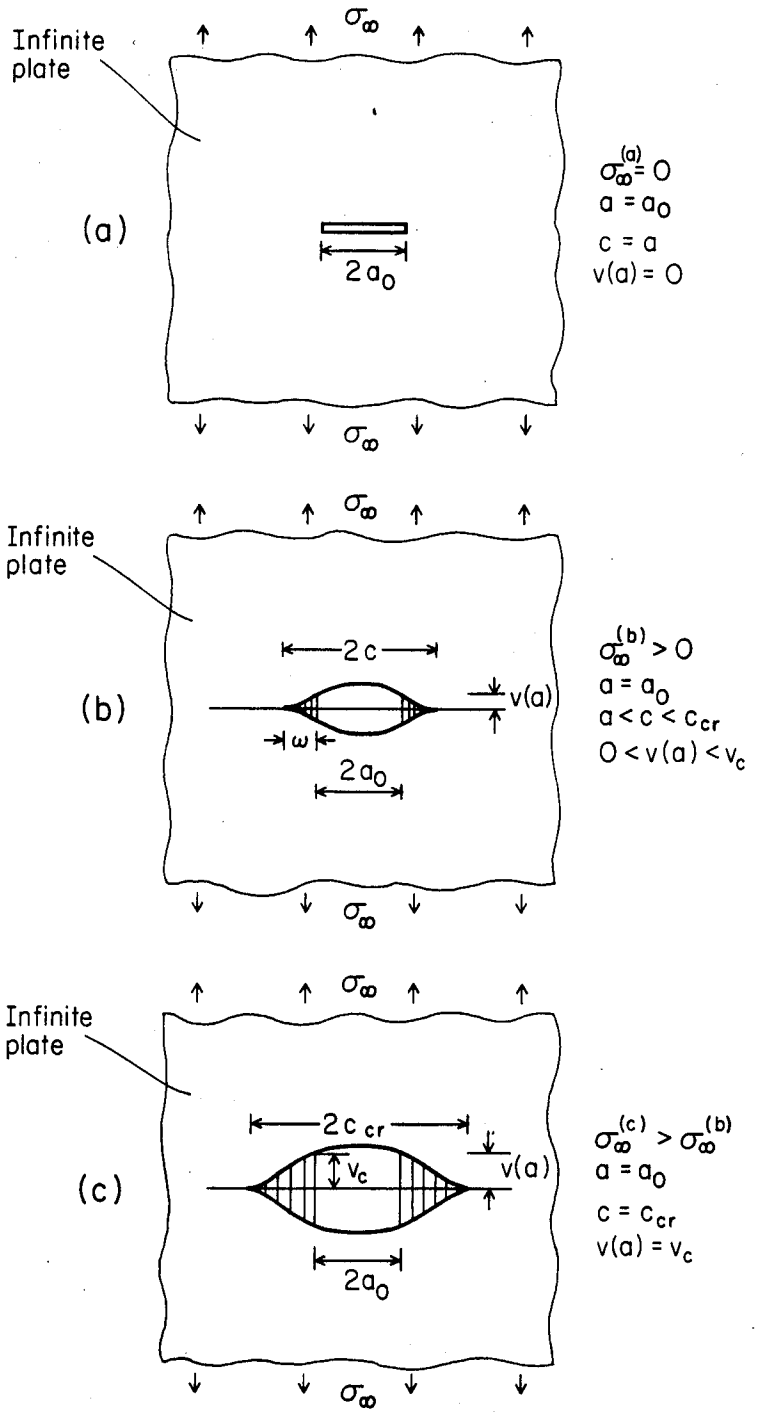

Figure 40. Craze growth initiating from a precut crack
(a) Initial precut crack, no far-field loading.
(b) Increasing far-field loading, no crack growth.
(c) Critical CTOD reached, crack growth imminent.

function of c for constant $a = a_o$ as shown in Figure 41. Five initial crack lengths are used (a_o= 0.3, 0.6, 0.9, 1.2, and 1.5). The curve representing quasi-static crack and craze growth referred to subsequently as the 'master' curve on which the CTOD always attains its critical value is also identified. On the 'master' curve, the craze and crack growth is unstable in the sense that σ_∞ must be reduced continually in order to maintain quasi-static.

For a_o=0.3 ($< a_{min}$),[30] σ_∞ increases from zero at point A monotonically to point B which lies on the nonphysical branch. As neither c nor 'a' can decrease (physically), one cannot follow the quasi-static equilibrium curve (henceforth the master curve) by gradually increasing or decreasing σ_∞. A jump is necessary to get back on the 'master' curve; this is achieved by dropping σ_∞ abruptly from point B to point C. In practice, quasi-static equilibrium will be difficult to maintain since σ_∞ must be known as a function of the craze length c in advance, and then prescribed and controlled. Most likely, the crack and craze would grow unstably from point B on. For $a_o \geq a_{min}$, it is possible to follow the master curve after c_{cr} is reached and maintain quasi-static growth with no 'jump'.

7.2. General p-v Models

Next let us consider the same problem as in Section (7.1) using p-v relations #1,3,5, and 6.[31] In contrast to the Barenblatt-Dugdale model, we find that for p-v relations that soften monotonically up to the point of fracture (models #1 through #5), instability may occur before the critical CTOD is reached at the crack tip. Briefly, the numerical analysis proceeds in the following sequence:

---

30. Here $a_{min} = \beta = \frac{\pi v_c}{2p_m} = 0.503$

31. The p-v relations #2 and #4 are not considered as they are of the same form as #1 and #3 respectively. (No new qualitative results are expected.)

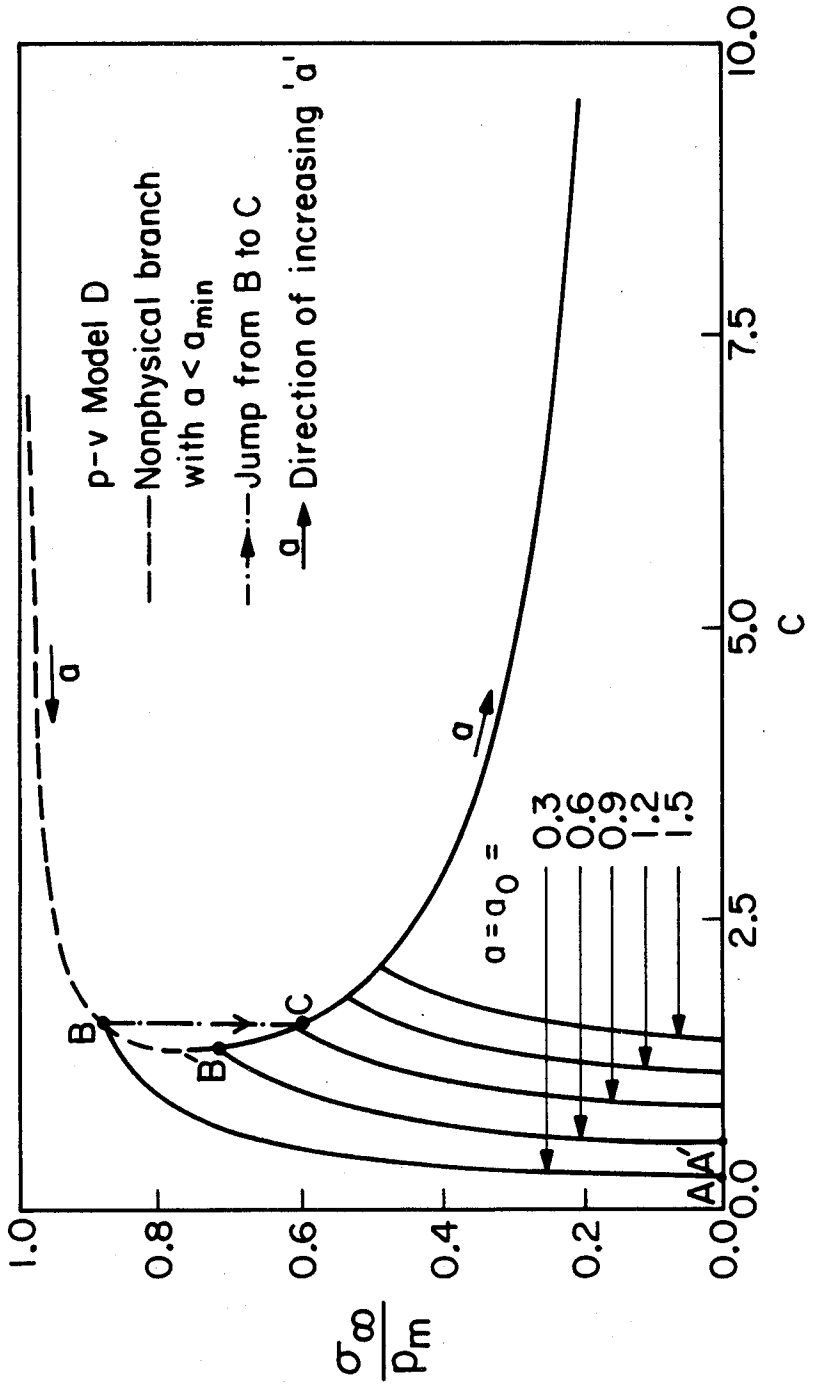

Figure 41. $\frac{\sigma_\infty}{p_m}$ as a function of c for a_o = 0.3, 0.6, 0.9, 1.2, and 1.5 for the Dugdale model 'D'.

i. Start with an a_o which corresponds to a 'c_{cr}' that lies on the master curve.

ii. Increase c gradually from a_o to c_{cr} in such way that the crack tip falls exactly on a discretized point x_i (see Figure 8). This avoids unnecessary interpolation.

iii. Find the solution, pre-specifying that p(x) vanish for $x \leq a_o$. The solution would automatically have $v(a) < v_c$ as long as $c < c_{cr}$.

As is evident from Figures 42 and 43, the results are very similar for p-v models #1 and #3. From the insets, one sees that, for $a_o = 0.3$, instabilities occur for both p-v models #1 and #3.

Specifically, let us consider a stress-controlled experiment (i.e. the far-field stress σ_∞ is prescribed). As σ_∞ is increased from zero up to point B, the CTOD, i.e., v(a) approaches the critical CTOD, v_c. At point B, any further increase in σ_∞ will cause the crack and craze to grow unstably since quasi-static growth will no longer be maintained at that stress level. If one reduces σ_∞ instead, keeping in mind that the craze length c cannot decrease while $a = a_o$ remains constant, point C could then be reached quasi-statically. Therefore, at point B, any small positive perturbation in σ_∞ or in a_o would cause the crack and craze to grow in an unstable manner. Note that the solution cannot 'jump' spontaneously from point A to point C because more work has to be done to further develop to craze zone and this is achieved by following the path ABC as discussed. Note that, if upon reaching point B, σ_∞ is maintained constant, the solution <u>cannot</u> simply jump across to point D on the master curve at the same level of σ_∞. This is because point D corresponds to $a < a_o$ and the crack cannot shrink from its initial length as no 'crack healing' is allowed.

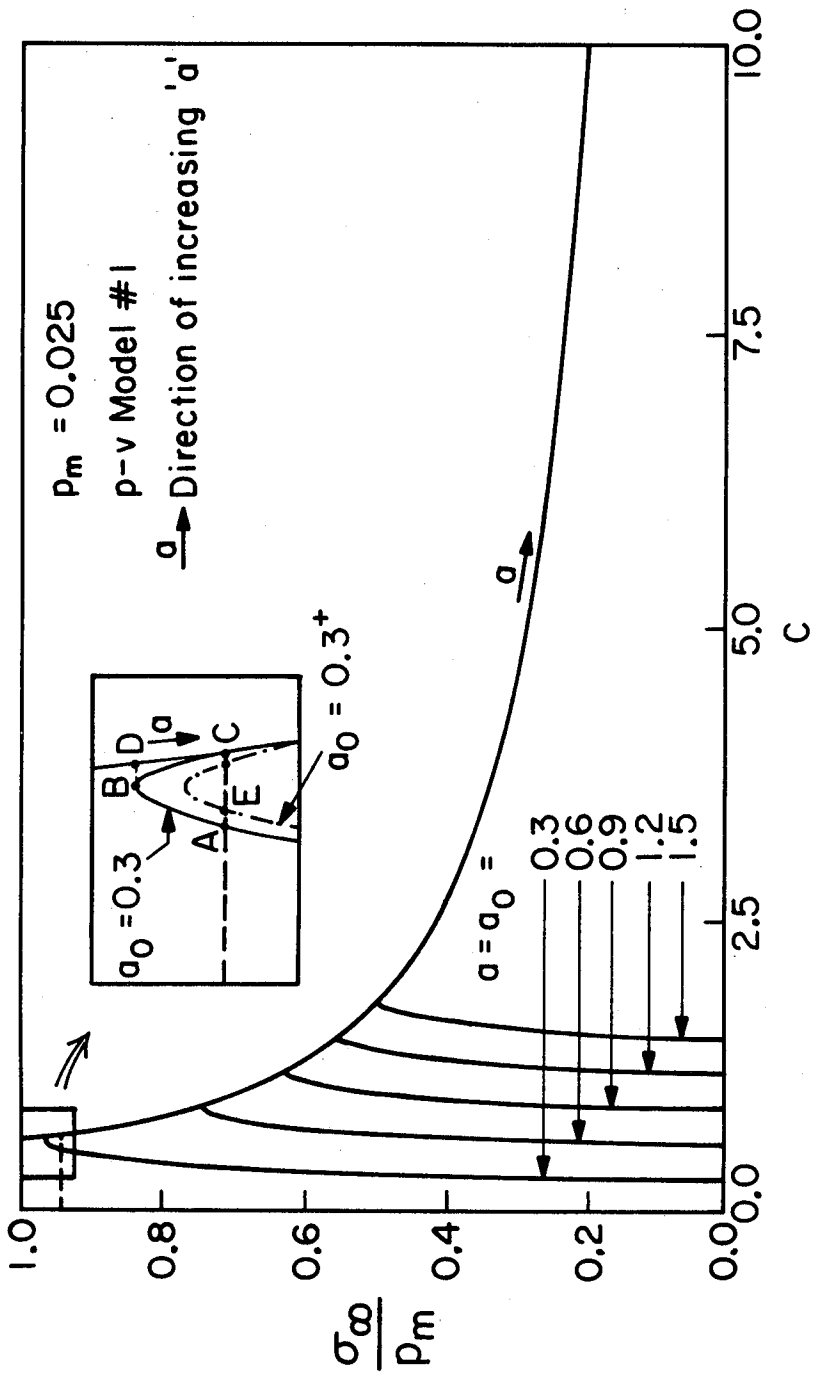

Figure 42. $\frac{\sigma_\infty}{p_m}$ as a function of c for a_o = 0.3, 0.6, 0.9, 1.2, and 1.5 for p-v model #1.

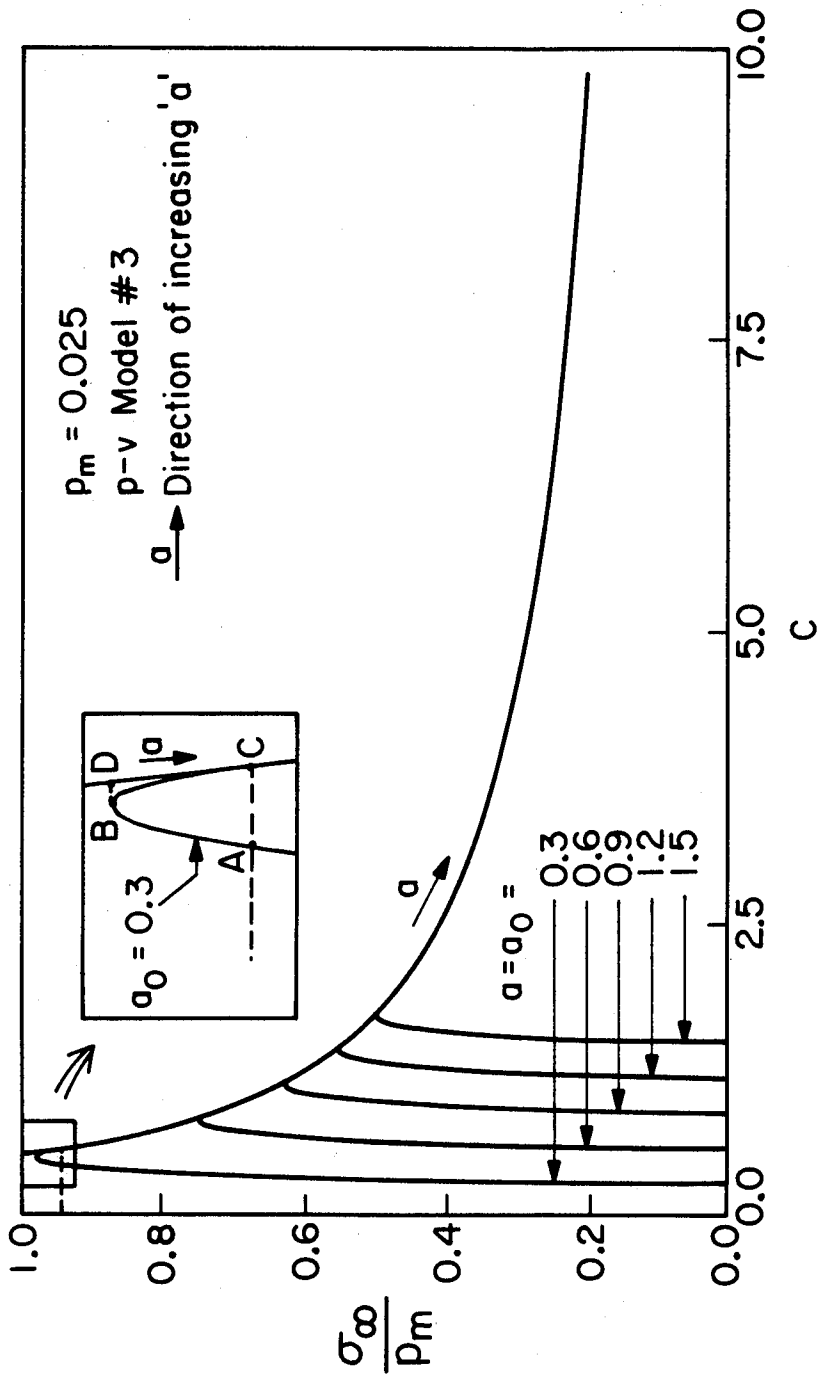

Figure 43. $\frac{\sigma_\infty}{p_m}$ as a function of c for a_o = 0.3, 0.6, 0.9, 1.2, and 1.5 for p-v model #3.

What happens, if at point A, one perturbs the system by cutting a fibril at the crack tip making a_o increase infinitesimally ? As depicted in Figure 42 (inset), the solution will simply jump from point A to a nearby point E which corresponds to $a_o = 0.3^+$ and stop. Thus the craze and crack at point A is stable since a small perturbation in a_o does not lead to total failure.

All the above discussions apply equally to p-v relation #5 with even more pronounced instability regimes. Figures 44 and 45 exemplify the various points made excellently. We see that for a p-v relation that softens sharply before leveling off and fails at relatively high v_c as in model #5, the instability occurs for a larger range of a_o. Note in passing that the unstable behavior is more pronounced for the shorter initial crack lengths.

We turn next to the results for p-v model #6 which rehardens after the initial softening and fails abruptly as in the Barenblatt-Dugdale model. In Figure 46, one sees that the unstable character observed in softening p-v models is clearly absent which closely resembles the result for the Barenblatt-Dugdale model shown Figure 41. These results indicate that in cases where craze fibrils fail in abrupt manners (as opposed to gradual softening to rupture), instability does not take place until the CTOD reaches its critical value v_c .

To summarize, it has been shown that, for fibril (or cohesive) force-displacement relationships with softening characteristics up to fracture, instabilities could occur before the critical crack tip opening displacement is reached at the crack tip especially for short initial crack lengths.

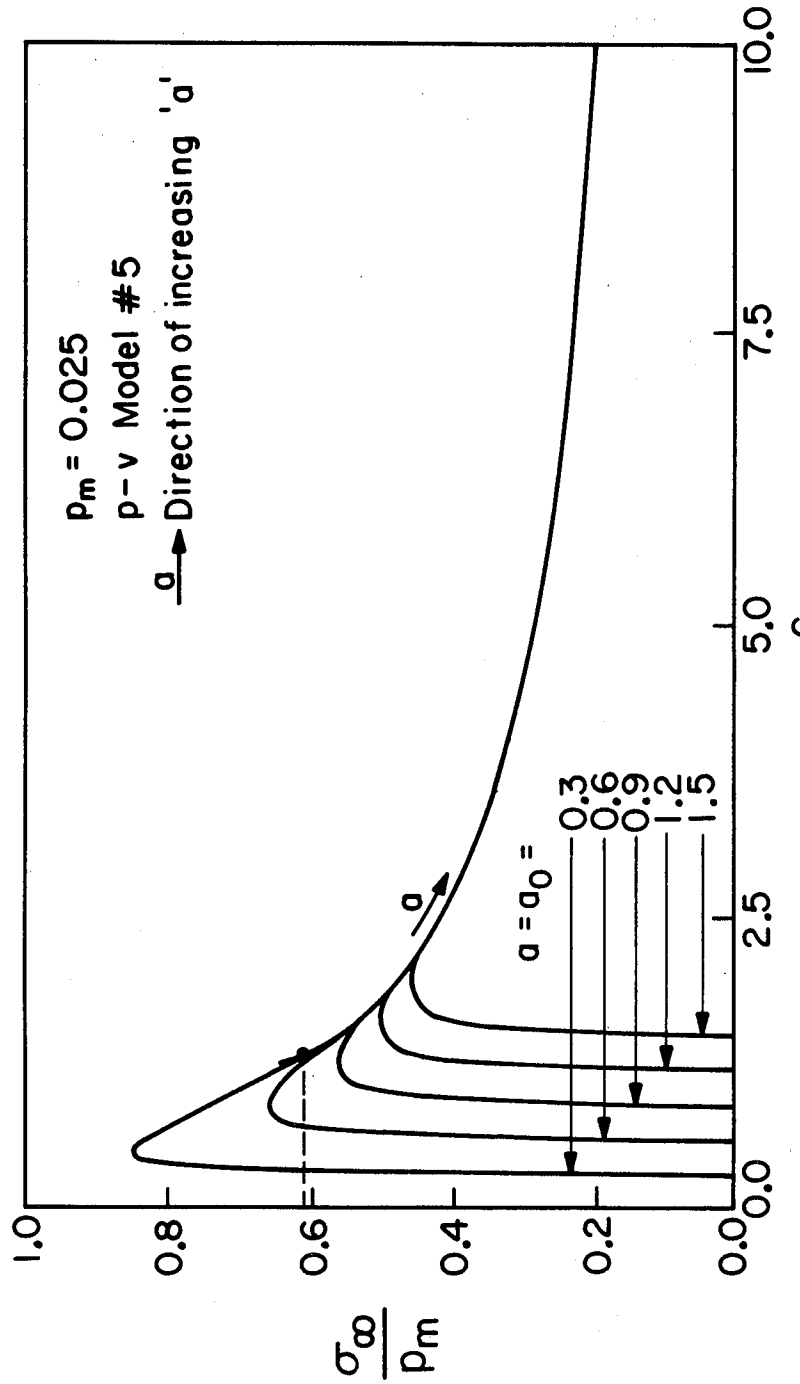

Figure 44. $\frac{\sigma_\infty}{p_m}$ as a function of c for a_o = 0.3, 0.6, 0.9, 1.2, and 1.5 for p-v model #5.

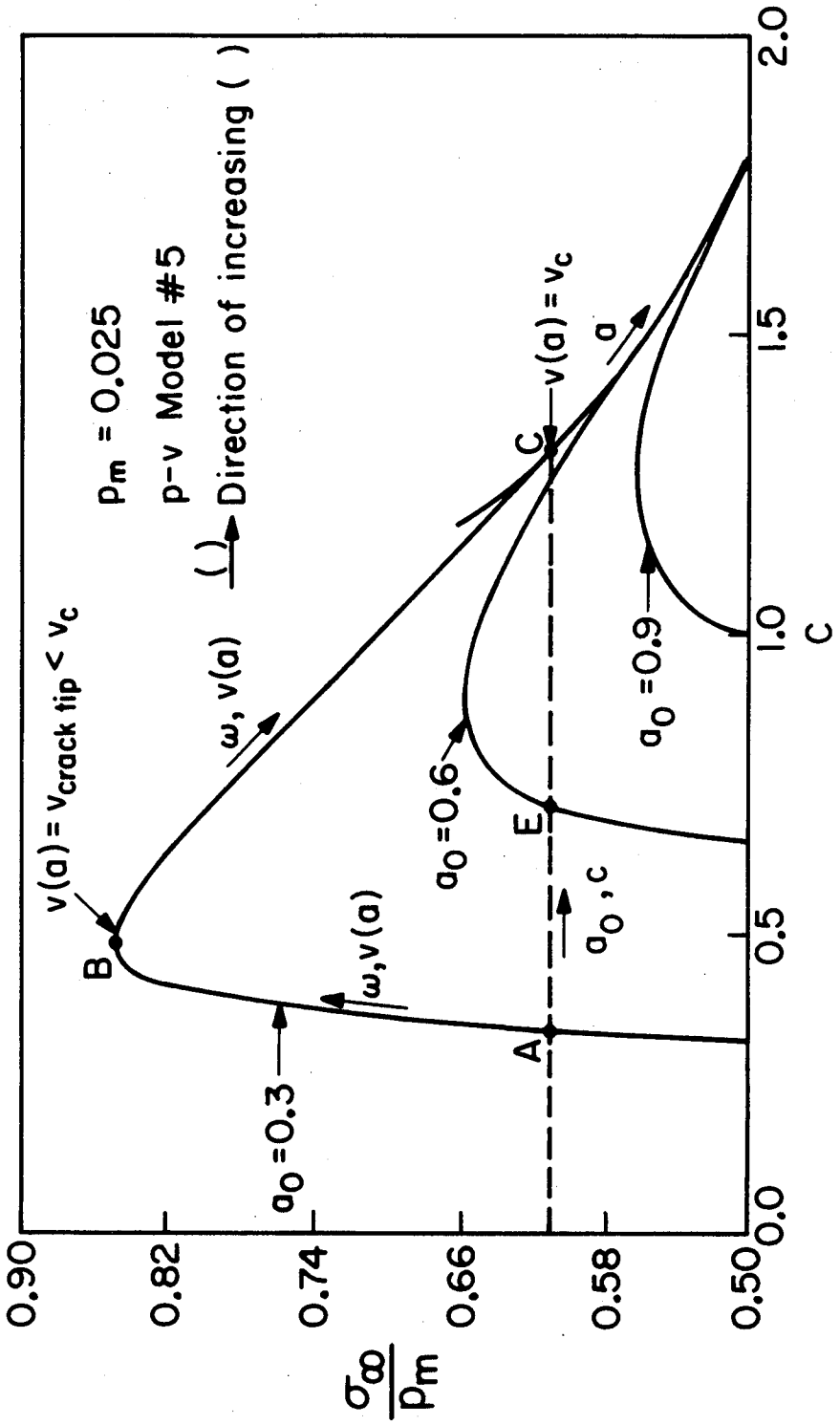

Figure 45. $\frac{\sigma_\infty}{p_m}$ as a function of c for a_o = 0.3, 0.6, 0.9, 1.2, and 1.5 for p-v model #5 (enlargement of a part of Figure 44).

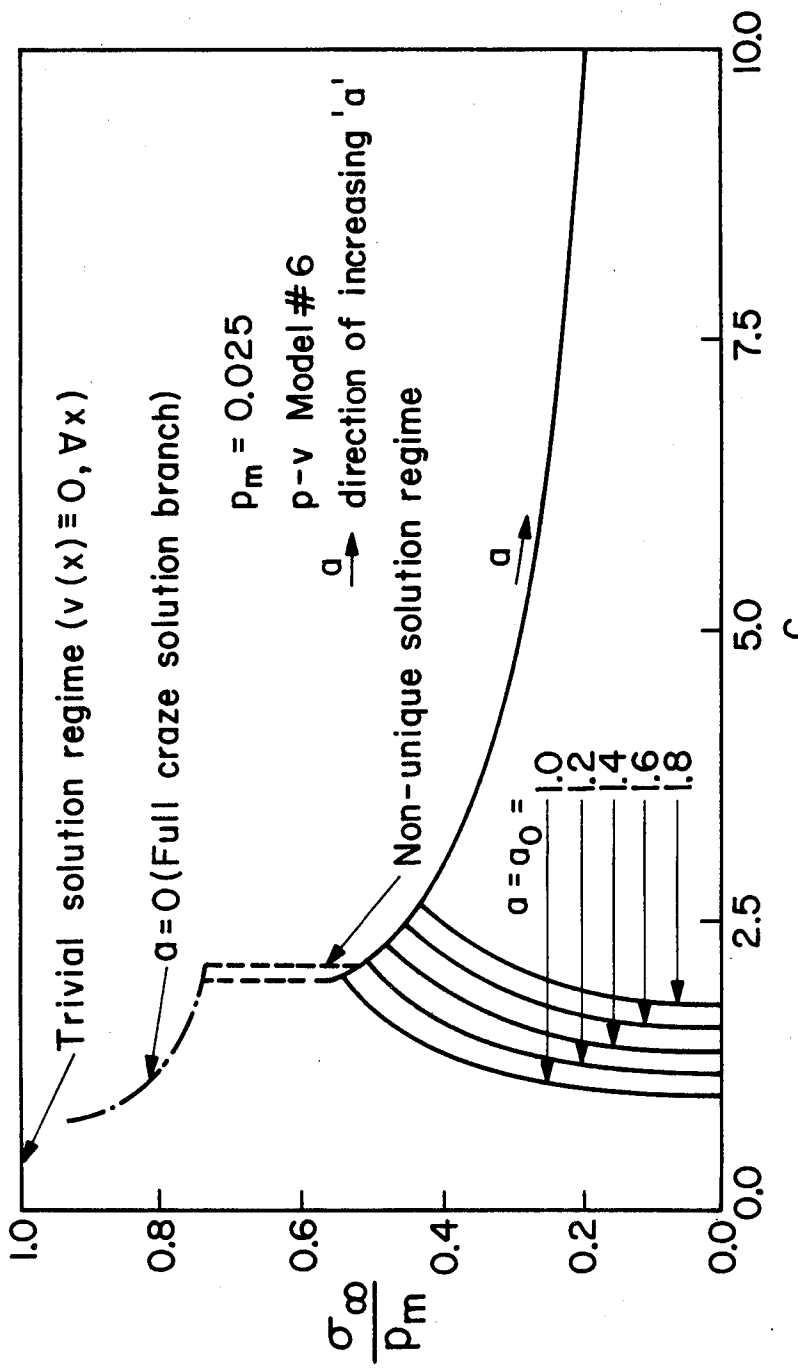

Figure 46. $\frac{\sigma_\infty}{p_m}$ as a function of c for a_o = 1.0, 1.2, 1.4, 1.6, and 1.8 for p-v model #6.

8. CONCLUSIONS AND SUGGESTIONS FOR FURTHER WORK

We have shown that the problem of a craze (with or without an internal crack) in an infinite plane under symmetrical loading may be solved exactly. The formulation and solution scheme are simple and straightforward. The implemented Picard's algorithm is effective and more economical than the Newton's method. The formulation can also be used, with definite advantage over the presently available schemes, to determine stress distribution profiles and the p-v relations from experimental displacement profiles.

Quasi-static crack and craze growth is investigated in detail. Six nonlinear p-v relation models are considered in the propagation study. Craze growth starting with a precut crack is also presented, instabilities are observed for softening p-v models. Energy dissipation rate consistent with the critical CTOD criterion is derived and computed.

As emphasized earlier, not enough is known about the p-v characteristics of the craze fibrils. Further investigation into the interplay between the surface drawing and creep mechanics should shed some light on how the p-v characteristics of fibrils change as the craze and crack grow; a first attempt along this line has been undertaken by Kramer and Hart [9]. On another front, experiments such as those performed by Kramer et al. [5,22,23] should be done for a wider range of craze and crack lengths to determine if the fibril p-v relation is invariant of c and 'a'. (And if so, to what extent ?)

Lastly, one should recognize that the present analysis may, equally well, be applied to the analysis of cracks. In such case, the p-v relation represents the crack tip cohesive stress-strain characteristics, thus generalizing the Dugdale model.

9. REFERENCES

1. Bucknall, C.B. "Toughened Plastic," Ch. 6, App. Sci. Publ., London, 1977, pp. 136-181.

2. Argon, A.S., Cohen, R.E., Gebizlioglu, O.S., and Schwier, C.E., "Crazing in Block Copolymers and Blends," Advances in Polymer Science, Vol. 52-53, H.H. Kausch (Ed.), Springer-Verlag Berlin, Heidelberg, 1983, pp. 275-334.

3. Kramer, E.J., Advances in Polymer Science, Vol. 52-53 Ch. 1, H.H. Kausch (Ed.), Springer-Verlag Berin, Heidelberg, 1983.

4. Argon, A.S. and Salama, M.M., "Growth of Crazes in Glassy Polymers," Phil. Mag., Vol. 36, 5, 1977, pp. 1217-1234.

5. Lauterwasser, B.D. and Kramer, E.J., "Microscopic Mechanisms of Craze Growth and Fracture," Phil. Mag. A., Vol. 39, 4, 1979, pp. 469-495.

6. Spurr, O.K. and Niegisch, W.D., "Stress Crazing of Some Amorphous Thermoplastics," J. Appl. Polym. Sci., Vol. 6, 23, 1962, pp. 585-599.

7. Kambour, R.P. and Kopp, R.W., "Cyclic Stress-Strain Behavior of the Dry Polycarbonate Craze," J. Polymer Science, A-2, Vol. 7, 1969, pp. 183-200.

8. Hull, D., "The Microstructure and Properties of Crazes," in Deformation and Fracture of High Polymers, Kausch, Hassell, and Jaffe (Eds.) Plenum Press, 1973, pp. 171-189.

9. Kramer, E.J. and Hart, E.W., "Theory of Slow, Steady State Crack Growth in Polymer Glasses," Polymer, Vol. 25, 1984, pp. 1667-1678.

10. Barenblatt, G.I., "The Mathematical Theory of Equilibrium Cracks in Brittle Fracture," in Advances in Applied Mechanics, Vol. VII, Academic Press, New York, 1962, pp. 59-129.

11. Dugdale, D.S., "Yielding of Steel Sheets Containing Slits," J. Mech. Phys. Solids, 1960, Vol. 8, pp. 100-104.

12. Rice, J.R., "Plastic Yielding at Crack Tip," Proceedings of the 1st Int'l Conf. on Fracture, Vol. I, Sendai, Japan, T. Yokobori et al. (Eds.), Japanese Soc. for Strength and Fracture of Materials, Tokyo, 1966, pp. 283-308.

13. Goodier, J.N. and Field, F.A., "Plastic Energy Dissipation in Crack Propagation," Fracture of Solids, D.C. Drucker and J.J. Gilman (Eds.), Wiley (Interscience), New York, 1963, pp. 103-118.

14. Goodier, J.N. and Kanninen, M., "Crack Propagation in a Continuum Model with Nonlinear Atomic Separation Laws," Technical Report No. 165, Div. of Eng. Mech., Stanford University,1966.

15. Atkinson, C. "An Iterative Scheme for Solving Problems Relating to Cracks Opening under a Displacement Dependent Internal Stress," Int. J. Fracture Mech., Vol. 6, 2, 1970, pp. 193-198.

16. Andersson, H. and Bergkvist, H., "Analysis of a Nonlinear Crack Model," J. Mech. Phys. Solids, Vol. 18, 1970, pp. 1-28.

17. Smith, E., "The Structure in the Vicinity of a Crack Tip: A General Theory Based on the Cohesive Zone Model," Eng. Fract. Mech., Vol. 6, 1974, pp. 213-222.

18. Knight, A.C., "Stress Crazing of Transparent Plastics: Computed Stresses at a Nonvoid Craze Mark," J. Polymer Sci, Part A, Vol. 3, 1965, pp. 1845-1857.

19. Sneddon, I.N., Fourier Transforms, McGraw-Hill, New York, 1951, p. 426.

20. Knauss, W.G., "Crack Propagation in Viscoelastic Diaspastically Non-Simple Solids: A Progress Report," Int. Union of Theoretical and Appl. Mech., Mech. of Viscoelastic Media and Bodies Symposium, Gothenburg, Sweden, J. Hult (Ed.), 1974, pp. 263-278.

A more extensive version can be found in Strength and Structure of Solid Materials, a joint Japan-USA seminar, Noordhoff International Publishing, Leyden; H. Miyamoto et al. (Eds.), 1976, pp. 389-416.

21. Verheulpen-Heymans, N. and Bauwens, J.C., "Effect of Stress and Temperature on Dry Craze Growth Kinetics during Low-Stress Creep of Polycarbonate," Part 1 & 2, J. Mat. Sci, Vol. 11, 1976, pp. 1-6 & 7-16.

22. Wang, W.V., and Kramer, E.J., "A Distributed Dislocation Stress Analysis for Crazes and Plastic Zones at Crack Tips," J. Mat. Sci, Vol. 17, 1982, pp. 2013-2026.

23. Donald, A.M. and Kramer, E.J., "The Entanglement Network and Craze Micromechanics in Glassy Polymers," J. Polymer Sci., Polymer Physics Edition, Vol. 20, 1982, pp. 1129-1141.

24. Bevan, L., "Finite Element and Boundary-Element Analysis of Craze Micromechanics," J. Appl. Polymer Sci, Vol. 27, 1982, pp. 4263-4272.

25. Sun, B.N. and Hsiao, C.C., "Nonlinear Quasi-fracture Behavior of Polymers," J. Appl. Phys., Vol. 57(2), 1985, pp. 170-174.

26. Walton, J.R. and Weitsman, Y., "Deformations and Stress Intensities Due to a Craze in an Extended Elastic Material," J. Appl. Mech., Vol. 51, 1, 1984, pp. 84-92.

27. Weitsman, Y., "Nonlinear Analysis of Crazes," J. Appl. Mech., Vol. 53, 1, 1986, pp. 97-102.

28. Kambour, R.P., "Stress-Strain Behavior of the Craze," Poly. Eng. and Sci., Vol. 8, 4, Oct. 1968, pp. 281-289. (In particular, p. 283, 2nd paragraph.)

29. Tada, H., Paris, P.C., and Irwin, G.R., The Stress Analysis of Cracks Handbook, Del Research Corporation, Hellertown, PA, 1973, p. 5.10.

30. Huang, N.C., "On the Size of the Cohesive Zone at the Crack Tip," J. Appl. Mech. (Brief Notes), Vol. 52, June 1985, pp. 490-492.

31. Schinker, M.G. and Doll, W., "Interference Optical Measurements of Large Deformations at the Tip of a Running Crack in a Glassy Thermoplastic," Physics Conference Series No. 47, J. Harding (Ed.), Inst. of Physics, Bristol, England, 1979, pp. 224-232.

32. Doll, W. et al., "A Time Independent Fracture Criterion for PMMA ?," Int. J. Fracture, Vol. 15, 1979, pp. R145-149.

APPENDIX

ABSTRACT

This appendix summarizes the results of an attempt to generalize the nonlinear cohesive zone model analyzed previously to the case where plastic deformation is not only confined to the crack path but spans the material surrounding the crack. Failure is, however, still allowed only along the prescribed crack path. The problem examined is formulated in terms of a compact tension specimen loaded by a displacement controlled machine. The material is elastic-plastic and is characterized by the classical J_2 - flow theory of plasticity. The specimen is modeled by a finite element mesh while the damaged-softened 'boundary layer' along which the crack is to propagate is represented by a row of nonlinearly softening springs. The springs' initial stiffness is (nearly) infinite, and the onset of softening occurs when a critical nodal force is reached and failure takes place at a critical separation distance.[1] When a spring fails, the crack advances by an increment equal to the dimension of the finite element adjoining the crack path much like in the case of the beam on a nonlinear foundation studied in Section 3 of Part I. The fracture energy is equal to the area under the spring's separation characteristics; material toughness would include the energy dissipated in plastic deformation. The definition of the problem is complete and no extra fracture criterion is needed, i.e., crack growth is totally controlled by the external loading.

The finite element program ABAQUS is employed for this purpose. The studies indicate that the solution is extremely sensitive to the size of the loading increment used, i.e., prescription of the solution path[2] is critical in avoiding erroneous results. More importantly, a

1. For the motivation of this spring design, see Section 1 of Part I and the discussion to follow in the introductory section of this appendix.

2. By 'solution path', we mean the loading history which proceeds in small increments. In problems where plastic deformation is described by the flow theory of plasticity, different sizes of increments taken to arrived at the same prescribed loading could

numerical difficulty is encountered as the spring at the crack tip starts to soften. The investigation suggests that additional constraints may need to be imposed on the manners by which the softening springs representing the 'boundary layer' are allowed to deform.

On another aspect of this study, we attempt to devise a proper scaling scheme for the springs so as to be able to derive consistent results from the finite element analyses independent of the mesh sizes employed. It was found that the fracture energy must vanish as the crack tip element size is decreased to zero, otherwise, the finite size of the fracture process zone must be accounted for by recognizing that the crack grows in discrete steps.[3]

---

yield different results.

3. The size of this 'discrete step' is a material characteristic and is determined physically by the failure mechanisms prevalent in the crack tip process zone.

1. INTRODUCTION

In this appendix, an attempt is made to extend the use of the non-linear cohesive zone model of the Barenblatt-Dugdale type to simulate crack growth in elastic-plastic materials. The motivation for the approach taken here is based on certain physical observations described below.

It is well recognized that cracks grow in different materials with varying degrees of ductility depending on the loading and on the environmental conditions. If the fracture process is relatively brittle, the crack surfaces separate in such a way that little plastic deformation is induced in the material surrounding the crack path. On the other hand, when the crack faces are formed through void nucleation, growth and coalescence, the 'effective' fracture energy turns out to be substantially higher than in brittle fracture because the extent of plastic deformation in the material adjacent to the path traversed by the crack is much greater. Thus, the material toughness and separation characteristics reflecting the failure mechanisms at the crack tip directly control the energy expenditure and the stress and strain fields around the crack front.

In view of the above discussion, it is clear that fracture analyses are necessarily incomplete if they do not incorporate the proper 'separation laws' which characterize the failure processes at and ahead of the crack tip. Let us consider that two distinct and interacting deformation modes exists: One is the plastic deformation described by the continuum theory of plasticity which occurs in the material surrounding the crack tip. The other mode of deformation incorporates the failure mechanisms caused by the interaction of microvoids in the fracture process zone resulting in eventual surface separation. In many instances, this process is confined to a very thin 'boundary layer' along the crack path.

It is natural to introduce a fracture model in which this 'boundary layer' is represented by a row of nonlinear springs whose characteristics reflect this separation mode of deformation discussed above while allowing the material surrounding the crack to respond plastically to the external loading and the crack-tip constraints imposed through the boundary layer.

The model discussed above is supported by the findings of Kanninen et al [1]. In these studies, fracture experiments were performed on center-cracked panels and compact tension specimens made of the 2219-T87 aluminum alloy or the A533-B steel. The experimental measurement of the applied load (or displacement) and crack growth history was then used as inputs to a finite element analysis from which a number of candidates (such as the crack tip opening displacement and angle) for stable crack growth parameters were extracted. This experimental-computational process termed the 'generation-phase' analysis involved imposing the known loading history in the finite element analysis and enforcing the corresponding crack growth history by gradually releasing the crack tip node one by one to simulate the experimental measurements. From their generation-phase analyses, it was found that the critical nodal force, F_c , at which the nodes were released and the fracture energy, γ ,[4] were relatively constant during crack propagation.[5] Based on these findings, the softening springs employed in our model are designed to of 'infinite' initial stiffness[6] with the softening starting at a critical nodal force, F_c , and the complete failure

4. Or the area under the curve of the crack tip nodal force versus the nodal displacement which is the work done by the system in order to generate new crack surfaces.

5. In private communication with Dr. Kanninen, he informed us that each node release generated approximately the same nodal force versus nodal displacement curve yielding the same fracture energy.

6. In this study, we make this initial stiffness equal 10^3 to 10^5 times the Young's modulus of the elastic-plastic material, the results to be discussed is insensitive to the exact value of this 'infinite' initial stiffness of the springs in this range.

at a critical separation distance, δ_c. Figure A-1a illustrates a typical 'nonlinearly-softening' spring.

Having laid down the motivation for introducing the 'boundary layer' model discussed above, we describe in the upcoming section its implementation through finite element modeling. The results of the finite element studies are summarized and interpreted in Section 3; the numerical difficulty encountered is discussed in detail. When the size of the finite elements along the crack path is decreased, it is necessary to scale the nonlinear springs accordingly in a proper manner so that the results from analyses using different finite element meshes are consistent. An attempt to find such a consistent scaling scheme is discussed in Section 4. Suggestions for overcoming some of the difficulties encountered in the study then follow in Section 5.

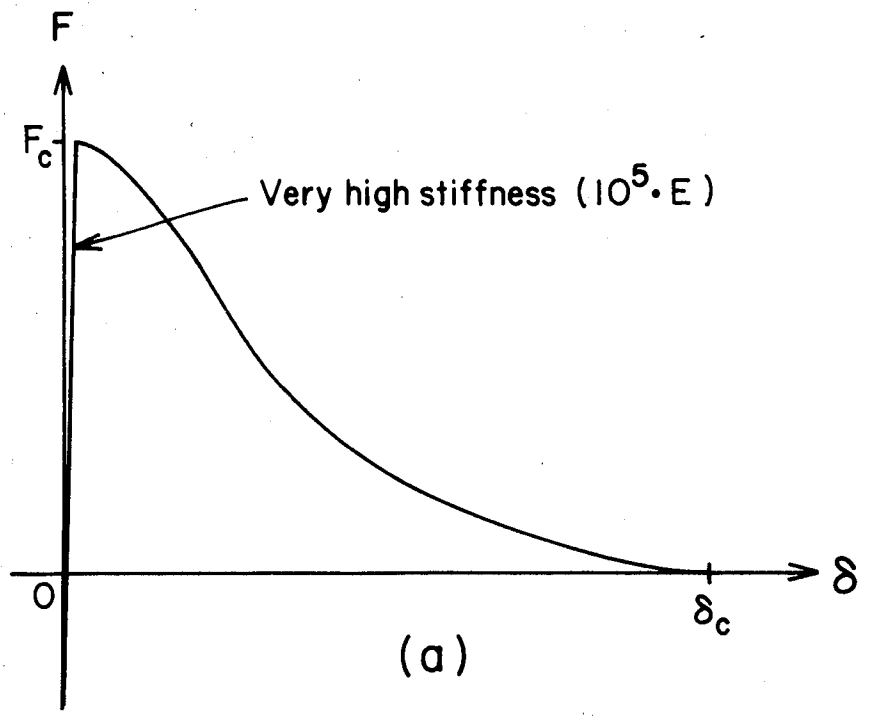

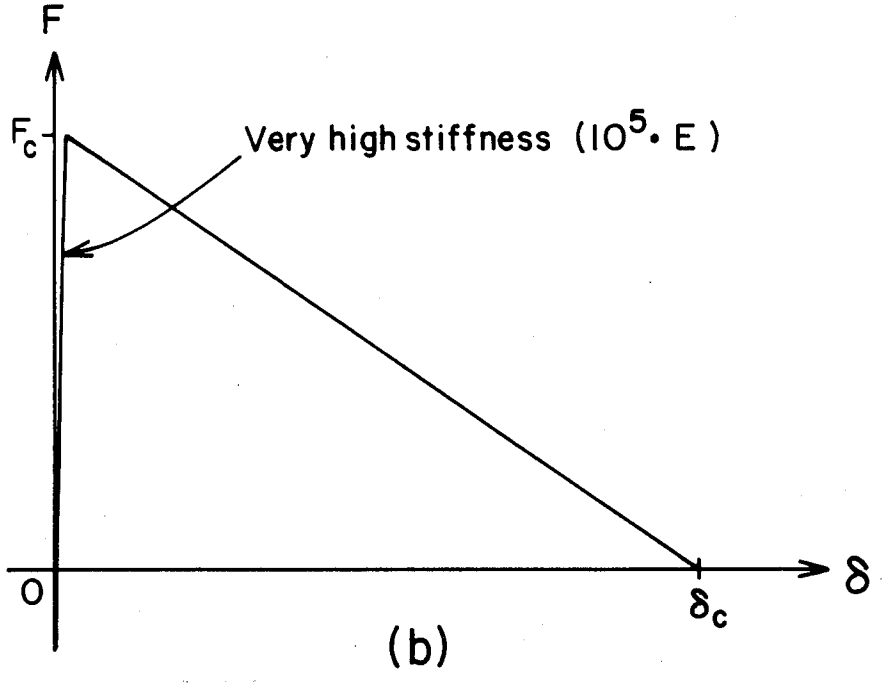

Figure A-1. Nonlinear springs used to model the behavior of the damage-softened 'boundary layer'.
(a) Nonlinearly-softening spring
(b) Linearly-softening spring

2. THE FINITE ELEMENT MODEL

In this section, we describe the specific problem we choose to study first. We rely on reference 1 for the input data, i.e., for the specimen dimensions, the material property as well as the 'generation-phase' fracture parameters used in designing the nonlinear springs.

We tested the model by attempting to duplicate the results in reference 1 using the data given there for the design of the finite element mesh and the softening springs. The experimental data and the values for F_c (see Figure A-1) and γ obtained from the 2219-T87 aluminum compact tension specimen tests were chosen. The problem was analyzed under the plane-stress conditions. The stress-strain behavior of the aluminum was approximated by a piecewise-linear hardening curve as is given in reference 1. The finite element program ABAQUS (version 4.5) running on an FPS-164 array processor with a VAX-11/780 as its host machine was employed for this purpose. Four-noded bilinear plane-stress elements were used to model the compact tension specimen. Nonlinear springs were used to restrain the vertical motion of the nodes along the crack path simulating the damage-softened 'boundary layer'.

The finite element mesh used in this study is shown in Figure A-2a with the detailed crack tip mesh in Figure A-2b.[7] The mesh consists of 385 elements, 12 identical springs, 429 nodes, and a total of 858 degrees of freedom with the smallest element size being 1.5 mm by 1.5 mm.[8] The crack path is modeled by a row of 'linearly-softening' springs the force-displacement behavior of which is shown in Figure A-1b. [9] The

7. By symmetry, only half of the specimen needs to be modeled. Also, throughout this study the plastic zone is always well contained within the boundary of the detailed mesh in Figure A-2b.

8. The element size of 1.5 mm by 1.5 mm is chosen for the initial studies as it adequately captures the deformation in the crack tip zone while keeping the computing time reasonable.

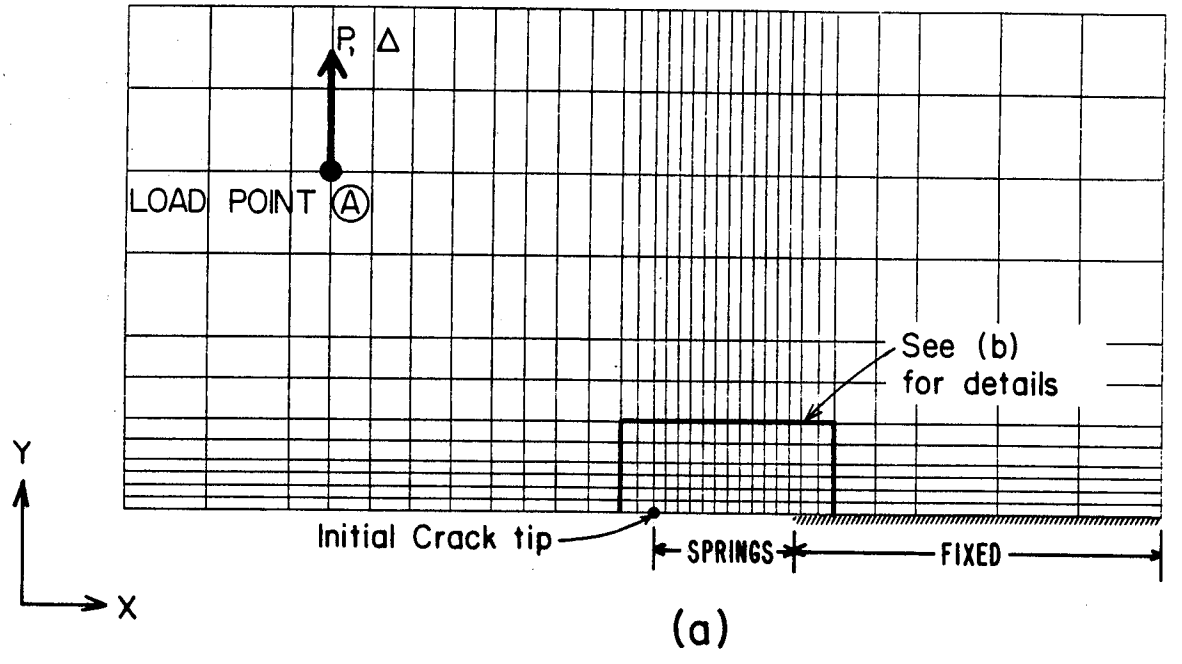

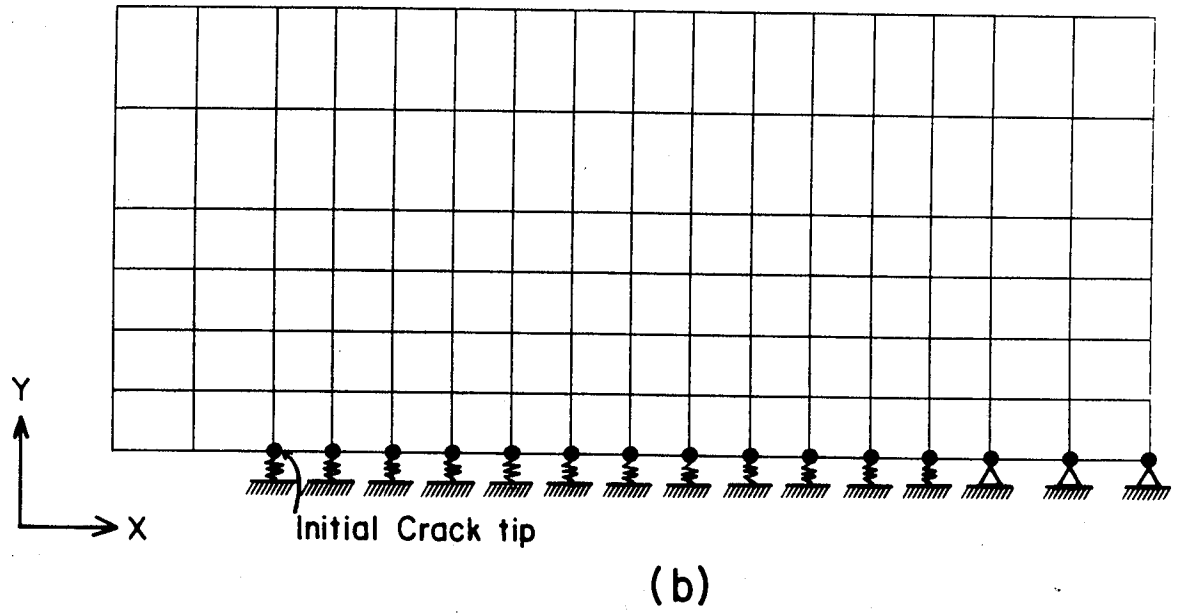

Figure A-2. The finite element mesh for the compact tension specimen.
(a) The overall mesh
(b) The detailed mesh of crack tip zone

rest of the nodes along the line of symmetry are fixed. The loading is accomplished through prescribing the displacement, Δ, at the node A, the reaction force at A then equals the applied load, P. The solution is effected by the usual Newton's iteration; a solution is considered attained when all residual nodal forces except at the nodes with prescribed displacements fall below 0.1% of the actual force values (in this case, P).[10]

9. We used 'linearly-softening' springs in this initial attempt for convenience as Dr. Kanninen indicated that the actual nodal unloadings in the analyses in reference 1 consistently followed a curved path just slightly below the linear path employed here. However the ABAQUS code is capable of handling general piecewise-linear springs.

10. Details of the ABAQUS code can be found in the ABAQUS Theory Manual published by Hibbitt, Karlsson and Sorensen, Inc., Providence, Rhode Island.

3. THE FINDING AND ITS INTERPRETATION

We next discuss a number of findings and attempt to give a suitable interpretation of the numerical difficulty encountered. Suggestions for improvement are left for the last section.

First of all, it is important to discuss the sensitivity of the results on the solution path (or loading history), in particular, the increment size of the loading employed in reaching a solution. In the initial attempts, an automatic incrementation scheme was employed. In this process, the step size of the displacement (loading) increment was adjusted continually in order to minimize the computation time: When convergence was judged unlikely for the current incremental step size based on the residual nodal forces at the end of each iteration, subdivision of the incremental step size took place until convergence was attained. On the other hand, when convergence was obtained twice and easily for the current step size, the step size would be increased. In most problems, this automatic scheme led to the same solution as would direct user control of the incremental step size. In this problem, the initial results obtained under the automatic incrementation scheme were very encouraging as we were able to simulate crack propagation very effectively.

It is necessary to verify these initial results by ensuring that they are independent of the particular solution path chosen by the automatic incrementation scheme employed. Attempts to duplicate the above results by directly controlling the incremental step size were unsuccessful as completely different results were obtained.[11] When the step size was kept very small and constant, we found that as the nodal force at the first spring (located at the crack tip) approached its critical value, F_c , the solution no longer converged. Moreover, at

11. The constant incremental step size used was the smallest step size needed for convergence when the automatic scheme was employed.

this stage, the applied displacement and load had far exceeded the values at which the result obtained through the automatic incrementation scheme indicated that crack propagation should occur. For example, at the load level at which the result of the automatic scheme indicated crack growth over a distance of 15 mm,[12] direct control of loading incrementation yielded a solution where the nodal force at the first spring was only approaching F_c.

In hindsight, it is not difficult to see why these initial attempts at using the automatic incrementation scheme fail: Consider a stage in the solution when the nodal force at the crack tip spring reaches, say, 90.0% of F_c, i.e., at point A in Figure A-3. If a large step is taken in the next increment, the convergent solution obtained could easily increase the crack tip nodal displacement such that a jump from point A to point B takes place. When this happens, the force-displacement relation of the spring is 'clipped' and is effectively different from what we prescribed, and an incorrect solution is obtained. Needless to say errors such as this propagate as the solution progresses, making subsequent results meaningless. Thus, in order to obtain the correct solution, one needs to ensure that the incremental step size is always small enough so that behavior such as illustrated in Figure A-3 is ruled out. In other words, the solution path must be taken such that the information contained in each spring is fully used.

Having recognized the above point, we continued the investigation by imposing a very small upper-bound on the incremental step size and allowing for smaller step sizes to be used when necessary.[13] It turned

12. Ten springs had been broken and the crack had propagated over ten elements' length.

13. Note that when the initially chosen small step size was fixed, we had no convergence as the crack tip spring started to soften; it is therefore necessary to allow for further subdivisions of the initial step size.

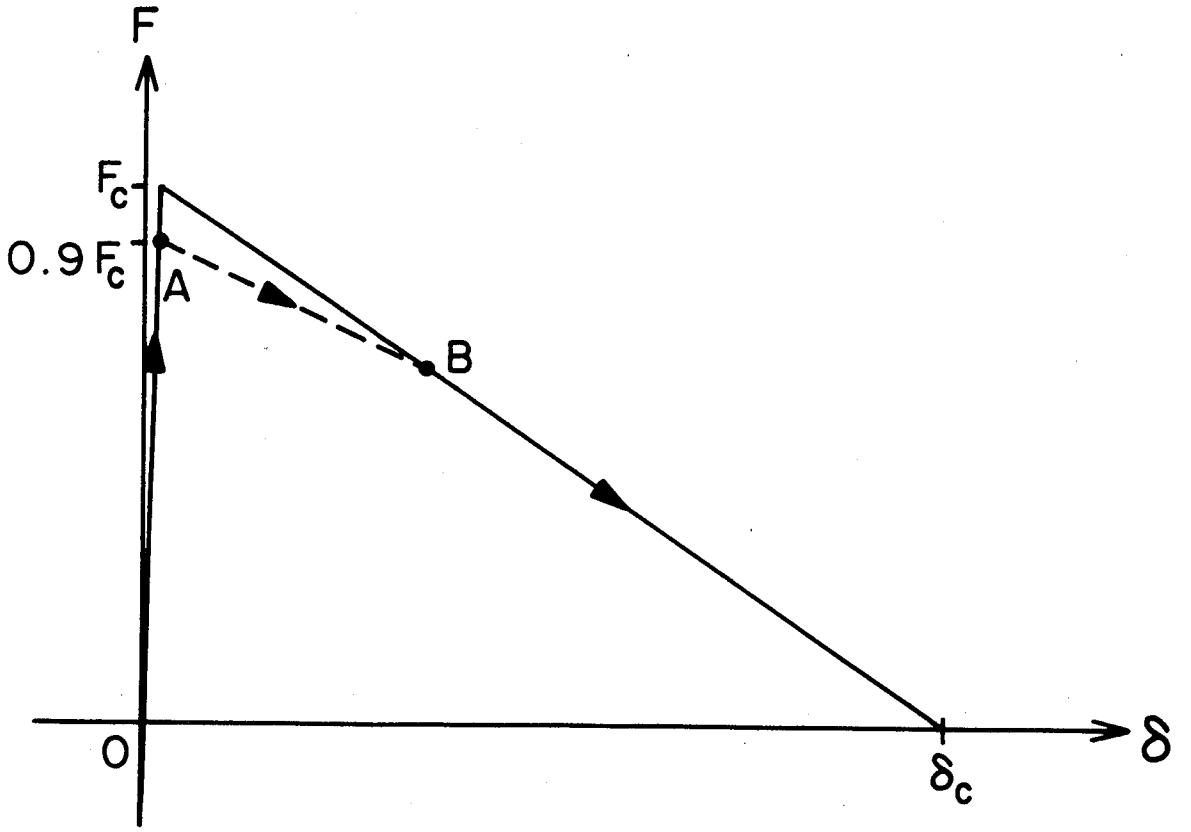

Figure A-3. Illustration of how an incorrect solution results when a large loading increment is taken.

out that extensive subdivisions of the step size occurred again once the softening of the crack tip spring started. The step size was allowed to decrease down to as low as 10^{-4} of the already small initial step size and the solution would still not converge.

To see if the onset of softening in the crack tip spring caused the non-convergence, we fixed all the nodes along the crack path leaving only the single spring at the crack tip active. Upon loading the system as before, the spring at the crack tip softened and was broken without further need for any subdivision of the step size; in this case, the spring was traced out fully in small steps as initially prescribed. The result of this test indicated that the numerical difficulty was likely to be caused by the interactions between the row of nonlinear springs and the plastically deforming solid.

It is very difficult to rigorously prove the above conjecture that, somehow, the coupling of these nonlinear softening springs and the elastic-plastic body is the source of the numerical problem encountered. However, we suspect that the model, in its present form, allow the springs representing the cohesive 'boundary layer' to deform too freely. In other words, it is likely that the problem is 'ill-posed' in its present form, and additional constraints need to be imposed in order to properly generalize the cohesive zone model to the case where the material body is elastic-plastic. An argument supporting this conjecture is given next.

Since its invention, the idea of a 'cohesive zone' has been used exclusively in connection with elastic solids the constitutive property of which imposes a 'smoothness' condition[14] on the deformed profile of the interface between the cohesive zone and the solid body. In our present model, however, the 'smoothness' condition does not exist since the elastic-plastic body is much more flexible in its freedom to deform

14. More precisely, the cohesive interface cannot exhibit a kink.

at the cohesive interface. This implies that the nonlinear cohesive layer does not necessarily need to possess a unique distribution of cohesive forces in order to satisfy all field equations. Therefore the non-convergence experienced when softening takes place at the crack tip spring possibly reflects the fact that at that stage in the solution process the newly formed stiffness matrix cannot seek out a consistent path which the incremental deformation of the system must follow, due to the excess of freedom in the present model. Before suggesting some possible remedies for this difficulty, let us digress for a moment to address another aspect of the present model which poses some further unresolved questions.

4. SOME COMMENTS ON FINITE-ELEMENT SCALING

In this section, we turn to another issue of importance in ensuring the self-consistency of the model proposed earlier. The issue is how one scales the nonlinear softening springs so that analyses using different element sizes along the crack path (which define the discrete incremental steps by which crack growth is simulated) yield the same results.

If the solid body is simply elastic and the cohesive behavior is such that a critical crack tip opening displacement is the proper criterion for fracture independent of the discretization of the crack path,[15] the scaling is very simple (see for instance, Section 3 of Part I). In the present model, however, no simple and consistent 'scaling' rules exist. The difficulty encountered is discussed below in its historical perspective.

In 1966 Rice showed that a Griffith-type energy balance for crack growth led to paradoxical results for solids that are modeled as elastic-plastic continua, since such solids provide no energy surplus in continuous crack advance to equate to a work of surface separation (or fracture energy) [2]. In essence, it was shown that when the material stress-strain relation entails the saturation of the flow stress to a finite value at large strain, there is no singularity in recoverable energy density at the crack tip. Thus there is no surplus external work over the plastic dissipation to furnish the required fracture energy, and therefore the crack cannot grow which is in contradiction to experimental observation. The paradox was resolved by the recognition that, in the real world, cracks grow in 'discrete' and

15. This is the case in the model of a beam on a nonlinear foundation analyzed in Part I. The critical crack tip opening displacement is independent of the incremental crack growth step since it is the product of the thickness of the cohesive interlayer and the critical strain both of which do not depend on the size of elements along the crack path.

'finite' steps the size of which is determined by the mode of failure in the crack tip process zone [3].

In reference 3, it is shown that the energy release rate (which is equivalent to our 'fracture energy') vanishes as the crack growth increment is decreased to zero. This conclusion is confirmed by extensive finite element analyses (see reference 4, for example). This means that the fracture energy calculated from a force-displacement diagram of a spring (such as Figure A-1) must not be interpreted as a physical quantity; but rather, as a value derived from the generation-phase analyses which depends on the size of the crack growth steps employed. According to the study of scaling conducted in reference 1, the critical nodal force, F_c , scales with the crack increment size, Δa, in an almost linear fashion whereas the fracture energy, γ, decreases as Δa is decreased but not quite as linearly as for F_c.

From the above discussion, it is clear that the scaling of the nonlinear springs representing the behavior of the cohesive 'boundary layer' is not based on any set of simple rules. As the findings in reference 1 suggest, the first attempt might be by linear scaling of both F_c and δ_c which would scale γ linearly as well. Subsequent refinements would have to be done through trial and error since the scaling is most likely nonlinear. We have, therefore, another unresolved issue in addition to the numerical difficulty described in Section 3. The problem of obtaining solutions from the present model which are independent of both the solution path and the finite element mesh has yet to be resolved.

5. SUGGESTIONS AND CONCLUSIONS

In this last section, we discuss a number of possible measures that may help overcome the numerical difficulty described in Section 3. At the present time, the suggestions given below cannot be implemented in the finite element program ABAQUS since it is proprietary and the FORTRAN source code is unavailable.

Based on the studies conducted thus far, we believe additional constraints have to be imposed on the model. In particular, the row of nonlinear softening springs must be controlled so that the resulting cohesive interface retains some degree of 'smoothness'. This can be accomplished in several ways, as discussed below. The most appropriate choice would be judged by how well each candidate performs in eliminating the numerical difficulty as well as in being able to closely simulate experimental measurements.

The simplest scheme is to freeze the movements of all the springs ahead of crack tip as soon as the crack tip spring reaches the critical nodal force F_c and allow only this one spring to break before reactivating the rest of the springs to continue the analysis. This method is, perhaps, too restrictive, and is not very different from releasing the crack tip node one at a time; thus it is rather inefficient as far as allowing crack growth to be completely controlled by external loading as we originally hoped to do. An alternative is to require that the extensions (or the vertical displacements) of the springs be monotonically decreasing starting from the first spring at the crack tip. This should ensure that the cohesive interface is fairly 'smooth'. Additionally, we may allow only positive increments in the extension of each spring, this would ensure that the softening of the damaged 'boundary layer' as modeled by the springs progresses monotonically and no artificial unloading occurs during the solution process. Other similar measures can also be tried provided the system is not perturbed excessively so as to result in erroneous solutions.

It is premature to claim the viability of the generalized cohesive zone model proposed here considering all the unresolved difficulties discussed in the previous two sections. Further investigations are needed to pass the final verdict on the potential of this model.

6. REFERENCES

1. Kanninen, M.F. et al., "Elastic-Plastic Fracture Mechanics for Two-Dimensional Stable Crack Growth and Instability Problems," Elastic-Plastic Fracture, ASTM STP 668, J.D. Landes, J.A. Begley, and G.A. Clarke (Eds.), 1979, pp. 121-150.

2. Rice, J.R., "An Examination of the Fracture Mechanics Energy Balance from the Point of View of Continuum Mechanics," Proceedings of the 1st Int'l Conf. on Fracture, Vol. I, Sendai, Japan, T. Yokobori et al. (Eds.), Japanese Soc. for Strength and Fracture of Materials, Tokyo, 1966, pp. 309-340.

3. Kfouri, A.P., "Continuous Crack Growth or Quantized Growth Steps ?," Int. J. Fracture Mech., Vol. 15, 1979, pp. 23-29.

4. Kfouri, A.P., and Rice, J.R., "Elastic/Plastic Separation Energy Rate for Crack Advance in Finite Growth Steps," Fracture 1977, the 4th Int'l Conf. on Fracture, Vol I, Waterloo, Canada, 1977, pp. 43-59.